

2003

Fatigue and Fracture of the FRP-Wood Interface: Experimental Characterization and Performance Limits

Yong Hong
University of Maine - Main

Follow this and additional works at: <http://digitalcommons.library.umaine.edu/etd>

 Part of the [Civil and Environmental Engineering Commons](#)

Recommended Citation

Hong, Yong, "Fatigue and Fracture of the FRP-Wood Interface: Experimental Characterization and Performance Limits" (2003).
Electronic Theses and Dissertations. 125.
<http://digitalcommons.library.umaine.edu/etd/125>

This Open-Access Thesis is brought to you for free and open access by DigitalCommons@UMaine. It has been accepted for inclusion in Electronic Theses and Dissertations by an authorized administrator of DigitalCommons@UMaine.

**FATIGUE AND FRACTURE OF THE FRP-WOOD INTERFACE:
EXPERIMENTAL CHARACTERIZATION AND PERFORMANCE LIMITS**

By

Yong Hong

B.S. Beijing Polytechnic University, China, 1993

A THESIS

Submitted in Partial Fulfillment of the

Requirements for the Degree of

Master of Science

(in Civil Engineering)

The Graduate School

The University of Maine

May, 2003

Advisory Committee:

Roberto A. Lopez-Anido, Assistant Professor of Civil Engineering, Advisor

Douglas J. Gardner, Professor, Wood Science and Technology

Eric Landis, Associate Professor of Civil Engineering

Lech Muszynski, Assistant Scientist, Wood Science and Technology

**FATIGUE AND FRACTURE OF THE FRP-WOOD INTERFACE:
EXPERIMENTAL CHARACTERIZATION AND PERFORMANCE LIMITS**

By Yong Hong

Thesis Advisor: Dr. Roberto A. Lopez-Anido

An Abstract of the Thesis Presented
in Partial Fulfillment of the Requirements for the
Degree of Master of Science
(in Civil Engineering)
May, 2003

A performance-based material evaluation methodology was developed to qualify FRP composite reinforcement bonded to glulam structural members for highway bridge applications. The objectives of this thesis are: a) to implement and correlate two methods to evaluate the fatigue and fracture performance of FRP-wood interfaces with associated performance limits; and b) to provide data and recommendations necessary to develop performance-based material specifications.

The first method is based on evaluating the apparent shear strength in a single-lap shear test by fatigue tension loading. The second method is based on evaluating the interface fracture toughness in Mode I or opening-mode using fracture mechanics. ASTM standard test procedures were identified as the basis for each method. However, these test procedures had to be modified and adapted for FRP-wood interfaces.

The research approach combined experimental techniques, data reduction methods and analytical tools. A laminating press was designed and calibrated for time-dependent effects to fabricate the test samples. Two material systems that passed adhesive screening tests were evaluated: E-glass/urethane pultruded composite sheet with

urethane adhesive (material system B) and E-glass/epoxy composite sheet by continuous lamination with epoxy adhesive (material system C). The fatigue performance of FRP-wood interfaces using a single-lap shear configuration was characterized by modifying ASTM D2339 standard test procedure. A fatigue performance-based evaluation criteria and associated limits were proposed. It was shown that material system C had higher apparent shear strength and better fatigue resistance than system B. Quality bonding was observed for both material systems in terms of high percentage of wood failure. Finite Element Analysis (FEA) was performed on a model simulating single lap shear specimens loaded in tension to analyze the peeling and shear stress distributions in the overlap area.

The Mode I fracture toughness of FRP composite and wood bonded interfaces was evaluated using flat double-cantilever beam (DCB) specimens. ASTM standard test procedure D5528 for unidirectional FRP composites was modified to characterize hybrid FRP-wood materials. Crack lengths and crack opening displacements were monitored during the experiments using a CCD digital camera system with digital image correlation. An important simplification was realized with flat DCB geometry with respect to other methods based on tapered specimens. Three data reduction methods were applied to compute interlaminar fracture toughness: modified beam theory, compliance calibration and shear corrected compliance. The three methods provided similar fracture toughness values. It was found that Mode I fracture toughness of material system C (epoxy adhesive) was significantly higher than that of material system B (urethane adhesive). It was demonstrated that this fracture method could be used to quantitatively discriminate and evaluate FRP-wood bonded material systems.

ACKNOWLEDGEMENTS

The author would like to thank Professor Roberto Lopez-Anido for his continuous guidance through every phase of this research project. I would also like to thank Professor Gardner, Professor Landis, Dr. Muszyński for their advice on this thesis. Besides, my sincere appreciation extends to Professor Goodell, Professor Dagher and Professor Davids for their comments on my research; to AEWCCerter laboratory staff for their technical assistance; to graduate students and undergraduate students for their help in conducting the experimental work. Without their help, this thesis would be an impossible mission.

The research was funded by the Federal Highway Administration and the Maine Department of Transportation through FHWA Contract DTFH61-99-C-00064- FRP Reinforced Glulams for Bridge Applications.

TABLE OF CONTENTS

| | |
|--|------|
| ACKNOWLEDGEMENTS..... | ii |
| LIST OF TABLES | xi |
| LIST OF FIGURES | xiii |
| Chapter | |
| 1. INTRODUCTION | 1 |
| 1.1 Introduction and Background | 1 |
| 1.2 Research Objectives and Outline | 3 |
| 1.3 Introduction of Adhesive Joints | 4 |
| 1.3.1 Advantages and Disadvantages of Adhesive Bonded Joints | 5 |
| 1.3.2 Common Adhesive Joint Types | 6 |
| 1.4 Comprehensive Review of the Test Methods | 7 |
| 1.4.1 Bond Strength of FRP-Wood and Wood-Wood Interface..... | 7 |
| 1.4.2 Adhesive Bonding of Metal-Metal | 8 |
| 1.4.3 Adhesive Bonding of FRP-Metal and FRP-FRP | 11 |
| 1.4.4 Fatigue Properties of Solid Wood and Jointed Wood | 15 |
| 1.4.5 Investigation of Lap Shear Test Method | 15 |
| 1.4.6 Relevant ASTM Standards | 16 |
| 1.5 Summary of Literature Review..... | 17 |
| 2. DESIGN, CALIBRATION AND APPLICATION OF A LAMINATING PRESS | |
| PROTOTYPE FOR FRP-GLULAM BILLETS | 20 |

| | |
|--|----|
| 2.1 Summary | 20 |
| 2.2 Introduction..... | 21 |
| 2.2.1 Background..... | 21 |
| 2.2.2 Objectives | 23 |
| 2.2.3 Literature Review | 24 |
| 2.3 Basic Principles and Design of the Clamping Device | 25 |
| 2.4 Analytical Calculation of the Clamping Pressure..... | 29 |
| 2.4.1 Empirical Model | 30 |
| 2.4.2 Phenomenological Model | 31 |
| 2.5 Calibration Procedure | 40 |
| 2.5.1 Torque versus Clamping Pressure | 42 |
| 2.5.1.1 Configuration | 42 |
| 2.5.1.2 Procedure | 42 |
| 2.5.2 Clamping Pressure Loss over Time..... | 43 |
| 2.5.2.1 Configuration | 43 |
| 2.5.2.2 Procedure | 43 |
| 2.5.3 Scaling Up | 45 |
| 2.6 Experimental Results and Discussion..... | 46 |
| 2.7 Modeling Results and Discussion..... | 49 |
| 2.7.1 Empirical Model | 49 |
| 2.7.2 Phenomenological Model | 52 |
| 2.8 Conclusions and Recommendations | 55 |

| | |
|-------------------|----|
| 2.9 Notation..... | 57 |
|-------------------|----|

3. SCREENING TESTS: EVALUATION OF DURABILITY AND SHEAR

| | |
|--|----|
| STRENGTH OF FRP-WOOD INTERFACES..... | 59 |
| 3.1 Summary..... | 59 |
| 3.2 Introduction..... | 59 |
| 3.3 Objective and Scope | 60 |
| 3.4 Literature Review..... | 60 |
| 3.5 Matrix of Material Systems | 63 |
| 3.6 Experimental Characterization of FRP Material Properties | 66 |
| 3.6.1 Mechanical Tests | 66 |
| 3.6.2 Ignition Loss Tests of FRP Composite..... | 66 |
| 3.7 Part One of Modified ASTM D2559: Resistance to Shear in Compression..... | 68 |
| 3.7.1 FRP-Wood Specimen Configuration..... | 68 |
| 3.7.2 FRP-Wood Specimen Fabrication | 70 |
| 3.7.3 Experimental Procedure..... | 70 |
| 3.7.4 Experimental Results..... | 71 |
| 3.7.5 Discussions of Experimental Results..... | 72 |
| 3.8 Part Two of Modified ASTM D2559: Resistance to Delamination During Accelerated Exposure | 75 |
| 3.8.1 FRP-Wood Specimen Configuration..... | 76 |
| 3.8.2 FRP-Wood Specimen Fabrication | 77 |
| 3.8.3 Experimental Procedure..... | 78 |

| | |
|---|----|
| 3.8.4 Experimental Results | 79 |
| 3.8.5 Discussion and Conclusion of Experimental Results | 83 |
| 3.9 Conclusions..... | 84 |

| | |
|--|-----|
| 4. FATIGUE PERFORMANCE OF FRP-WOOD INTERFACES USING A SINGLE-LAP SHEAR BY TENSION LOADING TEST | 85 |
| 4.1 Summary | 85 |
| 4.2 Introduction..... | 85 |
| 4.3 Objective and Scope | 87 |
| 4.4 Literature Review of Single-lap Shear Test Methods..... | 87 |
| 4.4.1 Adhesive Bonding of Metal-Metal | 87 |
| 4.4.2 Adhesive Bonding of FRP-Metal and FRP-FRP | 90 |
| 4.5 Materials | 92 |
| 4.6 Modified ASTM D2339: Strength Properties of Adhesives in FRP-Wood Construction in Shear by Tension Loading | 92 |
| 4.6.1 FRP-Wood Specimen Configuration..... | 92 |
| 4.6.2 FRP-Wood Specimen Fabrication | 93 |
| 4.6.3 Experimental Procedure..... | 96 |
| 4.6.3.1 Quasi-static Control Tests..... | 97 |
| 4.6.3.2 Fatigue Tests | 97 |
| 4.6.3.3 Residual Strength Tests..... | 98 |
| 4.6.4 Failure Mode..... | 98 |
| 4.6.5 Experimental Results..... | 100 |

| | |
|--|-----|
| 4.6.6 Analysis and Discussion of Experimental Results | 108 |
| 4.7 Fatigue Performance Criteria for Practical Application | 114 |
| 4.8 Conclusions and Recommendations | 116 |
| | |
| 5. FINITE ELEMENT ANALYSIS OF SINGLE-LAP SHEAR SPECIMEN UNDER TENSION LOADING | 119 |
| 5.1 Summary | 119 |
| 5.2 Introduction..... | 119 |
| 5.3 Objective and Scope | 120 |
| 5.4 Literature Review..... | 120 |
| 5.5 Element Type..... | 125 |
| 5.6 Material Properties..... | 126 |
| 5.6.1 Wood..... | 126 |
| 5.6.2 FRP | 126 |
| 5.6.3 Adhesive | 127 |
| 5.7 Boundary Conditions | 128 |
| 5.8 Element Meshing | 129 |
| 5.9 Convergence Study | 131 |
| 5.10 Results and Discussion | 140 |
| 5.11 Conclusions and Correlation with Experiments | 145 |
| | |
| 6. MODE I FRACTURE TESTING OF FRP-WOOD HYBRID FLAT DCB SPECIMENS..... | 148 |

| | |
|---|-----|
| 6.1 Summary | 148 |
| 6.2 Introduction of Fracture Toughness Tests | 148 |
| 6.3 Objective and Scope | 150 |
| 6.4 Literature Review of Fracture Test Methods | 150 |
| 6.4.1 Adhesive Bonding of FRP-Wood and Wood-Wood | 150 |
| 6.4.2 Adhesive Bonding of Metal-Metal and FRP-Metal..... | 153 |
| 6.4.3 Adhesive Bonding of FRP-FRP..... | 155 |
| 6.4.3.1 Data Reduction Methods..... | 155 |
| 6.4.3.2 Comprehensive Reviews..... | 156 |
| 6.4.3.3 Studies of Fatigue Behavior..... | 157 |
| 6.4.3.4 Effect of Substrate Material | 159 |
| 6.4.3.5 Effects of Loading Rate | 160 |
| 6.4.3.6 Effect of Starter Films and Precracking..... | 161 |
| 6.4.3.7 Effect of Post-cure Conditions..... | 161 |
| 6.4.3.8 Effect of Temperature | 162 |
| 6.4.3.9 Effect of Residual Stresses..... | 163 |
| 6.4.3.10 Fracture Behavior of Multidirectional Composite Laminates..... | 163 |
| 6.5 Summary and Discussion of the Literature Review | 163 |
| 6.6 Material Systems..... | 165 |
| 6.7 Modified ASTM D5528: Standard Test Method for Mode I Interlaminar Fracture Toughness of FRP-Wood Interface | 165 |
| 6.7.1 FRP-Wood Specimen Configuration..... | 165 |

| | |
|---|-----|
| 6.7.2 FRP-Wood Specimen Fabrication | 166 |
| 6.7.3 Experimental Procedure..... | 172 |
| 6.8 Image Analysis..... | 174 |
| 6.9 Data Reduction Methods..... | 176 |
| 6.9.1 Modified Beam Theory (MBT) Method..... | 178 |
| 6.9.2 Compliance Calibration (CC) Method..... | 179 |
| 6.9.3 Shear Corrected Compliance (SCC) Method | 180 |
| 6.10 Experimental Results | 181 |
| 6.11 Failure Mode..... | 185 |
| 6.12 Comparison of Data Reduction Methods..... | 187 |
| 6.13 Discussion of Experimental Results | 188 |
| 6.14 Conclusions and Recommendations | 191 |
| | |
| 7. CONCLUSIONS AND RECOMMENDATIONS | 194 |
| 7.1 Development of a Laminating Press..... | 194 |
| 7.2 Material Screening Tests..... | 195 |
| 7.3 Single-lap Shear Fatigue Tests..... | 196 |
| 7.4 Finite Element Analysis of Single-lap Shear Specimen | 198 |
| 7.5 Mode I DCB Fracture Tests..... | 199 |
| 7.6 Summary | 201 |
| | |
| REFERENCES | 203 |
| | |
| APPENDIX A – Calibration Procedure of the Laminating Press..... | 219 |

| | |
|---|-----|
| APPENDIX B – Standard Operation Procedure of Laminating Press | 222 |
| APPENDIX C – Work Instruction of Shear by Compression Loading Test..... | 223 |
| APPENDIX D – Work Instruction of Cycle Delamination Test | 226 |
| APPENDIX E – Work Instruction of Single-lap Shear Test by Tension Loading | 229 |
| APPENDIX F – Work Instruction of Mode I DCB Fracture Test..... | 233 |
| BIOGRAPHY OF THE AUTHOR..... | 237 |

LIST OF TABLES

| | | |
|------------|---|-----|
| Table 2.1 | Specifications of the Laminating Press..... | 28 |
| Table 2.2 | Stiffness Characteristics of the Press Components..... | 35 |
| Table 2.3 | Scaling Up Calculation | 46 |
| Table 2.4 | Constants of the Phenomenological Model | 52 |
| Table 2.5 | Constants of the Second Kelvin Element Used in the Prediction of the Retightening Behavior | 55 |
| Table 3.1 | Matrix of FRP-wood Material Systems for the Screening Tests..... | 65 |
| Table 3.2 | Matrix of PRO-SET Epoxy..... | 65 |
| Table 3.3 | Assembly Time and Clamping Pressure of Adhesives..... | 65 |
| Table 3.4 | FRP Mechanical Properties from Longitudinal Tensile Tests..... | 67 |
| Table 3.5 | FRP Mechanical Properties from Shear Tests | 67 |
| Table 3.6 | Fiber Volume Fractions | 67 |
| Table 3.7 | Shear Strength and Wood Failure | 73 |
| Table 3.8 | Material System Selected Based on the Screening Tests | 76 |
| Table 3.9 | Results of ASTM D2559 Cycle Delamination Tests of Material System D | 80 |
| Table 3.10 | Results of ASTM D2559 Cycle Delamination Tests of Material System B | 81 |
| Table 3.11 | Results of ASTM D2559 Cycle Delamination Tests of Material System C | 82 |
| Table 4.1 | Material Systems..... | 92 |
| Table 4.2 | Assembly Time and Clamping Pressure of Adhesives..... | 94 |
| Table 4.3 | SLS Test Results for Material System B | 101 |
| Table 4.4 | SLS Test Results for Material System C | 101 |

| | | |
|-----------|--|-----|
| Table 4.5 | Unpaired t-Test Result for Comparison of SLS Control Strength between Material System B and C | 109 |
| Table 4.6 | Unpaired t-Test Result for Material System B | 110 |
| Table 4.7 | Unpaired t-Test Result for Material System C | 110 |
| Table 4.8 | Correlations Between Shear Strength by Compression Loading and by Tension Loading | 114 |
| Table 5.1 | Material Properties Used in Finite Element Analysis..... | 128 |
| Table 5.2 | Meshing Parameters of the Four Different Meshes of FEA | 129 |
| Table 5.3 | Stress Concentration Factors for Material System B..... | 132 |
| Table 5.4 | Stress Concentration Factors for Material System C..... | 132 |
| Table 5.5 | Surface Nodal Forces of the Adhesive Layer and Tensile Loads for Material System B | 132 |
| Table 5.6 | Surface Nodal Forces of the Adhesive Layer and Tensile Loads for Material System C | 133 |
| Table 5.7 | Ratios of Average Peeling Stress to Average Shear Stress of the Surface of the Adhesive Layer for Material System B and C | 146 |
| Table 6.1 | Material System Selected Based on the Screening Tests | 165 |
| Table 6.2 | Assembly Time and Clamping Pressure of Adhesives..... | 169 |

LIST OF FIGURES

| | | |
|-------------|--|----|
| Figure 1.1 | Adhesive Joint Types (Army Research Laboratory 1999)..... | 6 |
| Figure 1.2 | Joint Geometry Effects (Army Research Laboratory 1999)..... | 7 |
| Figure 2.1 | Laminating Press | 21 |
| Figure 2.2 | Front View of the Laminating Press..... | 25 |
| Figure 2.3 | Effect of Springs on the Clamping Pressure Loss Due to Time Dependent Deformation | 27 |
| Figure 2.4 | Typical Clamping Force-time Curves | 30 |
| Figure 2.5 | Spring and Dashpot Elements | 31 |
| Figure 2.6 | Spring-dashpot Submodels..... | 32 |
| Figure 2.7 | Simplification of the Elastic Elements of the Models..... | 33 |
| Figure 2.8 | Simplified Spring-dashpot Models..... | 33 |
| Figure 2.9 | Configuration of the Calibration Setup of Torque versus Clamping Pressure..... | 41 |
| Figure 2.10 | Configuration of the Calibration Setup of Clamping Pressure Loss versus Time | 41 |
| Figure 2.11 | Calibration Curves of Clamping Pressure Loss versus Time..... | 44 |
| Figure 2.12 | Schematic Diagram of the Laminating Press with Wood Lay-ups | 45 |
| Figure 2.13 | Torque versus Clamping Load Calibration Curve with Steel Plates..... | 47 |
| Figure 2.14 | Torque versus Clamping Load Calibration Curve with Wood Laminations..... | 47 |
| Figure 2.15 | Correlation of Empirical Model with Experimental Results..... | 50 |
| Figure 2.16 | Prediction of the Retightening Effect from Empirical Model..... | 51 |
| Figure 2.17 | Predicted Retightening Behavior from the Empirical Model..... | 51 |
| Figure 2.18 | Correlation of Phenomenological Model with Experimental Results..... | 53 |

| | | |
|-------------|---|-----|
| Figure 2.19 | Typical Adhesive Effect | 53 |
| Figure 2.20 | Phenomenological Model Prediction due to Retightening after 30 Minutes | 54 |
| Figure 2.21 | Phenomenological Model Prediction due to Retightening after 60 Minutes | 54 |
| Figure 3.1 | FRP Composite Materials | 64 |
| Figure 3.2 | FRP Composite Materials after Ignition Tests | 68 |
| Figure 3.3 | Specimens for Modified ASTM D905 Shear Block Tests | 69 |
| Figure 3.4 | FRP-Wood Shear Block Specimens..... | 71 |
| Figure 3.5 | Shear Strength of the Shear Block Tests | 74 |
| Figure 3.6 | Wood Failure of the Shear Block Tests..... | 74 |
| Figure 3.7 | FRP-Wood Specimens for Cycle Delamination Test..... | 77 |
| Figure 3.8 | Specimens of Material System B after Cycle Delamination Tests..... | 81 |
| Figure 3.9 | Specimens of Material System C after Cycle Delamination Tests..... | 82 |
| Figure 4.1 | Specimen Configuration for Modified ASTM D2339 SLS Tests | 93 |
| Figure 4.2 | Test Panel and Test Sample of Single-lap Shear Tests | 94 |
| Figure 4.3 | Test Setup of the Single-lap Shear Test by Tension Loading | 96 |
| Figure 4.4 | Typical Static Failure Mode of SLS Specimens of System B..... | 99 |
| Figure 4.5 | Typical Static Failure Mode of SLS Specimens of System C..... | 99 |
| Figure 4.6 | Typical Fatigue Failure Mode of SLS Specimens for System B..... | 100 |
| Figure 4.7 | Typical Fatigue Failure Mode of SLS Specimens for System C..... | 100 |
| Figure 4.8 | Applied Number of Fatigue Cycles for Material System C (75%) | 101 |
| Figure 4.9 | SLS Control Strength for Material System B..... | 102 |

| | | |
|-------------|--|-----|
| Figure 4.10 | Percentage Wood Failure of Control Tests for Material System B..... | 102 |
| Figure 4.11 | SLS Control Strength for Material System C..... | 103 |
| Figure 4.12 | Percentage Wood Failure of Control Tests for Material System C..... | 103 |
| Figure 4.13 | Applied Number of Fatigue Cycles for Material System B | 104 |
| Figure 4.14 | Percentage Wood Failure of Fatigue Tests for Material System B | 104 |
| Figure 4.15 | Applied Number of Fatigue Cycles for Material System C | 105 |
| Figure 4.16 | Percentage Wood Failure of Fatigue Tests for Material System C | 105 |
| Figure 4.17 | SLS Residual Strength Tests for Material System B..... | 106 |
| Figure 4.18 | Percentage Wood Failure of Residual Strength Tests for System B | 106 |
| Figure 4.19 | SLS Residual Strength Tests for Material System C..... | 107 |
| Figure 4.20 | Percentage Wood Failure of Residual Strength Tests for System C | 107 |
| Figure 4.21 | SLS Strength Distribution of Material System B | 111 |
| Figure 4.22 | SLS Strength Distribution of Material System C | 111 |
| Figure 4.23 | Normal Probability Plot of the SLS Control Strength for System B..... | 112 |
| Figure 4.24 | Normal Probability Plot of the SLS Control Strength for System C..... | 112 |
| Figure 4.25 | Distribution of Fatigue Test Results..... | 113 |
| Figure 5.1 | Element Type: PLANE42(ANSYS 2001)..... | 125 |
| Figure 5.2 | Boundary Conditions Used in Finite Element Analysis..... | 129 |
| Figure 5.3 | Schematic of Mesh Refinement at the Right Overlap End (Box Area) | 130 |
| Figure 5.4 | Mesh Convergence for Peeling Stress Concentration Factors Loads for Material System B..... | 133 |
| Figure 5.5 | Mesh Convergence for Peeling Stress Concentration Factors Loads for Material System C | 133 |

| | | |
|-------------|--|-----|
| Figure 5.6 | Mesh Convergence for Shear Stress Concentration Factors Loads for Material System B | 134 |
| Figure 5.7 | Mesh Convergence for Shear Stress Concentration Factors Loads for Material System C | 134 |
| Figure 5.8 | Mesh Convergence for Nodal Forces of the Adhesive Surfaces Loads for Material System B | 135 |
| Figure 5.9 | Mesh Convergence for Nodal Forces of the Adhesive Surfaces Loads for Material System C | 135 |
| Figure 5.10 | Mesh Convergence for Peeling Stress Concentration Factors (Bottom Left) for Material System B | 136 |
| Figure 5.11 | Mesh Convergence for Peeling Stress Concentration Factors (Bottom Left) for Material System C | 136 |
| Figure 5.12 | Mesh Convergence for Peeling Stress Concentration Factors (Top Right) for Material System B | 137 |
| Figure 5.13 | Mesh Convergence for Peeling Stress Concentration Factors (Top Right) for Material System C | 137 |
| Figure 5.14 | Mesh Convergence for Shear Stress Concentration Factors (Bottom Left) for Material System B | 138 |
| Figure 5.15 | Mesh Convergence for Shear Stress Concentration Factors (Bottom Left) for Material System C | 138 |
| Figure 5.16 | Mesh Convergence for Shear Stress Concentration Factors (Top Right) for Material System B | 139 |

| | | |
|-------------|--|-----|
| Figure 5.17 | Mesh Convergence for Shear Stress Concentration Factors (Top Right) for Material System C | 139 |
| Figure 5.18 | Overall Peeling Stress Distribution (Mesh 1) for Material System B | 141 |
| Figure 5.19 | Overall Peeling Stress Distribution (Mesh 1) for Material System C | 141 |
| Figure 5.20 | Overall Shear Stress Distribution (Mesh 1) for Material System B | 141 |
| Figure 5.21 | Overall Shear Stress Distribution (Mesh 1) for Material System C | 141 |
| Figure 5.22 | Peeling Stress Distribution at the Ends of the Adhesive Layer (Mesh 4) for Material System B | 142 |
| Figure 5.23 | Peeling Stress Distribution at the Ends of the Adhesive Layer (Mesh 4) for Material System C | 142 |
| Figure 5.24 | Shear Stress Distribution at the Ends of the Adhesive Layer (Mesh 4) for Material System B | 142 |
| Figure 5.25 | Shear Stress Distribution at the Ends of the Adhesive Layer (Mesh 4) for Material System C | 142 |
| Figure 5.26 | Stress Concentration Factors of the Top Surface of the Adhesive Layer (Mesh 4) for Material System B | 143 |
| Figure 5.27 | Stress Concentration Factors of the Top Surface of the Adhesive Layer (Mesh 4) for Material System C | 143 |
| Figure 5.28 | Stress Concentration Factors of the Bottom Surface of the Adhesive Layer for Material System B | 144 |
| Figure 5.29 | Stress Concentration Factors of the Bottom Surface of the Adhesive Layer for Material System C | 144 |
| Figure 5.30 | Typical Failure Mode of Fatigue Tests | 147 |

| | | |
|-------------|---|-----|
| Figure 6.1 | Three Crack-propagation Modes..... | 149 |
| Figure 6.2 | Specimen Configuration for Modified ASTM D5528 Mode I Tests | 167 |
| Figure 6.3 | Hydraulic Press Used to Fabricate Specimens | 168 |
| Figure 6.4 | Test Panel and DCB Test Sample of Mode I Fracture Tests..... | 169 |
| Figure 6.5 | DCB Specimen with Hinges..... | 171 |
| Figure 6.6 | Test Setup of the Mode I Fracture Tests | 173 |
| Figure 6.7 | The Fracture Specimen Setup..... | 173 |
| Figure 6.8 | Image Analysis Using Sherlock | 175 |
| Figure 6.9 | Time Correlation of Data from Instron and CCD Camera | 176 |
| Figure 6.10 | Typical Curve of Loading-unloading Cyclic Tests | 177 |
| Figure 6.11 | DCB for Measurement of Mode I Fracture Toughness (Daniel and Ishai 1994)..... | 179 |
| Figure 6.12 | Modified Beam Theory (ASTM 2002)..... | 179 |
| Figure 6.13 | Compliance Calibration Method (ASTM 2002)..... | 180 |
| Figure 6.14 | Shear Corrected Compliance (SCC) Method (Gagliano and Frazier 2001)..... | 180 |
| Figure 6.15 | Typical Load-displacement Curve for FRP-Wood Specimen of System C..... | 181 |
| Figure 6.16 | Typical Plot of $\log(C)$ versus $\log(a)$ Using the Data from Figure 6.15..... | 182 |
| Figure 6.17 | Typical Plot of $C^{1/3}$ vs. Crack Length a Using the Data from Figure 6.15 | 182 |
| Figure 6.18 | Typical G_I vs. Crack Length Plot Comparison for Single Wood-wood Specimen of System B and C | 183 |
| Figure 6.19 | G_I vs. Crack Length Plot for Four FRP-Wood Specimens of System B..... | 183 |
| Figure 6.20 | G_I vs. Crack Length Plot for Four FRP-Wood Specimens of System C..... | 184 |

| | | |
|-------------|--|-----|
| Figure 6.21 | Typical G_I vs. Crack Length Plot Comparison for FRP-Wood Fracture Specimens of Material System B and C..... | 184 |
| Figure 6.22 | Typical Failure Mode of FRP-Wood Specimens of System B..... | 185 |
| Figure 6.23 | Typical Failure Mode of FRP-Wood Specimens of System C..... | 186 |
| Figure 6.24 | Typical Failure Mode of Wood-wood Specimens of System B..... | 186 |
| Figure 6.25 | Typical Failure Mode of Wood-wood Specimens of System C..... | 187 |
| Figure 6.26 | COV Comparison of Data Reduction Methods from Data of Single Typical Specimen of System B and C..... | 188 |

Chapter 1

INTRODUCTION

1.1 Introduction and Background

Wood has been one of the principal materials for bridge structures in the U.S. for hundreds of years. According to the National Bridge Inventory (NBI) kept by the Federal Highway Administration (FHWA), there are about 582,750 bridges, of which 38,298 are timber bridges and 39,503 are steel bridges with timber decks. Although wood is not the predominant material for building U.S. highway bridges, timber bridges are widely used on the secondary, local and rural highways to serve low volumes of traffic (Duwadi *et al.* 2000).

Wood has many advantages, such as lightweight, good resistance to freeze-and-thaw cycles and fatigue loads, and being one of the few renewable resources. Although wood has been proven to be a material suitable for transportation structures, it is necessary to develop and advance the systems to meet changing needs (Duwadi *et al.* 2000). On one hand, the cross-sectional dimensions and lengths of lumbers are limited by the size of the trees. On the other hand, wood usually has defects, such as knots, which can severely limit its load-carrying capacity. Furthermore, wood in its natural form, e.g., lumber or log, may not be the most efficient product for a particular load-carrying purpose (Bodig and Jayne 1992). Therefore, one of the most important technologies in this field was developed in U.S.: the application of glued laminated timber (glulam) in timber bridge construction using wet-use adhesives. Another advantage of glulam is that

the laminating process randomly disperses the strength-reducing characteristics of the lumber laminations throughout the member (Williamson 1996).

Traditional timber bridge designs often have difficulty producing adequate strength and stiffness for longer spans. To make the structure lighter and achieve longer spans, fiber-reinforced polymeric (FRP) composites are increasingly used in civil engineering applications (Lopez-Anido and Karbhari 2000). FRP can serve as both a substitute for high-quality laminations and a reinforcement material for glulam beams. Like reinforced concrete, glulam beams can be reinforced in tension to more efficiently use the wood's compressive strength. Glulam beams reinforced with FRP composites showed remarkable improvement in performance under short-term static loading and under long-term creep loading (Dagher 1996; Davids *et al.* 2000; Lopez-Anido and Xu 2002).

However, despite the satisfactory mechanical properties and corrosion resistance offered by the FRP composite system, its susceptibility to the synergistic effects of stress and environmental weathering, especially the lack of knowledge of integrity and durability of FRP-wood interfaces, hinders their widespread acceptance in bridge applications (Battles *et al.* 2000). Therefore, the current Federal Highway Administration (FHWA) funding includes provisions for development of the next generation of engineered wood-that is, hybrid glulam and fiber-reinforced wood composites-for vehicular bridge applications (Duwadi *et al.* 2000).

This Thesis is part of a research program titled "FRP reinforced glulams for bridge applications" funded by FHWA (Lopez-Anido *et al.* 2002). The study presented in this Thesis contributed to evaluating the durability of FRP-glulam through material

level testing and modeling. The overall goal was to develop a performance-based material evaluation methodology to allow prediction of FRP-glulam structural properties with acceptable tolerances, including both the short-term mechanical response and the long-term durability. The proposed test methods were adapted from current ASTM standards and modified when necessary. The methodology consisted of simple accelerated test methods and associated performance limits that are applicable to FRP reinforcement for glulam (Lopez-Anido *et al.* 2002).

1.2 Research Objectives and Outline

A performance-based material evaluation methodology has been developed to qualify FRP composite reinforcement bonded to glulam members for highway bridges. The objectives of this research study are: a) to define and correlate two methods to evaluate the fatigue performance of FRP-wood composite interfaces with associated performance limits; and b) to provide data and recommendations necessary to develop performance based material specifications.

The first method is based on evaluating the apparent shear strength in a single-lap shear test by tension loading (Chapter 4). Finite Element Analysis (FEA) was performed on a model simulating single lap shear specimens loaded in tension to analyze the peeling and shear stress distributions in the overlap area (Chapter 5).

The second method is based on evaluating the interface fracture toughness in the opening-mode (Mode I in fracture mechanics) (Chapter 6). ASTM standard test procedures were identified as the basis for each method. However, these test procedures were modified and adapted for FRP-wood composite interfaces.

A laminating press was designed and calibrated for time-dependent effects to fabricate the test samples (Chapter 2). As screening test methods, two parts of ASTM D2559 standard test procedure were modified and adapted to characterize durability and shear strength of hybrid FRP-wood interface: delamination test and shear block test in compression (Chapter 3). They were used to screen several candidate material systems. Only material systems passed the screening tests were selected for further evaluations. Finally, the conclusions and recommendations of each chapter are summarized (Chapter 7).

The research approach combines experimental techniques, data reduction methods and analytical tools. A servo-hydraulic testing frame was used to conduct the single-lap shear fatigue tests for two types of FRP composite systems bonded to wood. An electro-mechanical testing frame was used to conduct the Mode I fracture mechanics tests. Crack lengths and crack opening displacements were monitored during the experiments using a digital camera system with digital image correlation software.

1.3 Introduction of Adhesive Joints

For FRP reinforced wood structures, questions about life and/or long-term performance of the bond interface are usually related to fatigue and to the effects of a harsh environment. For material level tests, the test methods should be developed using small specimens, which are capable of providing useful information for the material selection and design of large-scale structures.

Fatigue tests of a few days at a high frequency may provide useful information for a much longer time, even years for the same material under similar loading but a lower

frequency. The failure due to fatigue of a coupon-level specimen should be able to be related to the performance of the prototype structure. It requires that mechanisms of failure are often the same in lab specimen geometries as those in the prototype structure (Brinson and Grant 1986).

1.3.1 Advantages and Disadvantages of Adhesive Bonded Joints

One of the greatest challenges in the design of hybrid structures is the prediction of the bond properties. The material discontinuities, and often, the interruptions geometry of the structure, always produce local highly stressed areas.

In general, adhesive bond is structurally more efficient than mechanical fastening because it provides better opportunities to minimize stress concentrations. Furthermore, adhesive joints have improved fatigue resistance. Because most adhesives are polymeric materials that exhibit viscoelastic properties, they can absorb mechanical energy applied to the joint and dissipate the energy as heat. This property is particularly important for bridge structures. Although adhesive joints do require a much larger contact area between the adherends and the adhesive to carry the same load as a mechanical fastener, it is not an issue for FRP reinforced glulam beams.

However, adhesive joints are highly sensitive to manufacturing deficiencies, including poor bond techniques and sensitivity of the adhesive to environmental effects, such as temperature and moisture. Although surface preparation and bond techniques have been well developed, lack of attention to detail in the bond operation may lead to deficiencies. Lack of reliable inspection methods is another big challenge to prevent adhesive joints being used in primary structures. While ultrasonic and X-ray inspection may reveal gaps in the bond, there is no nondestructive evaluation technique currently

available to detect low interfacial strength between the bond and the adherends.

Assurance of bond quality and adequate load transfer capability has been a continuing problem in adhesive joints (Army Research Laboratory 1999).

1.3.2 Common Adhesive Joint Types

A series of typical bonded joint configurations is shown in Figure 1.1.

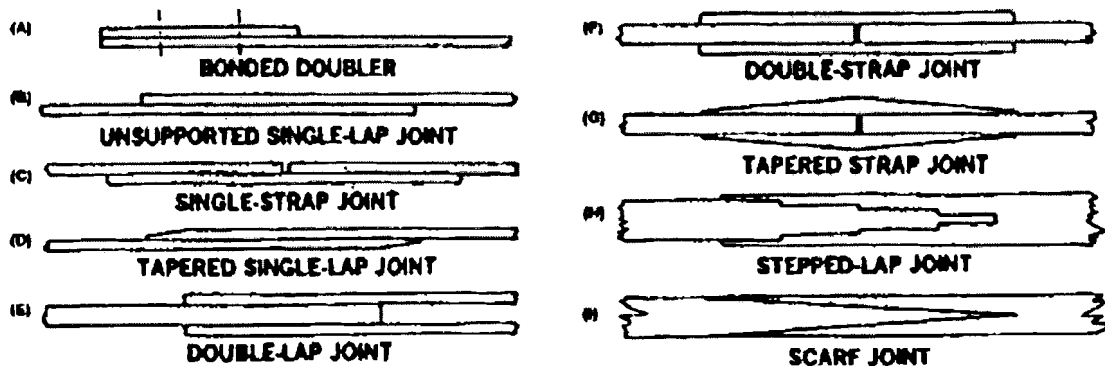


Figure 1.1 Adhesive Joint Types (Army Research Laboratory 1999)

Single lap joints (B) with uniformly thick adherends are the least efficient joint type because the eccentricity of geometry generates significant bending of the adherends that magnifies the peel stresses. Peel stresses are also present in the case of symmetric double lap (E) and double strap joints (F). Tapering of the adherends, (D) and (G), can be used to eliminate peel stresses in areas of the joint where the peel stresses are tensile.

Scarf joints (I) are theoretically the most efficient because it's possible to completely eliminate stress concentrations from these types of joint. Step lap joint (H) is a practical solution of bond thick members to transfer high loads if sufficiently many short steps of sufficiently small "rise" in each step are used, while maintaining sufficient overall length of the joint. A progression of joint types which represent increasing strength capability from the lowest to the highest is shown in Figure 1.2.

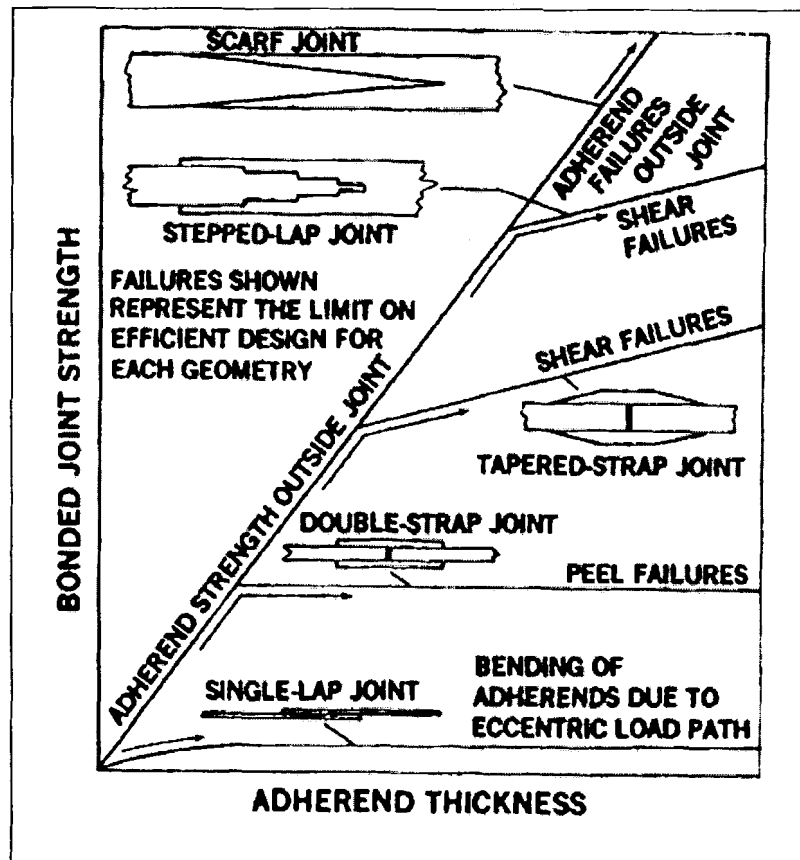


Figure 1.2 Joint Geometry Effects (Army Research Laboratory 1999)

1.4 Comprehensive Review of the Test Methods

A great variety of standard test methods have been developed to characterize adhesive bonded joints between different adherend materials. These test methods are continually updated and revised. All tests can generally be classified into four groups, i.e., shear, tension, peel, and fracture toughness (Tong and Steven 1999). In this section, a comprehensive literature review of general techniques used for characterizing structural adhesive-bonded wood or FRP joints is presented.

1.4.1 Bond Strength of FRP-Wood and Wood-Wood Interface

Since solid wood contoured beams require special efforts for machining and bondline consolidation, a new specimen configuration was developed to evaluate wood-

adhesive joints (Scott *et al.* 1991). It was an extension of the contoured double cantilever beam (CDCB) test and generally followed the procedures outlined in ASTM D3433. Samples were prepared by bond thin wood laminates to contoured aluminum beams, i.e., used the metal-backed wood beam to measure the toughness of the wood-wood bond line.

To evaluate the ultimate shear strength, bond-interface integrity, and percent wood failure of FRP-wood interfaces, shear block tests were conducted as described in ASTM D905 (Gardner *et al.* 1994). A finite element model was developed to analyze the stress of the FRP-wood bond interface under dry and wet conditions (Barbero *et al.* 1994). The results from the experimental program were used to validate the numerical model.

An experimental characterization of the opening-mode (Mode I) fracture toughness of bonded interfaces was presented for wood-wood and FRP-wood hybrid laminates (Davalos *et al.* 1997; Davalos *et al.* 1998). A bi-layer CDCB specimen was developed, which consists of constant thickness adherends bonded to straight tapered sections of an easily machinable material.

1.4.2 Adhesive Bonding of Metal-Metal

The fatigue behavior of adhesively bonded aluminum joints was investigated analytically and experimentally (Romanko and Jones 1980). The thick-adherend single-lap shear joint was selected as the “model joint” to reduce the bending moment in the overlap area. Linear elastic and three-element linear viscoelastic finite element stress analyses were conducted. The specimens were subjected to sinusoidal fatigue tests at several frequencies, humidity and temperatures.

Four ASTM standards used in measuring lap-shear strength, impact strength, peel strength as well as fatigue strength of adhesive bonding were evaluated (Zalucha 1981).

The structural influence of the scrim cloth on the fracture behavior of adhesive-bonded joints was investigated through thick adherend single-lap shear specimens (Francis and Gutierrez-Lemini 1982). The scrim cloth is generally utilized in the adhesive to control the adhesive thickness in a bonded joint. The mat may represent a built-in defect located near the tip of a crack at an adhesive-adherend interface. The finite element method (FEM) was used to analyze the thick adherend single-lap specimen configuration.

The relationship between static and fatigue strength for four different specimen types was reviewed: single-lap shear, edge-delamination, double cantilever beam, and creaked-lap-shear. It was found that the ratio of static strength to fatigue strength varied from 2.3 to 4.7, depending on the adhesive and specimen configuration (Johnson and Mall 1984).

An estimation of fatigue strength was conducted for a lap joint bonded by an epoxy-polyamide adhesive (Imanaka *et al.* 1986). Based on the assumption that the fatigue strength of the lap joint is dominated by the maximum tensile stress, the fatigue strength of the lap joint was estimated from the S-N curve of the adhesive bonded butt joint of the thin wall tube with has a uniform stress distribution. The estimated fatigue strength of the lap joint agreed well with the experimental results. Furthermore, it gave a conservative estimation.

In another study, a method of estimating the fatigue life of adhesively bonded lap joints was developed based on the stress analysis in adhesive layer with FEM (Imanaka *et*

al. 1988). First, cyclic tensile fatigue tests were conducted for adhesively bonded lap joints with different lap length and adhesive layer thickness. Then the results were evaluated from the viewpoint of the maximum values of both tensile and shear stress obtained numerically, instead of the apparent stress.

The fatigue behavior of two adhesives intended for use in automotive body-shell construction was evaluated using simple lap shear test-pieces (Harris and Fay 1991). In the context of aerospace applications where joints are designed with long overlaps and are configured to minimize stress concentrations, the single lap shear joint has been criticized as not being suitable for evaluating the fatigue resistance of adhesive joints because of the high shear and peel stress concentrations that arise in the adhesive layer at the ends of the overlap. Therefore, for aerospace applications, the cracked lap shear joint is always employed for the assessment of fatigue resistance, which is described as “joint independent”. However, for automotive applications, where shorter overlap lengths and simpler joint designs are used, the single lap shear joint is more representative, but it’s not “joint independent”.

The reason that Mode II type crack propagation has been generally less investigated than that occurring under Mode I was described (Edde and Verreman 1995). However, in bonded joints, Mode II has been shown to be a major contributor to crack propagation. It was suggested that a tapered end-notched flexure (TENF) specimen could be used to solve the deficiencies of ENF specimen. The proposed contour prevents the sudden and high acceleration of cracks that hinders usage of the ENF specimen.

A new backface strain technique to detect fatigue crack initiation in adhesive-bonded lap joints was developed (Zhang *et al.* 1995). With the assistance of this

technique, it was found that a fatigue crack initiates in the adhesive but to propagate towards the interface to continue its growth on the interface and to cause the final separation of the joint along the interface. It was concluded that the lifetime in the long-life regime was dominated by the resistance of the adhesive to fatigue crack initiation.

A specific test was developed to investigate the shear behavior of adhesive joints under both monotonic and fatigue loading using a short overlap-thick adherend configuration (Blanchard *et al.* 1996).

A fracture mechanics approach was used successfully to examine the cyclic fatigue behavior of adhesively bonded joints, which consisted of aluminum-alloy substrates bonded using epoxy structural adhesive (Fernando *et al.* 1996). The fatigue tests were conducted in both dry and wet environments. A TDCB joint specimen was employed under nominally mode I cyclic loading.

A study was conducted to investigate fatigue failure criteria for adhesive-bonded joints under combined stress conditions (Imanaka and Iwata 1996). Two types of adhesively bonded joints specimens were used: the scarf joint and the butterfly-type butt joint. The stress distributions were analyzed by a FEM. The results showed that the maximum principal, the von Mises equivalent and the maximum shear stresses in the uniform stress region of the adhesive layer at the endurance limit are correlated with the principal stress ration.

1.4.3 Adhesive Bonding of FRP-Metal and FRP-FRP

An experimental and analytical investigation were conducted, based on fracture mechanics methodology to study the fatigue failure of adhesively bonded composite joints (Mall *et al.* 1982). Two configurations of crack-lap-shear specimens were applied,

which simulate the real-world condition of mixed-mode failure (combination of shear and peel stresses). The tests showed that the joints fatigued by cyclic debonding of adhesive only. The progress of the debonding interface was tracked by photographing photo-elastic material bonded to the composite. The debonding growth rate was then correlated with the different strain-energy-release rates. It correlated very well with total strain-energy-release rate.

In another study, adhesively bonded composites joints were investigated to characterize both the static and fatigue debonding growth mechanism under Mode I (DCB) and Mixed I and II loadings (cracked-lap-shear) (Mall and Johnson 1986; Mall and Yun 1987). It was found that total strain-energy release rate appeared to be the driving parameter for debonding growth under static and fatigue loadings and static data alone are insufficient for safe joint design. If so, it would require the characterization of cycle debonding under Mode I loading only. It would be simpler and easier to test and calculate the G_T .

The role of interlaminar fracture toughness on the cyclic delamination growth resistance and interaction of Mode I and Mode II components of cyclic loading (Mall 1989) were investigated. Three types of specimens were applied: DCB, CLS and end-notched flexure (ENF) specimens to characterize the cyclic delamination (and debonding) growth mechanism under Mode I, Mixed Mode I-II and Mode II conditions, respectively. It was found that the normalized delamination growth resistance for laminated composites under cyclic loading decreases with the increase of static interlaminar fracture toughness.

Ways and means to obtain good mechanical property information for the adhesive layer were considered, which can be effectively used in finite element to durability prediction (Brinson and Grant 1986). After reviewing several currently used methods for the determination of bonded joint durability, it was found that the mechanical properties derived from tensile tests of the bulk adhesive are not good indicators. The Boeing wedge-crack test was considered to be a much better method to evaluate adherend surface treatment, which is tantamount to evaluating the interface. Finally, a new torsion test method was introduced, which is capable to give the needed shear properties of the adhesive for FEM use.

Several types of fatigue tests were conducted to obtain the carbon FRP fatigue strengths in different loading modes (Martin and Sage 1986). It was recognized that the short beam shear test is a valid method for composite shear testing and it is well documented both dynamically and statically. It was suggested that shear fatigue tests for the composite could be found adequately by the short beam shear test so that $\pm 45^\circ$ bar tests are not necessary.

The residual Mode II delamination fracture toughness following exposure to low cycle fatigue loading and moisture at 50°C was characterized (Kenig *et al.* 1989). Experimental results showed that the matrix and fiber/matrix interface dominated behavior in shear loading and was insensitive to short-term exposure to both fatigue and moisture, but sensitive to long-term exposure.

Carbon FRP adherends and epoxy adhesive were used to simulate aircraft structural joints (Gilmore and Shaw 1993). The joint geometry used was a variation of a cracked-lap shear joint. The samples were fatigued at five different combinations of

temperatures and humidity. The results showed that temperatures, humidity and support medium considerably affected the fatigue behavior of adhesive joints.

The fracture mechanics method was applied to study the fatigue behavior of adhesively-bonded joints, which consisted of an epoxy-film adhesive bonding fibre-composite substrates (Kinloch and Osiyemi 1993). DCB specimens were used to get relationship between the rate of crack growth per cycles and the maximum strain-energy release rate. Then these data were modeled and used to predict the fatigue lifetime of bonded single-lap joints.

Embedded adhesive joint configuration was also used to perform fatigue tests on FRP/steel joints at different temperatures (Hattori and Iwasa 1995). FEM was applied to perform the stress analyses of the joint model.

The results of wedge testing (ASTM D3762) were reported for adhesive bonded joints made from dry, and water-immersed and dried, carbon FRP laminates (Armstrong 1996). Both mechanical abrasion and peel ply surfaces were used as the surface preparation. It was found that all the peel ply surfaces gave interfacial failure. This suggests that in view of the extensive use of peel plies in industry it would seem that further research is required to achieve more durable bonds.

Interfacial fracture toughness tests of the DCB specimens were conducted for studying adhesion between the aluminum and carbon FRP sheets (Lawcock *et al.* 1997). Tensile tests, interlaminar shear tests and residual strength tests were also performed.

A method of estimating the fatigue strengths of adhesively bonded single-lap, cracked single-lap and single-step double lap joints composed of carbon FRP and an

aluminum alloy was proposed based on two stress-singularity parameters (Ishii *et al.* 1999).

1.4.4 Fatigue Properties of Solid Wood and Jointed Wood

A detailed review of wood fatigue literatures was presented (Tsai and Ansell 1990). Some species of wood were fatigue tested under load control in four-point flexure over several R ratios at several moisture contents. It was discovered that fatigue life is largely species independent when normalized by static strength. It was also found that moisture has a detrimental effect on fatigue life not only in reducing the static strength but also in accelerating the fatigue damage process. Optical microscopy was used to study the development of compression creases as a function of fatigue test duration.

An extensive review of wood fatigue literatures was carried out (Bond and Ansell 1998a; Bond and Ansell 1998b). The fatigue performance of scarf-jointed laminated wood composites was assessed, which were used to manufacture wind turbine blades and establish simple fatigue design procedures. Furthermore, a method was developed of predicting lifetime to failure for any wood composite system subjected to a complex load-time history.

1.4.5 Investigation of Lap Shear Test Method

The single lap shear test specimen was investigated in a combined experimental and analytical study (Guess *et al.* 1977). The shear strengths of two structural adhesives with the conventional thin adherent lap shear specimen and with several thick adherent configurations were measured. The test results were anomaly explained by finite element analyses of the shear and normal stress gradients in the adhesive layer.

The behavior of interface cracks in adhesively bonded lap-shear joints was investigated (Wang and Yau 1982). An analysis method was applied which was based on conservation laws in elasticity for nonhomogeneous solids and fundamental relationships in fracture mechanics of dissimilar materials. Fundamental nature of the interfacial flaw behavior in lap-shear adhesive joints is examined in detail.

A geometrically nonlinear finite element analysis of cohesive failure in typical joints was conducted (Dattaguru *et al.* 1984). Cracked-lap-shear joints were chosen for the analysis. Results obtained from linear and nonlinear analysis show that nonlinear effects, due to large rotations, significantly affect the calculated mode I and mode II strain-energy-release rates. Results from the analysis agreed well with experimentally measured joints opening displacements.

1.4.6 Relevant ASTM Standards

The available quasi-static test methods are:

- **D905** Standard Test Method for Strength Properties of Adhesive Bonds in Shear by Compression Loading (Single lap shear test, Wood-Wood)
- **D2339** Standard Test Method for Strength Properties of Adhesives in Two-Ply Wood Construction in Shear by Tension Loading (Laminated Assemblies shear test, Wood-Wood)
- **D3165** Standard Test Method for Strength Properties of Adhesives in Shear by Tension Loading of Single-Lap-Joint Laminated Assemblies (Laminated Assemblies shear test, Metal-Metal)
- **D3762** Standard Test Method for Adhesive-Bonded Surface Durability of Aluminum (Wedge Test)

- **D3983** Standard Test Method for Measuring Strength and Shear Modulus of Nonrigid Adhesives by the Thick-Adherend Tensile-Lap Specimen
- **D5528** Standard Test Method for Mode I Interlaminar Fracture Toughness of Unidirectional Fiber-Reinforced Polymer Matrix Composites (Fracture DCB test, FRP)
- **D5868** Standard Test Method for Lap Shear Adhesion for Fiber Reinforced Plastic (FRP) Bonding (Single lap shear test, FRP-FRP or FRP-Metal)

The available fatigue test methods are:

- **D3166** Standard Test Method for Fatigue Properties of Adhesives in Shear by Tension Loading (Metal/Metal)
- **D3479** Standard Test Method for Tension-Tension Fatigue of Polymer Matrix Composite Materials
- **D6115** Standard Test Method for Mode I Fatigue Delamination Growth Onset of Unidirectional Fiber-Reinforced Polymer Matrix Composites

1.5 Summary of Literature Review

Significant research efforts have been dedicated to investigate mechanical properties and predict durability of adhesive bonded joints. However, relatively little work has been done to characterize and qualify the durability performance of hybrid FRP-wood composites for structural applications. In particular to FRP-wood interfaces subjected to moisture and temperature cyclic loads as well as permanent and fatigue loads, it is necessary to develop a performance-based material evaluation methodology to predict the structural properties through material-level testing and modeling, which should be applicable to all FRP reinforcement types (Lopez-Anido *et al.* 2002).

Among all kinds of adhesively bonded joints which have been used to investigate bonding behaviors under different circumstances, two specimen configurations are extremely popular and widely investigated: single-lap shear (SLS) specimen and Double cantilever beam (DCB) specimen.

The single-lap is one of the most commonly used specimen configurations to develop, evaluate and compare different adhesives and bonded products, including manufacturing quality control. The specimens are economical, practical, and easy to fabricate and test. Furthermore, many ASTM standards of this type of joints have been developed for wood, FRP composite and adhesives and for both quasi-static and fatigue testing. Through single-lap fatigue tests, we can get valuable information of fatigue properties of FRP-wood interfaces. Therefore, single-lap shear test by tension loading was selected as one of the two test methods of this study.

In developing material-based fatigue tests, we assume that fatigue failure takes place in the adhesive (called cohesive failure) or between the adhesive and the adherend (called adhesive failure). The true strength of an adhesive is a material property independent of the joint geometry, adherend properties, and load. However, the true shear strength cannot be easily determined using single-lap specimens. Many factors may affect the apparent single-lap shear strength, such as the size and shape of the specimen, the properties of the adherends and the presence of internal stresses or flaws. Thus, single-lap shear tests may not be adequate to evaluate the fatigue performance of FRP-wood interfaces (ASTM 2002).

Fracture mechanics methods have been used to correlate crack growth behavior in adhesive joints. Mode I fracture test is usually recommended to evaluate an adhesive

interface bond strength. In general, the Mode I critical fracture toughness, or critical energy release rate, can be much lower than that of Mode II fracture (Davalos *et al.* 1998). Fracture toughness is a material property independent of the joint geometry, adherend properties, and load. These properties of adhesive bonds are important in terms of characterizing adhesives, predicting adhesive joint strength and service life. Furthermore, ASTM standards for both Mode I quasi-static and fatigue tests are available. Therefore, the Mode I fracture test was selected as the other test method of this study.

The literature review characterizing durability and shear strength of hybrid FRP-wood interfaces is presented in Chapter 2. The literature review related to single-lap test by tension loading and Mode I fracture test is presented in Chapter 4 and Chapter 6, respectively.

Chapter 2

DESIGN, CALIBRATION AND APPLICATION OF A LAMINATING PRESS PROTOTYPE FOR FRP-GLULAM BILLETS

2.1 Summary

The conceptual design, modeling and calibration procedure of a mechanical clamping device for fabricating wood and fiber-reinforced polymer (FRP) composite laminated billets for ASTM D2559 cycle delamination tests and ASTM D905 shear block tests are presented. Quality bonding of the billets requires clamping the laminate under uniformly distributed pressure of specified level for a span of time necessary for the resin to cure. Specific time and pressure level to be applied depend on the type of resin and species of wood used. To meet the requirements, a mechanical clamping device was designed that provides control over the applied stress level and is capable of maintaining the minimum required pressure up to 24 hours. A calibration procedure was developed to adjust for the flow of the excessive resin being pressed out of the glue-lines in the first stage of clamping, as well as the nonlinear time-dependent behavior of the laminate material. The calibration procedure involved correlation between the average torque applied when tightening the four closing nuts and the clamping pressure between the steel plates. In addition, a procedure to determine the laminate material specific clamping pressure over 24 hours was established.

2.2 Introduction

2.2.1 Background

This chapter gives a brief overview of the concepts, results and main problems encountered during the design, modeling and calibration of a clamping device for fabrication of laminated billets for ASTM D2559 test and ASTM D905 shear block test, as shown in Figure 2.1.

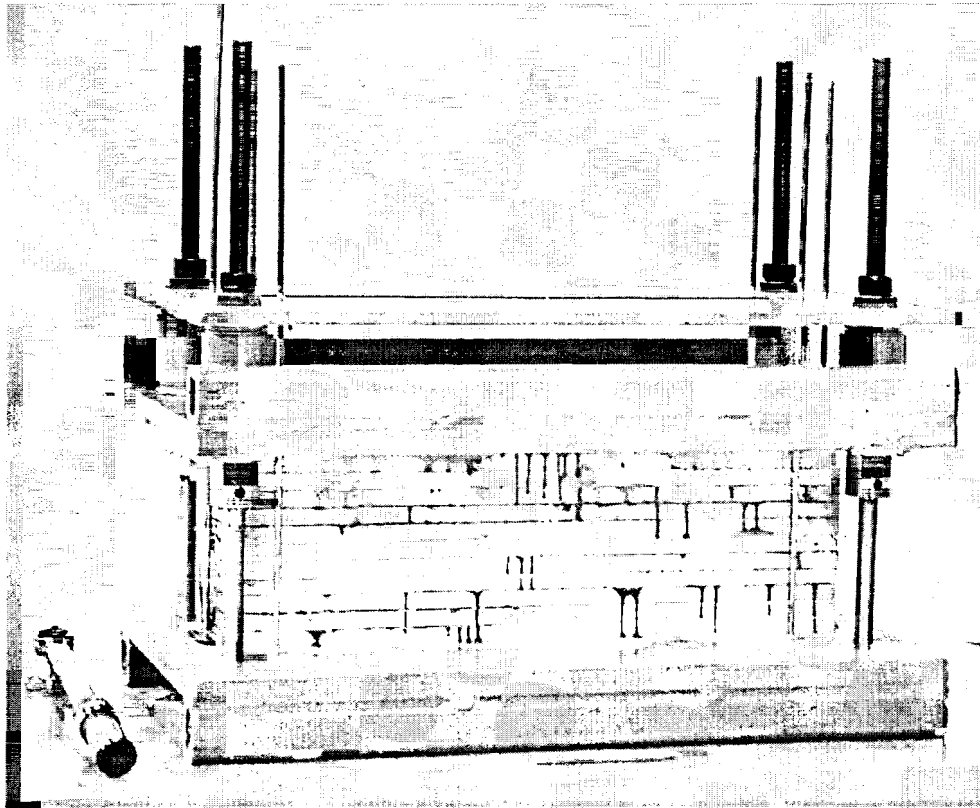


Figure 2.1 Laminating Press

As described in Chapter 2, ASTM D2559 is the specification to test adhesives for structural laminated wood products for exterior use (wet use). The requirements of the adhesive are based on the performance of the adhesive in laminated wood as measured by: a) resistance to shear by compression loading (ASTM D905 (ASTM 2000a)); b) resistance to delamination during accelerated exposure to wetting and drying; and c)

resistance to deformation under static load (ASTM 2000b). This clamping device is designed to fabricate test joints specified in part (a) and (b) of the standard.

The cyclic delamination test of ASTM D2559 requires that the specimens be prepared by bonding 6 wood laminations of nominal dimensions 19-mm (0.75-in) thick, 127 mm (5-in) wide and 602-mm (23.7-in) long. Twenty shear block samples for ASTM D905 can be prepared from bonding two wood laminations of the same dimensions. Basically, the billet fabrication process involves clamping the laminations with the proper clamping pressure for a span of time necessary for the adhesive to cure. Specific times and pressures to be applied depend on the type of resin and species of wood used for lamination of the billets. It is assumed, however, that the good quality bonding requires the clamping pressure to be distributed uniformly over all adhesive layers and maintained at a required constant level over the recommended time span.

To ensure that the clamping pressure is maintained on the required level, the clamping device must: 1) provide basic control on the pressure magnitude; and 2) compensate for the pressure loss due to time-dependent deformation of the laminates.

One ideal solution could be using an automatic hydraulic press capable of maintaining the required clamping pressure over a required period of time. However, dedicating such a press for fabricating testing billets, which require up to a 24-hour period, is typically too expensive. On the other end, simple hydraulic presses or hydraulic jack systems, for which the position of plates is fixed after application of an initial pressure, cannot maintain the required pressure over 24 hours.

The pressure loss is due to the nonlinear time-dependent properties of laminated material (stress relaxation) and viscous behavior of the adhesive trapped in the gluelines.

When the press is closed and the initial pressure is applied, the lay-up and the spring system are subjected to instantaneous elastic deformation. Then, the lay-up continues delayed deformation, which primarily is dominated by the viscous flow of the excess of the liquid resin being squeezed out from the glue-lines. When the excessive resin is pressed out, the time-dependent deformation of the lay-up is dominated by that of the laminate material (wood).

To make up for this time-dependent deformation, a mechanical laminating press may be designed to apply the load by means of a spring system, which can minimize the clamping pressure loss after the position of the clamping plates are fixed.

2.2.2 Objectives

The general objective of this chapter is to design and calibrate a laminating press for fabricating FRP-wood laminated billets for ASTM D2559 cycle delamination test and ASTM D905 shear block test. The specific objectives are:

- 1) Determine required design and performance parameters of the laminating press.
- 2) Develop mathematical models (empirical and phenomenological) to predict the behavior of the press under load;
- 3) Calibrate the laminating press to determine: a) the torque-clamping pressure relationship (elastic behavior); b) the clamping pressure loss-time relationship (viscoelastic behavior); c) the model parameters; and d) the amount of the initial pressure and the optimum retightening time.
- 4) Validate the model with the parameters obtained from the experiments;
- 5) Develop a standard operation procedure for the laminating press.

2.2.3 Literature Review

A practical application of maintaining applied pressure on wood laminations is the design of stress laminated timber (SLT) bridge decks (Barger *et al.* 1993; Crews 1998). SLT decks are constructed by laminating together pieces of timber which have been placed on edge to achieve the desired width. The laminating is achieved by compressing individual timber members together by applying a prestress in the transverse direction through steel bars and anchorage system. The designed prestress shall not exceed the short-term characteristic bearing strength (compression perpendicular to face grain) of the timber. It was suggested that permissible creep losses should be restricted such that the minimum level of compressive prestress does not become less than 700 kPa in hardwood decks and 500 kPa in softwood decks. When necessary, restressing must be carried out for the deck to meet the performance requirements.

Another practical application of applying pressure on wood laminations through mechanical method is a clamping system developed at the university of Maine for fabricating FRP-glulam beams in AEWC center (AEWC 2002). A laminated beam is placed between two steel plates. The clamping pressure is applied by tightening the nuts through evenly spaced thread rods along the beam by an adjustable click-type torque wrench.

Springs were used to minimize the clamping pressure loss over time due to the viscoelastic behavior of wood in a compression-type deformation tester (ASTM 2000c). It was developed to test the resistance to deformation under static loading for structural wood laminated specimens. Laminated specimens are clamped between the top plate and

the base plate. The clamping pressure is applied by tightening the nuts through the top threads of the for tension rods.

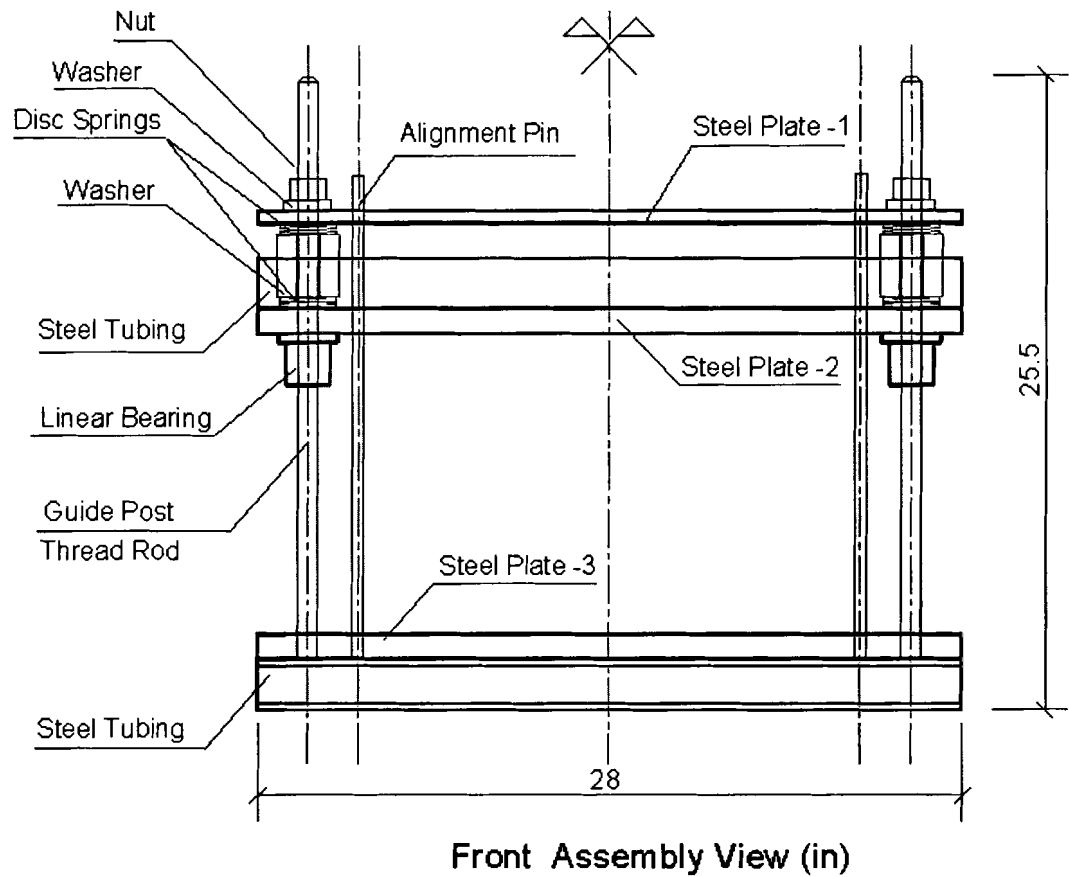


Figure 2.2 Front View of the Laminating Press

2.3 Basic Principles and Design of the Clamping Device

The laminating press was designed to meet the following requirements:

- 1) producing a uniform clamping pressure of specified level in all glue-lines of the laminate;
- 2) maintaining the minimum required pressure over the required clamping time;
- 3) bonding hybrid FRP-wood laminated billets to be used in ASTM D2559 delamination tests.

The dimensions of the laminating press were determined so that the press can be used to fabricate the delamination specimens specified in ASTM D2559. The core components of the press are three steel plates (top, middle and bottom), four guiding posts, four linear bearings, and four sets of disc springs, as shown in Figure 2.2.

All of the components of the laminating press were designed to meet the strength requirements as well as the stiffness requirements with proper safety factors. Since laminated billets are clamped between the middle plate and the bottom plate, these two plates were designed to be able to sustain the design load with adequate strength and stiffness. The stiffness was acquired by reinforcing the steel plates with tube stiffeners. The top plate works as a large washer to distribute the clamping pressure uniformly among the four guiding posts.

The uniform distribution of the clamping pressure is ensured by proper/regular geometry of the lamination (surfaces are parallel and plane), and the clamping device (clamping plates are plane, parallel and stiff). For this reason, a system of guiding posts and linear bearings was used. The linear bearings were mounted on the bottom side of the middle plate. They can slide along the middle part of the guiding posts to ensure parallel position of the steel plates and uniform clamping stress distribution.

The guiding posts were made from steel rods with threads on both ends. The bottom threads were used to connect them to the bottom plate. The clamping pressure is applied by tightening the nuts through the top threads of the guiding posts. To get precision control of the clamping pressure, a micrometer adjusting torque wrench was used. When the preset torque has been reached, the wrench can indicate that by a few degrees of free travel accompanied by an audible “click” signal. Hydraulic oil was used

as the lubricant to minimize the friction between the nuts and the top threads of the guiding posts.

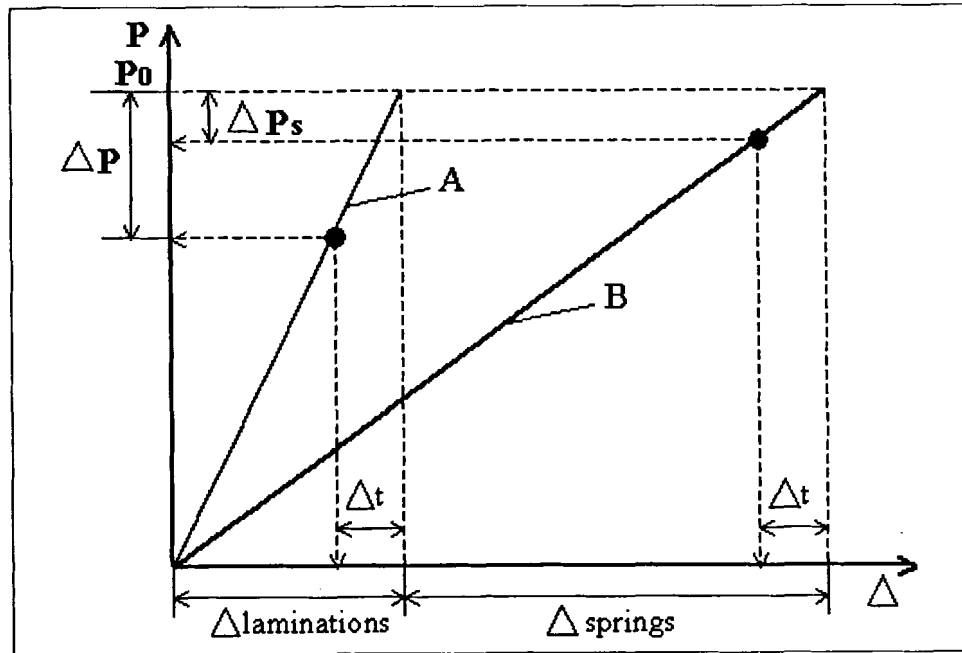


Figure 2.3 Effect of Springs on the Clamping Pressure Loss Due to Time Dependent Deformation

Note: A and B-load-deformation curves without and with springs; Δ_t - time dependent deformation; ΔP and ΔP_s - pressure loss due to Δ_t without and with springs; $\Delta_{\text{laminations}}$ and Δ_{springs} - deformation of wood laminations and springs.

Sets of four disc springs arranged in series were used to minimize the clamping pressure loss over time due to flow of the excessive resin and the viscoelastic behavior of wood. They were placed between the washers and the plates. Using the springs arranged in series extends the working range of the set without changing the maximum load capacity. The extended working distance of the springs makes up for the time-dependent deformation of the lay-up to minimize the clamping pressure loss. The effect of springs on the clamping pressure loss due to time dependent deformation can be illustrated by Figure 2.3. Since springs can partially compensate the time dependent deformation of the clamped lap-ups, the pressure loss due to this deformation can be reduced. Six alignment

pins were setup around the billets to prevent the layers from slipping during the clamping and to keep good alignment of the layers.

The load level corresponding to compressing the disc springs to flat is regarded as the maximum working load (77.2 kN). Theoretically, it is possible to tighten the nuts even further and significantly increase the clamping pressure. However, the benefit of pressure loss compensation is gone beyond this point.

The laminating press has the capacity to accommodate two wood billets at a time. Each of the two billets has six wood laminations and five adhesive layers. The total cost of this device is \$1,500, including materials and fabrication. The specifications of the laminating press are summarized in Table 2.1.

Table 2.1 Specifications of the Laminating Press

| | |
|--|--|
| External dimensions (L x W x H) | 711 x 432 x 648 mm (28 x 17 x 25.5 in) |
| Nominal dimensions of the ASTM D2559 delamination billet (with 6 wood laminations) | 602 x 127 x 114 mm (23.7 x 5 x 0.75 in) |
| Net weight | 186 kg (410 lb) |
| Maximum clamping load | 77.2 kN (17,350 lb) |
| Maximum clamping pressure | 1 MPa (145 psi) |
| Total cost | \$1,500 |

The clamping pressure may be either calculated analytically as a function of deformation imposed on the lay-up after closing the clamping plates (measured as vertical advance of nuts on the threaded rods); or determined indirectly from the torque

necessary to tighten the closing nuts. A disadvantage of the analytical calculation is that the result always depends on the compliance of the lay-up, which in turn depend on the wood species and viscosity of the resin used for the billet. In the second case, a torque versus pressure characteristic curve has to be determined.

2.4 Analytical Calculation of the Clamping Pressure

A theoretical or empirical model can be helpful for both interpretation and prediction of observed mechanical behavior of the lay-up and press components under clamping load. To characterize the mechanics response of the laminating press during wood billet fabrications, empirical and phenomenological models are developed to simulate the behavior of the laminating press.

The empirical model consists of arbitrary equations fitted to the experimental data based on the curve similarity. Although using arbitrary mathematical expressions to fit experimental data is a simplistic approach, it may have some practical usefulness. However, it offers only limited guarantee that the equations are valid for any conditions other than the one used in the calibration tests, since it is not based on clear mechanical principals. Another problem associated with this type of approach is that there is little if any basis for comparison of the data obtained by different investigators (Bodig and Jayne 1992).

A more fundamental approach involves phenomenological modeling of creep and stress relaxation of the lay-up and press elements by means of rheological elements. Complex modeling of the clamping press may be built up from elementary mechanical models often visualized by analogical representation of springs and dashpots. Typical

clamping force-time curves of wood lay-up without adhesive layer, with adhesive layers, and with adhesive layers and retightening are shown in Figure 2.4.

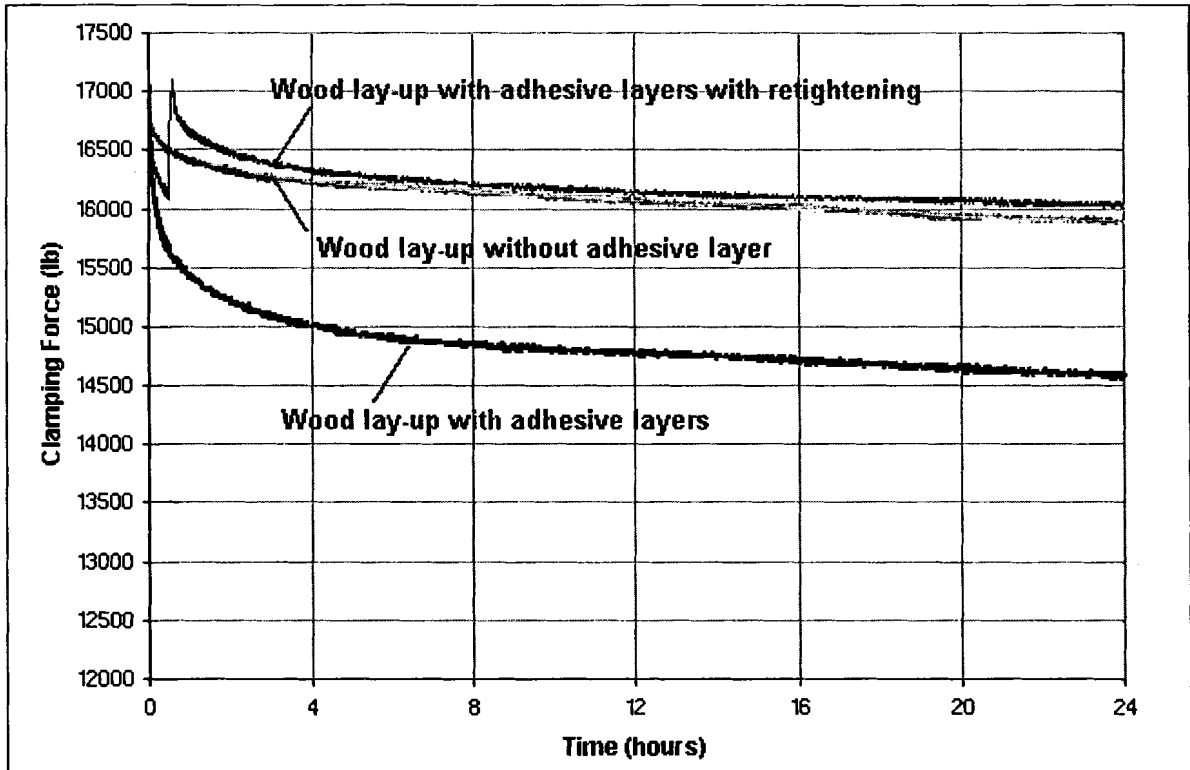


Figure 2.4 Typical Clamping Force-time Curves

2.4.1 Empirical Model

The empirical model is based on curve-fitting of arbitrary mathematical functions to the experimental data. Logarithmic and power type equations are fitted against the clamping pressure loss data shown in Figure 2.11. The general model equations are as follows:

$$\text{Logarithmic:} \quad \Delta P_{loss}(t) = A \ln(t) + B \quad (2.1)$$

$$\text{Power:} \quad \Delta P_{loss}(t) = C(t)^D \quad (2.2)$$

where t is the clamping time, and A , B , C and D are unknown parameters. The effect of retightening is handled by shifting the points of the original curve “down” along the y-

axis so that ΔP_{loss} is reset to zero, as shown in Figure 2.16. Therefore, the following equation can be used to calculate the pressure loss with retightening:

$$\Delta P_{loss}(t) = \begin{cases} \Delta P(t) & \text{when } t < t_r \\ \Delta P(t) - \Delta P(t_r) & \text{when } t \geq t_r \end{cases} \quad (2.3)$$

2.4.2 Phenomenological Model

A phenomenological model of time dependent interaction between press elements and the lay-up is developed. It is based on elementary rheological elements, which may be represented by springs and dashpots, as shown in Figure 2.5.

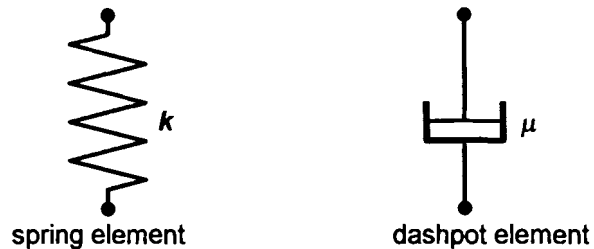


Figure 2.5 Spring and Dashpot Elements

The following assumptions are made in developing the models:

1. Deflection of the press plates is negligible and thus the steel plates are regarded perfectly stiff.
2. Elastic characteristics of the “active” clamping press elements (springs and the guiding rods) are known (or readily measurable from the first calibration experiment).
3. Elastic modulus of wood in compression is known (FPL 1999) (or readily measurable).
4. The delayed elastic deformation of wood is of viscoelastic nature and may be modeled with a Kelvin element.

5. The time-dependent deformation of the glue-lines and the influence of that excessive resin is squeezed out may be modeled with a Kelvin element.

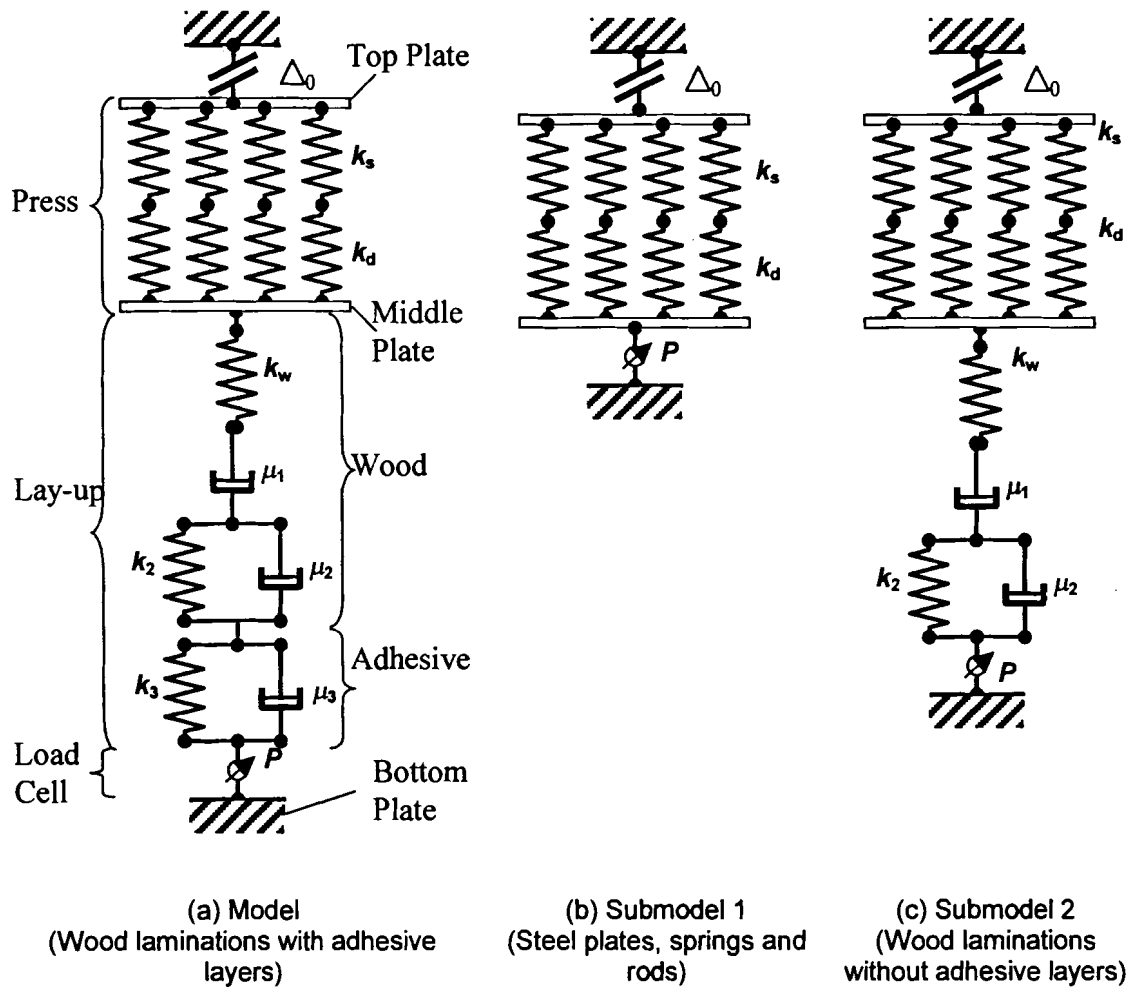


Figure 2.6 Spring-dashpot Submodels

Note: Δ_0 – the initial displacement of the laminating press system; k_s , k_d and k_w - the nominal spring characteristic constant of the steel rods, disc springs and wood laminations; μ_1 , μ_2 , and μ_3 – the reciprocal of the damping constant of the dashpots; k_2 and k_3 - the nominal spring characteristic constant of the Kelvin elements.

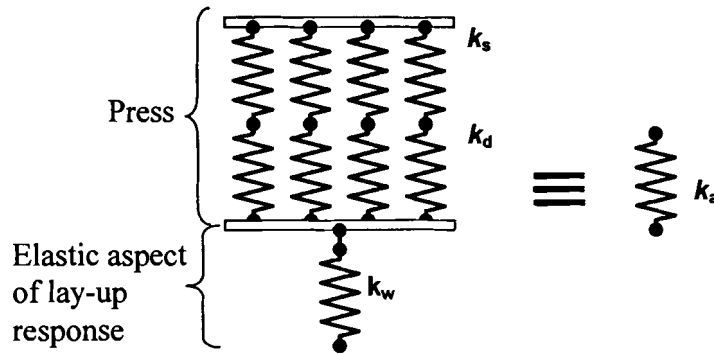


Figure 2.7 Simplification of the Elastic Elements of the Models

Note: Elastic elements of the press and elastic aspect of the lay-up response are represented by a single spring of the apparent spring characteristic constant k_a ; k_s , k_d and k_w - the same as shown in Figure 2.6.

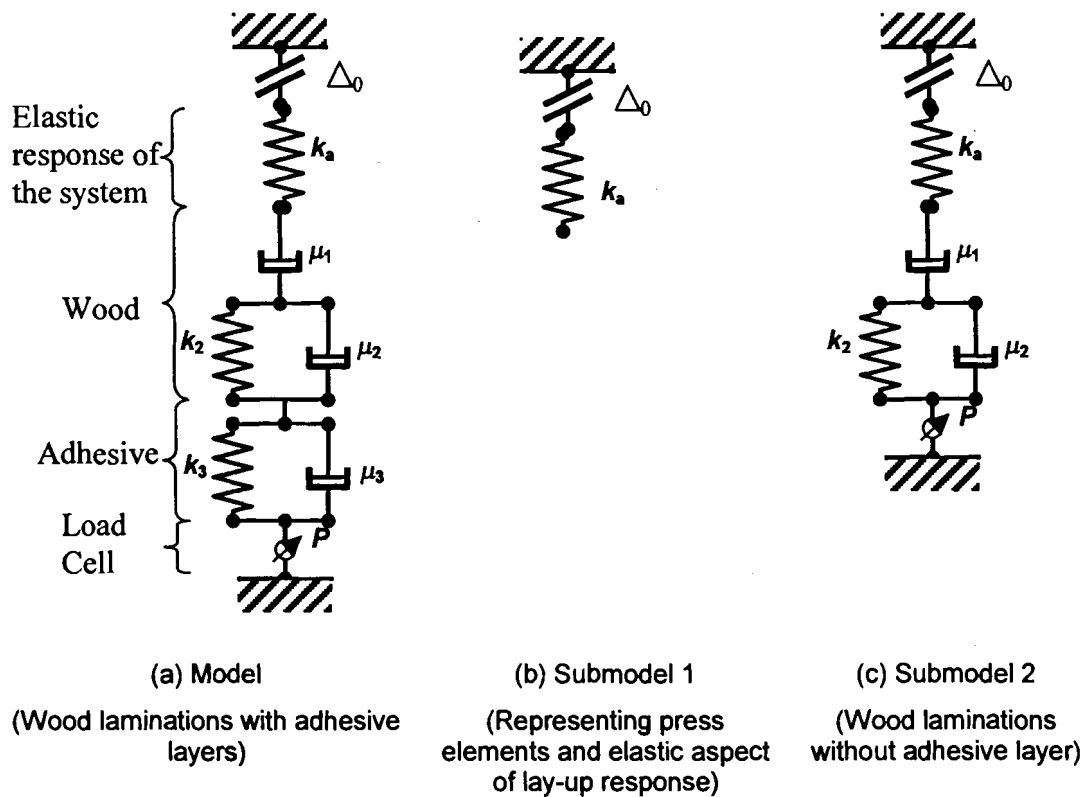


Figure 2.8 Simplified Spring-dashpot Models

Note: μ_1 , μ_2 , μ_3 , k_2 and k_3 - the same as shown in Figure 2.6. k_a - the same as shown in Figure 2.7.

The model of the press with lay-up (wood laminations and adhesive layers) is shown in Figure 2.6a. It can be further simplified by replacing the elastic aspects of the system response by a single spring with an apparent spring constant k_a . The resulting model consists of a series arrangement of a Maxwell body and two Kelvin bodies as shown in Figure 2.8a. The explanation of the elements is as follows: 1) the first set of springs enclosed by the top and middle plates of the press represents four sets of disc springs (k_d) and four threaded rods (k_s); 2) the four-element Burger body characterized by parameters k_w , μ_1 , k_2 and μ_2 represents viscoelastic properties of wood; the two-element Kelvin body characterized by parameters k_3 and μ_3 represents the non-linear response of the adhesive layers as the resin is gradually squeezed out. Since the three components of deformation are additive, they are joint in series. The detailed description of the model and the meaning of the parameters is described later in this section.

Since the elastic parameters of the active press elements (springs and guiding rods) as well as the elastic characteristics of wood are known, they may be represented by a single apparent combined spring characteristic constant k_a in the simplified model representation, as shown in Figure 2.7. The simplified spring-dashpot general model and the two submodels are shown in Figure 2.8. The apparent combined spring characteristic constant k_a for the press with 4 guiding poles, 4 sets of 4 disc springs and the lay-up loaded may be calculated as following:

$$\frac{1}{k_a} = \frac{1}{4} \left(\frac{4}{k_d} + \frac{1}{k_s} \right) + \left(\frac{1}{k_w} \right) \quad (2.4)$$

The nominal spring characteristic constant of the disc springs k_d is given in Table 2.2. The spring constant of the guiding posts (steel rods) k_s is calculated as follows:

$$k_s = A_s E_s / h_s \quad (2.5)$$

where $A_s E_s$ is the tensile stiffness and h_s is the working length of the guiding posts.

The spring characteristic constant of the wood lay-up is defined as:

$$k_w = A_w E_w / h_w \quad (2.6)$$

where $A_w E_w$ is the compressive stiffness and h_w is the height of the lay-up. The clamping pressure in the wood lay-up of known dimensions and elastic properties is calculated using k_d and k_s . The characteristics of the press components and the lay-up (*Southern yellow pine*) used for the calculations are given in Table 2.2.

Table 2.2 Stiffness Characteristics of the Press Components

| Disc springs | | Guiding posts | | Wood Lay-up | | |
|--------------|--------------------------|---------------|---|-------------|---|---------------------------------|
| | | | | | 1 billet with 4 laminations | 2 billets with 6 laminations |
| | | h_s | 406 mm (16 in) | h_w | 76 mm (3 in) | 229 mm (9 in) |
| | | A_s | 484 mm ² (0.75 in ²) | A_w | 76,451 mm ² (118.5 in ²) | |
| | | E_s^b | 200 GPa (29,000 ksi) | E_w^c | SYP: 606 MPa (87,910 psi) | |
| k_d^a | 20 kN/mm (114 kip/in) | k_s | 140 kN/mm (800 kip/in) | k_w | 616 kN/mm (3,516 kip/in) | 231 kN/mm (1,319 kip/in) |

a: (MSC 1999); b: (Segui 1998); c: (FPL 1999).

The resulting values of the apparent combined spring characteristic constant k_a of the press with wood lay-up are: 1) 18.7 kN/mm (106.9 kip/in) for one wood billet with 4 laminations and 17.8 kN/mm (101.7 kip/in) for two wood billets with 6 laminations, which is equivalent to 29.7 kN (6.68 kip); and 2) 28.3 kN (6.36 kip) of clamping load increase per every single-coil advance (or one full rotation) of the closing nut.

The above values were calculated specifically for *Southern yellow pine* (SYP) and have to be recalculated every time a material of different mechanical properties is

laminated. No slack between the plates and the wood lay-up is assumed. Then, the clamping force P or clamping pressure p may be calculated as functions of the average vertical advance of the nuts on the threaded rods h_a :

$$P = \Delta h_a \cdot k_a \quad (2.7)$$

$$p = \frac{P}{A_w} = \frac{\Delta h_a k_a}{A_w} \quad (2.8)$$

The maximum capacity of the disc springs or the load to keep the springs flat is 19.3 kN (4,337 lbs), which is equivalent to maximum clamping pressure of 1.0 MPa (145 psi). The clamping pressure of 0.76 MPa (110 psi), which is recommended for SYP, is obtained when the springs are loaded 76% of their maximum capacity.

To determine the viscoelastic parameters of this model, a three-step calibration procedure was designed: step 1) determination of the torque-clamping pressure relationship (steel plates); step 2) measurement of clamping pressure loss on a stack of wood laminations without resin; and step 3) measurement of clamping pressure loss on a stack of wood laminations with resin. Each calibration step is represented by the general phenomenological model or one of its submodels expressed in terms of basic rheological elements, as shown in Figure 2.6. Components of the model equations are fitted against the experimental data acquired in calibration tests. For each test, the initial clamping pressure was applied to the wood lay-up by tightening of the closing nuts on the threaded rods.

The magnitude of the clamping load was monitored by a load cell during the calibration experiments. Since the distance between clamping plates is too small to accommodate two wood billets and the load cell at the same time, the height of the calibration lay-up was reduced to four wood laminations. Then, the results are

recalculated to determine the clamping pressure for the actual lay-up with two wood billets.

The total deformation within the constrained system after the initial loading may be expressed as:

$$\Delta_{tot} = \Delta_e + \Delta_t = 0 \quad (2.9)$$

where Δ_{tot} , Δ_e , and Δ_t are the total, the elastic, and the delayed or time-dependent deformation of springs, steel rods and the wood billet, respectively.

Since the elastic characteristic of the system k_a is known, the magnitude of the time-dependent component of the deformation may be calculated from the measured load:

$$\Delta_t = -\Delta_e = -\frac{P(t)}{k_a} \quad (2.10)$$

Since wood is a viscoelastic material, a dashpot with a damping constant ($1/\mu_1$) may be used to model the behavior of wood. In the case of the wood laminations without adhesive layers, the delayed elastic deformation may be calculated from the constitutive ordinary differential equation of the Kelvin element:

$$P(t) = k_2 \Delta_t + \mu_2 \dot{\Delta}_t \quad (2.11)$$

where $P(t)$ is the clamping load as a function of time, k_2 is the elastic characteristic constant and $1/\mu_2$ is the damping constant of the first Kelvin element. The solution of equation (2.11) is:

$$\Delta = \int_0^t P(\tau) e^{-(t-\tau)(k_2/\mu_2)} d\tau \quad (2.12)$$

where τ is a time variable within the integral.

In the case of the wood laminations with adhesive layers, the time-dependent deformation model has to take into account the deflection of the glue-lines and the influence of that excessive resin is squeezed out. This nonlinear time-dependent deformation may be calculated from the constitutive ordinary differential equation of another Kelvin element with the same form as equation (2.11). The adjusted equation takes the following form:

$$\Delta_i(t) = \int_0^t P(\tau) \cdot e^{-(t-\tau)k_2/\mu_2} d\tau + \int_0^t P(\tau) \cdot e^{-(t-\tau)k_3/\mu_3} d\tau \quad (2.13)$$

where k_3 is the elastic characteristic constant and $1/\mu_3$ is the damping constant relating to the adhesive. Substituting equations (2.10) and (2.13) into equation (2.9), results in:

$$-\frac{P(t)}{k_a} + \mu_1 \int_0^t P(t) dt + \int_0^t P(\tau) \cdot e^{-(t-\tau)k_2/\mu_2} d\tau + \int_0^t P(\tau) \cdot e^{-(t-\tau)k_3/\mu_3} d\tau = 0 \quad (2.14)$$

Taking the first derivative of Equation (2.14) and rearranging the equation, results in:

$$\frac{1}{k_a} \dot{P}(t) + \mu_1 P(t) + \frac{1}{k_2} P(t) e^{-t(k_2\mu_2)} + \frac{1}{k_3} P(t) e^{-t(k_3\mu_3)} = 0 \quad (2.15)$$

This equation may be rewritten as:

$$\dot{P}(t) + P(t) \left(k_a \mu_1 + \frac{k_a}{k_2} e^{-t(k_2\mu_2)} + \frac{k_a}{k_3} e^{-t(k_3\mu_3)} \right) = 0 \quad (2.16)$$

which is a first-order linear ordinary differential equation. Its solution takes the following form:

$$P(t) = C * \exp \left(k_a \mu_1 t + \frac{k_a}{k_2^2 \mu_2} (1 - \exp(-tk_2\mu_2)) + \frac{k_a}{k_3^2 \mu_3} (1 - \exp(-tk_3\mu_3)) \right) \quad (2.17)$$

From the initial boundary condition $P(t=0)=P_0$, results in $C=P_0$, where P_0 is the initial clamping load. Therefore, the solution can be written as:

$$P(t) = P_0 * \exp \left(\underbrace{k_a \mu_1 t}_{A} + \underbrace{\frac{k_a}{k_2^2 \mu_2} (1 - \exp(-tk_2 \mu_2))}_{B} + \underbrace{\frac{k_a}{k_3^2 \mu_3} (1 - \exp(-tk_3 \mu_3))}_{C} \right) \quad (2.18)$$

Based on the submodel 2 shown in Figure 2.8(c) and equation (2.18), the damping constant $1/\mu_1$ of the dashpot, the elastic characteristic constant k_2 and the damping constant $1/\mu_2$ of the first Kelvin element can be determined by fitting the experimental data of wood lay-ups without adhesive layer. The effect of adhesive layers may be separated by subtracting the deformation of wood laminations measured without adhesive layers from the total deflection of the lay-up with resin. A typical clamping pressure loss-time diagram due to adhesive effect is shown in Figure 2.19. Then, based on the general model shown in Figure 2.8(a) and equation (2.18), these data can be used to determine the elastic characteristic constant k_3 and the damping constant $1/\mu_3$ of the second Kelvin element.

Also based on the general model shown in Figure 2.8(a) and equation (2.18), these constants can be used to predict the press behavior after retightening. The clamping pressure is released completely before retightening, and it takes about 10 minutes to reapply the pressure. It is assumed that the delayed elastic aspect of wood deformation (component B of equation (2.18)) experiences significant recovery. For practical calculations, complete recovery may be assumed. Consequently, the delayed elastic deformation at t_r after retightening starts at the same rate as at t_0 . This is reflected in equation (2.19) by modifying time argument to $(t-t_r)$. The other two components (A and C) are considered to be irrecoverable, and after retightening, the deformation restarts

from the values read at t_r . Therefore, equation (2.17) can be rewritten with new boundary conditions as (2.19):

$$P_r(t) = P_0 * \exp\left(k_a \mu_1 t + \frac{k_a}{k_2^2 \mu_2} (1 - \exp(-(t - t_r) k_2 \mu_2)) + \frac{k_a}{k_3^2 \mu_3} (1 - \exp(-t k_3 \mu_3))\right) - C_r \quad (2.19)$$

where C_r is a constant added to the equation to satisfy the boundary conditions. It can be calculated from the following equation:

$$C_r = P_0 * \exp\left(k_a \mu_1 t_r + \frac{k_a}{k_3^2 \mu_3} (1 - \exp(-t_r k_3 \mu_3))\right) \quad (2.20)$$

Therefore, the following equation can be used to calculate the clamping force with retightening:

$$P_R(t) = \begin{cases} P(t) \text{ from (3.18)} & \text{when } t < t_r \\ P_r(t) \text{ from (3.19)} & \text{when } t \geq t_r \end{cases} \quad (2.21)$$

2.5 Calibration Procedure

The calibration procedure involves two stages: 1) determination of the basic correlation between the magnitude of torque while tightening the closing nuts and the clamping pressure; 2) determination of the clamping pressure loss with time.

The Phenol Resorcinol Formaldehyde (PRF) adhesive used in the calibration was Resorsabond 4242 Resin mixed with 4553 Hardener from Georgia-Pacific Resins, Inc. It has a viscosity of 3000 - 6000 cps at 25°C. Its gel time is 2.25 - 2.75 hours at 25°C. The clamping pressure of 0.69-1.03 MPa (100-150 psi) is recommended for Western softwoods and Southern pine (Borden 1993). The minimum clamp curing time is 18 hours at 18°C.

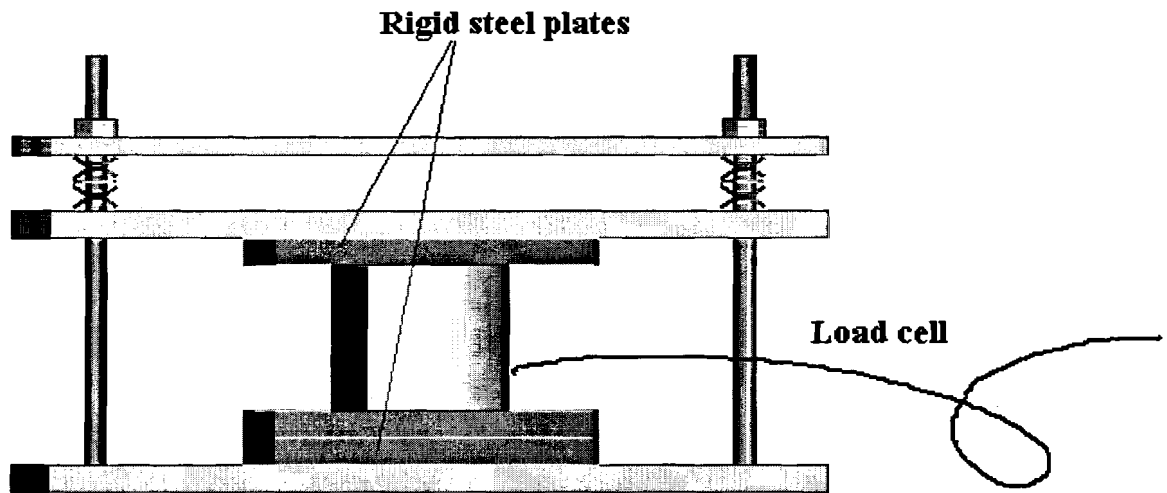


Figure 2.9 Configuration of the Calibration Setup of Torque versus Clamping Pressure

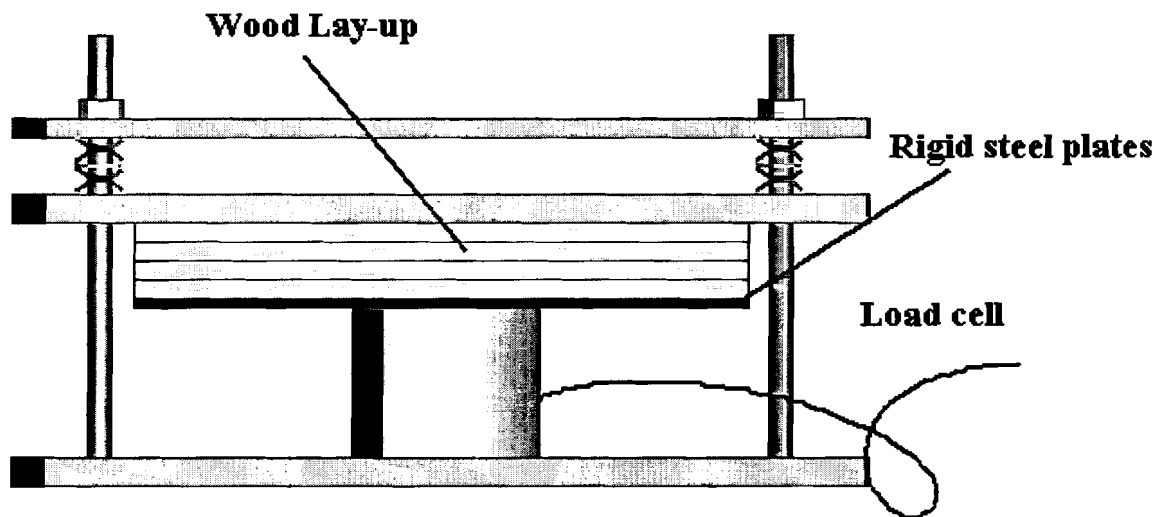


Figure 2.10 Configuration of the Calibration Setup of Clamping Pressure Loss versus Time

2.5.1 Torque versus Clamping Pressure

The clamping pressure may be determined indirectly from the level of torque necessary to tighten the closing nuts. The advantage of using the torque versus clamping pressure calibration curve is that this characteristic is independent of the laminate material. At this stage, the objective was to determine the basic correlation between the magnitude of torque while tightening the closing nuts and the clamping pressure between the plates.

2.5.1.1 Configuration

A torque wrench was used for measurement of the magnitude of torque while tightening individual closing nuts. The clamping force between the plates was measured with an Instron load cell of 100 kN (22 kip) capacity. Two materials were used to conduct the calibration: steel plates (see Figure 2.9) and wood laminations (see Figure 2.10). For the calibration with steel plates, additional steel plates were used to fill the space between the load cell and the clamping plates.

2.5.1.2 Procedure

The closing nuts were tightened gradually in a crisscross manner. The clamping force was recorded at definite torque levels: 13.6, 20.3, 27.1, 33.9, 40.7, 47.5, 54.2, 61.0, 67.8, 74.6 N-m (10, 15, 20, 25, 30, 35, 40, 45, 50 and 55 ft-lbs). Each time before tightening the nuts up to the next torque level, all nuts were loosened to the zero load level.

After preliminary calibration runs, it appeared that the linear range of the calibration curve is affected by the arrangement of the disc springs and depends

significantly on the amount of friction between the disc spring rims and the reaction surfaces. During the following runs, significant extension of the linear range was obtained by: 1) rearranging the disc springs; 2) applying hydraulic oil to the threads and under the head of bolts to reduce the friction of the moving parts; and 3) polishing the reaction surfaces (plates and washers) which worked in contact with the spring rims.

The details of the calibration procedure for steel plates and wood laminations are shown in the Appendix.

2.5.2 Clamping Pressure Loss over Time

At this stage, the objective was to determine the clamping pressure loss with time. The device was designed so that the working distance of the springs makes up for the time-dependent deformation of the lay-up to minimize the clamping pressure loss. This procedure also had two stages: 1) lay-ups of wood laminations without adhesive layers and 2) lay-ups of wood laminations with adhesive layers.

2.5.2.1 Configuration

To separate the influence of nonlinear behavior of the wood laminations from that of the viscous flow of the adhesive layers, the calibration tests were conducted separately on lay-ups of wood laminations with and without adhesive layers. The configuration is the same as that of calibration of torque versus clamping pressure with wood laminations, as shown in Figure 2.10.

2.5.2.2 Procedure

The closing nuts were gradually tightened to the torque of 74.6 N-m (55 ft-lbs) in a crisscross manner. Data acquisition of the clamping load and time was performed

continuously with Labview software throughout the tests. Two tests of wood lay-ups without adhesive layers were tested first, and then the same procedure was used for the lay-ups with adhesive layers.

For the lay-ups with adhesive layers, at the beginning of the clamping time, the clamping pressure would decrease significantly due to the flow of the excessive resin being squeezed out from the glue-lines. At first, two tests were conducted without retightening the nuts. The results showed that this was not adequate. Then, to minimize this loss, two tests were conducted with loosening and retightening the nuts once after 30 minutes and 60 minutes, respectively. Retightening the nuts one hour after first closing the press was determined to be a sufficient way to reduce further pressure loss due to the resin squeeze out.

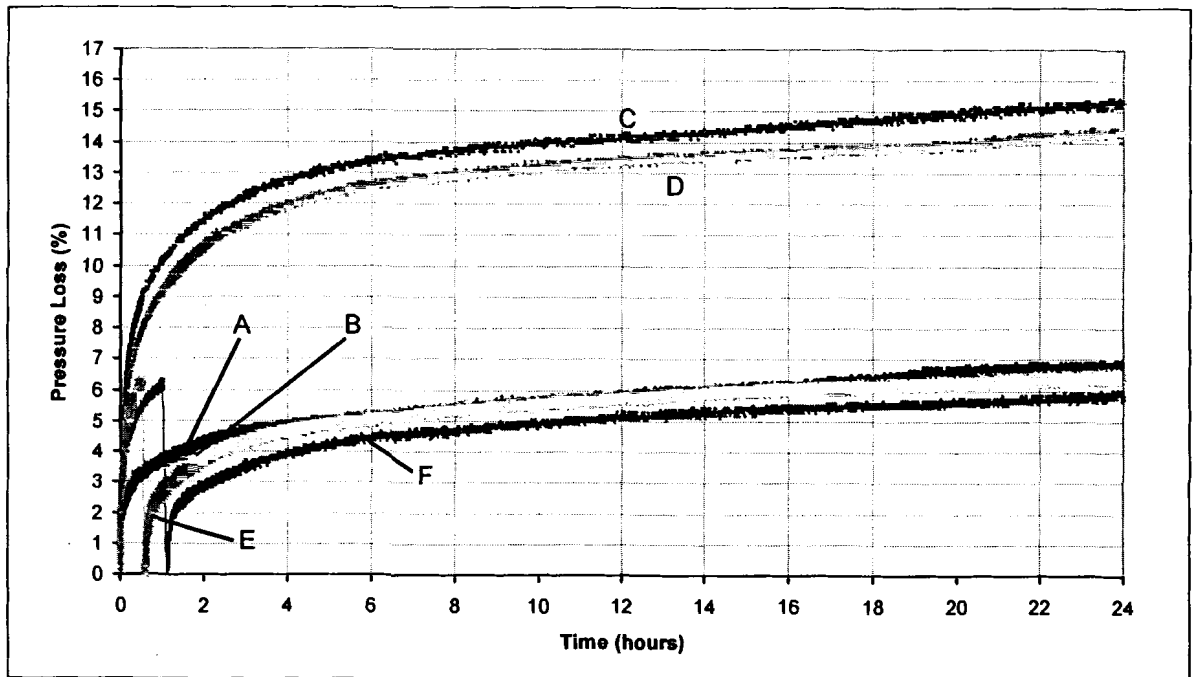


Figure 2.11 Calibration Curves of Clamping Pressure Loss versus Time

All of the test results are shown in Figure 2.11. Tests A and B correspond to wood lay-ups without adhesive layer. Tests C and D correspond to wood lay-ups with adhesive layers without retightening. Tests E and F correspond to wood lay-ups with adhesive layer with retightening after 30 and 60 minutes, respectively.

There are several possible ways to determine the retightening time. The predictions obtained from the empirical model and the phenomenological are two of them. There may be another simple way to preselect it. For example, if it is assumed that the maximum tolerance of pressure loss is 10%, then a horizontal line can be drawn at 10% level in the pressure loss-time chart of lay-ups without retightening to get an intersection point with the test curve. This in turn can be used to get the relevant clamping time. This time could be selected at the first trial retightening time, but it should not be less than the adhesive gel time.

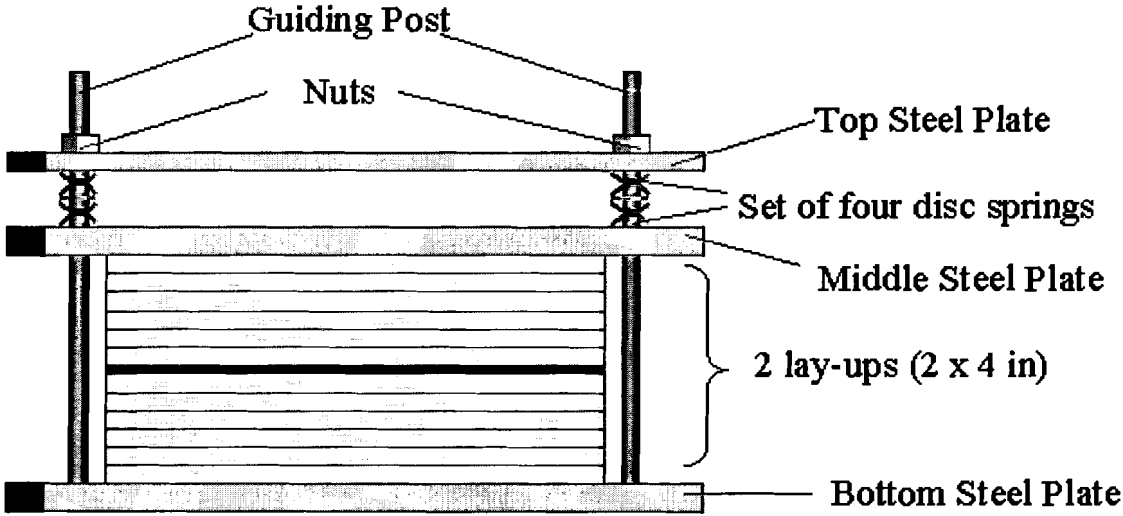


Figure 2.12 Schematic Diagram of the Laminating Press with Wood Lay-ups

2.5.3 Scaling Up

The laminating press has the capacity to accommodate two wood billets at a time. Each of the billets may have up to six wood laminations and five adhesive layers, as

shown in Figure 2.12. A simplistic analytical method was used to scale up the calibration results from lay-up of four wood laminations and three adhesive layers used in the calibration tests to lay-up of twelve laminations and ten adhesive layers used in regular press operation to get the pressure loss versus time relationship of the real case.

Since all elements of the press are arranged in series, it may be assumed that each wood lamination and adhesive layer of the regular lay-up has the same deformation-time characteristic as that of the calibration lay-up. Therefore, the pressure loss effect is proportional to the number of wood laminations and adhesive layers. The pressure loss effect obtained from the calibration tests was scaled up by multiplying the ratio of the number of wood laminations of regular lay-ups to that number of lay-ups used in the calibration tests. The ratio is 3 in this case. The result is shown in Table 2.3. It should be noted, however, that the calculations were conducted for pressure loss values after retightening, which explains less significant effect of the adhesive layers.

Table 2.3 Scaling Up Calculation

| Lay-up | Total Pressure loss after 24 hours |
|--|------------------------------------|
| 4 wood laminations + 3 adhesive layers | 6.15 % |
| 12 wood laminations + 10 adhesive layers | 18.45 % |

2.6 Experimental Results and Discussion

The calibration curves of torque versus clamping pressure with steel plates and wood laminations are shown in Figure 2.13 and Figure 2.14, respectively. A linear relationship up to the 74.6 N-m (55 ft-lbs) torque level and similar slopes are observed in both figures. According to the calibration curve, it is possible to control the desired clamping pressure by setting up a proper torque level.

equations did not fit the experimental data and therefore were not further considered. To consider retightening, the modeled curve was shifted back to the initial clamping pressure at the retightening time, as shown in Figure 2.16. This approach was applied to predict the press behavior after retightening, as shown in Figure 2.17. However, when compared with the actual experimental data from the tests with retightening, it was found that they did not agree in this case. As previously mentioned, since this type of empirical approach is not based on the mechanics of the laminating press system, it offers limited guarantee that the equations are valid for any conditions other than the one described. However, empirical models may be used for preliminary approximation under certain conditions. In this case, the empirical model can predict the pressure loss after 12 hours and 24 hours with reasonable accuracy ($\pm 1\%$).

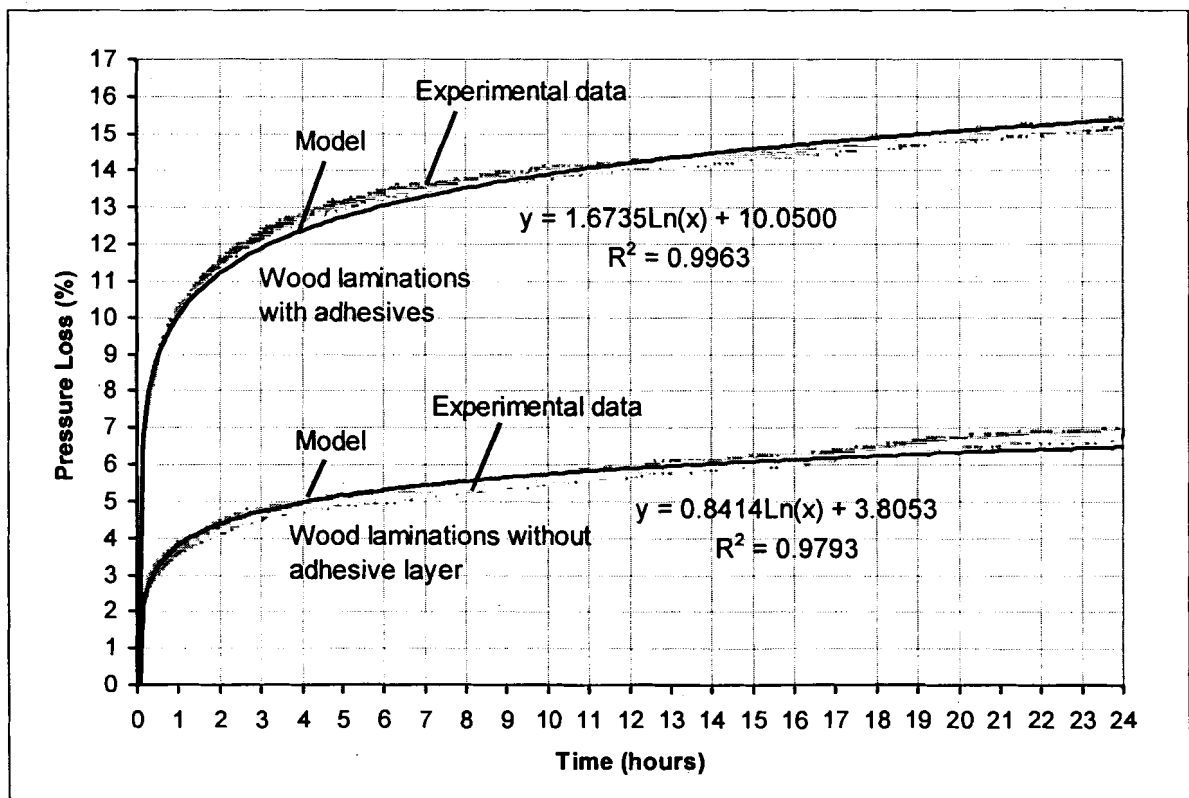


Figure 2.15 Correlation of Empirical Model with Experimental Results

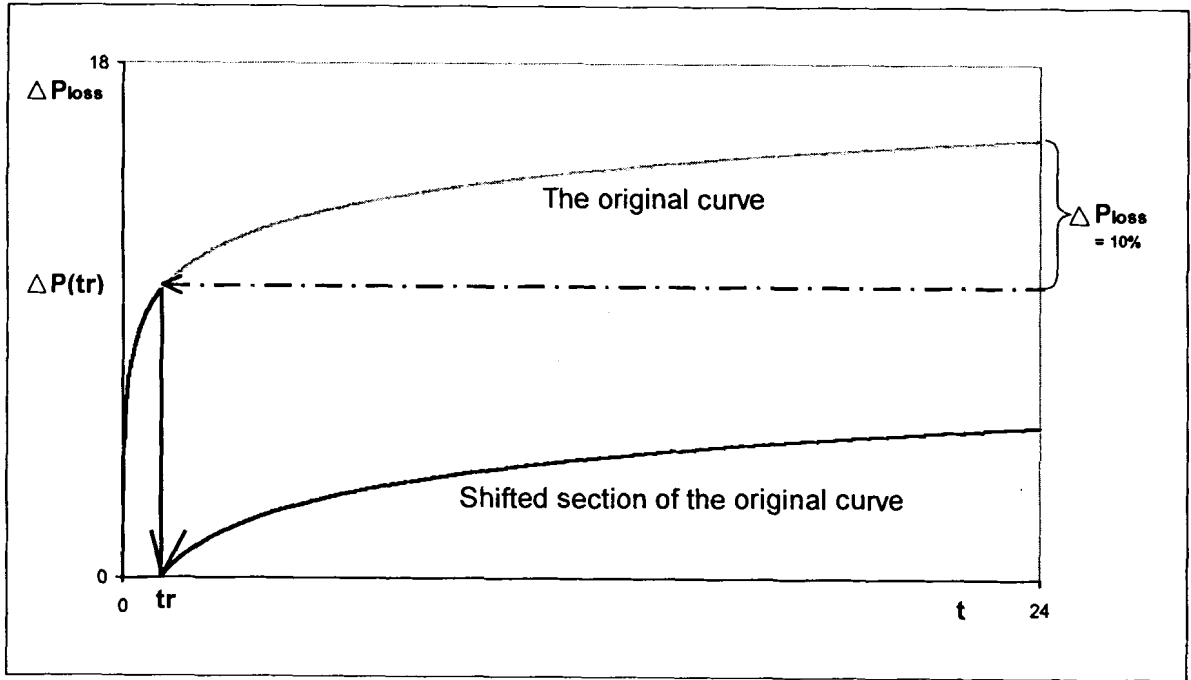


Figure 2.16 Prediction of the Retightening Effect from Empirical Model

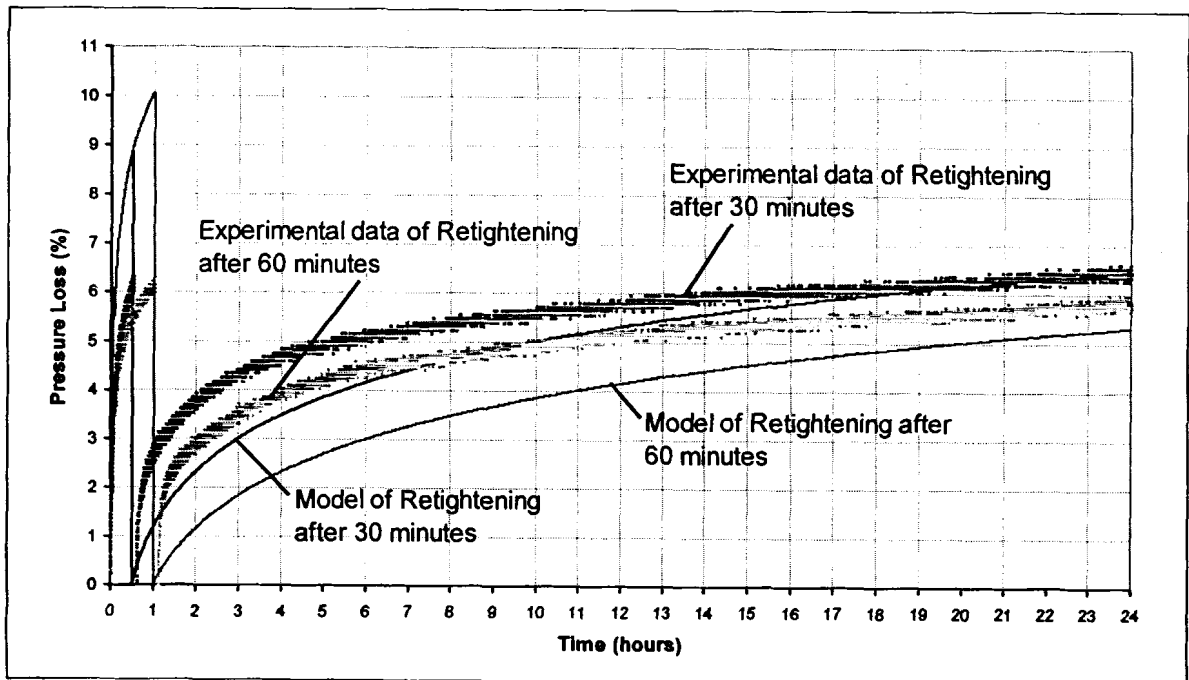


Figure 2.17 Predicted Retightening Behavior from the Empirical Model

2.7.2 Phenomenological Model

Based on the submodel 2 shown in Figure 2.8(c) and equation (2.18), the damping constant $1/\mu_1$ of the dashpot, the elastic characteristic constant k_2 and the damping constant $1/\mu_2$ of the first Kelvin element can be determined by fitting the experimental data of wood lay-ups without adhesive layer, as shown in Figure 2.18. Then, based on the general model shown in Figure 2.8(a) and equation (2.18), these data were used to determine the elastic characteristic constant k_3 and the damping constant $1/\mu_3$ of the second Kelvin element by fitting the experimental data of wood lay-ups with adhesive layers, which is also shown in Figure 2.18. The constants are listed in Table 2.4.

Table 2.4 Constants of the Phenomenological Model

| k_a | μ_1 | k_2 | μ_2 | k_3 | μ_3 |
|--------------------------|---|---------------------------|---|--------------------------|---|
| 20 kN/mm (114 kip/in) | 5.65E-8 mm/hour-N (9.9E-9 in/hour-lbs) | 154 kN/mm (879 kip/in) | 1.88E-5 mm/hour-N (3.3E-6 in/hour-lbs) | 87 kN/mm (498 kip/in) | 2.85E-5 mm/hour-N (5.0E-6 in/hour-lbs) |

Then, also based on the general model shown in Figure 2.8(a) and equation (2.21), these constants were used to predict the press behavior after retightening. As discussed in the previous section, the shape of the experimental data has some variation primarily due to the variability of the resin distribution. To get conservative results, the experimental data with the maximum clamping pressure loss was used in the modeling. When matching the predicted data with the actual data, the constants of the adhesive elements, k_3 and μ_3 , were adjusted to account for this variability. The predicted results of retightening after 30 and 60 minutes are shown in Figure 2.20 and Figure 2.21, respectively. The constants used in the second Kelvin element are shown in Table 2.5.

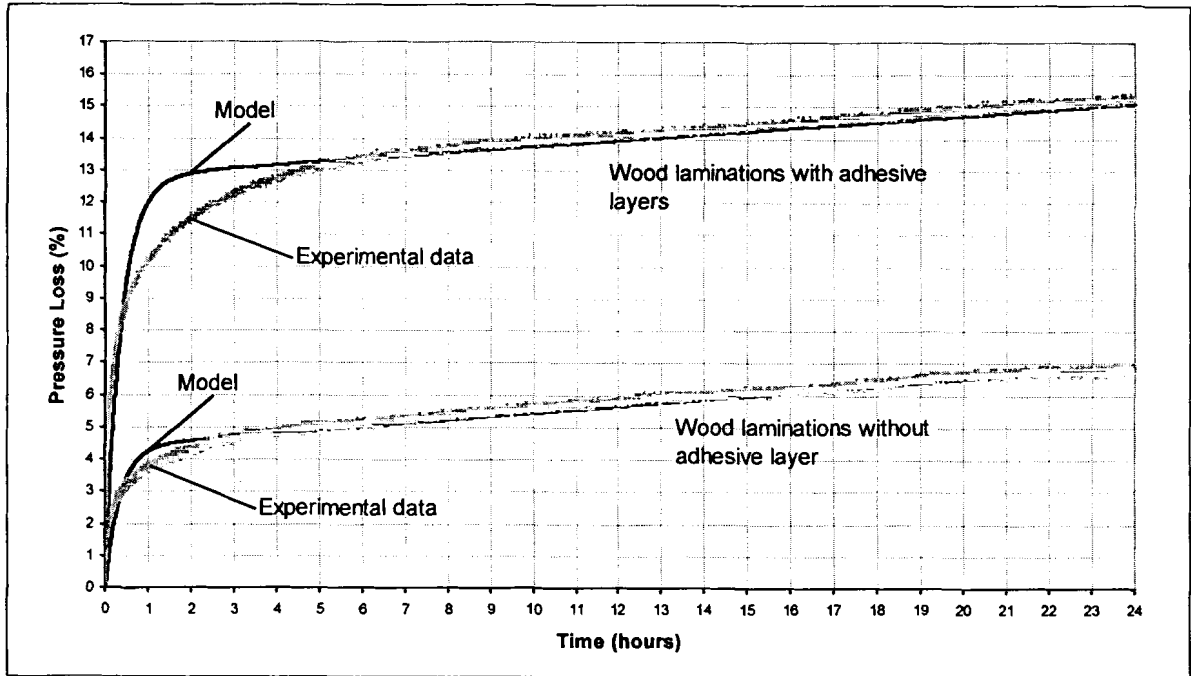


Figure 2.18 Correlation of Phenomenological Model with Experimental Results

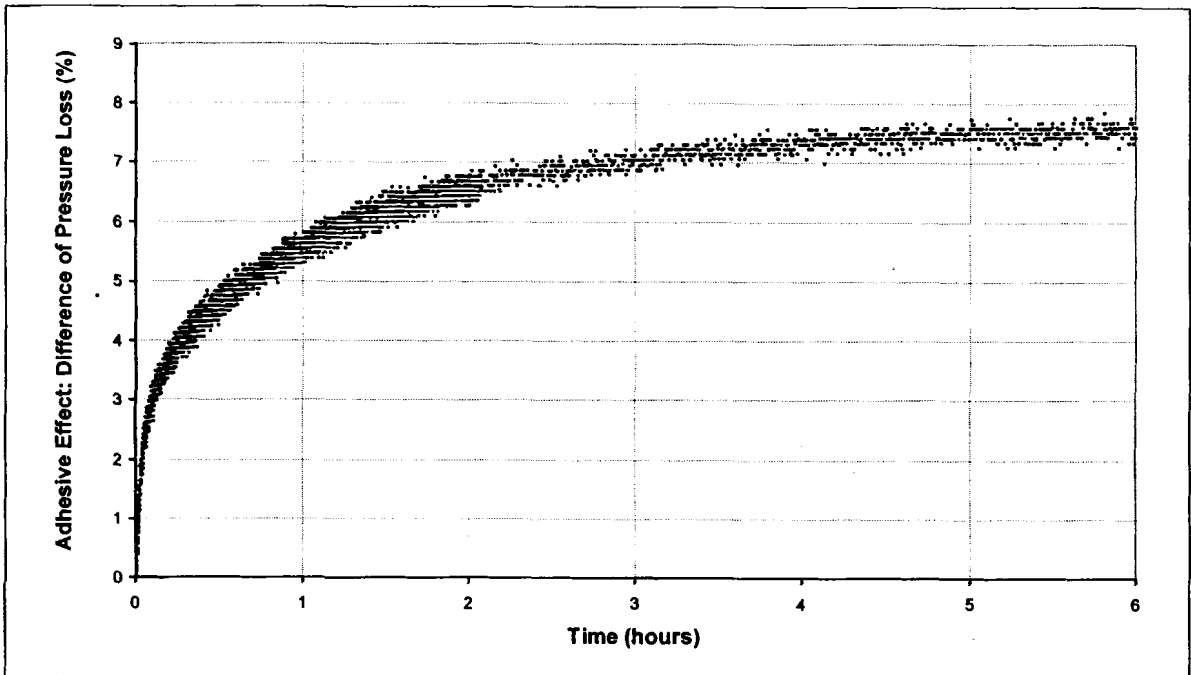


Figure 2.19 Typical Adhesive Effect

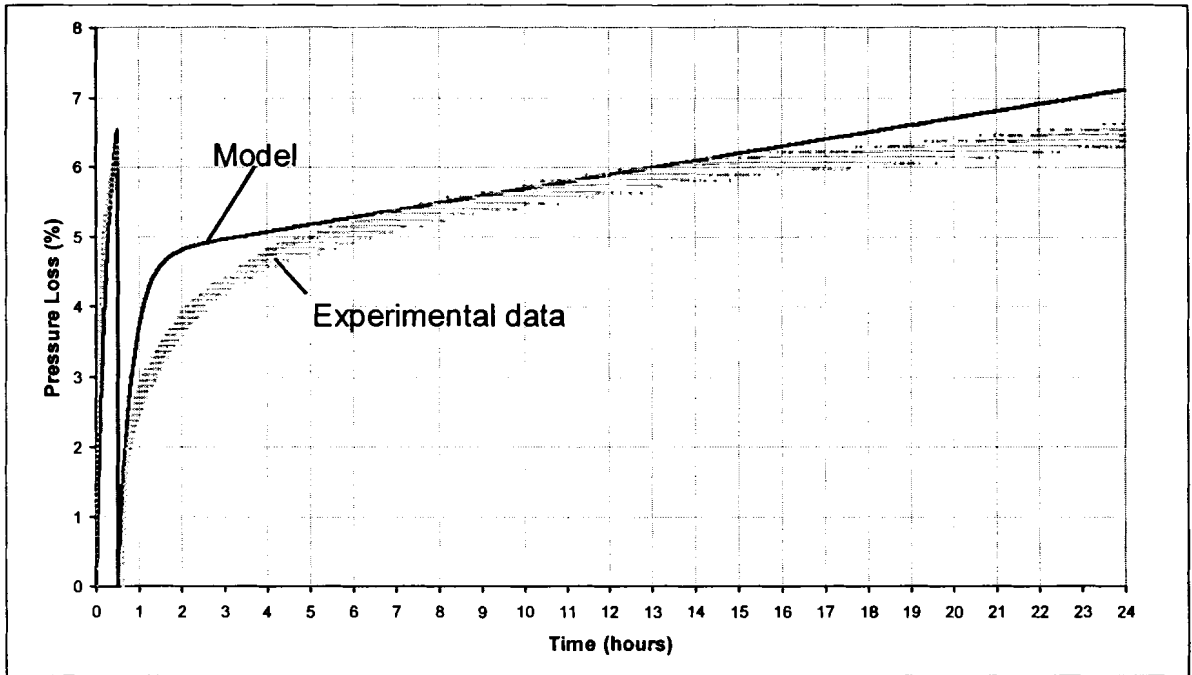


Figure 2.20 Phenomenological Model Prediction due to Retightening after 30 Minutes

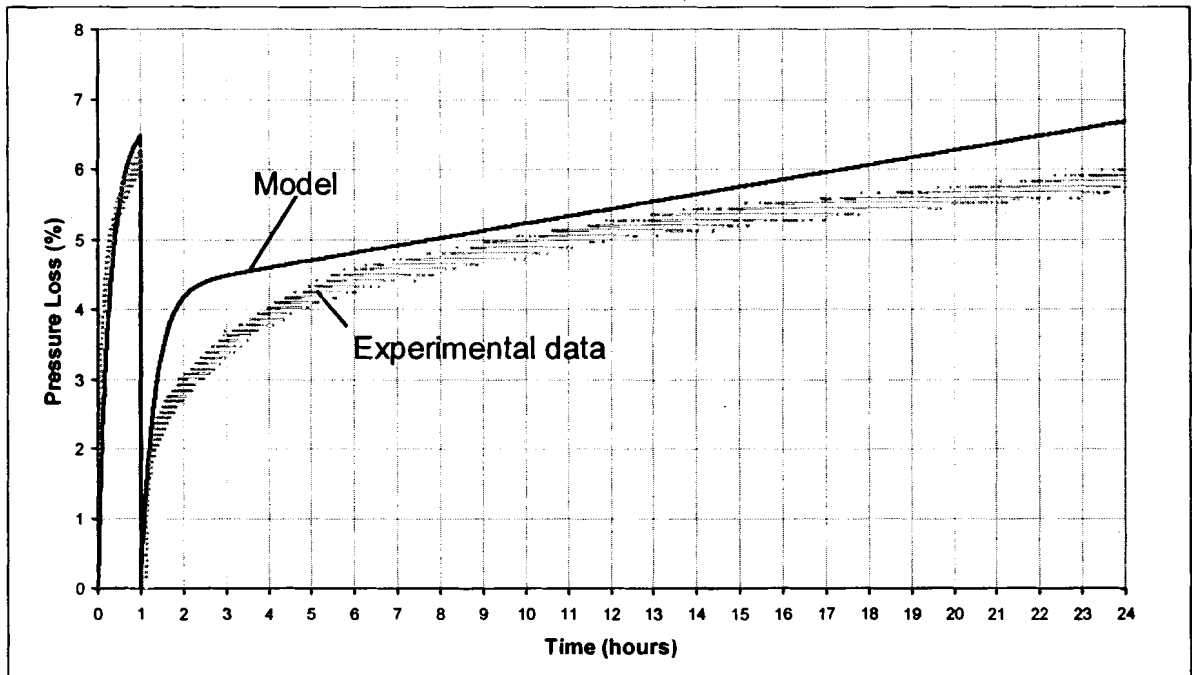


Figure 2.21 Phenomenological Model Prediction due to Retightening after 60 Minutes

Table 2.5 Constants of the Second Kelvin Element Used in the Prediction of the Retightening Behavior

| Retightening Time (mins) | k_3 | μ_3 |
|--------------------------|---------------------------|--|
| 0 | 87 kN/mm (498 kip/in) | 2.85E-5 mm/hour-N (5.0E-6 in/hour-lbs) |
| 30 | 131 kN/mm (750 kip/in) | 3.05E-5 mm/hour-N (5.35E-6 in/hour-lbs) |
| 60 | 166 kN/mm (950 kip/in) | 3.05E-5 mm/hour-N (5.35E-6 in/hour-lbs) |

The phenomenological model, which is based on the mechanics of the laminating press system, was found to be able to predict the pressure-time behavior with reasonable accuracy. The minimum required clamping time for this resin is 12 hours, but for convenience, the actual clamping time is usually around 24 hours when fabricating specimens. The phenomenological model can give reasonable and conservative predictions of the maximum pressure loss for both cases.

2.8 Conclusions and Recommendations

Calibration experiments were conducted to obtain the torque-clamping pressure relationship and the clamping pressure loss-time relationship. The standard operation procedure (work instruction) for the laminating press was developed, and is presented in the Appendix.

Based on the research findings presented in this chapter, the following conclusions are drawn:

- 1) The laminating press is capable of applying reasonably constant and uniform clamping pressure over the time span required to create quality adhesive bonding of the billets for ASTM D2559 and ASTM D905 standard tests. After retightening, the pressure loss over the adhesive curing time (up to 24 hours) was within 19%.
- 2) A phenomenological model and an empirical model were developed to be able to predict the pressure-time behavior of the laminating press system with acceptable accuracy.
- 3) The optimum retightening time and the amount of the initial pressure were determined. For wood billets bonded with this PRF resin, one hour is the proper retightening time, and the initial pressure should be 0.86 MPa (125 psi).

The following recommendations are suggested:

- 1) Lubricant should be applied regularly to reduce the friction between the nuts and the top threads of the guiding posts.
- 2) Since the top plates are relatively heavy (105 kg), two people are needed to operate the press. To operate the system by one person, two jacks may be used to lift up the top plates of the press, one on each side.
- 3) The parameters of the press and the models were calculated specifically for Southern yellow pine and PRF adhesive. If the materials of the lay-ups are changed (wood and/or adhesive), the press has to be recalibrated and the parameters have to be recalculated.

2.9 Notation

The following symbols are used in this chapter:

| | | |
|--------------------------|---|--|
| A_s | = | Cross-section area of the steel guiding posts |
| A_w | = | Cross-section area of the wood lay-up |
| E_s | = | Elastic modulus of structural steel |
| E_w | = | Elastic modulus of wood in transverse direction |
| F | = | Clamping force |
| h_a | = | Average vertical advance of nuts on the threaded rods |
| h_s | = | Working length of the steel guiding posts |
| h_w | = | Height of the clamped lay-up |
| k_2 | = | Elastic constant for the first Kelvin element |
| k_3 | = | Elastic constant for the second Kelvin element |
| k_a | = | Apparent combined spring characteristic constant of the press system |
| k_d | = | Spring constant of the disc springs |
| k_s | = | Spring constant of the steel rods |
| k_w | = | Spring characteristic constant of the wood lay-up |
| P | = | Clamping pressure |
| ΔP_{loss} | = | Clamping pressure loss |
| t | = | Clamping time |
| t_r | = | Retightening time |
| Δ_0 | = | Initial displacement of the laminating press system |
| Δ_e | = | Elastic deformation of springs, rods and the lay-ups |
| Δ_t | = | Delayed or time-dependent deformation of wood lay-ups |

- Δ_{tot} = Total deformation of springs, rods and the lay-ups
- $1/\mu_1$ = Damping constant representing viscous property of wood
- $1/\mu_2$ = Damping constant of the first Kelvin element
- $1/\mu_3$ = Damping constant of the second Kelvin element
- τ = Time variable within the integral

Chapter 3

SCREENING TESTS: EVALUATION OF DURABILITY AND SHEAR STRENGTH OF FRP-WOOD INTERFACES

3.1 Summary

In this chapter, the durability of the FRP-wood interface under hydrothermal stresses was studied. The proposed methodology was to identify material performance indicators of the FRP-wood bonded interface (hydrothermal cycling and shear strength). Two parts of ASTM D2559 standard test procedure were modified and adopted to characterize hybrid FRP-wood materials: delamination test and shear block test in compression. The modifications were needed to account for the presence of the FRP. They were used as pass/fail screening test methods to evaluate several commercially available candidate material systems. Only those material combinations that passed the tests were selected for further evaluation.

3.2 Introduction

Fiber-reinforced polymer (FRP) composites are used for reinforcement of glulam bridges in exterior environments. Therefore, material and durability properties of the FRP-wood interfaces need to be characterized based on mechanical tests and accelerated aging methods. In this chapter, the durability of FRP-wood interface is examined based on a part of modified ASTM D2559 (ASTM 2000b) hydrothermal cycling to assess delamination. The effects of HMR coupling agent as wood primer were also examined. The shear strength of the FRP-wood bonded interface was studied by conducting another

part of modified ASTM D2559. The specimen configuration was modified according to ASTM D905 (ASTM 2000e) shear resistance to compression loading test.

3.3 Objective and Scope

The objective of this chapter is to develop a material-level test method and associated acceptance criteria to investigate the integrity/durability of FRP-wood bond lines under accelerated hydrothermal stresses. Two parts of ASTM D2559 standard test procedures were selected and modified to account for hybrid FRP-wood materials: accelerated delamination test and shear block test in compression.

The following steps were conducted according to the chapter objective: a protocol based on modified ASTM test procedures was developed; the specimen configuration was determined; a standard procedure for specimen fabrications and testing was drafted; acceptance criteria of the experimental results were proposed, and a set of experiments was conducted to validate the test method and acceptance criteria.

3.4 Literature Review

An experimental program was performed to evaluate the ultimate shear strength, bond-interface integrity, and percentage of wood failure of adhesive-bonded FRP-wood interface under dry and wet conditions (Gardner 1994). Dry and water-saturated FRP-wood shear block tests were conducted following a modified ASTM D 905 testing procedure to evaluate shear strength and percent wood failure of FRP-wood interfaces. A 5-cycle vacuum –pressure-soak-dry testing procedure was also used based on modified ASTM D1101 to evaluate the integrity of the bond interface under exterior use. It was

found that RF adhesive showed the greatest promise for bonding both polyester and vinylester FRP composites to wood for exterior applications. A finite element model was developed to analyze the stress of the FRP-wood bond interface under dry and wet conditions (Barbero *et al.* 1994). The results of this experimental program were used to validate the numerical model.

A Coupling Agent HydroxyMethylated Resorcinol (HMR) was developed to increase the delamination resistance and shear strength of adhesive bonds of wood products as a wood surface primer (Vick 1995). Modified ASTM D2559 and ASTM D 905 were used to evaluate the durability of FRP-wood bonds. When they modified the specimen configuration of ASTM D2559, they substituted the top and the bottom wood layers by two FRP layers. It was found that when bonding phenolic FRP to wood with vinylester adhesive and with HMR primer, the resistance to delamination was extraordinary.

Epoxy adhesives can provide good bonds to wood in dry conditions. Epoxies also have some unique properties, such as gap filling, strong, durable, room temperature curing, etc. But when used in wet conditions, the bonds delaminate. Research was conducted to evaluate the durability of epoxy-bonded FRP-wood bonds enhanced by HMR primer (Vick 1997). The results showed that the HMR primer increased delamination resistance, shear strength, wood failure and deformation resistance so that epoxy bonds passed the ASTM D 2559 tests. In the following study, some experiments were conducted to define the optimum range of reaction time when adhesion was maximum for epoxy bonds to HMR-primed Douglas-fir (Vick 1998b). The capability of

epoxies bond to both wood and plastics presents an opportunity for making strong and durable composites from FRP and wood.

One-part polyurethane adhesives are general-purpose adhesives. They are well known for their excellent adhesion, flexibility, high cohesive strength, low-temperature performance, and amenable curing speeds. A study was performed to determine the strength and durability of representative commercial polyurethane wood adhesives in bonds to hardwood and softwood (Vick 1998a). It was found that the dry shear strength, dry wood failure and wet shear strength were at least as strong as bonds of RF structural adhesive on Douglas-fir. But the percentages of wet wood failure were much lower than those of the RF adhesive. Furthermore, the ASTM D2559 delamination test caused severe delamination of polyurethane bonds in lumber laminates of Douglas fir. In a subsequent study, the adhesion-enhancing capabilities of the HMR coupling agent for polyurethane were evaluated (Vick 2000). It was found that the HMR primer greatly increased the durability of the polyurethane bonds. When the wood surfaces were primed with HMR, one-part polyurethane adhesives can meet the strength and durability requirements of the ASTM D2559.

Recently, a qualification program was developed to evaluate the service performance of FRP-wood bonded interfaces (Davalos 2000). Two types of FRP-wood bonds were studied: phenolic and epoxy. First, the service performance and durability of FRP-wood interface bonds were evaluated using a modified ASTM D2559 delamination test. The same specimen configuration of a previous study (Vick 1995) was used. Then, the apparent shear strengths of bonded interfaces under both dry and wet conditions were obtained from modified ASTM D905 shear block tests. For phenolic bonds, the effects of

HMR coupling agent, clamping pressure and assembly time were studied. For epoxy bonds, only the effect of HMR coupling agent was investigated. It was found that the modified ASTM D2559 standard test could be successfully applied to study and optimize bonding parameters. Then, the average shear strengths can be obtained from modified ASTM D905 test for the best combination of parameters.

3.5 Matrix of Material Systems

Three material systems were selected in the screening tests: B, C and D. For each material system, FRP type, wood species, adhesive type and surface primer type were specified. The material systems for the screening tests are shown in Table 3.1.

Three commercially available FRP materials were considered: (1) E-glass /urethane pre-consolidated sheet fabricated by pultrusion process from Creative Pultrusions, Inc., two types of the FRP sheets were investigated: “all roving” materials and materials with “CSM (Chopped Strand Mat)”; (2) E-glass/epoxy pre-consolidated sheet fabricated by continuous lamination process from Gordon Composites, Inc. (3) Carbon fiber/phenolic resin impregnated paper (CF/P) composite sheet from Toho Rayon Co. Ltd. (Ogawa 2000);

These three FRP composite materials are made with two types of reinforcing fibers: E-glass and Carbon, and three types of polymeric matrices: phenolics, urethane and epoxy. The pictures of the FRP composite materials are shown in Figure 3.1

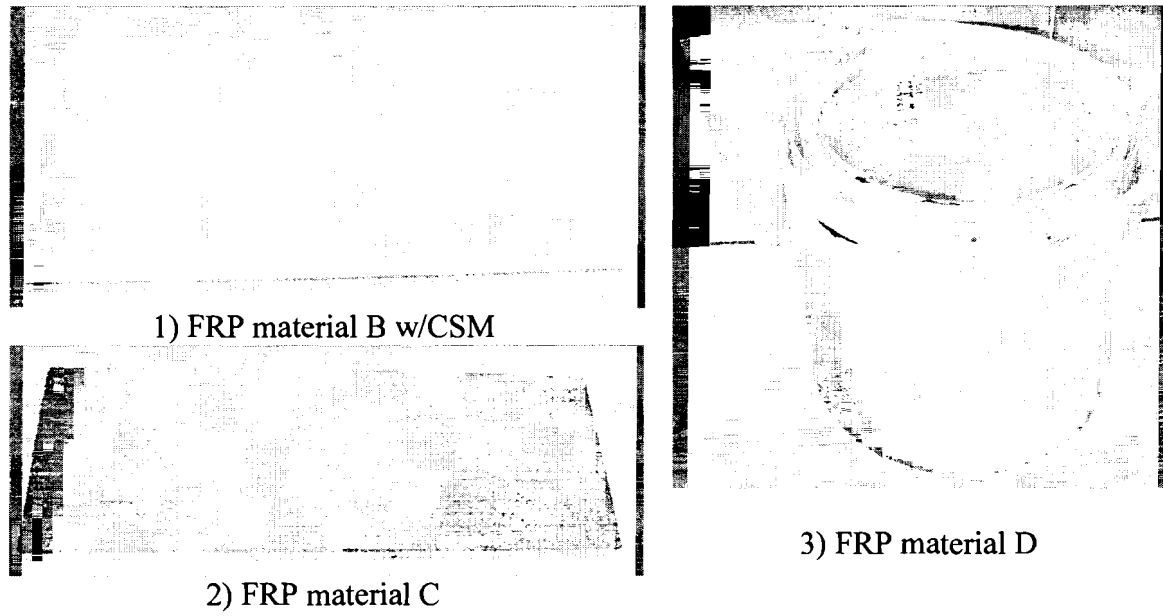


Figure 3.1 FRP Composite Materials

For FRP material system D, a two-part Phenol Resorcinol Formaldehyde (PRF) wood adhesive from Borden Chemical, Inc. was used to bond FRP to wood. It consists of Cascophen LT-5212 resin and Cascoset FM-6210 hardener. This adhesive was also used to bond the thin FRP sheets together to achieve proper thickness. For FRP material B, two types of a one-part moist-cure polyurethane adhesive were used: a) ISOGRIP 3030D from Ashland Chemical Inc. and b) ReactITE 8143 from Franklin International. For FRP material C, three epoxy adhesives were used: G1, G2 and G3, as shown in Table 3.2. They are two-part epoxy adhesives from Gougeon Brothers, Inc. The Assembly Time and Clamping Pressure of the adhesives are shown in Table 3.3.

Table 3.1 Matrix of FRP-wood Material Systems for the Screening Tests

| Material system | FRP Composite | FRP Fabrication | Wood Species | Adhesive | Wood Primer |
|------------------------|---|--------------------------------|---------------------|---------------------------------|--------------------|
| D | Carbon/phenolics w/ pulp paper (0.8 mm thick) | Bond pulp paper to CF prepreg. | DF & SYP | PRF | No |
| B | E-glass/ urethane: All roving & CSM (6.35 mm thick) | Pultrusion | DF | Ashland Urethane ISOGRIP 3030D | w/ & w/o |
| | | | | Franklin urethane ReactITE 8143 | HMR |
| C | E-glass/epoxy (19 mm thick) | Continuous lamination | DF | PRO-SET Epoxy: G1, G2 & G3 | HMR |

Table 3.2 Matrix of PRO-SET Epoxy

| Adhesive | Resin | Hardener |
|-----------------|---------------|-----------------|
| G1 | 176 | 276 |
| G2 | XR 01-113-53A | XH 01-113-53B |
| G2 | XR 01-113-53C | XH 01-113-53D |

Table 3.3 Assembly Time and Clamping Pressure of Adhesives

| Adhesive | PRF | Franklin Urethane | Ashland Urethane | Epoxy G1, G2 & G3 |
|---------------------------------|------------|--------------------------|-------------------------|------------------------------|
| Open/closed Assembly Time (min) | 5/30 | 5/20 | 5/20 | 5/20 |
| Clamping Pressure (psi) | > 110 | 60 | 50 | 20 |

Two wood species were used in the testing with FRP material system D: Douglas-fir (DF) and southern yellow pine (SYP). For FRP material B and C, only DF was used.

As described in the literature review, when used as a wood surface primer, HydroxyMethylated Resorcinol (HMR) can significantly increase the delamination resistance and shear strength of epoxy and urethane adhesive-bonded wood products (Vick 1995). In this study, the effects of the HMR primer were investigated for material B. For material C, the wood surfaces next to the FRP strips of all of the specimens were treated with the HMR primer.

3.6 Experimental Characterization of FRP Material Properties

3.6.1 Mechanical Tests

To obtain mechanical properties of FRP materials, material characterization tests based on ASTM standard test procedures were conducted. The longitudinal moduli, the tensile strength and the in-plane Poisson's ratio were determined according to the ASTM D3039 (ASTM 2000d). The results are shown in Table 3.4. The apparent interlaminar shear strength was determined according to ASTM D2344 (ASTM 2000a). (Lopez-Anido 2002). The in-plane shear modulus was obtained from ASTM D5379 V-notched shear tests (ASTM 2000f). The results are shown in Table 3.5.

3.6.2 Ignition Loss Tests of FRP Composite

The ignition test of ASTM D2584 (ASTM 2000c) was used to obtain weight percentage of E-glass fiber for FRP composite B (with CSM) and C. Then, the typical E-glass fiber density of 2.55 g/cm^3 was used to compute the fiber volume fraction. Five samples were tested for each material. All samples were placed in crucibles and placed into a muffle furnace at 565°C to burn out the resin. The weights of samples before

ignition and the residues after ignition were recorded. The test results are listed in Table 3.6.

Table 3.4 FRP Mechanical Properties from Longitudinal Tensile Tests

| FRP Material | Tensile Modulus (GPa) | COV (%) | Tensile Strength (MPa) | COV (%) | Poisson's Ratio | COV (%) |
|--------------|-----------------------|---------|------------------------|---------|-----------------|---------|
| B | 44.3 | 1.4 | 898 | 11.7 | 0.30 | 7.2 |
| C | 38.2 | 0.8 | 705 | 0.83 | 0.30 | 1.2 |
| D | 88.1 | 3.7 | 1341 | 7.0 | - | - |

Table 3.5 FRP Mechanical Properties from Shear Tests

| FRP Material | In-plane Shear Modulus (MPa) | COV (%) | Interlaminar Shear Strength (MPa) | COV (%) |
|--------------|------------------------------|---------|-----------------------------------|---------|
| B | 3649 | 3.2 | 28.0 | 7.00 |
| C | 3301 | 3.4 | 44.9 | 1.58 |
| D | - | - | 24.6 | 5.16 |

Table 3.6 Fiber Volume Fractions

| FRP Material | V_f (%) | COV. (%) |
|-------------------------|-----------|----------|
| E-glass/urethane w/ CSM | 59.9 | 0.9 |
| E-glass/epoxy | 46.4 | 1.5 |

The orientations of E-glass fibers can be readily observed after the ignition tests, as shown in Figure 3.2. For FRP material B, three CSM layers were placed on the top, middle, and bottom of the unidirectional fibers, respectively. For FRP material C, all of the fibers were unidirectional.

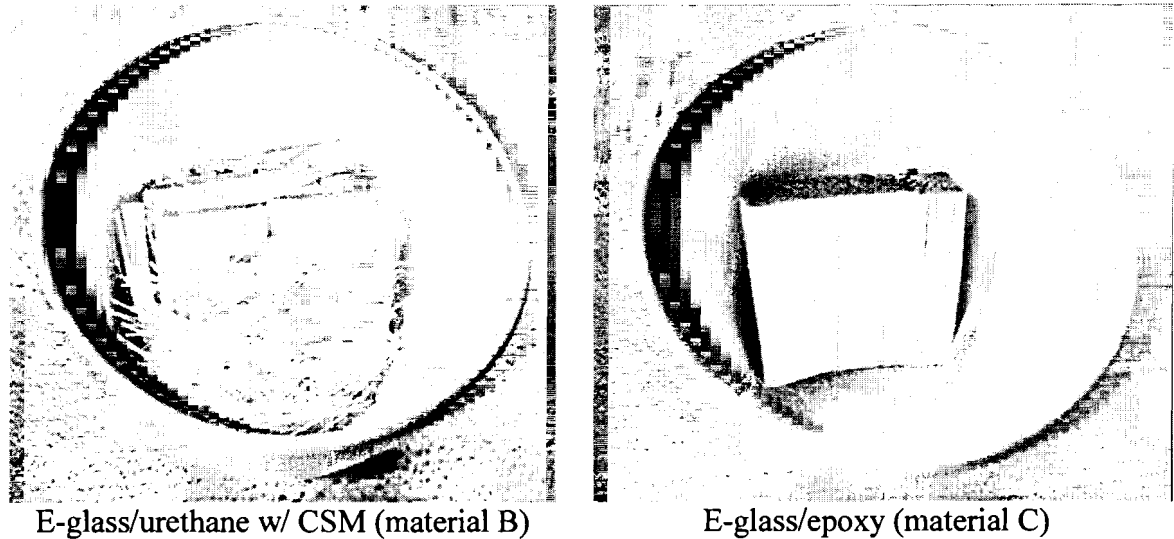


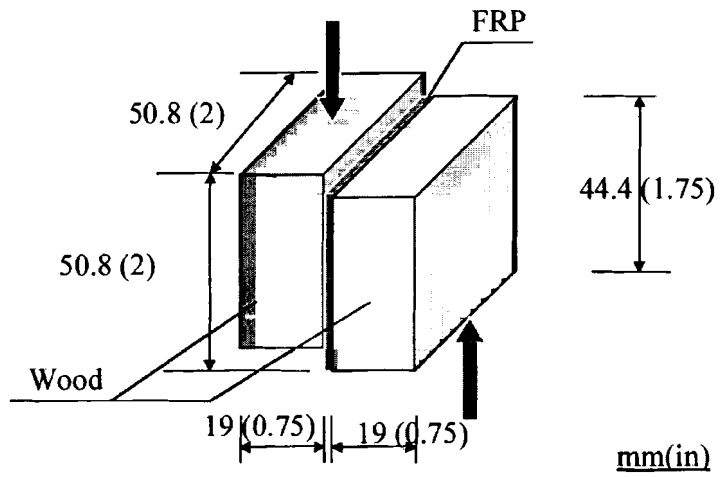
Figure 3.2 FRP Composite Materials after Ignition Tests

3.7 Part One of Modified ASTM D2559: Resistance to Shear in Compression

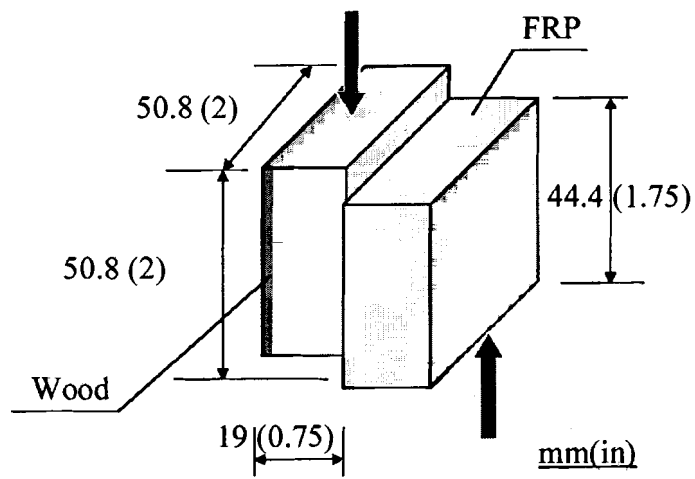
Shear block tests were conducted according to the modified ASTM D2559. The specimen configuration was modified according to ASTM D905 to account for the FRP composite substrate. The effects of the HMR primer and FRP surface treatment were studied. Although shear testing by compression loading of wet (saturated) samples are not required by ASTM D2559, this evaluation was considered important to assess durability under exterior use (Lopez-Anido *et al.* 2000).

3.7.1 FRP-Wood Specimen Configuration

The configuration of the ASTM D905 was modified to account for the FRP composite substrate. Two cases are specified corresponding to thin and thick FRP materials. For FRP with thickness less than ¼-in, one FRP layer is added between two wood substrates. For thick FRP materials, the FRP substrate is used to substitute one wood substrate. The shear block specimen configurations are shown in Figure 3.3.



(a) For thin FRP materials: A & B



(b) For thick FRP materials: C

Figure 3.3 Specimens for Modified ASTM D905 Shear Block Tests

3.7.2 FRP-Wood Specimen Fabrication

The specimen fabrication has the following steps specified in a standard work instruction (AEWC 2001a):

1. Cut each piece of wood lamination to nominal 19-mm (0.75-in) thick, 127 mm (5-in) wide and 602-mm (23.7-in) long (determined by the laminating press). Plane the lamination surface.
2. Apply HMR Primer to the wood surfaces.
3. Cut each piece of FRP to 127 mm (5-in) wide and 602-mm (23.7-in) long; abrade the FRP surfaces with 80-grit sand paper; wipe the sanded surface with a lint-free, acetone-saturated rag.
4. Apply the adhesive uniformly to the contacting faces of each lamination in accordance with manufacturer's instructions; place the laminated wood members under proper pressure for a period of time at the glue-line temperature specified by the manufacturer of the adhesive.
5. Cut the FRP-wood laminations into the samples as shown in Figure 3.3. A picture of the test samples is shown in Figure 3.4.

3.7.3 Experimental Procedure

All dry samples were conditioned in an environmental chamber with 65% RH and 24°C for more than two weeks before testing. For the wet samples, a vacuum pressure of 200 mm Hg was applied for 10 minutes first, then a pressure of 0.52 MPa (75 psi) was applied and held for 30 minutes.

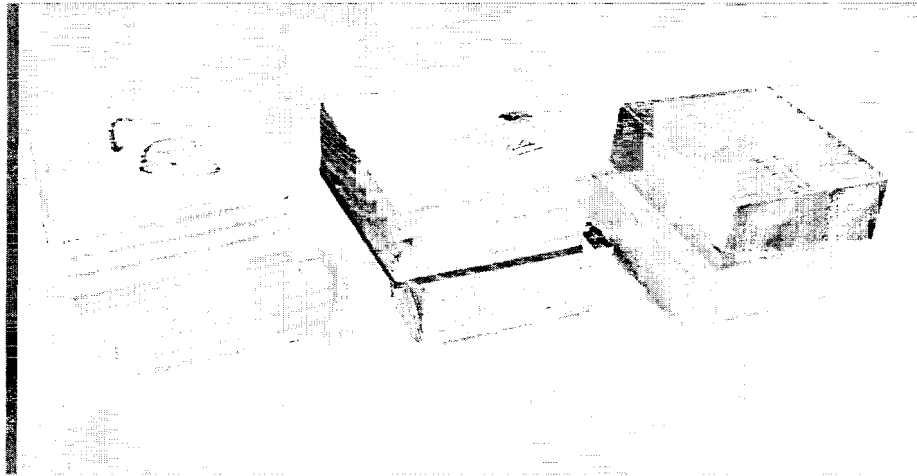


Figure 3.4 FRP-Wood Shear Block Specimens

A testing fixture required to shear the interface by compression loading was used as specified in the ASTM D905. An Instron 8801 servo-hydraulic testing frame was used to apply load on the testing fixture with a loading rate of 5mm/minute until failure. Interface shear stress is achieved by applying compression force on the self-adjusting bearing.

The average shear strength of the adhesive bonding line was obtained by dividing the maximum compression force with the glue line area between the two laminations. The percentage of wood failure was also recorded to the nearest 5% for each test specimen.

3.7.4 Experimental Results

The minimum requirement of average shear strength of ASTM D2559 for wood-to-wood bonding using DF and SYP are 7.38 MPa (1070 psi) and 9.04 MPa (1310 psi) respectively. For both wood species, the standard also requires that the average wood failure shall be not less than 75 %. The criteria of ASTM D2559 were accepted in this

research. Because there is only one wood bond surface instead of two, the required minimum wood failure may be reduced, e.g. to 50%, to account for the presence of the FRP substrate. However, further experimental investigations may be necessary to determine a proper performance limit. The results of the shear block tests shown in Table 3.7. Shear strength and wood failure of selected material combinations are shown in Figure 3.5 and Figure 3.6, respectively.

3.7.5 Discussions of Experimental Results

For FRP material system D bonded to DF and SYP, the shear block strength met the minimum requirement of the standard. However, both of the material combinations had very low percentages of wood failure in both dry and wet conditions. Each FRP layer consisted of 3 CF/P sheets. Most of the delaminations occurred in the FRP-paper interfaces. Therefore, both of the material combinations for FRP material system D failed in the shear block tests.

For FRP material system B, the effects of addition of CSM near to the FRP surface and application of HMR coupling agent for wood priming were investigated. In the dry condition, all of the material combinations produced relatively high shear strengths. But in wet condition, the HMR coupling agent dramatically improved adhesion of the polyurethane adhesives on DF and FRP. When wood surfaces were not primed with HMR, the wet wood shear strength and wet wood failure were significantly lower.

Table 3.7 Shear Strength and Wood Failure

| FRP Material | Primer/ Adhesive | Wood Species | Dry | | Wet | |
|----------------------------|-------------------|--------------|------------------------------|----------------|------------------------------|----------------|
| | | | Shear Strength (MPa) (COV %) | Wood Failure % | Shear Strength (MPa) (COV %) | Wood Failure % |
| D | PRF | SYP | 8.4 (23.3) | 19 | 4.8 (38.7) | 6 |
| D | PRF | DF | 7.9 (15.6) | 7 | 5.8 (19.1) | 20 |
| B: All roving ¹ | Franklin Urethane | DF | 12.9 (22.8) | 56 | 4.5 (12.1) | 19 |
| B: w/ CSM | Franklin Urethane | DF | 11.5 (16.9) | 69 | 5.7 (15.6) | 6 |
| B: All roving ¹ | HMR/ F. Urethane | DF | 13.2 (11.5) | 41 | N.A. | N.A. |
| B: w/ CSM | HMR/ F. Urethane | DF | 15.6 (8.9) | 30 | 9.4 (3.7) | 26 |
| B: All roving ¹ | ISPGRIP Urethane | DF | 8.0 (21.9) | 37 | 4.9 (13.2) | 2 |
| B: w/ CSM | ISPGRIP Urethane | DF | 10.3 (10.9) | 18 | 4.9 (12.4) | 2 |
| B: All roving ¹ | HMR/ I. Urethane | DF | 9.8 (17.3) | 38 | 6.0 (3.2) | 64 |
| B: All roving ² | HMR/ I. Urethane | DF | 9.1 (13.1) | 75 | 6.3 (12.2) | 71 |
| B: w/ CSM | HMR/ I. Urethane | DF | 10.9 (9.4) | 68 | 6.2 (13.9) | 76 |
| C | HMR/ Epoxy G1 | DF | 16.7 (3.1) | 93 | 11.2 (3.2) | 98 |
| C | HMR/ Epoxy G2 | DF | 17.1 (2.2) | 95 | 7.7 (5.1) | 93 |
| C | HMR/ Epoxy G3 | DF | 10.3 (4.1) | 90 | 6.0 (7.9) | 94 |

1: Surfaces were hand sanded; 2: Surfaces were machine sanded.

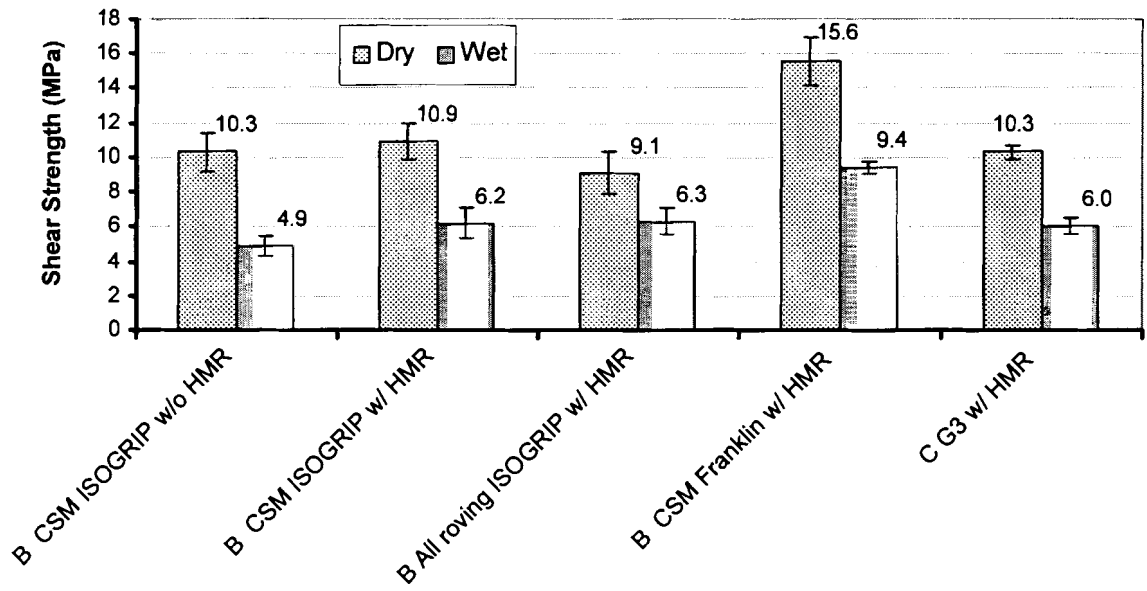


Figure 3.5 Shear Strength of the Shear Block Tests

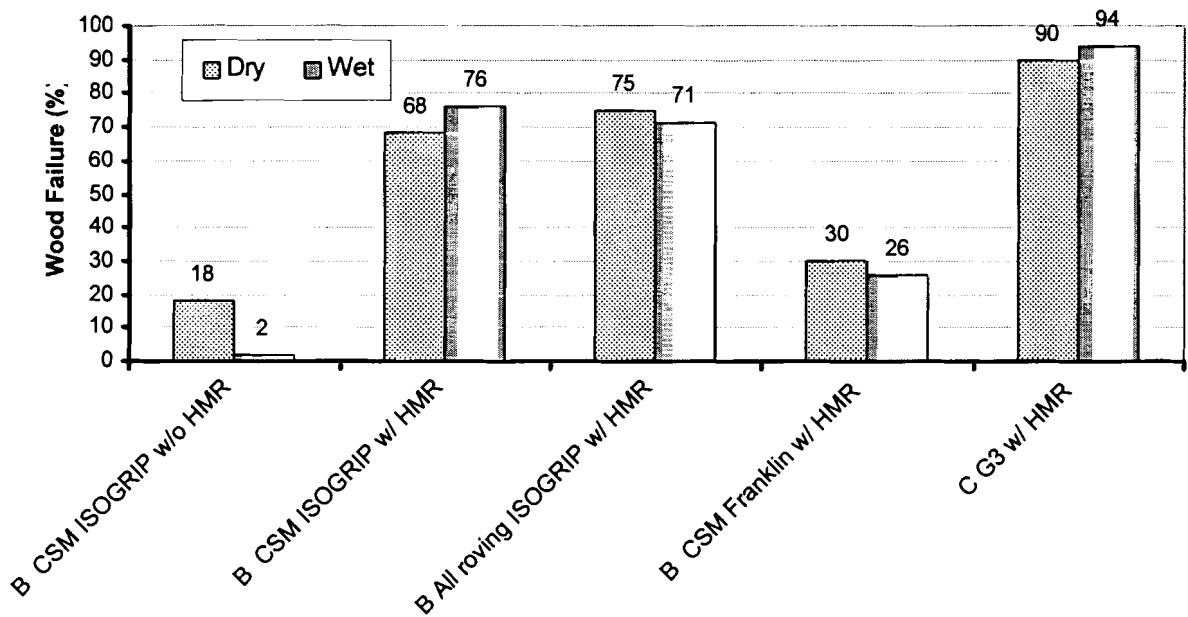


Figure 3.6 Wood Failure of the Shear Block Tests

Because of the large variation of wood properties, the behaviors of CSM and all roving material with machine sanded surfaces may be considered similar. The samples bonded with the Franklin adhesive had higher shear strength than those bonded with the Ashland adhesive in both dry and wet conditions. All of the material combinations for FRP material B with HMR primer passed the shear block tests.

Both the Franklin adhesive and the Ashland adhesive worked well (material system B). However, since Franklin adhesive is designed as a high performance finger jointing product, it has a rapid cure rate, which makes it difficult to be used to bond FRP to glulam beams due to the short assembly time. Therefore, for the subsequent tests, only the Ashland adhesive was used with FRP material system B.

For material C, all of the three adhesives passed the shear block tests. However, only G3 adhesive passed the cycle delamination tests. Therefore, only G3 adhesive was used in the subsequent tests.

Material system D failed in the screening tests. The interface of the carbon-phenolic sheet and phenolic-impregnated paper proved to be the weakest link. This material system was eliminated from the subsequent tests. An alternative Carbon FRP composite reinforcement was proposed.

The material systems selected for further evaluation are listed in Table 3.8.

3.8 Part Two of Modified ASTM D2559: Resistance to Delamination During Accelerated Exposure

Cycle delamination tests were conducted according to the modified ASTM D2559. The standard was modified to account for the FRP composite substrate. The

experiments were used to examine the integrity/durability of FRP-wood bond lines under accelerated hydrothermal stresses. The experiments examined the integrity of several material systems in terms of the measurement of delamination ratios of FRP-wood interfaces.

Table 3.8 Material System Selected Based on the Screening Tests

| Material System | FRP composite | FRP fabrication | Wood species | Adhesive | Wood Primer |
|------------------------|------------------------------|------------------------|---------------------|----------------------------|--------------------|
| B | E-glass/ urethane: w/ CSM | Pultrusion | DF | Urethane: ISOGRIP 3030D | HMR |
| C | E-glass/epoxy | Continuous lamination | DF | Epoxy: PRO-SET G3 | HMR |

3.8.1 FRP-Wood Specimen Configuration

The specimen configuration was modified according to the ASTM D2559 to account for the presence of the FRP. The configuration and dimensions of the glulam are the same as specified by the ASTM standard. A FRP layer was added to only one surface of the glulam beam. For the thickness of the FRP layer, two cases are specified corresponding to minimum and maximum FRP thickness expected in glulam reinforcement. The minimum thickness for pre-consolidated FRP materials is one consolidated sheet or one fabric layer. The maximum thickness is the maximum thickness required for specific project. In this study, the maximum thickness of E-glass FRP (material B and C) is 19mm (3/4"). For carbon fiber reinforcements, the maximum thickness is divided by the modular ratio between the FRP and the baseline E-glass FRP. For FRP material system D (CF/P), the maximum thickness was determined as 9.5mm

(3/8"). The configurations of the FRP-wood specimens with maximum FRP thickness are shown in Figure 3.7.

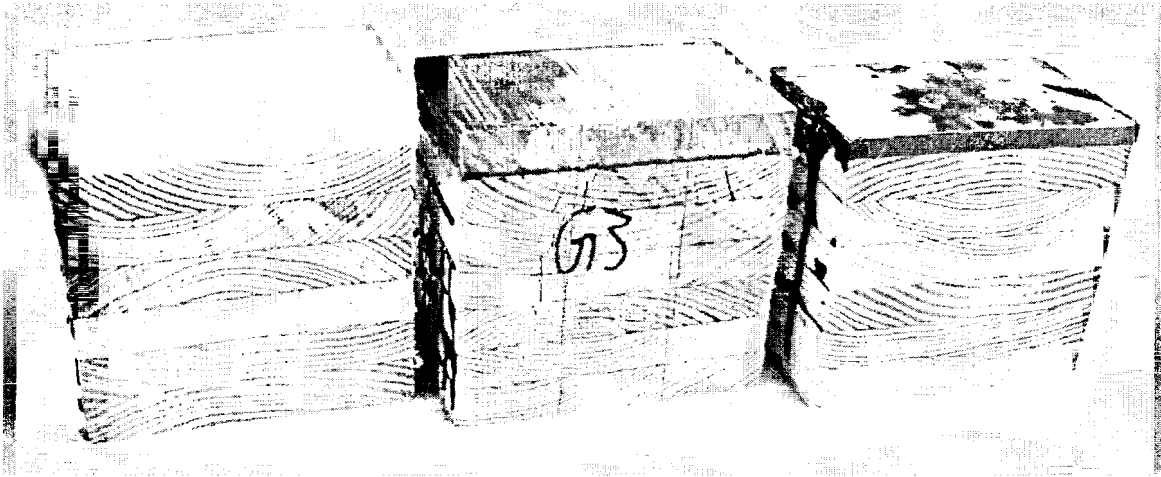


Figure 3.7 FRP-Wood Specimens for Cycle Delamination Test

3.8.2 FRP-Wood Specimen Fabrication

All of the test specimens were fabricated in the laboratory. Grade structural selected Douglas-fir lumber with nominal size of 25×150mm (1"×6") were used to fabricate glulam specimens. They were stored in the conditioning chamber with 24°C and 65% of RH for about two months. The moisture content was about 12% when fabricating.

The fabrication of FRP-wood laminated specimens was followed by a standard work instruction (AEWC 2002a). A standard work instruction for proportioning, mixing, applying and obtaining ingredients for HMR primer for bonding FRP to wood was also applied (AEWC 2001; Lopez-Anido *et al.* 2000).

The fabrication procedure steps are:

1. Prepare six pieces of wood with dimensions of nominal 19-mm (0.75-in) thick, 127 mm (5-in) wide and 602-mm (23.7-in) long.

2. Apply PRF adhesive on only one surface of each lumber with the rate of 387.5 g/m². Six wood laminations were clamped together with a pressure of 110 psi for 24 hours by a laminating press, which is introduced in Chapter 3.
3. Refresh only one surface of the resulting glulam beam with a planer. Prepare and apply the HMR primer to that wood surface 16 hours before the application of the adhesive.
4. Clean the FRP surfaces with Acetone. Sand the surfaces with 80-grit sandpaper. Wipe the surface with clean towels before the solvent dries.
5. Apply the adhesive uniformly only to the wood face in accordance with manufacturer's instructions. Apply the FRP layer only to one surface of the laminated wood beam.
6. Place the FRP reinforced laminated wood members under pressure using the laminating press for a period of time and at the glue-line temperature specified by the manufacturer of the adhesive.

When cutting FRP-glulam specimens, trim 46-mm (1.8-in) off each end of the beam and discard it. The remaining portion was cut into six 75 mm (3") long parts. For each material system, at least two beams (12 samples) were fabricated and tested.

3.8.3 Experimental Procedure

As specified in ASTM D2559 test procedure, the cycle delamination test consists of three hydrothermal cycles. The FRP-wood hybrid specimens were exposed to three types of accelerated environmental conditions: vacuum/pressure water saturation, oven drying and steaming.

Immediately after the three cycles, the images of the specimens were taken using a digital camera. Then, they were examined to measure interface delaminations using image analysis techniques. The total delamination length of the FRP-wood interface on each end-grain surface of the specimens was measured to get the delamination ratio. For the material systems in this study, the 5% delamination limit as specified by the ASTM D2559 for softwood species was adopted.

3.8.4 Experimental Results

The results and pictures of specimen after cycle delamination for material system D are shown in Table 3.9.

For material system B, the effect of addition of a continuous strand mat (CSM) near to the FRP surface was studied. The effect of application of HMR wood primer was also evaluated by shear block tests, which is presented later in this chapter. The results of shear block tests showed that the HMR primer greatly increased the bonding properties between the urethane adhesive and wood, especially in wet use. Therefore, the material systems without HMR primer were eliminated from the matrix of the cycle delamination tests. Two FRP surface treatments were evaluated for all roving materials (without CSM): hand sanded and machine sanded. The results of material system B are shown in Table 3.10. The specimen pictures after delamination tests are shown in Figure 3.8.

Table 3.9 Results of ASTM D2559 Cycle Delamination Tests of Material System D

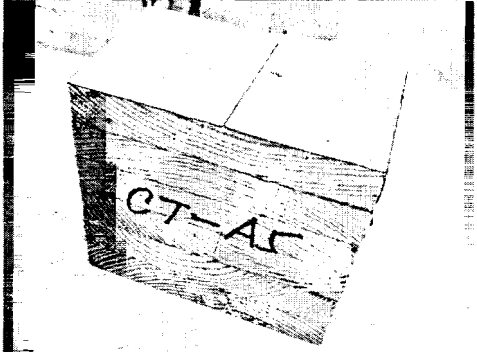
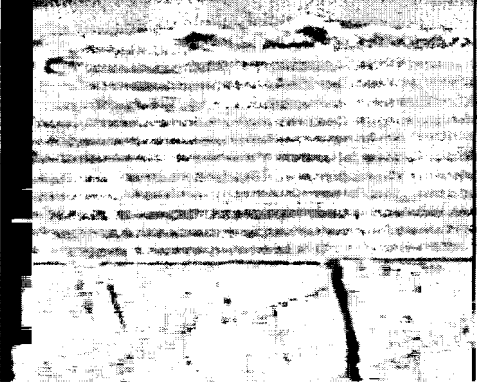
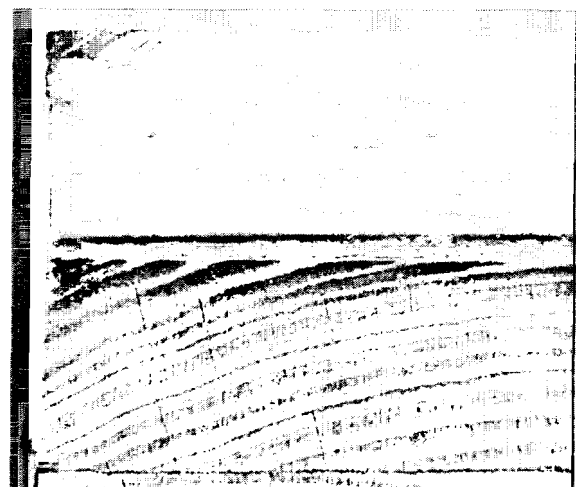
| FRP Thickness | Image Right After Testing | Results |
|--|---|--|
| Minimum: 0.8 mm (1 layer). 12 samples. |  | Passed. No delamination in interface. Cracks only existed along the fiber direction in FRP. |
| Maximum: 19 mm (12 layers). 12 samples. |  | Failed. Delamination ratio: 33% for SYP, 11% for DF. Delaminations occurred both in FRP/wood interface and FRP/FRP interfaces. |

Table 3.10 Results of ASTM D2559 Cycle Delamination Tests of Material System B

| E-glass/urethane | FRP Thickness | FRP Surface Treatment | Result |
|---------------------------------|----------------------|--------------------------------|---|
| CSM w/ HMR (Franklin) | Minimum (1/4") | Sanded by the manufacturer. | Passed. No delamination. |
| CSM w/ HMR (Franklin) | Maximum (3/4") | Sanded by the manufacturer. | Passed. No delamination. |
| All roving w/ HMR (Franklin) | Maximum (3/4") | Sanded with 80-grit sandpaper. | Passed. No delamination. |
| CSM w/ HMR (Ashland) | Minimum (1/4") | Sanded by the manufacturer. | Passed. No delamination. |
| CSM w/ HMR (Ashland) | Maximum (3/4") | Sanded by the manufacturer. | Passed. No delamination. |
| All roving w/ HMR (Ashland) | Maximum (3/4") | Sanded with 80-grit sandpaper. | Failed after the 1 st cycle. |
| All roving w/ HMR (Ashland) | Maximum (3/4") | Sanded with the belt sander. | Passed. No delamination. |



1) All Roving w/HMR



2) CSM w/HMR

Figure 3.8 Specimens of Material System B after Cycle Delamination Tests

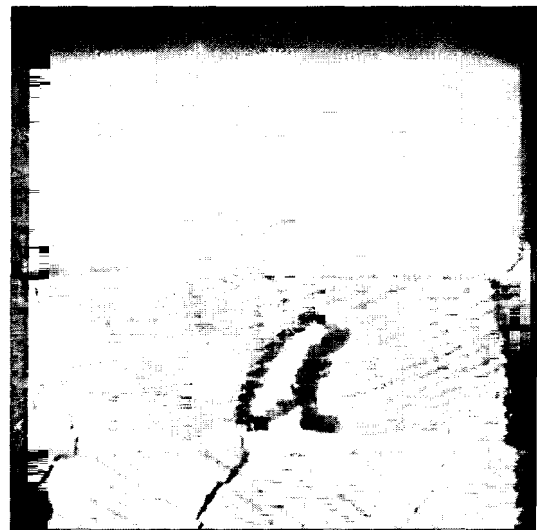
For material system C, three epoxy adhesives were tested. The bonding surface of FRP layers was sanded with 80-grit sandpaper by hand. For the material combinations that failed in the tests, double spread adhesive application was used to study the effect. The results of material system C are shown in Table 3.11. The specimen pictures after delamination tests are shown in Figure 3.9.

Table 3.11 Results of ASTM D2559 Cycle Delamination Tests of Material System C

| E-glass/epoxy | Adhesive Application | Result |
|----------------------|-----------------------------|--|
| G1 w/ HMR | Single spread. | Failed after the 1 st cycle |
| G2 w/ HMR | Single spread. | Failed after the 1 st cycle |
| G3 w/ HMR | Single spread. | Passed. No delamination |
| G1 w/ HMR | Double spread. | Failed. 27 % delamination. |
| G2 w/ HMR | Double spread. | Failed. 24 % delamination. |
| G1 w/ HMR | Double spread. | Failed after the 1 st cycle |
| G2 w/ HMR | Double spread. | Failed after the 1 st cycle |



1) G1



2) G2

Figure 3.9 Specimens of Material System C after Cycle Delamination Tests

3.8.5 Discussion and Conclusion of Experimental Results

Material system D failed in the test. Large delaminations were observed in the FRP-wood interface and FRP-FRP interfaces for both SYP and DF. It was shown that delaminations usually occurred between the carbon-phenolic sheet and the phenolic-impregnated paper. The phenolic-impregnated paper was found to be dry and brittle when stored in the lab (RH in winter is approximately 15 to 25%). For subsequent tests, the roll of CF/P material was conditioned in the environmental chamber (65%RH and 23°C) for more than one month before fabricating, but no significant improvement was observed.

For material system B, two types of FRP materials were tested: all roving and CSM. Two types of polyurethane adhesives were used: Franklin ReacTITE 8143 and Ashland ISOGRIP 3030D. The HMR wood primer was used in all of the material combinations. The surfaces of both materials had been sanded before shipment. The material with CSM passed the test without delamination for both adhesives. The all roving materials failed in the first test with the Ashland adhesive and passed the test with Franklin adhesive. When the surfaces were sanded with a belt sander (machined sanded), the all roving materials passed the second test with the Ashland adhesive. It was shown that the CSM-wood interfaces have better delamination resistance than all roving-wood interfaces with the same surface treatment (hand sanded).

For material system C, three types of epoxy adhesives were tested. Only G3 adhesive passed the test with no delamination. Although double spread application was used in the subsequent tests for G1 and G2 adhesives, both of them failed again.

For FRP sheets fabricated by pultrusion and continuous lamination process (material B and C), only the configurations with the maximum thickness (3/4-in) were

tested. This is because the strength and the stiffness are usually adequate to prevent crack initiation in the cyclic delamination tests.

3.9 Conclusions

The following conclusions were drawn based on the experimental findings:

1. An effective bonding interface was achieved between E-glass/urethane composite and DF by priming the wood surface with HMR.
2. For material system B, both the CSM material sanded by hand and the all roving material sanded by machine passed the delamination tests and shear block tests. Because the extra surface treatment may increase the cost, the all roving material was eliminated from the matrix of the subsequent tests. Only the CSM material was selected for further evaluation.
3. An effective bonding interface was achieved between E-glass/epoxy composite and DF by priming the wood surface with HMR.
4. It was found that the HMR primer significantly improved the bond strength and durability of the epoxy FRP-wood interface. This experimental findings is in agreement with published results (Davalos 2000; Lopez-Anido 2000).
5. It was found that the shear block test is not as sensitive as the delamination tests to discriminate adhesive systems. For example, for material system C, all of the three adhesives had good shear strength and wood failure, but only G3 adhesive passed the cycle delamination test. The delamination test of ASTM D2559 was successfully used to discriminate the effect of several bonding parameters and select the best material combinations for further evaluation. These conclusions are in agreement with existing recommendations (Davalos 2000).

Chapter 4

FATIGUE PERFORMANCE OF FRP-WOOD INTERFACE USING A SINGLE-LAP SHEAR BY TENSION LOADING TEST

4.1 Summary

The fatigue performance of FRP-wood interface using a single-lap shear by tension loading test is characterized. ASTM D2339 standard test procedure was modified and adapted to characterize hybrid FRP-wood bonded materials. ASTM D2339 was developed to evaluate adhesive bonded wood-wood specimens using a single-lap shear test by tension loading. Modifications in the test method were made to account for the presence of the FRP material. Two material systems that passed adhesive screening tests were evaluated: material system B (E-glass/urethane pultruded composite sheet with urethane adhesive) and material system C (E-glass/epoxy composite sheet by continuous lamination with epoxy adhesive). It was shown that the modification and application of the ASTM test method were successful. The fatigue performance-based evaluation criteria and associated limits were also proposed.

4.2 Introduction

Joining of dissimilar materials, wood and FRP composite, by adhesive bonding is required for reinforcement of glulam members. Therefore, the performance of adhesive-bonded joints need to be evaluated to develop specifications for use in load bearing glulam structures. When adhesive-bonded joints are used for primary load bearing

structures, the mechanical performance of the joint, especially the fatigue performance, becomes a major concern (Zhang *et al.* 1995).

Because of its simple geometry and good representation of real structures, the single-lap joint has been widely used to assess the mechanical behavior of adhesive joints of metals and FRP composite materials. Significant research effort has been conducted in this field by combining experimental techniques and analytical tools. However, limited work has been done to investigate fatigue performance of hybrid FRP-wood adhesive joints by single-lap shear tests.

Most of the attempts to understand the fatigue failure processes in adhesive joints have been limited to the post-failure examination of the fracture surfaces after failure, which often does not provide sufficient information on the damage processes contributing to the final fracture. One method to assess the damage processes in adhesive joints during fatigue loading is to detect the stiffness loss of the specimen as related to the initiation and propagation of fatigue cracks. However, a major disadvantage of this approach is that the overall stiffness is not sensitive to localized damage, such as the initiation of a fatigue crack (Zhang *et al.* 1995).

In this study, wood is a material with relatively low strength compared with the FRP composites, which can make it even more difficult to measure the change in the stiffness of the specimens. Therefore, in this study, residual strength tests were conducted for specimens surviving after fatigue cyclic tests using the same test methods for quasi-static control tests. Then, the results were compared with those from control tests to investigate any possible damage accumulation due to fatigue cyclic tests.

4.3 Objective and Scope

The objective of this chapter is develop a material-level test method and associated acceptance criteria to investigate interfacial fatigue performance of FRP-wood bondlines based on single-lap shear (SLS) tests by tension loading. Two ASTM standard test procedures were selected and modified to account for hybrid FRP-wood materials: ASTM D2339 for wood-wood adhesive joints and ASTM D3166 for fatigue performance of metal-metal joints.

The following steps were conducted to support the chapter objective: a protocol based on modified ASTM test procedures was developed; the specimen configuration was determined; a standard procedure for specimen fabrications and testing was drafted; acceptance criteria of the experimental results was proposed, and a set of experiments was conducted to validate the test method and acceptance criteria.

4.4 Literature Review of Single-lap Shear Test Methods

4.4.1 Adhesive Bonding of Metal-Metal

The fatigue behavior of adhesively bonded aluminum joints was investigated analytically and experimentally (Romanko and Jones 1980). In this study, the thick-adherend single-lap shear joint was selected as the “model joint” to reduce the bending moment in the overlap area. The specimens were subjected to sinusoidal fatigue loads at several frequencies, humidity and temperatures. Linear elastic and 3-D linear viscoelastic finite element analysis (FEA) was conducted to calculate stress distributions in the adhesive interlayer. Damage was found to initiate in the high stress regions and propagate

with further load cycling. It was found that crack growth rate was sensitive to temperature, moisture, loading frequency and wave shape.

The relationship between static and fatigue strength of epoxy-bonded aluminum specimens was reviewed for four different specimen types: single-lap shear, edge-delamination, double cantilever beam, and cracked-lap-shear (Johnson and Mall 1984). It was pointed out that the average shear stress value to be very misleading as a material strength parameter of the adhesive because of the relatively high peel and shear stress concentrations near the end of the laps. However, the SLS specimen may be used to compare static and fatigue strengths for the same adhesive system if the configuration and materials are identical. For example, for epoxy bonded aluminum SLS specimens, the static failure stress is almost 2.5 times of the maximum cyclic stress to survive one million cycles.

The estimation of fatigue strength has been conducted for single-lap joints with steel adherends bonded by an epoxy-polyamide adhesive (Imanaka *et al.* 1988). The results of FEA showed that the maximum tensile stress at the lap end well exceeds the maximum shear stress at the same location. First, cyclic tensile fatigue tests were conducted for adhesively bonded lap joints with different lap length and adhesive layer thickness. Then, the standardized fatigue strengths were compared with those of adhesively bonded butt joints of a thin wall tube under both cyclic tensile fatigue loading and fully reversed torsional load conditions. The results indicated that fatigue strength of lap joints evaluated from the maximum tensile stress of the adhesive layer agreed well with that of adhesively bonded butt. It was confirmed that the fatigue strength of the lap

joint could be conservatively estimated from the S-N curve of the adhesive bonded butt joint of the thin wall tube, which has a uniform stress distribution.

The fatigue behavior of two adhesives intended for use in automotive body-shell construction was assessed using single-lap shear specimens with steel adherends (Harris and Fay 1991). In this study, it was found that fatigue life is dominated by a crack initiation phase over a wide temperature range, which is associated with the build up of creep deformation in the adhesive layer. In this research work, the effects of load amplitude, test temperature, specimen configuration and adhesive type on fatigue life were considered in relation to static joint strength. It was found that, in the context of aerospace applications, joints are usually designed with long overlaps and are configured to minimize stress concentrations. Therefore, in this field, the single lap shear joint has been criticized as not being suitable for evaluating the fatigue resistance of adhesive joints because of the relatively high shear and peel stress concentrations that arise in the adhesive layer at the ends of the overlap. Thus, for aerospace applications, the cracked-lap shear joint is always employed for the assessment of fatigue resistance, which is described as “joint independent”. However, for automotive applications, where shorter overlap lengths and simpler joint designs are used, it was found that the single lap shear joint is more representative, although it’s not “joint independent”.

A new backface strain technique to detect fatigue crack initiation in adhesive-bonded lap joints was developed based on the special strain distribution (Zhang *et al.* 1995). During the test, the fatigue crack initiation was detected by the switch in the direction of the strain variation. Tensile and fatigue tests and FEA of epoxy bonded steel single-lap joints were conducted. With the assistance of this technique, a fatigue crack

was found to initiate in the adhesive but to propagate towards the interface to continue its growth and to cause the final fracture of the joint along the interface. It was concluded that the lifetime in the long-life region was dominated by the resistance of the adhesive to fatigue crack initiation.

4.4.2 Adhesive Bonding of FRP-Metal and FRP-FRP

The fatigue behavior of adhesive-bonded single-lap joints, which consisted of an epoxy-film adhesive bonding FRP composite substrates was studied (Kinloch and Osiyemi 1993). The rate of crack growth per cycle was measured as function of the maximum strain energy release rate using a double cantilever beam specimen. Then, these data were modeled and used to predict the fatigue lifetime of bonded single-lap joints. The agreement between the theoretical predictions and experimental results for the fatigue behavior of the single-lap joints was found to be excellent.

Static tensile tests of adhesively bonded single-lap joints with cross-ply FRP adherends were conducted (Kairouz and Matthews 1993). The stresses in the joint were determined using large displacement finite element analysis to account for non-linear geometric effects. A numerical crack simulation was used to determine approximately stress/strain redistribution after initial cracking. The numerical predictions were compared with joint experimental performance and failure modes.

An exploratory experimental evaluation was conducted to investigate the effect of through-thickness stitching on the fatigue life of balanced composite single-lap joints (Jain *et al.* 1998). Since the test joints were fabricated by a resin transfer molding technique, there was no adhesive layer at the joint, and failure typically occurred at the interface of the adherends caused by the peel stresses. Experimental results indicated that

stitches remained intact during crack propagation. No failure of the stitches occurred till the crack propagated to the middle of the specimen prior to complete failure. It was seen that for any given fatigue load, the stitched specimens exhibited larger number of cycles to failure and therefore exhibit better fatigue performance.

Tensile fatigue tests for adhesively bonded aluminum /CFRP single-lap joints were conducted (Ishii *et al.* 1999). The crack initiation and propagation behaviors were observed using a micro-video camera. A method of estimating the fatigue strengths of adhesively bonded single-lap joints based on two stress-singularity parameters was developed.

A simple generalized model was developed for predicting the stiffness of a single-lap joint (Owens and Lee-Sullivan 2000a; Owens and Lee-Sullivan 2000b). The model considered each component of the joint as separate spring elements. Therefore, each element sustained different levels of deflection. The individual deflections due to tension loading were found using basic mechanics analysis and by applying the Adams-Peppiat stress equation for adhesive bonded lap joints. The model can also be used to predict the stiffness loss due to adhesive bond fracture by accounting for the shorter overlap length due to cracking. Experimental testing was performed for FRP-aluminum single-lap joints bonded with flexible or rigid adhesives to verify this model. The results showed that the joint stiffness was more affected by the response of the adherends to the test temperature than by the modulus of the thin adhesive layer. It was found that the model was capable of predicting the joint stiffness and the rate of stiffness loss with crack growth. However, since the model did not account for other failure modes such as delamination and interfacial tearing, the stiffness loss due to such failures was underestimated.

4.5 Materials

The characteristics of the two material systems selected are listed in Table 4.1.

Table 4.1 Material Systems

| Material System | FRP Composite | FRP Fabrication | Wood Species | Adhesive | Wood Primer |
|------------------------|------------------------------|--------------------------|----------------------|-----------------------------|--------------------|
| B | E-glass/ urethane: w/ CSM | Pultrusion | DF: quarter- sawn | Urethane: ISOG RIP 3030D | HMR |
| C | E-glass/epoxy | Continuous lamination | DF: quarter- sawn | Epoxy: PRO-SET G3 | HMR |

4.6 Modified ASTM D2339: Strength Properties of Adhesives in FRP-Wood

Construction in Shear by Tension Loading

Single-lap shear quasi-static and fatigue tests were conducted according to the modified ASTM D2339. The standard was modified to account for the FRP composite substrate. The experiments were used to examine the integrity of two FRP-wood-adhesive material systems in terms of the measurement of apparent single-lap shear strength, fatigue cycles and percentage of wood failure of FRP-wood interfaces.

4.6.1 FRP-Wood Specimen Configuration

The configuration of the ASTM D2339 was modified to account for the FRP composite substrate. The FRP substrate was used to substitute one wood substrate. The grip length of the specimen was increased to fit the jaws of the testing frame. For pre-consolidated FRP materials, the thickness of the FRP layer is one consolidated sheet or one fabric layer. For both material system B and C, the FRP materials are pre-consolidated with the thickness of 6.3mm (0.25in). The minimum thickness of the wood

layer is depended on the strength of the wood specie to assure shear failure instead of tensile failure.

Finite element analysis (FEA) was conducted to optimize the wood thickness by approximately matching the axial stiffness of FRP and wood, as explained in Chapter 5. To balance the substrates of the single-lap shear joints, stress concentrations can be minimized and premature wood failure can be prevented. Based on the results of FEA and preliminary tests, the thickness of the wood layer was specified as 8 mm for DF. The single-lap shear specimen configuration is shown in Figure 4.1.

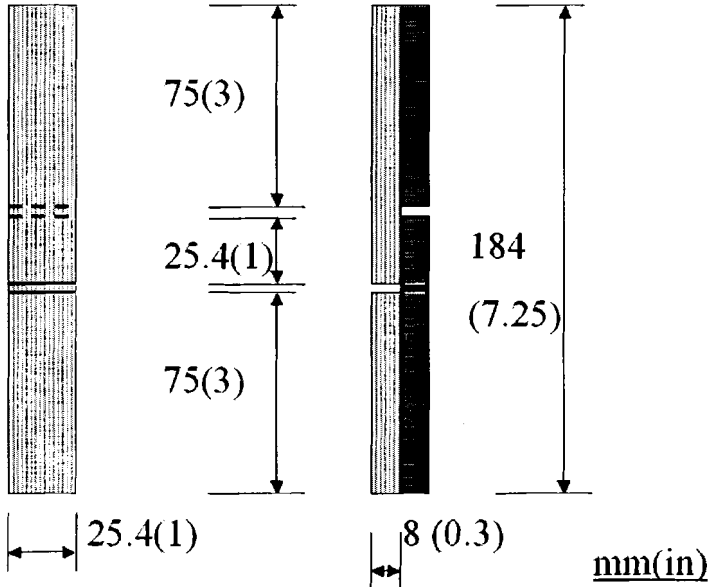


Figure 4.1 Specimen Configuration for Modified ASTM D2339 SLS Tests

4.6.2 FRP-Wood Specimen Fabrication

The test specimens were fabricated in the laboratory. Grade structural selected Douglas-fir lumber with size of 19×150mm (nominal 1”×6”) were used to fabricate glulam specimens. To get uniform surface properties for such a small specimen, only Douglas-fir lumber with quarter-sawn orientation were used. They were stored in a

conditioning chamber at 24°C and 65% of RH for more than two months. The moisture content was approximately 12% during fabrication.

The fabrication of FRP-wood laminated specimens followed a standard work instruction (AEWC 2002). A standard work instruction for proportioning, mixing, applying and obtaining ingredients for HMR primer for bonding FRP to wood was also applied (AEWC 2001; Lopez-Anido *et al.* 2000).

The test joints were fabricated using the laminating press introduced in Chapter 3. The assembly time and clamping pressure are listed in Table 4.2.

Table 4.2 Assembly Time and Clamping Pressure of Adhesives

| Adhesive | Urethane | Epoxy |
|-------------------------|----------|-------|
| Open/closed | 5/20 | 5/20 |
| Assembly Time (min) | | |
| Clamping Pressure (psi) | 50 | 20 |

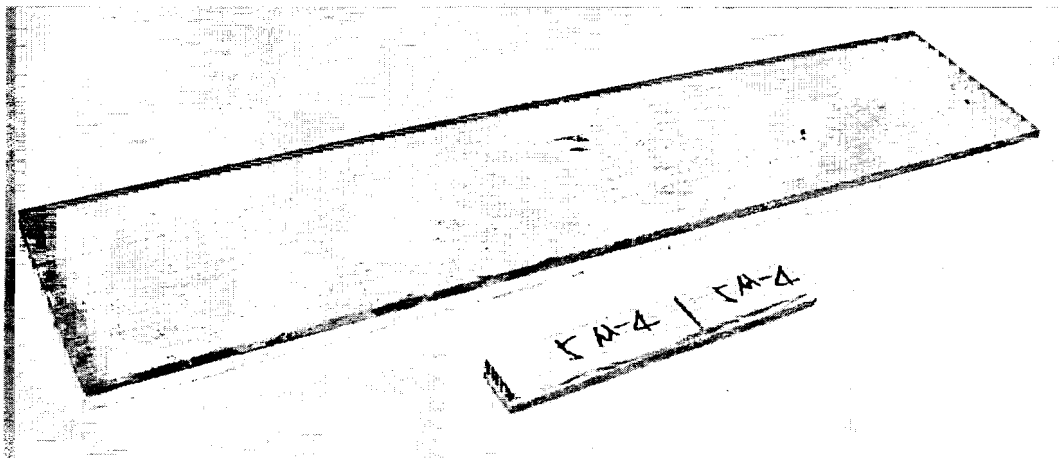


Figure 4.2 Test Panel and Test Sample of Single-lap Shear Tests

The test panel and test sample are shown in Figure 4.2. The fabrication procedure for one test panel consists of eight steps as follows:

1. A wood substrate with dimensions of 8 mm (0.315 in) thick, 127 mm (5 in) wide and 602 mm (23.7 in) long was prepared.
2. One surface of the wood lumber was refreshed with a planer. HMR primer was prepared and applied to that wood surface 16 hours before the application of the adhesive.
3. One surface of the FRP substrate was cleaned with Acetone. The surface was sanded with 80-grit sandpaper and wiped with a clean towel before the solvent dries.
4. The adhesive was applied uniformly only to the wood surface in accordance with the manufacturer's instructions. Then, the FRP layer was applied to the wood lumber.
5. The FRP-wood laminated panel was applied under pressure using the laminating press for a period of time and at the glue-line temperature specified by the manufacturer of the adhesive.
6. One-inch strip was trimmed off and discarded along the transverse direction from one end of the panel using a table saw with a diamond blade. Then, the lumber was cut to three 7.25-in long panels along the transverse direction. The other end was also discarded.
7. A notch was cut on the FRP layer 3-in from the end of each panel along the transverse direction. Another notch was cut on the wood layer 3-in from the other end of each panel along the transverse direction.

can provide more reliable and repeatable results. Thus, only this orientation was used to conduct all of the tests.

The crossheads of the testing machine were aligned manually to prevent premature torsion failure of the specimen. The specimens should be perfectly aligned in such a position that an imaginary vertical line would pass through the center of the bonded area and through the points of suspension. Ensure that the edge of the lap is 25.4 mm (1 in.) from the edge of the grip. The clamping pressure of 40 psi was selected to prevent crushing failure of the wood layer and slippage in the grip area.

4.6.3.1 Quasi-static Control Tests

First, 20% of the specimens were tested under quasi-static loading to get the control ultimate single-lap shear strength. To investigate possible effects due to post-curing of the adhesive, control tests of another 20% of the specimens were conducted after the fatigue tests. For quasi-static control tests, a monotonic tensile load is applied till failure with a loading rate of 3.5 kN/min as specified in ASTM D2339 test procedure. The ultimate tensile load was recorded. The apparent single-lap shear strength of the bonding line was obtained by dividing the maximum tensile force with the overlap shear area between the wood notch and the FRP notch. The percentage of surface failure in the wood substrate was also recorded to the nearest 5% for each test specimen.

4.6.3.2 Fatigue Tests

Fatigue tests can usually be conducted at several selected stress levels such that failures occur with regular spacing over a range varying from at least 1 million cycles to not less than 2000 cycles (Gere and Timoshenko 1997). S-N curves can be used to characterize the fatigue properties. S-N curves relate demand (stress or strain, S) and capability (cycles-to-failure, N). All engineering S-N curves use a logarithmic axis for

cycles, and the dependent variable, cycles, is plotted on the x-axis. Wood has relatively low shear strength parallel to the fiber direction compared to the strengths of FRP composites. For example, the typical shear strength of DF is 6.3 MPa, while the typical in-plane shear strength of E-glass/epoxy is 45 MPa. Preliminary test results showed that the failure usually occurred within the wood substrate near the wood-adhesive interface. The ultimate tensile load was approximately 4 kN. Two stress levels, which represent 50% and 75% of the ultimate SLS strength respectively, were investigated.

The proposed limit number of fatigue cycles was 3 million. For the 50% SLS strength stress level, some of the specimens failed during the fatigue tests and others passed 3 million cycles. For the 75% SLS strength stress level, all of the specimens failed prematurely, exhibiting a broad variation in the number of cycles to failure.

Sinusoidal tension-tension axial load was used to conduct the fatigue tests. The average apparent shear stress in the overlap area was 3.1 MPa (450 psi). Fatigue tests were conducted at a constant amplitude with a stress ratio of $R = 0.1$ and a frequency of 20 Hz. Therefore, the maximum tensile load is 2.0 kN and the minimum tensile load is 0.2 kN. Specimens were tested for 3 million load cycles if no failure occurred earlier.

4.6.3.3 Residual Strength Tests

Residual strength tests were conducted for the specimens that survived after 3 million cycles. The testing procedure was the same as the one used for the quasi-static control tests.

4.6.4 Failure Mode

Typical failure modes of quasi-static control tests for FRP-wood specimens of material systems B and C are shown in Figure 4.4/Figure 4.5, respectively. For both material systems, the failure mode was highly dependant on the wood density. For wood

with higher densities (such as late wood), adhesive failure occurred. For wood with lower densities (such as early wood), wood failure occurred.

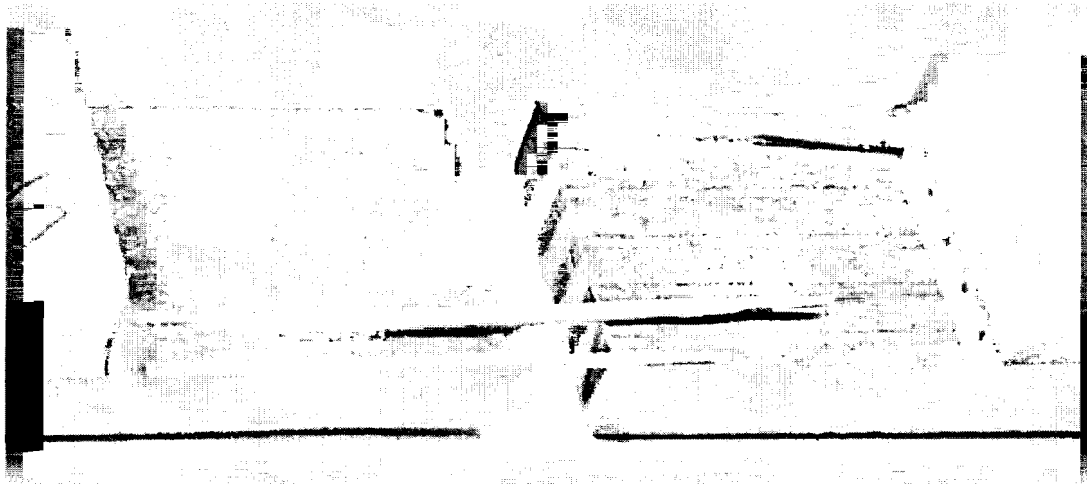


Figure 4.4 Typical Static Failure Mode of SLS Specimens of System B

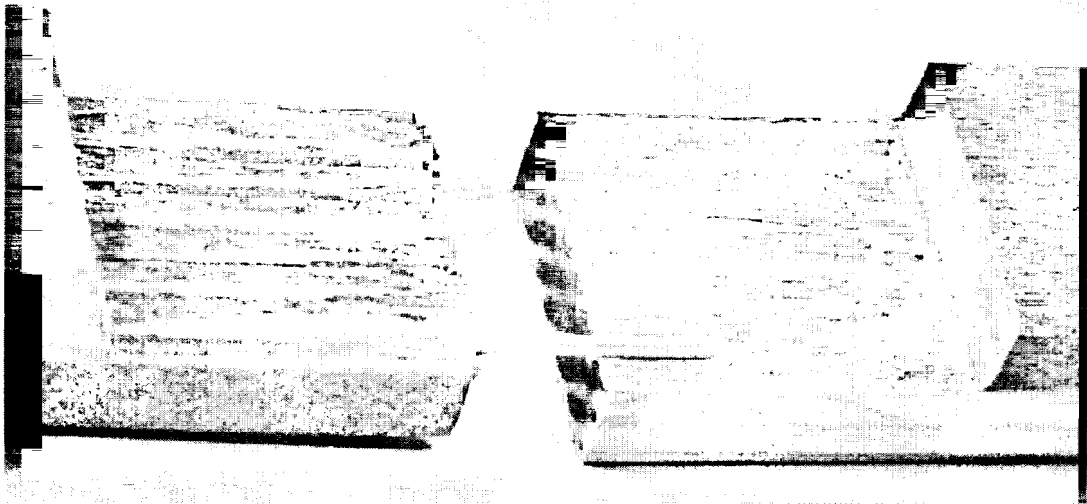


Figure 4.5 Typical Static Failure Mode of SLS Specimens of System C

Typical fatigue failure modes for FRP-wood specimens of material systems B and C are shown in Figure 4.6 and Figure 4.7, respectively. For material system B, the cracks usually formed at a point near the FRP composite sheet notch within the wood substrate, and gradually propagated to the wood notch until reaching failure. For system C, two typical fatigue failure modes were observed. The cracks either had the same failure mode

described for system B, as shown in Figure 4.7, or propagated along the FRP-wood interface, as shown in Figure 4.5.

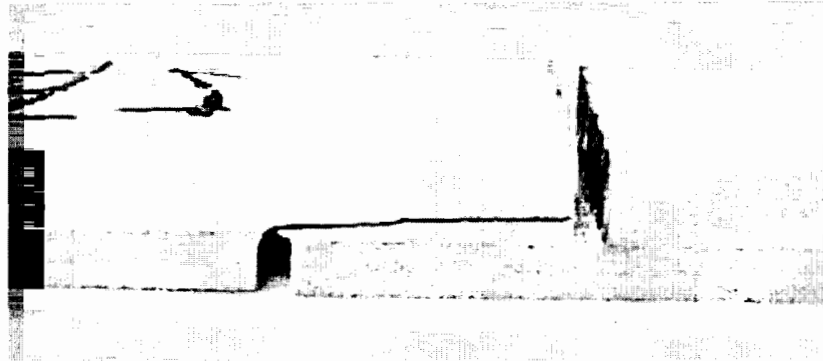


Figure 4.6 Typical Fatigue Failure Mode of SLS Specimens for System B

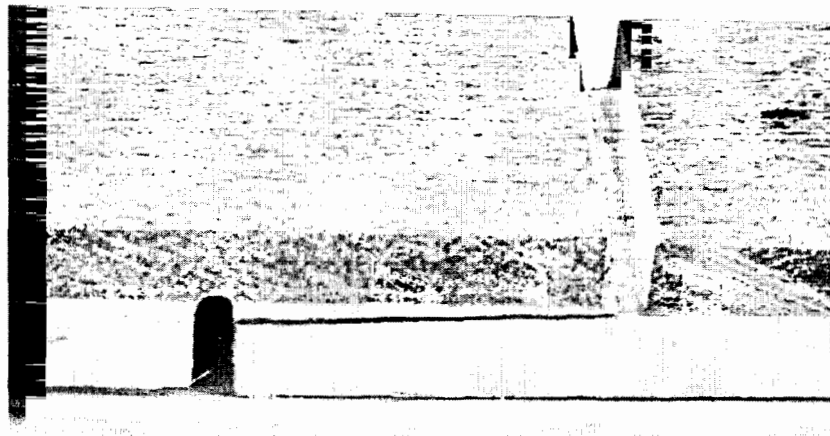


Figure 4.7 Typical Fatigue Failure Mode of SLS Specimens for System C

The failure mode of the residual strength tests was similar to that of the quasi-static control tests for both material systems.

4.6.5 Experimental Results

One panel of material system C was evaluated at 75% SLS control strength as shown in Figure 4.8. In Figure 4.8, each sample index number represents a specific specimen. Only one stress level was further studied, which corresponds to 50% of the ultimate single-lap shear strength from quasi-static control tests. Six panels of system B

and five panels of system C at 50% SLS control strength were evaluated. The fatigue performance evaluation for systems B and C at 50% of SLS is presented in Table 4.3 and Table 4.4, respectively. The test results are shown in Figure 4.9 to Figure 4.20. Each panel index number represents a group of specimens cut from that specific test panel.

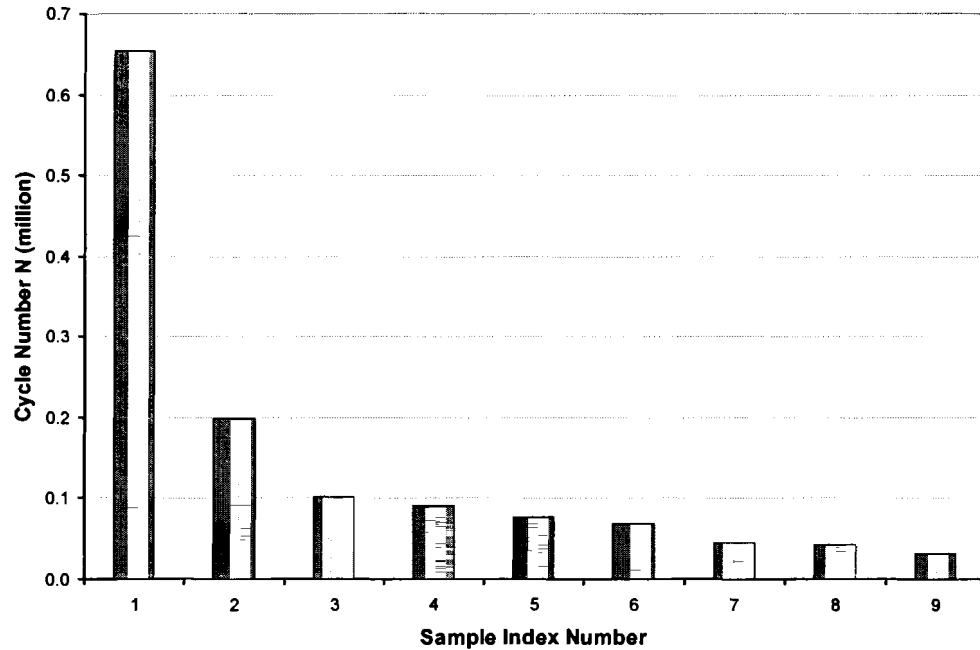


Figure 4.8 Applied Number of Fatigue Cycles for Material System C (75%)

Table 4.3 SLS Test Results for Material System B

| Test Type | Sample size | SLS strength MPa (COV %) | Wood Failure % | Number of Samples passed 3 million cycles (%) |
|--------------------------------|-------------|--------------------------|----------------|---|
| Control | 24 | 6.9 (19.0) | 77 | - |
| Fatigue Failure | 38 | - | 70 | 11 (29) |
| Fatigue with Residual Strength | 11 | 7.4 (16.6) | 72 | - |

Table 4.4 SLS Test Results for Material System C

| Test Type | Sample size | SLS strength MPa (COV %) | Wood Failure % | Number of Samples passed 3 million cycles (%) |
|--------------------------------|-------------|--------------------------|----------------|---|
| Control | 27 | 7.7 (19.3) | 81 | - |
| Fatigue Failure | 32 | - | 90 | 19 (59) |
| Fatigue with Residual Strength | 19 | 7.4 (13.6) | 76 | - |

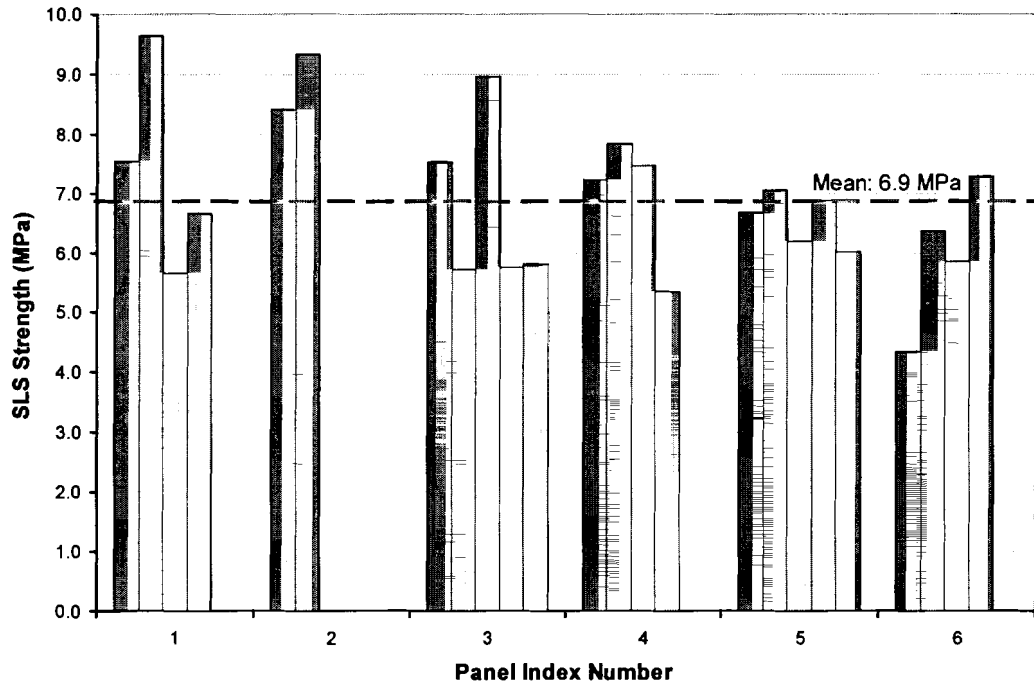


Figure 4.9 SLS Control Strength for Material System B

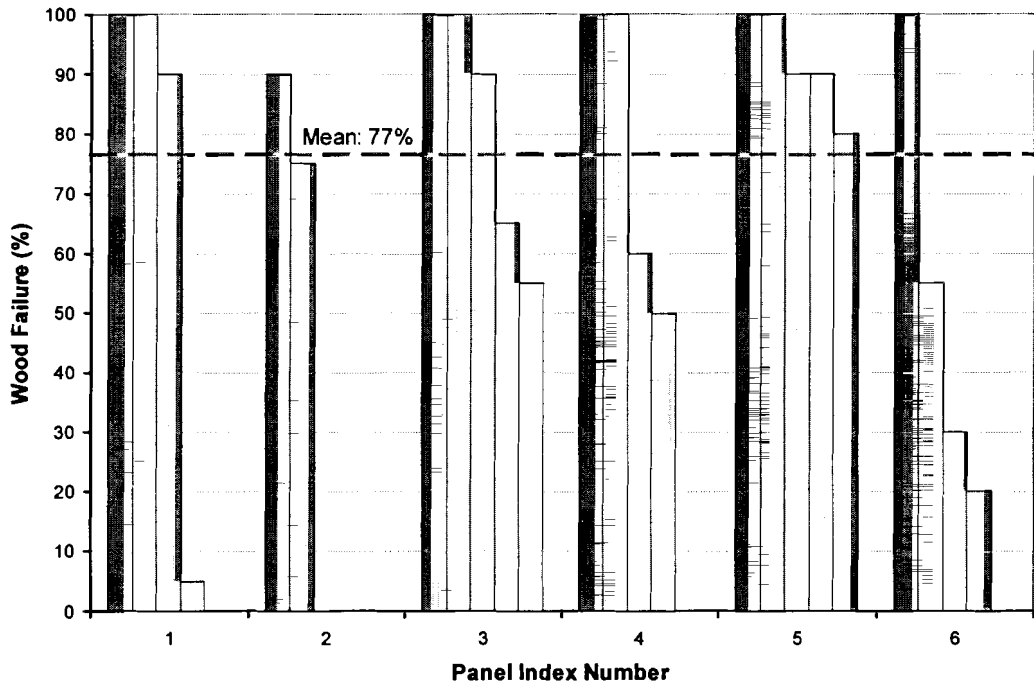


Figure 4.10 Percentage Wood Failure of Control Tests for Material System B

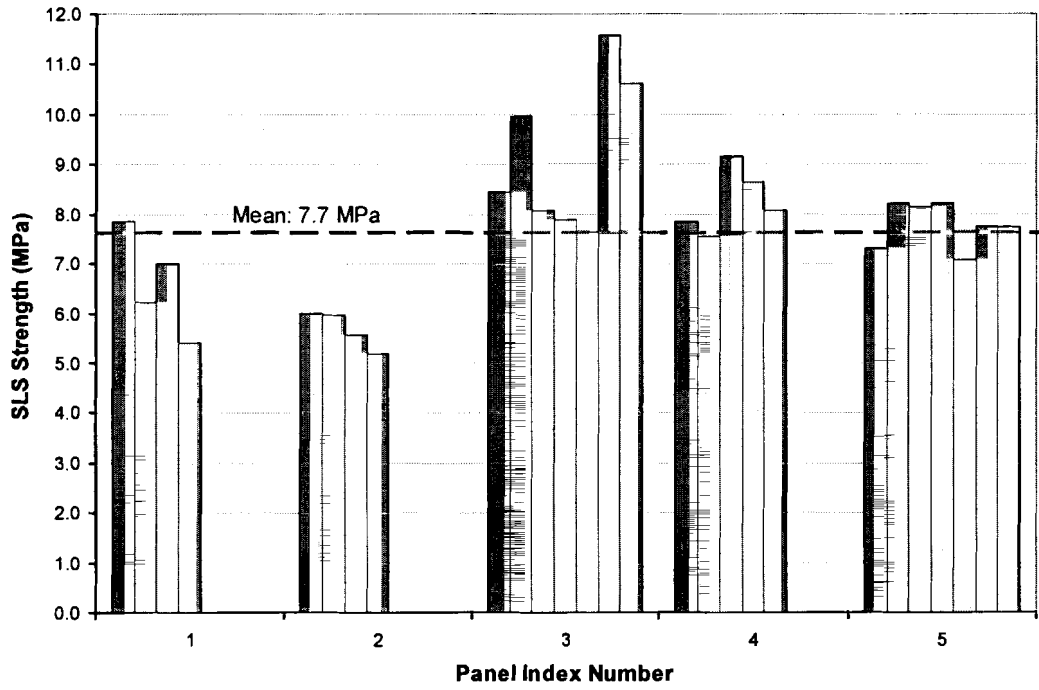


Figure 4.11 SLS Control Strength for Material System C

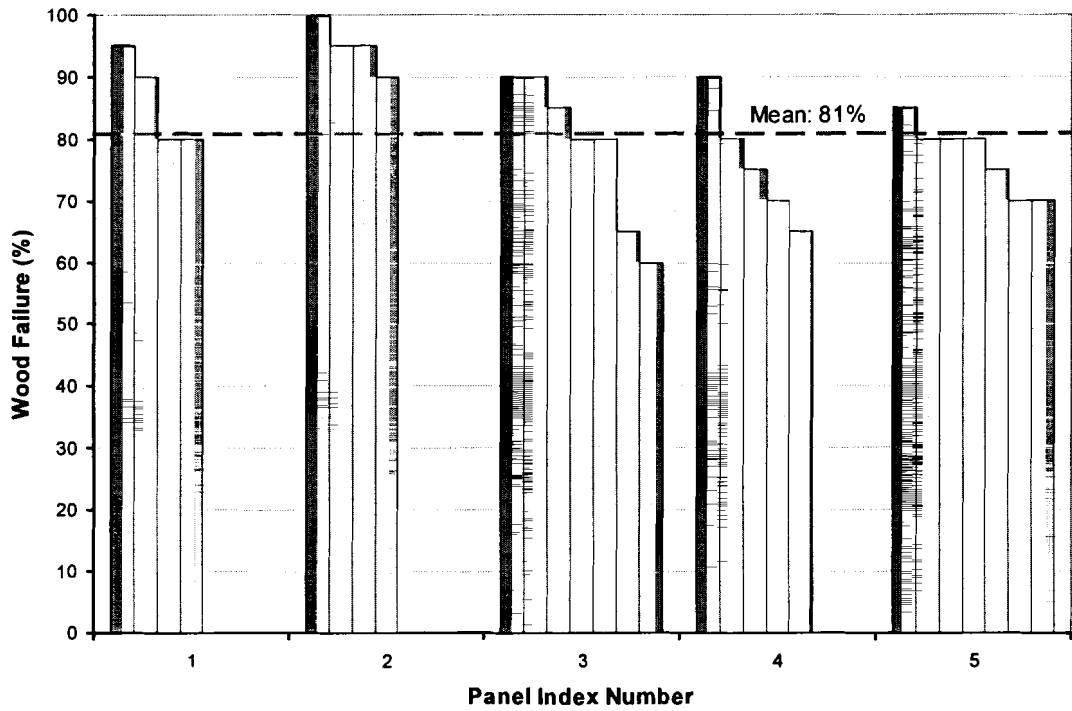


Figure 4.12 Percentage Wood Failure of Control Tests for Material System C

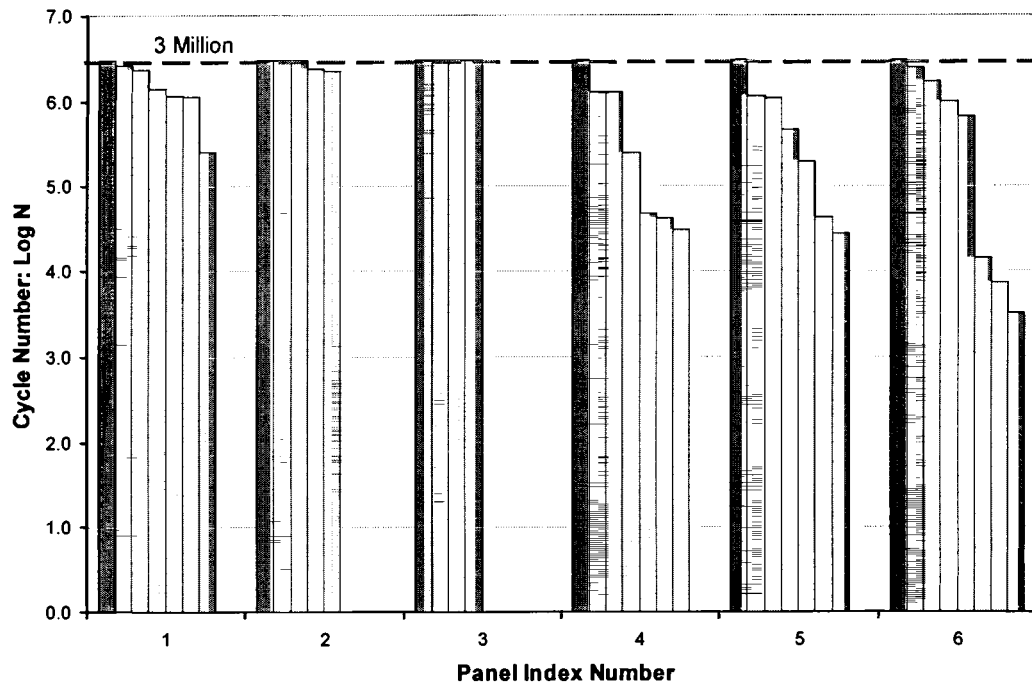


Figure 4.13 Applied Number of Fatigue Cycles for Material System B

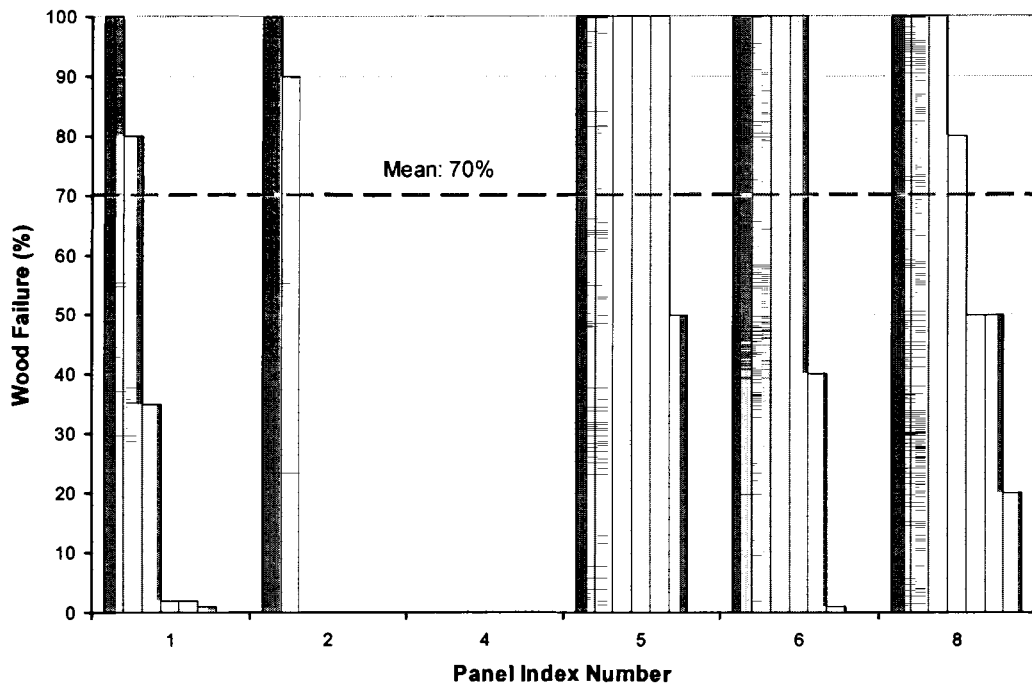


Figure 4.14 Percentage Wood Failure of Fatigue Tests for Material System B

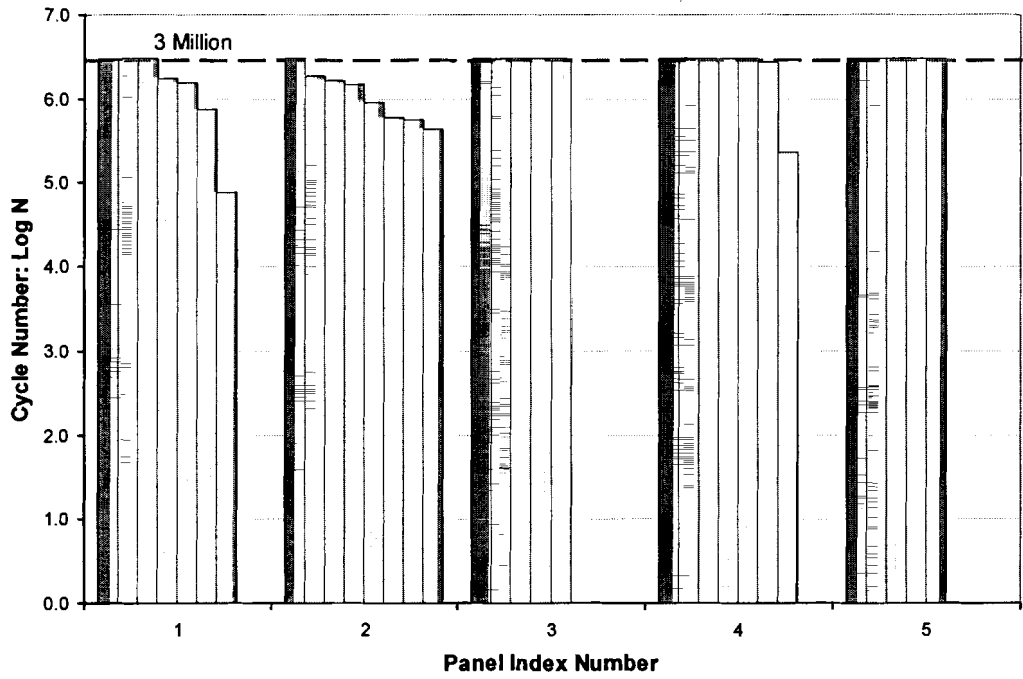


Figure 4.15 Applied Number of Fatigue Cycles for Material System C

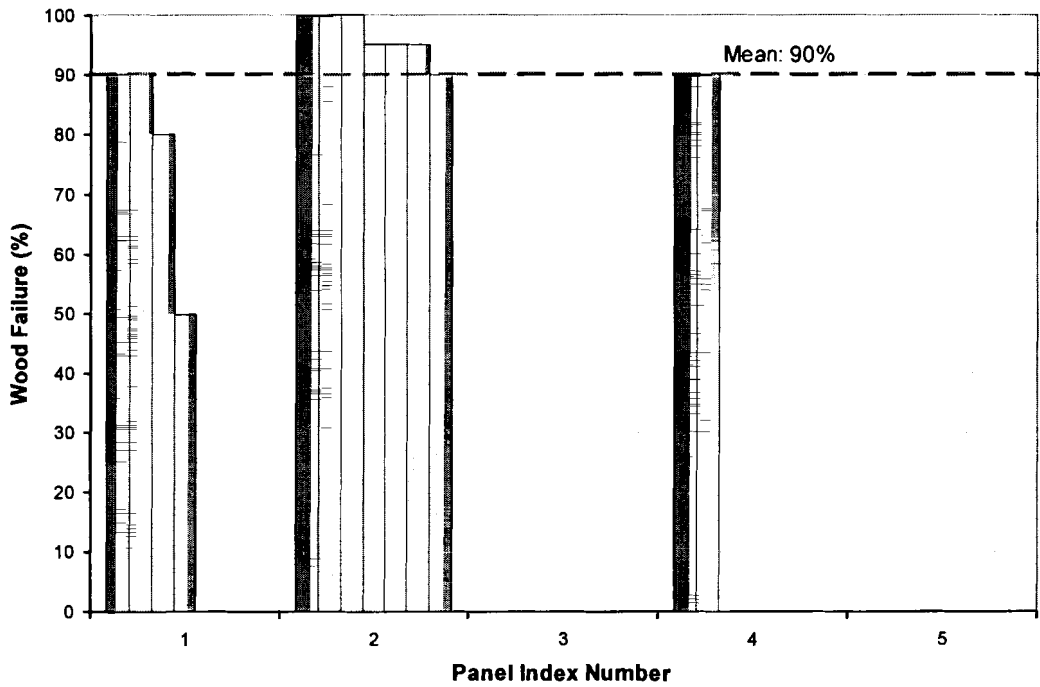


Figure 4.16 Percentage Wood Failure of Fatigue Tests for Material System C

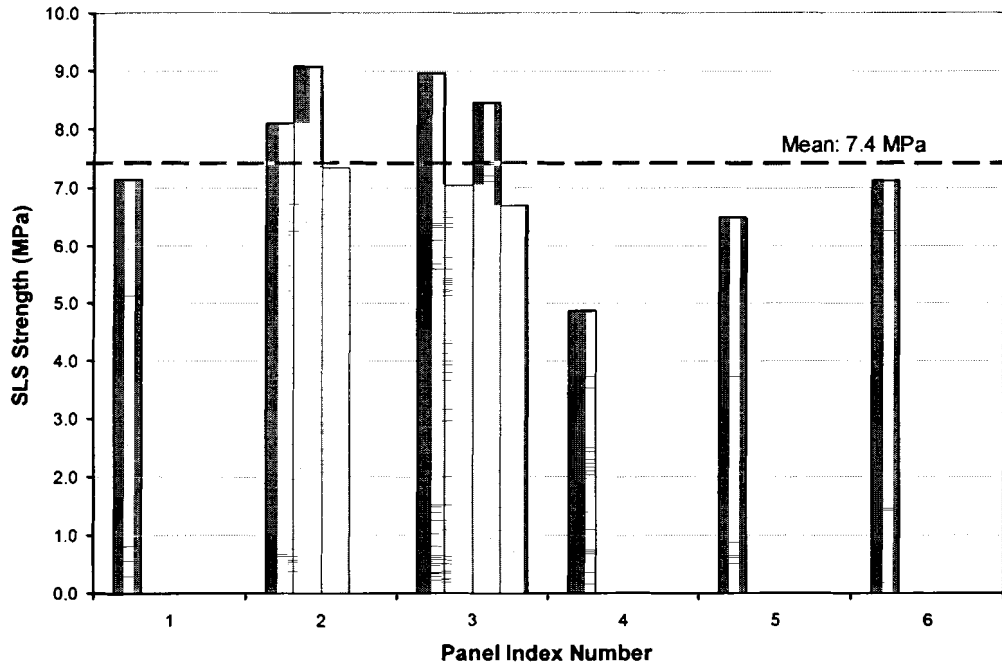


Figure 4.17 SLS Residual Strength Tests for Material System B

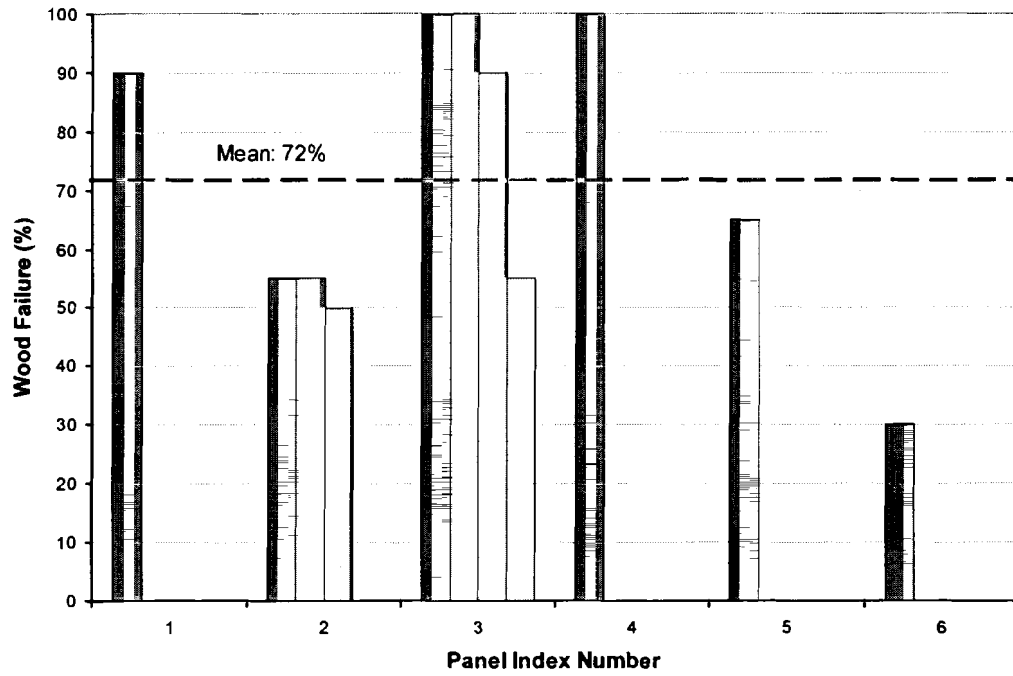


Figure 4.18 Percentage Wood Failure of Residual Strength Tests for System B

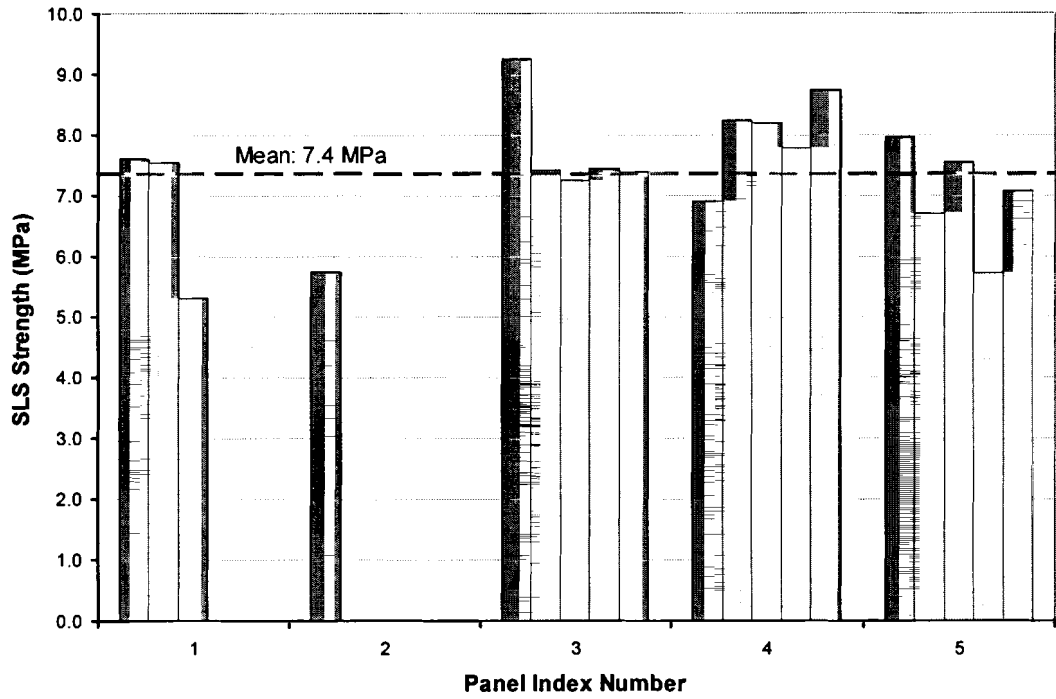


Figure 4.19 SLS Residual Strength Tests for Material System C

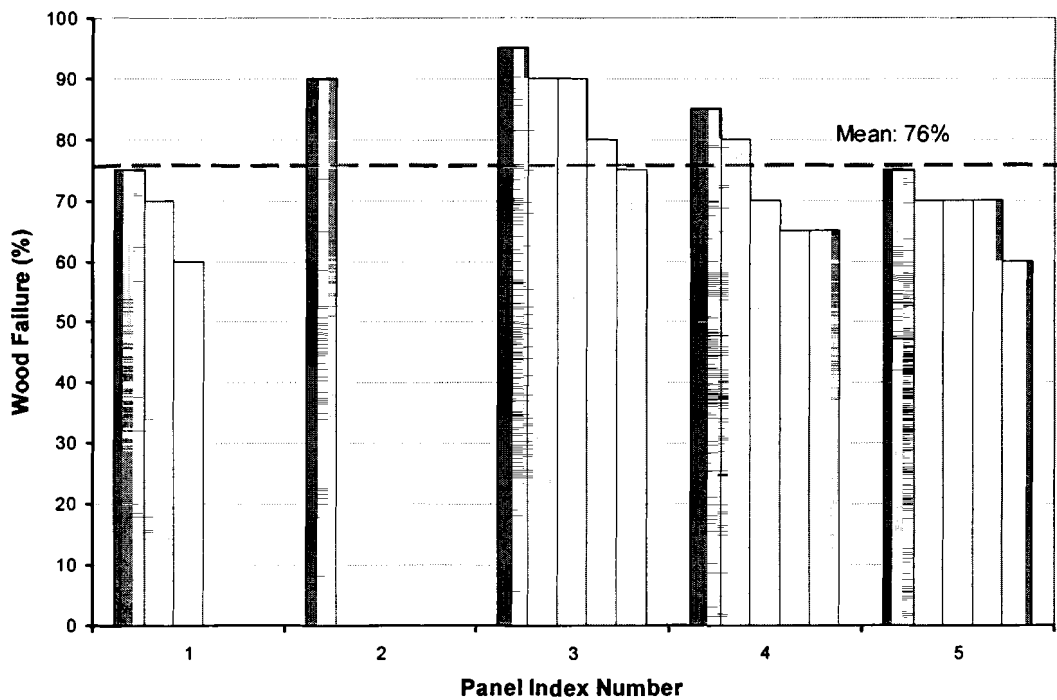


Figure 4.20 Percentage Wood Failure of Residual Strength Tests for System C

4.6.6 Analysis and Discussion of Experimental Results

To compare the results of material systems B and C, the same configuration and applied stress level were used in both systems. First, the result of unpaired t-Test showed that the difference of SLS control strength between system B and system C was significant, as shown in Table 4.5. Second, fewer specimens from system B (29%) passed 3 million fatigue cycles than those from system C (59%). Third, the average percentage of wood failure of system B was lower than that of system C. High wood failure usually indicates that quality bonding is achieved between wood and FRP. A few specimens from system B even had wood failure as low as 0%. However, almost all of the specimens from system C had relatively high wood failure (usually more than 90%). Forth, for system B, the single-lap shear fatigue properties of specimens from different panels have significant variations; even specimens from the same panel may have significantly different properties. For system C, the fatigue resistance was more uniform. Therefore, it may be assumed that the differences of fatigue properties between system B and system C are significant. Since the same specimen geometry, the same surface treatment and the same fabrication procedure were used, if it is assumed that the variations of wood, FRP and adhesive properties were the same, it may be assumed that the differences were due to the properties of material systems themselves.

The SLS control strength distribution for material systems B and C are shown in Figure 4.21 and Figure 4.22, respectively. If it is assumed that the observations follow a normal distribution, the normal probability plots can be used to check the normality assumption. The normal probability plots for system B and C from SYSTAT are shown in Figure 4.23 and Figure 4.24, respectively. There is no obvious problem with the normal distribution assumption for system B. For system C, a relatively significant

departure from normality was observed. However, since only a limited numbers of samples were tested, the statistical response was not fully characterized.

Table 4.5 Unpaired t-Test Result for Comparison of SLS Control Strength between Material System B and C

| t-Test: Two-Sample Assuming Equal Variances | | |
|--|--------------------|-------------------|
| | <i>Variable 1</i> | <i>Variable 2</i> |
| Mean | 6.898375266 | 7.739051031 |
| Variance | 1.711646926 | 2.233775603 |
| Observations | 24 | 27 |
| Pooled Variance | 1.988694795 | |
| Hypothesized Mean Difference | 0 | |
| df | 49 | |
| t Stat | -2.12494099 | |
| P(T<=t) one-tail | 0.019329814 | |
| t Critical one-tail | 1.676551165 | |
| P(T<=t) two-tail | 0.038659627 | |
| t Critical two-tail | 2.009574018 | |

The residual strength of test samples as affected by fatigue cycling was also investigated. The unpaired t-Tests were conducted for systems B and C to compare the SLS control strength with the residual strength, as shown in Table 4.6 and Table 4.7, respectively. From the analysis, no significant difference was observed. Therefore, it may be assumed that no significant difference between the results from the control tests and the residual strength tests, which means no damage accumulation due to fatigue tests.

Since most of the failure occurred in the wood substrates, it may be assumed that wood is the weakest material in this configuration. As mentioned in the literature review of Chapter 1, the fatigue strength of wood is actually much higher than that of crystalline materials when compared to the static strength limit of the substance in the bending and tension tests. However, this research shows that wood is weak to resist fatigue shear load by tension loading parallel to the fiber direction. Furthermore, if no damage accumulation

due to fatigue tests is assumed, it may be in turn assumed that the wood fatigue failure is brittle. Since most of the samples were observed to fail in the wood substrates during the fatigue tests, which are the desired fatigue failure mode, it may be assumed that quality bonding was achieved.

Table 4.6 Unpaired t-Test Result for Material System B

| t-Test: Two-Sample Assuming Equal Variances | | |
|--|---------------------|-------------------|
| | <i>Variable 1</i> | <i>Variable 2</i> |
| Mean | 6.881207103 | 7.383473315 |
| Variance | 1.782053618 | 1.497112779 |
| Observations | 23 | 11 |
| Pooled Variance | 1.693009606 | |
| Hypothesized Mean Difference | 0 | |
| df | 32 | |
| t Stat | -1.052991958 | |
| P(T<=t) one-tail | 0.150115614 | |
| t Critical one-tail | 1.693888407 | |
| P(T<=t) two-tail | 0.300231228 | |
| t Critical two-tail | 2.036931619 | |

Table 4.7 Unpaired t-Test Result for Material System C

| t-Test: Two-Sample Assuming Equal Variances | | |
|--|--------------------|-------------------|
| | <i>Variable 1</i> | <i>Variable 2</i> |
| Mean | 7.739051031 | 7.355708566 |
| Variance | 2.233775603 | 0.995111467 |
| Observations | 27 | 19 |
| Pooled Variance | 1.727049365 | |
| Hypothesized Mean Difference | 0 | |
| df | 44 | |
| t Stat | 0.974124176 | |
| P(T<=t) one-tail | 0.167660067 | |
| t Critical one-tail | 1.680230071 | |
| P(T<=t) two-tail | 0.335320134 | |
| t Critical two-tail | 2.0153675 | |

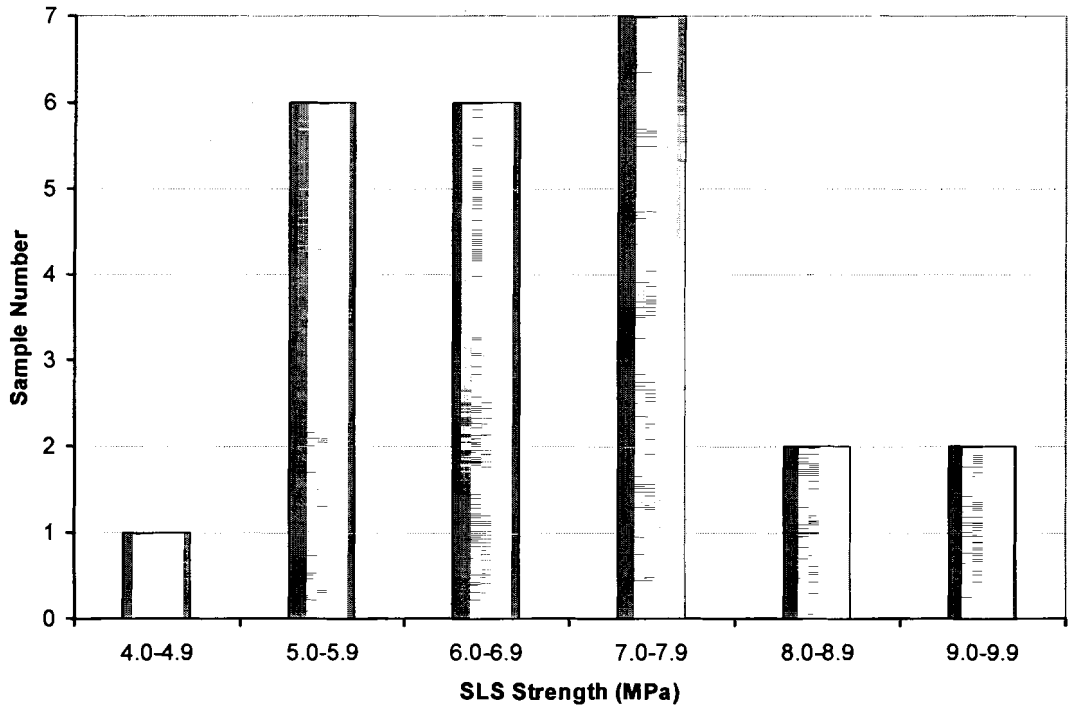


Figure 4.21 SLS Strength Distribution of Material System B

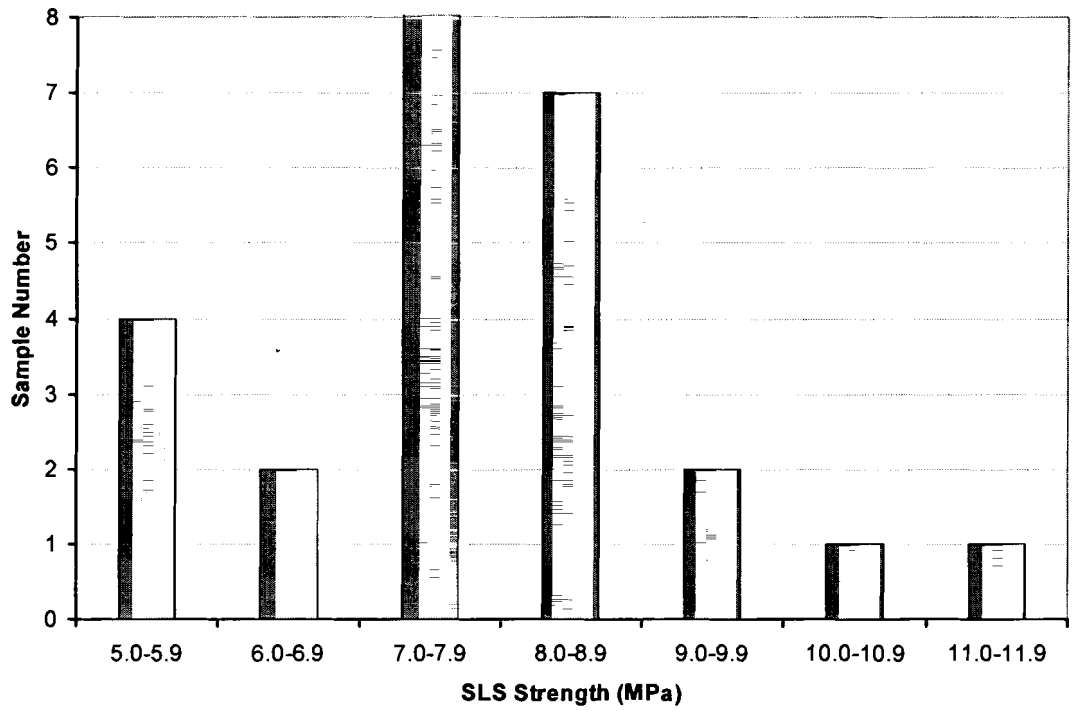


Figure 4.22 SLS Strength Distribution of Material System C

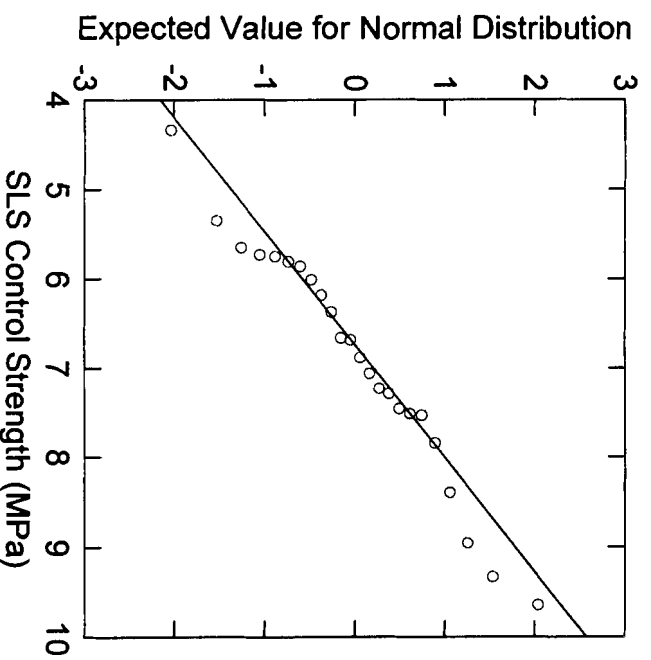


Figure 4.23 Normal Probability Plot of the SLS Control Strength for System B

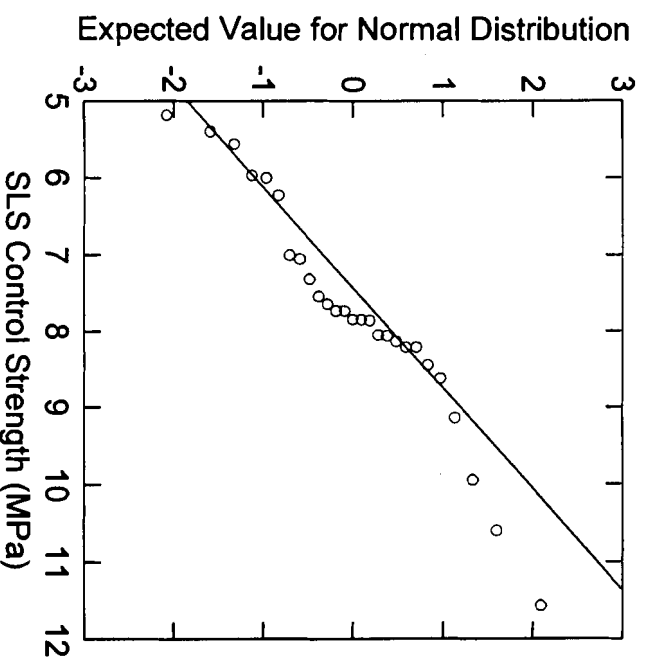


Figure 4.24 Normal Probability Plot of the SLS Control Strength for System C

The distribution of fatigue-cycle numbers for systems B and C are shown in Figure 4.25. More samples need to be tested to choose the minimum requirement of fatigue number with proper statistical reliability. From the test results, it was found that the slope of the curves in Figure 4.25 decreases considerably after 2 million load cycles. Based on this observation, the conventional number of fatigue cycles, 2 million, typical for bridge structures is considered acceptable for FRP-wood interfaces.

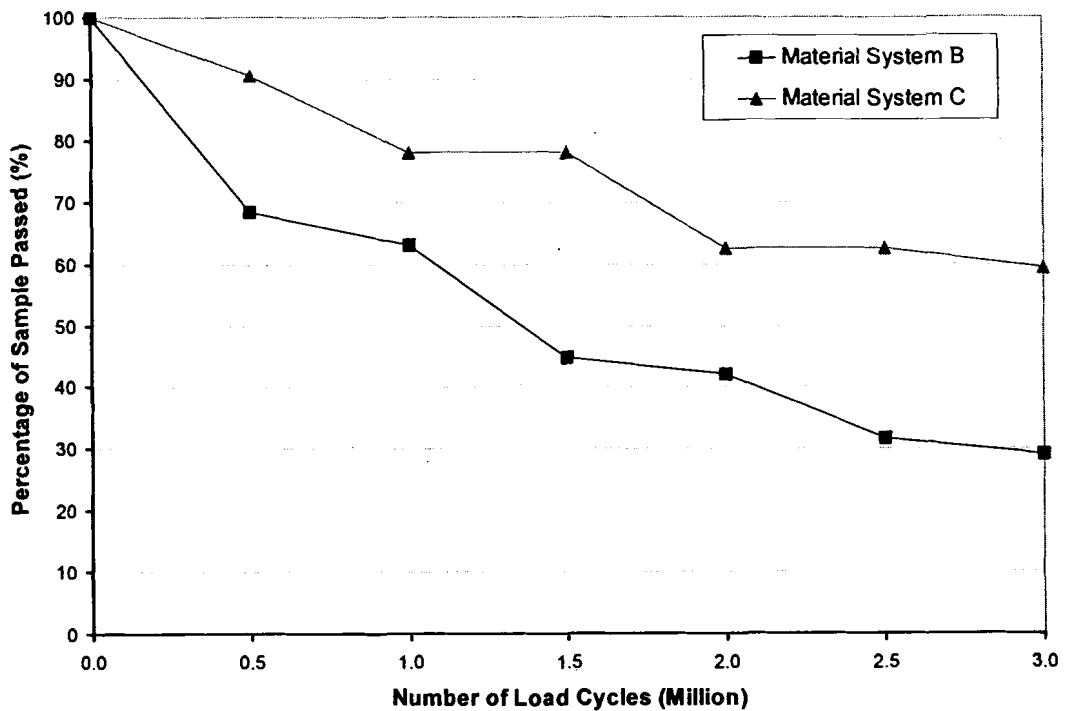


Figure 4.25 Distribution of Fatigue Test Results

Since the bonding strength between adhesive and wood was usually stronger than the wood strength, the crack usually formed at a point near that corner within the wood, and gradually propagated to the wood notch till failure. When the bonding strength was lower than the wood strength (such as high density wood), the cracks propagated along the FRP-wood interface and resulted in low wood failure percentage.

The correlations between the apparent SLS strength and the shear block strength reported in Chapter 2 for both material systems are listed in Table 4.8. The shear block strength is higher than the SLS strength for both material systems. In SLS test, the FRP-wood interface is subjected to the combination of the peeling stress and shear stress with high stress concentrations, as shown by the finite element analysis presented in Chapter 5. It is well known that the peel strength of an adhesive can be orders of magnitude less than its shear strength (Pocius 1997). It may be assumed that the existence of the peeling stress and stress concentrations weakened the apparent bonding strength.

Table 4.8 Correlations Between Shear Strength by Compression Loading and by Tension Loading

| Material System | Shear Strength MPa (COV %) | | Wood Failure (%) | |
|-----------------|----------------------------|-----------------|---------------------|-----------------|
| | Compression Loading | Tension Loading | Compression Loading | Tension Loading |
| B | 10.9 (9.4) | 6.9 (19.0) | 68 | 77 |
| C | 10.3 (4.1) | 7.7 (19.3) | 90 | 81 |

4.7 Basis for Fatigue Performance Criteria

Fatigue performance criteria can be based on the following considerations:

- 1) ASTM D2339 standard test procedure was modified and applied to evaluate fatigue performance of adhesively bonded FRP-wood single-lap shear specimens.
- 2) Single-lap shear control tests were conducted with a loading rate of 3.5 kN/min to evaluate SLS control strength.
- 3) The SLS control strength and percentage wood failure were correlated with those of shear by compression loading (shear block).

- 4) Fatigue tests were conducted in load-controlled mode with constant load amplitude. Two million load cycles were applied to the samples at one stress level, which was determined by 50% of SLS control strength. A cyclic frequency of 20 Hz was adopted. The ratio between maximum and minimum load was $R = 0.1$.
- 5) Residual strength was evaluated with a loading rate of 3.5 kN/min for the specimens survived after 2 million load cycles.
- 6) Percentage of wood failure was evaluated for control tests, fatigue tests and residual tests.

The following experimental findings can be used as a preliminary basis for fatigue performance criteria. However, the author recognizes that the experimental results are limited to two material systems, and evaluation of other material system is required to establish performance limits or recommendations.

- 1) The ratios of single-lap shear control strength to shear block strength obtained from the two material systems tested were ranged from 0.63 to 0.75.
- 2) The ratios of minimum numbers of surviving specimens after 2 million cycles to the total sample number for cyclic fatigue tests obtained from the two material systems tested were ranged from 0.42 to 0.62.
- 3) The residual strength should not be statistically less than the control strength.
- 4) The mean percentage of wood failure for control tests, fatigue tests and residual tests obtained from the two material systems tested were ranged from 77% to 81%.

4.8 Conclusions and Recommendations

A standard ASTM test method was modified and applied successfully to evaluate fatigue performance of adhesively bonded FRP-wood single-lap shear specimens. The corresponding fatigue performance-based evaluation criteria and associated limits were proposed. Two material systems were evaluated: system B and C. This fatigue test is necessary but not enough to characterize the FRP-wood interface. The advantage of this test is that the interface is subjected to cyclic stress. The disadvantage of this test is the stress concentrations at the notches. Besides, this test does not provide actual material property but an apparent property that depends on a complex stress state including both shear and peeling. However, in actual glulam beam, there is also a complex stress state including both shear and peeling. The main contribution of this study is to establish a protocol to apply single-lap shear under fatigue loading to evaluate FRP-wood interfaces.

Based on the research findings presented in this chapter, the following conclusions are drawn:

- 1) It was shown that material system C presented stronger bonding strength and better fatigue resistance than system B when tested in single-lap shear configuration. Quality bonding was observed for both material systems in terms of high percentage of wood failure.
- 2) Since no statistically significant difference was observed between the control strength and the residual strength for both material systems, it may be assumed that there was no damage accumulation due to fatigue tests.

The following recommendations are suggested:

- 1) Since both material systems B and C passed the delamination tests and shear block tests, ASTM D2559 alone is not sufficient to discriminate the differences between them. Furthermore, performance evaluation tests presented in Chapter 2 are not sufficient to predict whether a bonded interface has good fatigue resistance. Therefore, single-lap shear fatigue tests are considered necessary to evaluate performance requirements of FRP composite reinforcement systems for glulam in highway bridge applications.
- 2) Wood bonding properties (strength and wood failure) are highly dependent on the density of the wood. To evaluate the effects, sample groups with different wood densities should be tested. Within each group, wood lumber should have similar densities and surface pattern to minimize the variation of experimental results.
- 3) The desired SLS strength of an eligible FRP-wood specimen should be controlled by the shear strength of wood parallel to the grain, which is indicated by high wood failure.
- 4) To investigate the effects of possible adhesive strength change due to the post-curing with time, 50% of quasi-static control tests should be conducted after fatigue tests.
- 5) If most of the specimens passed 3 million cycles (e.g., 75%), it may be necessary to increase the stress level to get the information of fatigue failure mode (e.g., the percentage of interface wood failure).
- 6) Since the overlap area is subjected to the shear stresses as well as peel stresses, the fatigue failure process was a process of fracture under the combination of Mode I (Opening Mode) and Mode II (Forward Shear Mode). Therefore, the Mode I fracture toughness may control the overall single-lap shear strength. Thus, the Mode I fracture

toughness study presented in Chapter 6 should also be considered as an important indicator of fatigue resistance of FRP-wood bonding.

Chapter 5

FINITE ELEMENT ANALYSIS OF SINGLE-LAP SHEAR SPECIMEN UNDER TENSION LOADING

5.1 Summary

The quasi-static tests of FRP-wood single-lap shear specimen by tension loading were modeled using 2-D linear elastic Finite Element Analysis (FEA). Finite element simulations were carried out by using ANSYS. Numerical predictions of peeling and shear stress distribution along the overlap area were correlated to the experimental results. The stress condition of the FRP-wood interface can be characterized by the ratio of the average peeling stress to the average shear stress of the adhesive surface. The lower this ratio, the less peeling stresses are developed, and consequently, the more desirable the stress field results. It was found that elastic modulus of adhesives have significant influence on the stress conditions of the single-lap shear configuration. The failure mode prediction from the finite element models matched well with fatigue experiments, which shows that the cracks always started at a point near the FRP notch.

5.2 Introduction

The theoretical analysis of the single-lap joint has been conducted for over 60 years. Since the 1970s, the finite element method (FEM) has been increasingly used to study the adhesively bonded single-lap joint. It has been proven to be a powerful tool to obtain stress and strain distributions along a loaded joint.

Significant efforts of many researchers have been dedicated to study the behavior of all kinds of single-lap joints. Their work can be subdivided into several categories: materially linear elastic or non-linear; geometrically linear or nonlinear; balanced joints (with two identical adherends) or bi-material hybrid joints; two dimensional or three dimensional; adherends with square edges or with optimized shapes; adhesive layer with or without spew fillets; adhesive/adherend interface with or without cracks (based on fracture mechanics); analysis based on or not based on stress singularity parameters, etc.

5.3 Objective and Scope

The objective of this chapter is to develop a FE model to investigate peeling and shear stress distributions on FRP-wood interfaces of single-lap shear specimens by tension loading. The influence of material properties on the stress concentrations are also evaluated, and the analysis results are correlated with the experimental results of FRP-wood single-lap shear fatigue tests described in Chapter 4.

5.4 Literature Review

A combined experimental and analytical study was conducted to evaluate the single-lap shear specimen (Guess *et al.* 1977). Two structural adhesives were tested with both the conventional thin adherend configuration and thick adherend configuration. It was found that failure of thin specimens was controlled by the peeling strength of the adhesive/adherend interface rather than by the adhesive shear strength. It was also found that apparent shear strengths of the two adhesives measured with thin specimens were

opposite the results from thick specimens. FEA of the shear and normal stress gradients was used in the adhesive layer to explain this anomaly.

A comprehensive review of the strength prediction methods for lap joints was presented, especially with composite adherends (Adams 1989). Classical linear elastic solutions of the lap joint problems were discussed as well as the more advanced versions of the same type. Local stress concentrations at discontinuities were also discussed. Finite element techniques were shown to be the best way of treating the non-linear mechanics and material behavior in real joints, which can be used not only to predict the strength of joints but also the failure mode.

An experimental program was performed to evaluate the ultimate shear strength, bond-interface integrity, and percentage of wood failure of adhesive-bonded FRP-wood interface under dry and wet conditions (Gardner *et al.* 1994). Dry and water-saturated FRP-wood shear block tests were conducted following a modified ASTM D 905 testing procedure to evaluate shear strength and percent wood failure of FRP-wood interfaces. A 3-D finite element model was developed to analyze the stress of the FRP-wood bond interface under dry and wet conditions (Barbero *et al.* 1994). The adhesive layer was not considered in the simulation. With the exception of the supports, it was found that the shear stress is quite uniform at the bond interface. It was also found that the mechanical and moisture load effects can be treated approximately as linearly cumulative.

The single-lap joint is well known to be the most sensitive to changes in geometrical parameters. It is also well known that there are discontinuities of material and geometry at the overlap region. These discontinuities cause singularities in the stress fields near the vertex of the bonding edges and very high stress concentrations. A study

of the shape optimization of bi-material single-lap joints was performed (Hu *et al.* 1998). First, the free-edge stress singularity and condition for its disappearance near the vertex of bonding edges were investigated theoretically. Then, Bezier function was used to represent the geometrical boundary shape for design. The influences of material properties, lap length and critical value of intensity of stress singularity on the strength and optimum design shapes were discussed.

Spew (or fillet) is defined as the portion of adhesive that is squeezed out from the lap area and forms a bead at the lap ends as the two substrates are assembled. Spew is always present in an adhesive joint, but is usually neglected in the stress analysis of adhesively bonded joints. The presence of spews can reduce peak stresses and therefore increase the joint strength. The reduction in peak stresses is related to the shape and size of the spew. The effect of spew geometry on the peak stresses and stress distributions was investigated in epoxy bonded E-glass/vinylester composite single-lap joints (Lang and Mallick 1998). A linear 2-D plain strain analysis with isotropic materials was performed using ANSYS. The stress distributions and peak stresses across the lap length at the interface for joints with different spew geometries was determined and compared to those of the square ended single-lap joints. It was shown that the stress concentrations can be significantly reduced by shaping the spew to provide a smoother transition in joint geometry.

A geometrically nonlinear, 2-D FEA was performed to determine the stress and strain distributions across the adhesive thickness for laminated composite single-lap joints without spew fillets (Li *et al.* 1999). It was found that both the peeling and shear stresses at the bond free edges changed significantly across the adhesive thickness. It was

also observed that the peak shear and peeling stresses increased with the bond thickness and adhesive elastic modulus. In a subsequent research, FEA was used to investigate the behaviors of balanced single-lap joints (Li and Lee-Sullivan 2001). The effects of following factors were compared: (i) plane stress and plane strain conditions; (ii) simply supported and fully fixed boundary conditions; (iii) filleted and unfilleted overlap end geometries; and (iv) different adhesives.

One parameter governing the strength of the adhesive joints is the concentrated stress distribution due to the stress singularity at the corners of the adhesive/adherend interface. Recently, stress-singularity parameters have been used to evaluate the strength of adhesive joints. 2-D FEA was conducted for CFRP/Aluminum thick adherend single-lap joints with spew fillets and several other lap shear configurations (Ishii *et al.* 1999). An evaluation method was developed for the fatigue endurance limit based on two stress-singularity parameters and verified it experimentally by fatigue tests.

Three-dimensional viscoplastic analysis of adhesively bonded single lap joint with square edges was performed, considering material and geometric nonlinearity (Pandey and Narasimhan 2001). A comprehensive literature review of both the analytic and the FE technique was also performed for studies on 2-D and 3-D single lap joint model. Steel was used as the adherend. The adhesive layer was modeled as elasto-viscoplastic and adherend as linearly elastic. Observations had been made in particular on peeling and shear stresses in the adhesive layer. The results were compared among different types of analysis of 2-D and 3-D models. It was found that viscoplastic analysis gave the reduced stresses at the end of overlap than the elastic solution. It was also found that peeling stress values were close to plane strain at the edges. It was concluded that 3-

D analysis showed significantly different distributions of stresses from the plane strain analysis away from the central region. 3-D analysis was recommended for behavioral study and joint design specimen configuration.

Special 2-D and 3-D adhesive elements were developed for geometrical nonlinear FEA of adhesively bonded single-lap joints (Andruet *et al.* 2001). In the 2-D analysis, adherends were represented by Bernoulli beam elements with axial deformation and the adhesive layer by plane stress or plane strain elements. The 3-D elements consist of shell elements that represent the adherends and solid brick elements to model the adhesive. This technique resulted in small models with faster convergence than conventional 3-D models. This model can include debonds as well as cracks within the adhesive. Therefore, it can be used for durability analysis of adhesive joints.

Experiments on single-lap composite joints showed that fracture of the bondline was a primary mechanism under both static and fatigue loadings. A geometrically nonlinear model was developed to study stress fields in single-lap adhesively bonded composite joints containing cracks of different lengths (Kayupov and Dzenis 2001). It was observed that stresses, energy release rates and stress intensity factors varied nonlinearly with the crack length, but there was a near-linear relationship between the stress intensity factors and the load for cracks of constant length. It was also found that the critical energy release rates for fast crack propagation in the final stage of fatigue life were 2-3 times lower than those for the cracks propagating under quasi-static loading.

5.5 Element Type

FRP-wood single-lap shear specimens were modeled using a 2-D Structural Solid element called PLANE42 (ANSYS 2001). This is a four-node plane element (plane stress or plane strain) with two degrees of freedom at each node: translations in the nodal x and y directions. Since the interesting area is the adhesive layer at the overlap area, and the adhesive width is large compared to its thickness and should provide lateral restraint to the adhesive, it may be assumed that the front and rear faces of an element are fully restrained against displacement. Therefore, the plane strain option of the PLANE42 element was used in the modeling, as shown in Figure 5.1. It is assumed that no normal strain in the z direction and no shear strains in the xz and yz planes.

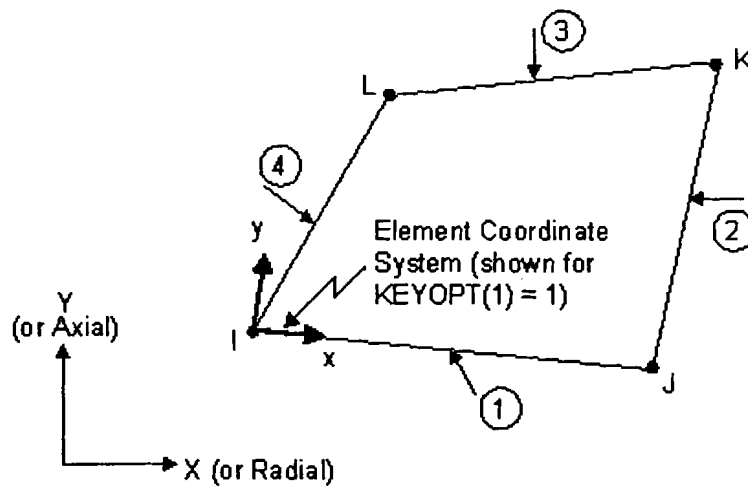


Figure 5.1 Element Type: PLANE42(ANSYS 2001)

5.6 Material Properties

5.6.1 Wood

The wood is structural selected grade, quarter sawn Douglas fir. It is modeled as a linear elastic orthotropic material. From the tensile tests, $E_L = 12000$ MPa. The elastic properties of softwoods can be predicted as functions of E_L (FPL 1999). For Douglas fir with $E_L = 12000$ MPa, $E_R = 820$ MPa, $E_T = 600$ MPa, $G_{LR} = 770$ MPa, $G_{LT} = 940$ MPa, $G_{RT} = 80$ MPa. The Poisson's ratios for Douglas fir at approximately 12% moisture content were also got from the wood handbook (FPL 1999), which are listed in Table 5.1. According to the coordinates of this FE analysis, the axis L, T and R are equivalent to axis x, y and z, respectively.

5.6.2 FRP

Material System C is a unidirectional GC-67-UB E-glass/epoxy composite sheet material fabricated by continuous lamination process and provided by Gordon Composites, Inc. The average thickness is 6.3 mm. It is modeled as a linear elastic orthotropic material. The longitudinal and transverse modulus of this material were obtained from ASTM D3039 tensile tests, which are $E_L = 36000$ MPa and $E_T = 10100$ MPa, respectively. The in-plane Poisson's ratio is 0.30, which was also obtained from ASTM D3039 tensile tests. The out-of-plane Poisson's ratio calculated based on micromechanics of composite materials is 0.84, which is not reasonable. Therefore, the out-of-plane Poisson's ratio is assumed to be the same value as that of in-plane. The in-plane shear modulus is 3300 MPa, which was obtained from ASTM D5379 V-notched shear tests. The out-of-plane shear modulus was calculated based on micromechanics of composite materials, which is 2700 MPa. According to the coordinates of this FE

The adhesive used in Material System C is two-part (liquid/liquid) epoxy adhesive G3 provided by Gougeon Brothers, Inc. It has two components: XR 01-113-53C resin and XH 01-113-53-D hardener. It was modeled as a linear elastic isotropic material. The elastic modulus was obtained from tensile tests, which is $E = 2900$ MPa. The thickness of the adhesive layer was assumed to be 0.2 mm. The Poisson's ratio is assumed to be 0.4 based on the literature reviews. The properties are listed in Table 5.1.

Table 5.1 Material Properties Used in Finite Element Analysis

| Materials | E (MPa) | G (MPa) | Poisson's Ratio |
|-----------------------------------|---------------------|--------------------------|------------------------------|
| Wood: Quarter Sawn Douglas fir | $E_x = 12000$ | $G_{xy} = 940$ | $\nu_{xy} = 0.45$ |
| | $E_y = 600$ | $G_{yz} = 80$ | $\nu_{yz} = 0.39$ |
| | $E_z = 820$ | $G_{xz} = 770$ | $\nu_{xz} = 0.29$ |
| Adhesive: Urethane | $E = 540$ | - | $\nu = 0.40$ |
| Adhesive: Epoxy | $E = 2900$ | - | $\nu = 0.40$ |
| FRP: E-glass/urethane sheet | $E_x = 43600$ | $G_{xy} = G_{xz} = 3700$ | $\nu_{xy} = \nu_{xz} = 0.30$ |
| | $E_y = E_z = 13100$ | $G_{yz} = 3400$ | $\nu_{yz} = 0.30$ |
| FRP: E-glass/epoxy sheet | $E_x = 36000$ | $G_{xy} = G_{xz} = 3300$ | $\nu_{xy} = \nu_{xz} = 0.30$ |
| | $E_y = E_z = 10100$ | $G_{yz} = 2700$ | $\nu_{yz} = 0.30$ |

5.7 Boundary Conditions

The boundary conditions were shown in Figure 5.2. On the left end of the specimen, each node was defined as a hinge which was fixed both in x and y directions. On the right end of the specimen, each node was defined as a roller, which was fixed in y direction and was applied a 0.1 mm displacement in x direction to generate the horizontal tensile force.

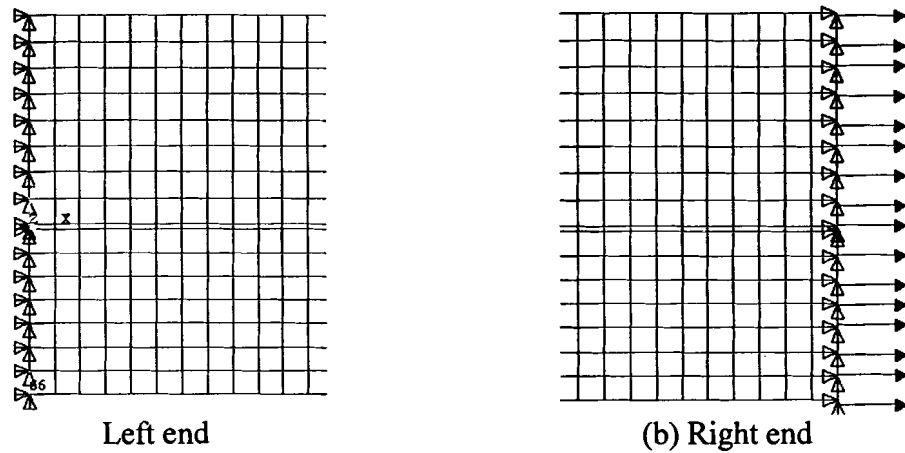


Figure 5.2 Boundary Conditions Used in Finite Element Analysis

5.8 Element Meshing

The automatic area mesh function in ANSYS 5.7 was used. Four mesh sizes of rectangular elements were used in the adhesive layer to conduct the convergence study, as shown in Table 5.2. The thickness of the adhesive layer was 0.2 mm. Mesh 1 has only one element along the adhesive thickness, which assumed that the stress distribution is identical across the adhesive layer thickness. Mesh 2, 3 and 4 have 2, 3, and 4 elements along the adhesive thickness respectively, which can be used to investigate the stress distribution across the adhesive thickness. A detailed schematic of the four mesh sizes of the adhesive layer in the overlap area is shown in Figure 5.3.

Table 5.2 Meshing Parameters of the Four Different Meshes of FEA

| Mesh | No. of Elements | No. of Nodes | Adhesive Layer in the Overlap Area | | |
|------|-----------------|--------------|------------------------------------|----------------------------------|-------------------------------------|
| | | | Element length (mm) | No. of elements along the length | No. of elements along the thickness |
| 1 | 4283 | 4611 | 0.25 | 102 | 1 |
| 2 | 17533 | 17957 | 0.125 | 204 | 2 |
| 3 | 24020 | 24548 | 0.083 | 307 | 3 |
| 4 | 30527 | 31156 | 0.0625 | 407 | 4 |

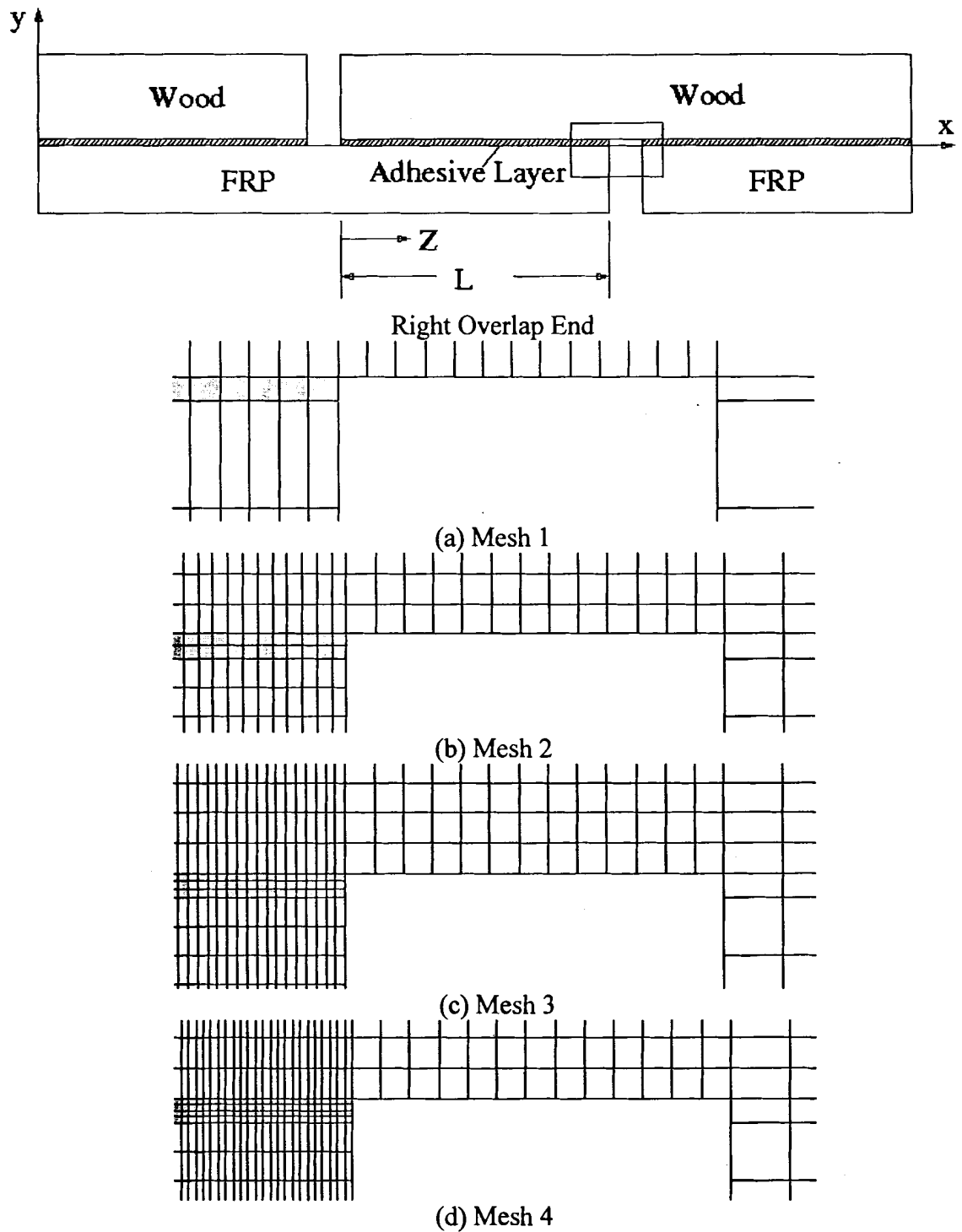


Figure 5.3 Schematic of Mesh Refinement at the Right Overlap End (Box Area)

5.9 Convergence Study

The principal results sought were the shear and peeling (normal) stress distributions along the adhesive layer in the overlap area. All of the stresses presented in the figures have been normalized by dividing the calculated values by the average shear stress, to get the shear and peeling stress concentration factors. The average shear stress is defined as the applied tensile load divided by the overlap area. The stress distribution along the bond line of length L is normalized in terms of z/l , which is the coordinate position along the joint.

The maximum values of the shear and peeling concentration factors calculated from the four mesh sizes are summarized in Table 5.3 and Table 5.4 for material system B and C, respectively. Since both of the stress concentration factors occurred at the corners at the end of the overlap area, the values of top left corner (TL), top Right corner (TR), bottom left corner (BL) and bottom right corner (BR) are listed in the table. The mesh convergence results of the maximum stress concentration factors are shown in Figure 5.4 to Figure 5.7. The mesh convergence results of the stress concentration factors at the end of the overlap are shown in Figure 5.10 to Figure 5.17.

The sums of peeling forces and compressive forces at the adhesive-adherend interface were calculated from the nodal forces, which are summarized in Table 5.5 and Table 5.6 for material system B and C, respectively. The tensile load for each mesh was also listed in the tables, which was calculated from the reactions. The mesh convergence results are shown in Figure 5.8 and Figure 5.9 for material system B and C, respectively.

Table 5.3 Stress Concentration Factors for Material System B

| Mesh | Peeling Stress Concentration Factors | | | | Shear Stress Concentration Factors | | | |
|------|--------------------------------------|------|------|------|------------------------------------|------|------|------|
| | TL | TR | BL | BR | TL | TR | BL | BR |
| 1 | 3.55 | 2.58 | 3.55 | 2.58 | 1.34 | 3.14 | 1.34 | 3.14 |
| 2 | 3.10 | 5.51 | 4.75 | 2.87 | 1.34 | 3.25 | 1.66 | 3.06 |
| 3 | 2.74 | 7.94 | 5.82 | 2.02 | 1.37 | 3.33 | 1.82 | 2.94 |
| 4 | 2.53 | 9.64 | 6.64 | 1.78 | 1.37 | 3.49 | 1.95 | 2.92 |

Table 5.4 Stress Concentration Factors for Material System C

| Mesh | Peeling Stress Concentration Factors | | | | Shear Stress Concentration Factors | | | |
|------|--------------------------------------|-------|-------|------|------------------------------------|------|------|------|
| | TL | TR | BL | BR | TL | TR | BL | BR |
| 1 | 4.92 | 2.56 | 4.92 | 2.56 | 1.84 | 4.26 | 1.84 | 4.26 |
| 2 | 3.44 | 6.43 | 7.05 | 3.25 | 1.76 | 4.51 | 2.26 | 3.77 |
| 3 | 3.04 | 9.92 | 8.72 | 2.12 | 1.71 | 5.08 | 2.64 | 3.59 |
| 4 | 3.02 | 12.75 | 10.07 | 1.86 | 1.69 | 5.67 | 2.96 | 3.53 |

Table 5.5 Surface Nodal Forces of the Adhesive Layer and Tensile Loads for Material System B

| Mesh | Nodal Forces (N/mm) | | | | Tensile Load (N/mm) |
|------|---------------------|-------------|----------------|-------------|---------------------|
| | Top Surface | | Bottom Surface | | |
| | Peeling | Compressive | Peeling | Compressive | |
| 1 | 45.04 | 59.79 | 45.04 | 59.79 | 126.31 |
| 2 | 44.87 | 59.57 | 44.86 | 59.56 | 125.39 |
| 3 | 45.18 | 59.88 | 45.08 | 59.77 | 125.36 |
| 4 | 44.95 | 59.65 | 44.80 | 59.50 | 125.35 |

Table 5.6 Surface Nodal Forces of the Adhesive Layer and Tensile Loads for Material System C

| Mesh | Nodal Forces (N/mm) | | | | Tensile Load (N/mm) |
|------|---------------------|-------------|----------------|-------------|---------------------|
| | Top Surface | | Bottom Surface | | |
| | Peeling | Compressive | Peeling | Compressive | |
| 1 | 45.79 | 59.94 | 45.79 | 59.94 | 128.20 |
| 2 | 45.28 | 59.66 | 45.24 | 59.63 | 126.61 |
| 3 | 45.48 | 59.87 | 45.46 | 59.85 | 126.59 |
| 4 | 45.33 | 59.72 | 45.24 | 59.64 | 126.62 |

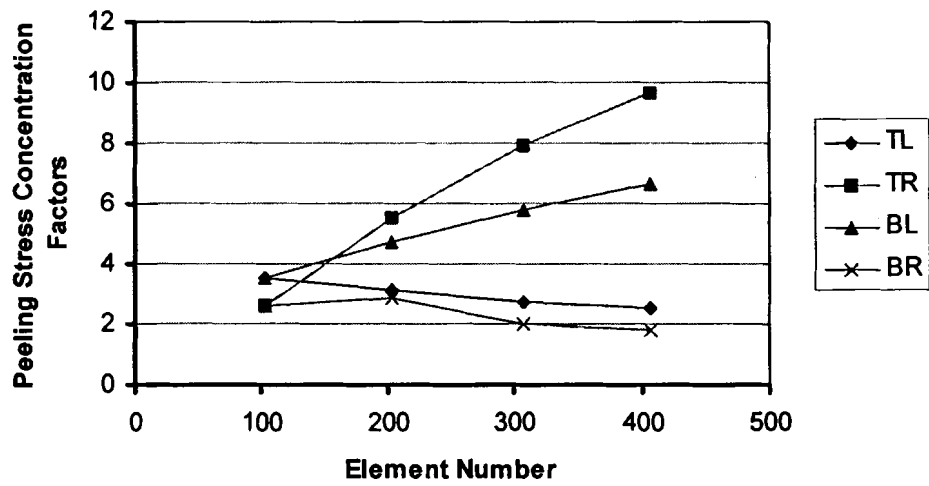


Figure 5.4 Mesh Convergence for Peeling Stress Concentration Factors Loads for Material System B

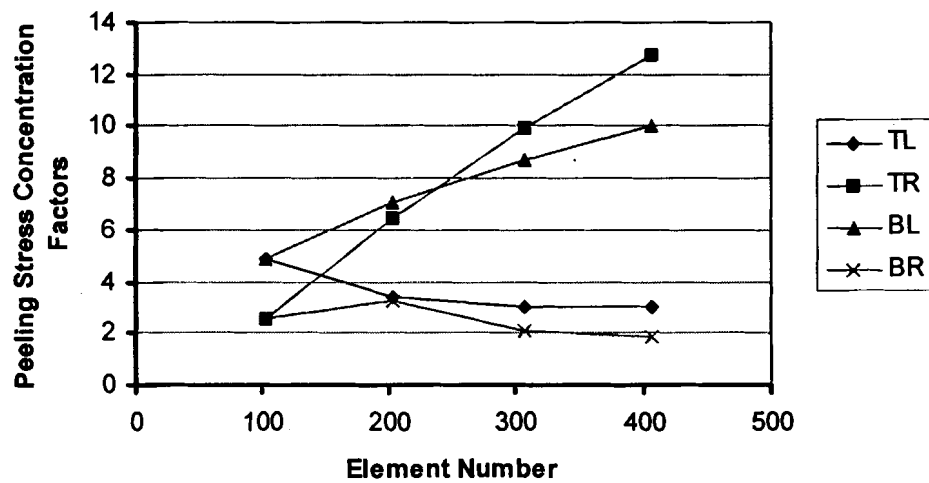


Figure 5.5 Mesh Convergence for Peeling Stress Concentration Factors Loads for Material System C

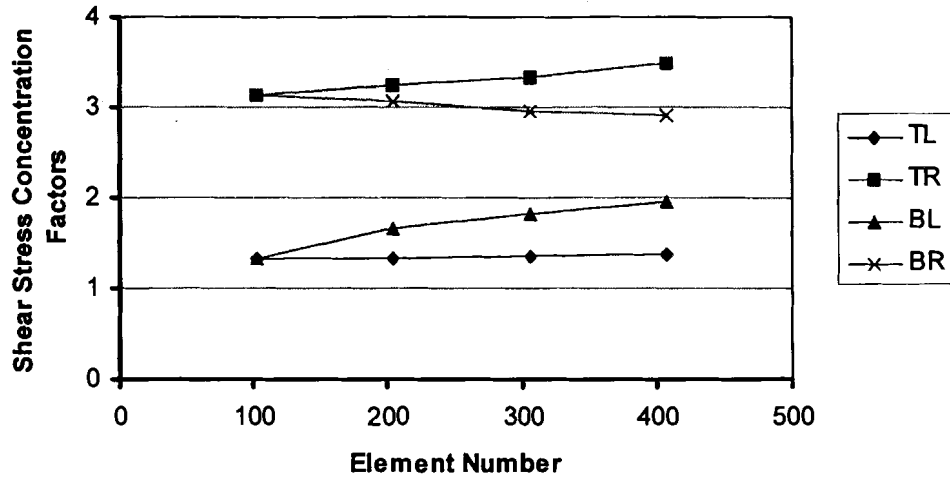


Figure 5.6 Mesh Convergence for Shear Stress Concentration Factors Loads for Material System B

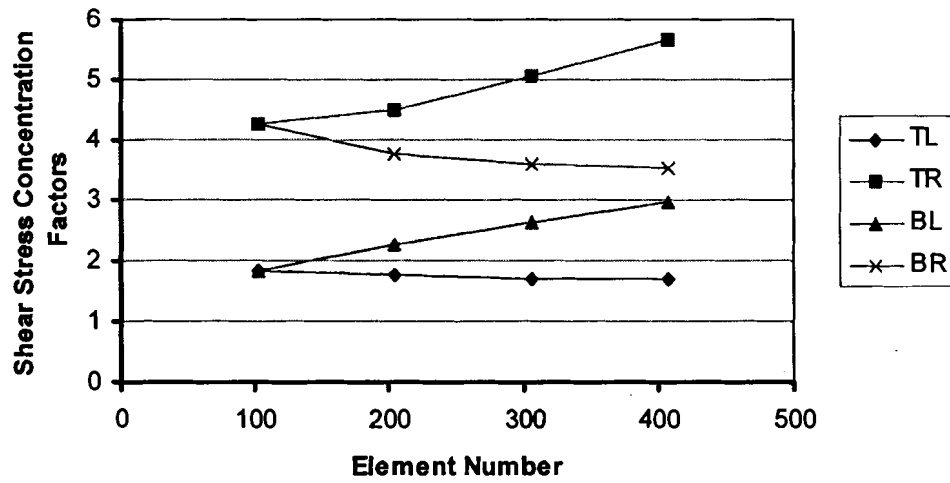


Figure 5.7 Mesh Convergence for Shear Stress Concentration Factors Loads for Material System C

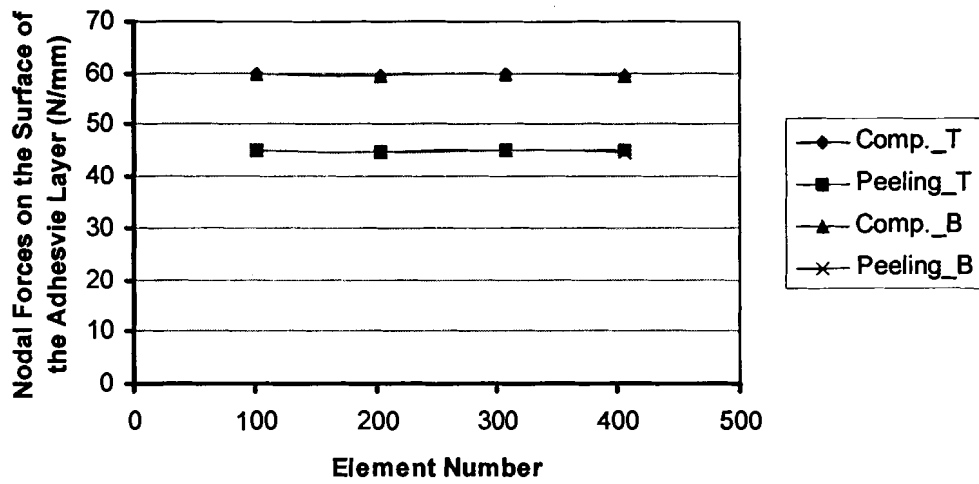


Figure 5.8 Mesh Convergence for Nodal Forces of the Adhesive Surfaces Loads for Material System B

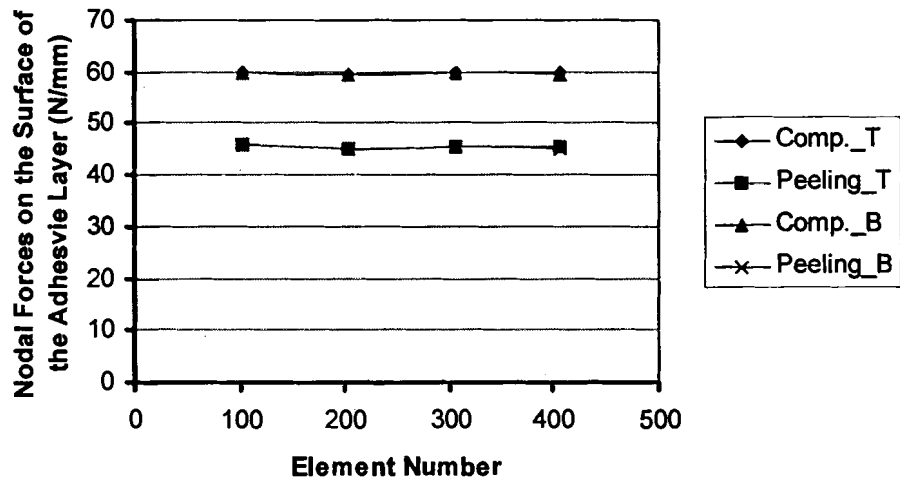


Figure 5.9 Mesh Convergence for Nodal Forces of the Adhesive Surfaces Loads for Material System C

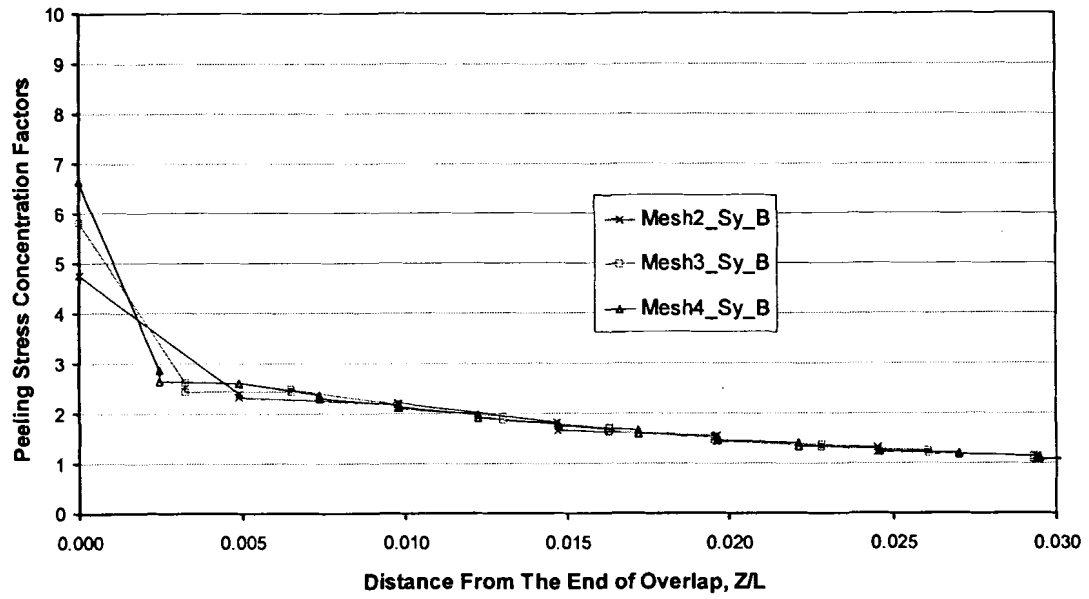


Figure 5.10 Mesh Convergence for Peeling Stress Concentration Factors (Bottom Left) for Material System B

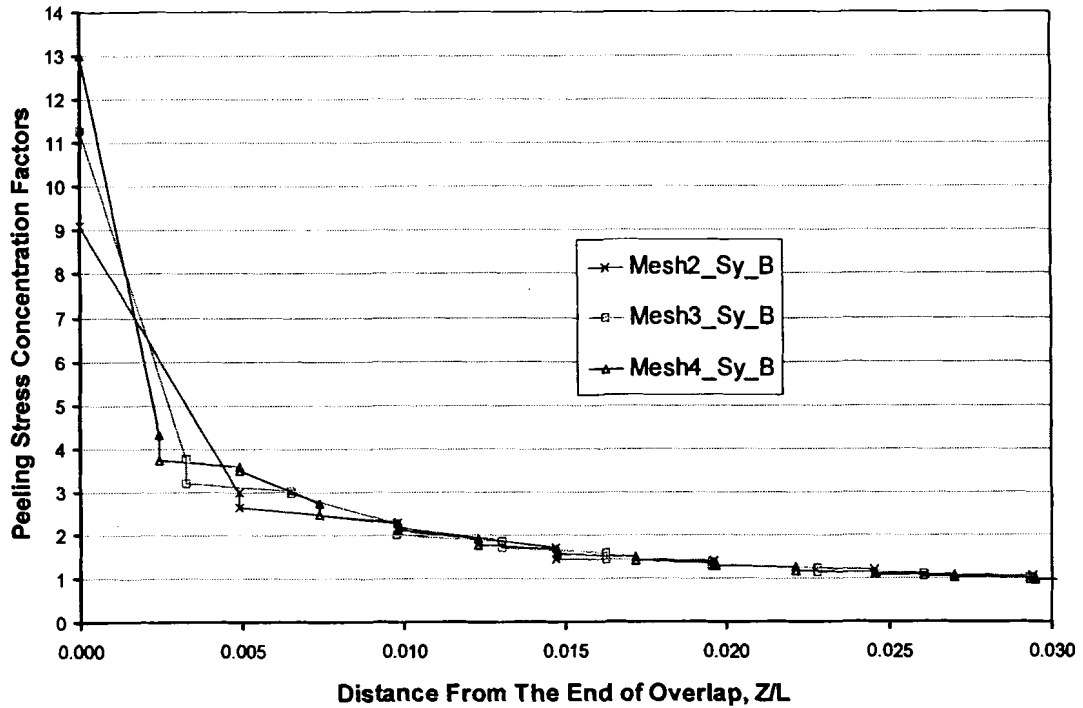


Figure 5.11 Mesh Convergence for Peeling Stress Concentration Factors (Bottom Left) for Material System C

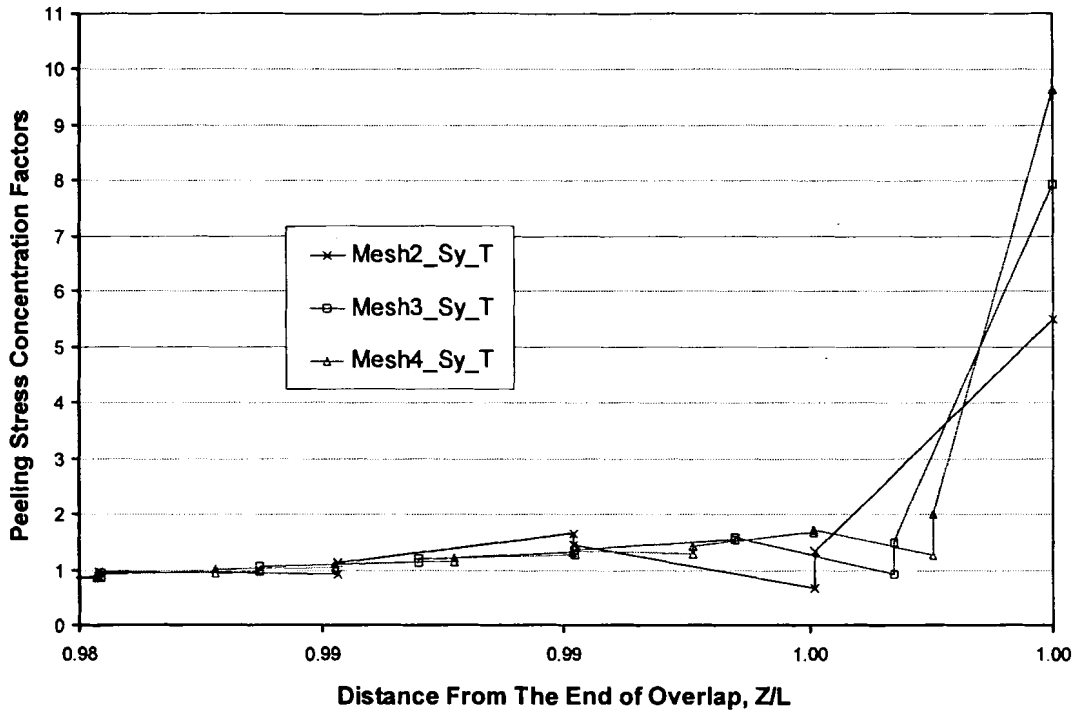


Figure 5.12 Mesh Convergence for Peeling Stress Concentration Factors (Top Right) for Material System B

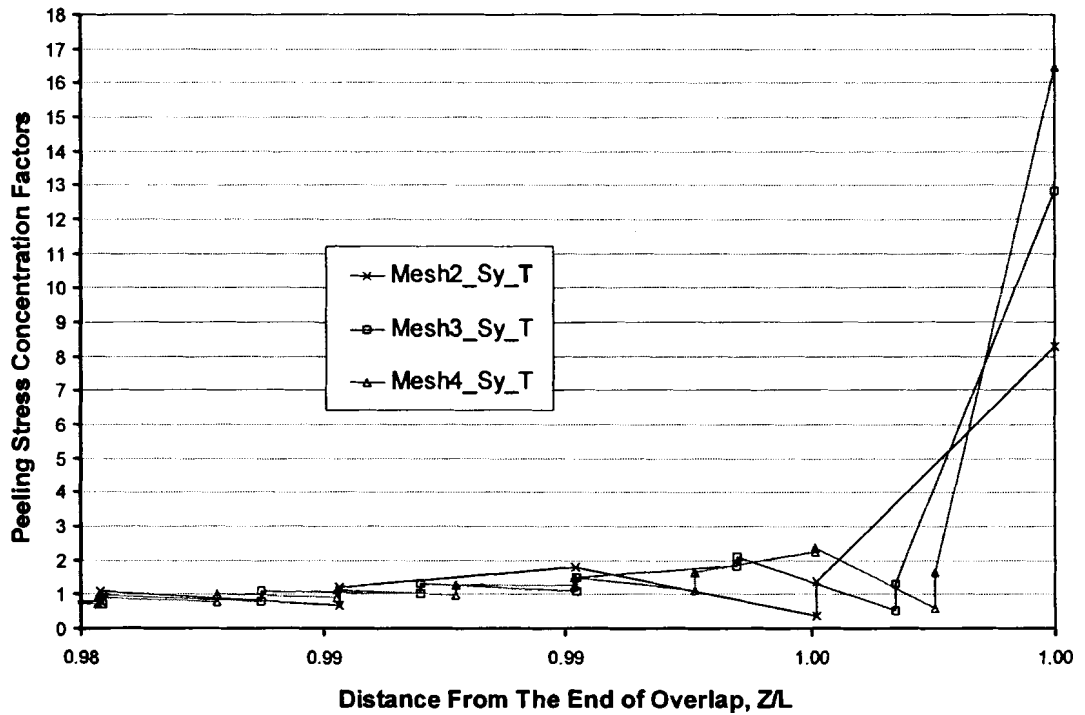


Figure 5.13 Mesh Convergence for Peeling Stress Concentration Factors (Top Right) for Material System C

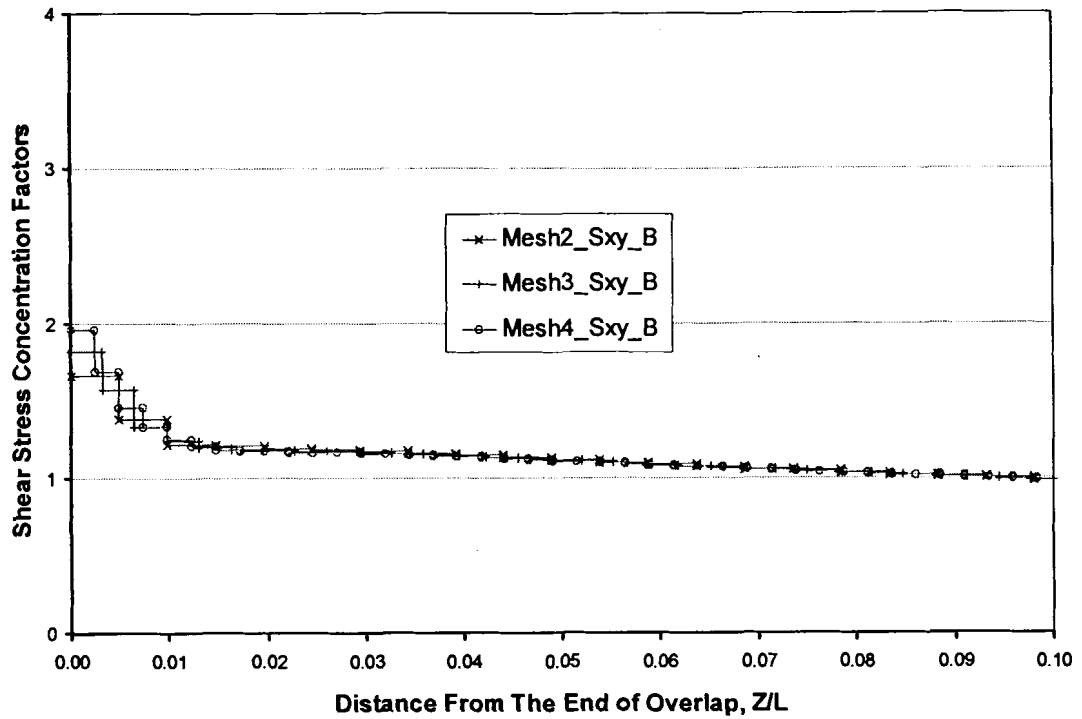


Figure 5.14 Mesh Convergence for Shear Stress Concentration Factors (Bottom Left) for Material System B

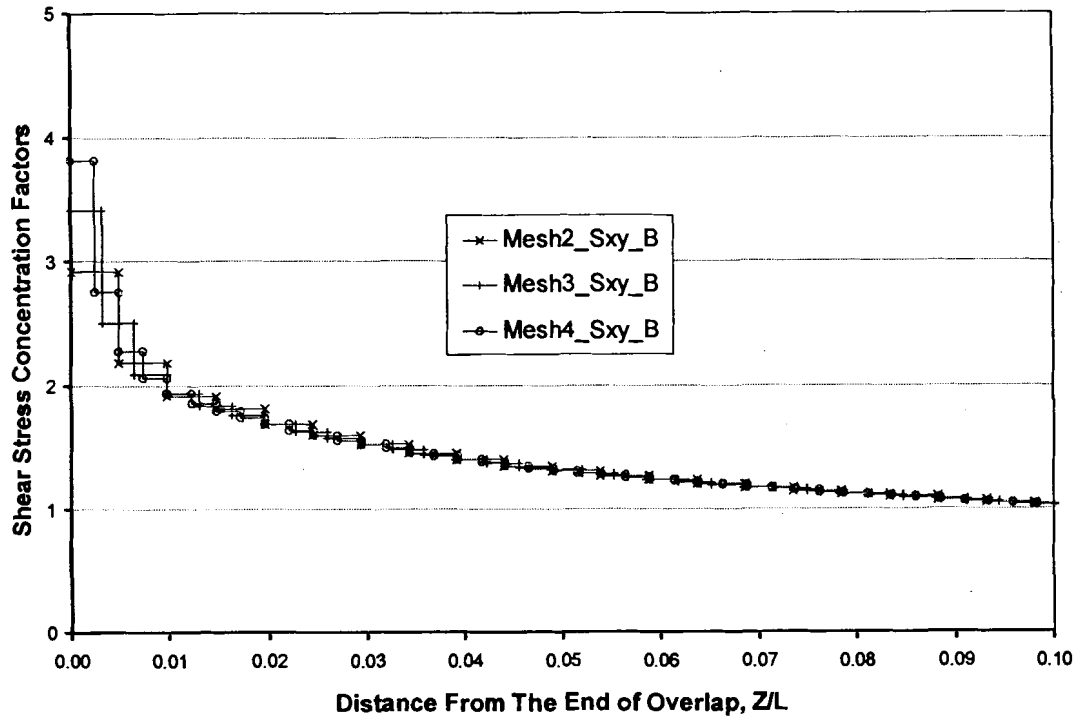


Figure 5.15 Mesh Convergence for Shear Stress Concentration Factors (Bottom Left) for Material System C

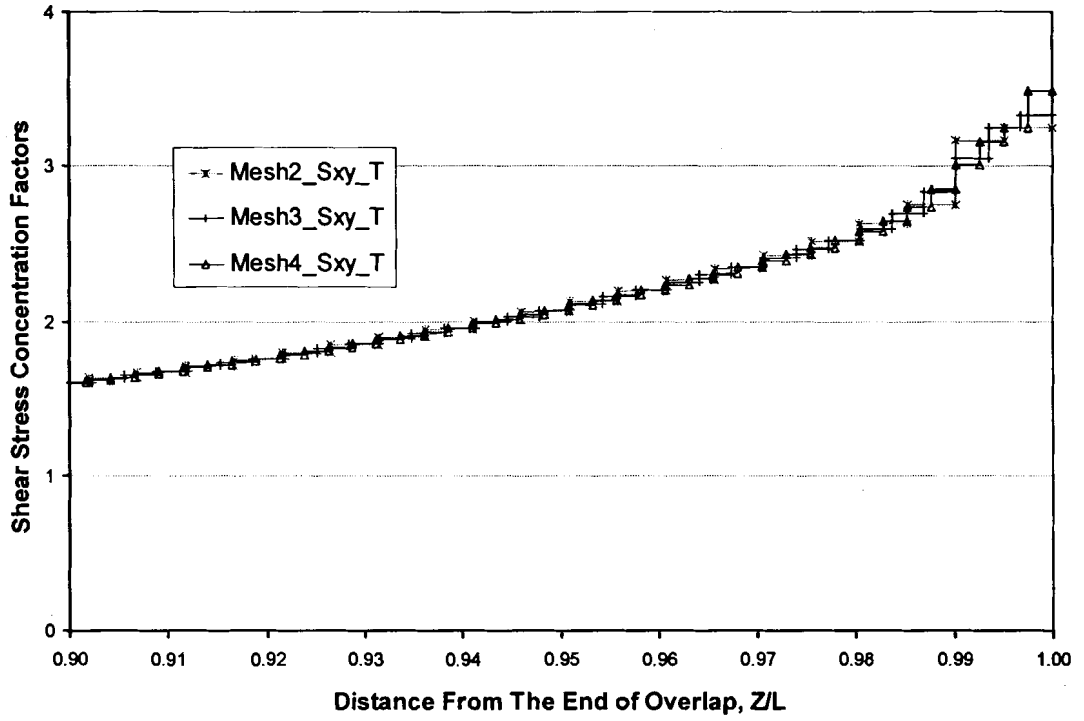


Figure 5.16 Mesh Convergence for Shear Stress Concentration Factors (Top Right) for Material System B

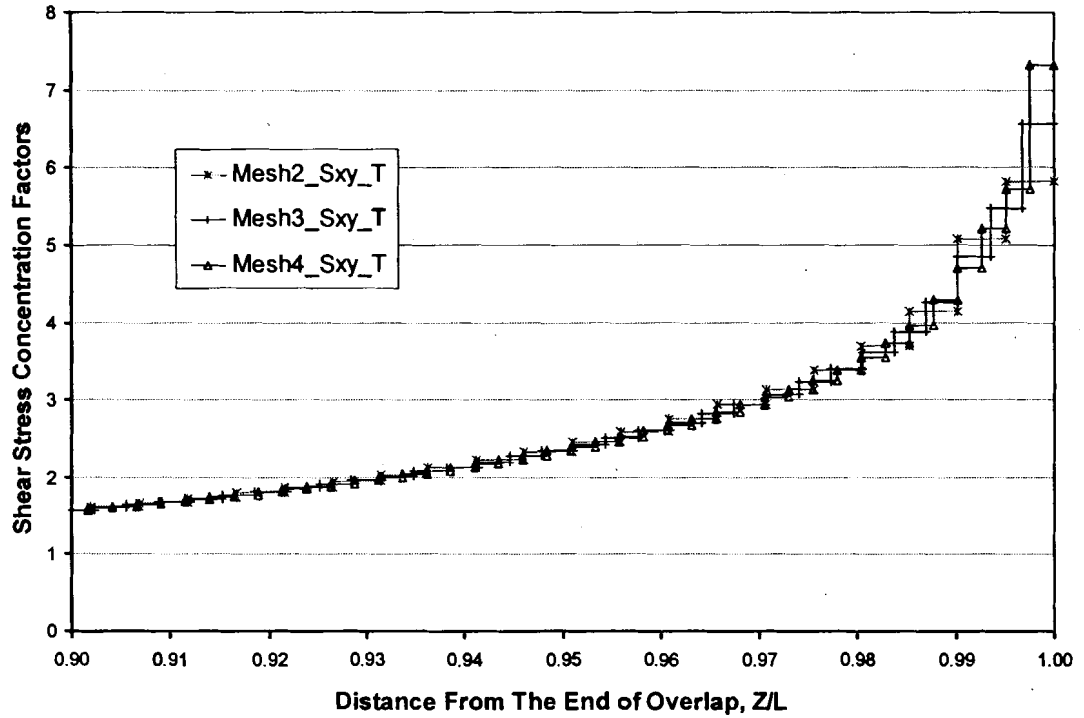


Figure 5.17 Mesh Convergence for Shear Stress Concentration Factors (Top Right) for Material System C

From the convergence study, the peeling stress concentration factors were not convergent at the top right corner and the bottom left corner of the adhesive layer, which indicated that singularities existed at these regions. The results of mesh convergence indicate that Mesh 4 is adequate for this study.

5.10 Results and Discussion

Although element solutions are more accurate, in order to clearly show the trends of the stress distributions, nodal solutions are used in the figures. For better comparison, same type of figures for material system B and C are put together.

The overall peeling and shear stress distributions for material system B and C are shown in Figure 5.18 to Figure 5.21. The overall deformed shape is also shown in the pictures. These results are calculated from Mesh 1. The peeling and shear stress distributions of the adhesive layer at the end of the overlap area are shown in Figure 5.22 and Figure 5.25. The peeling and shear stress concentration factors of the top and bottom surfaces of the adhesive layer in the overlap area are shown in Figure 5.26 to Figure 5.29. These results are calculated from Mesh 4.

For the distributions of the stress concentration factors, similar trends are found for material system B and C. First, the peeling and shear stress distributions are not uniform along the adhesive-adherend interfaces, and the maximum values of both peeling and shear concentration factors occurred at the corner of the FRP notch (top right corner). Second, the peeling stress concentration factors are not convergent at the FRP and wood notches (bottom left corner and top right corner), which indicate that peeling stress singularity exists at these locations. Since it is well known that adhesives are generally good in shear and weak in tension (peeling), this may further indicate that the failure of

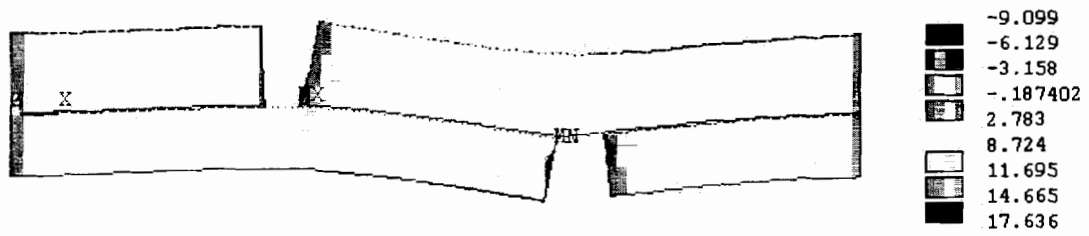


Figure 5.18 Overall Peeling Stress Distribution (Mesh 1) for Material System B

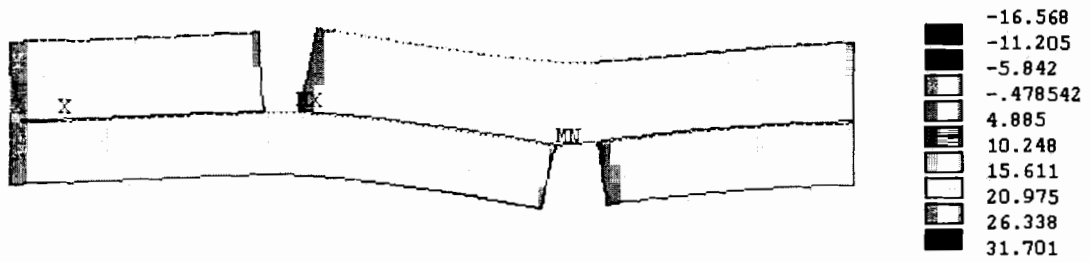


Figure 5.19 Overall Peeling Stress Distribution (Mesh 1) for Material System C

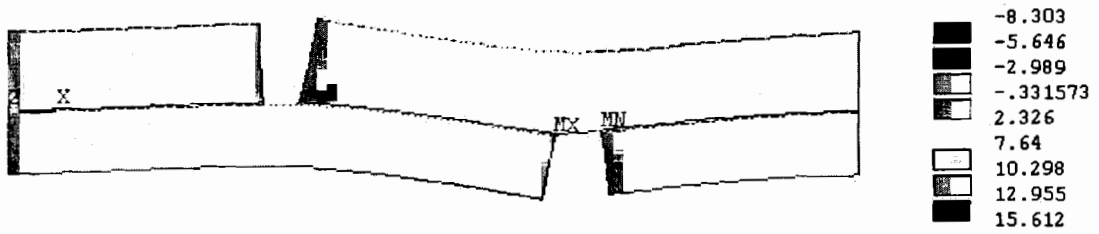


Figure 5.20 Overall Shear Stress Distribution (Mesh 1) for Material System B

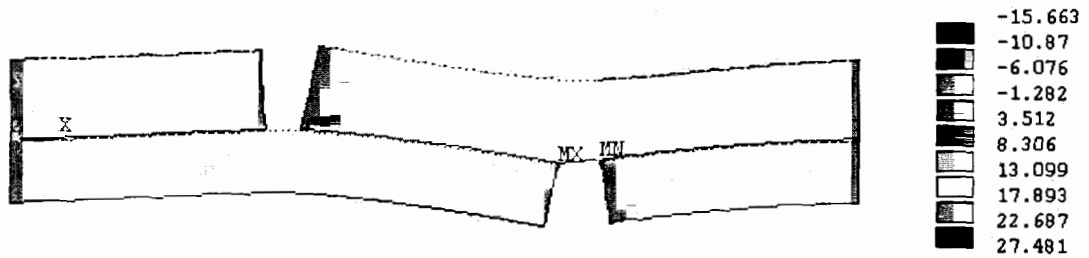


Figure 5.21 Overall Shear Stress Distribution (Mesh 1) for Material System C

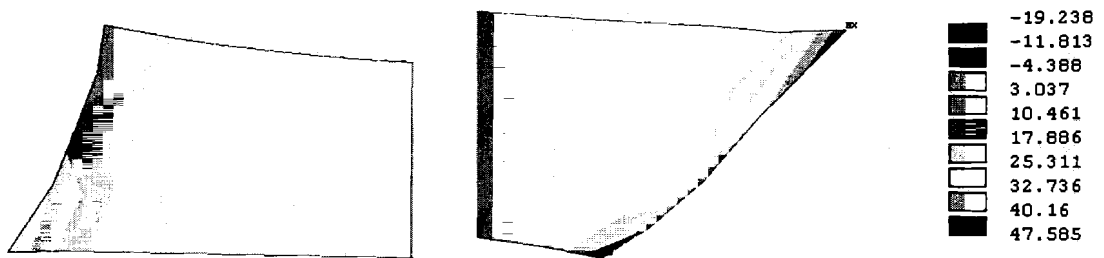


Figure 5.22 Peeling Stress Distribution at the Ends of the Adhesive Layer (Mesh 4) for Material System B

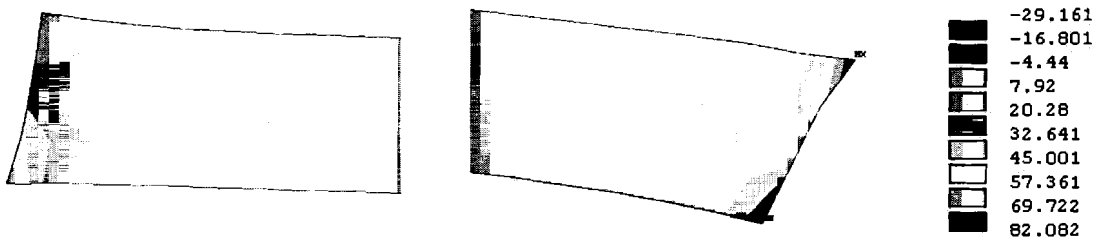


Figure 5.23 Peeling Stress Distribution at the Ends of the Adhesive Layer (Mesh 4) for Material System C

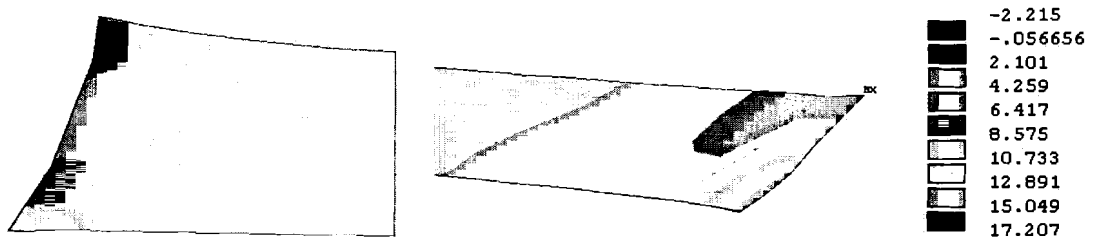


Figure 5.24 Shear Stress Distribution at the Ends of the Adhesive Layer (Mesh 4) for Material System B

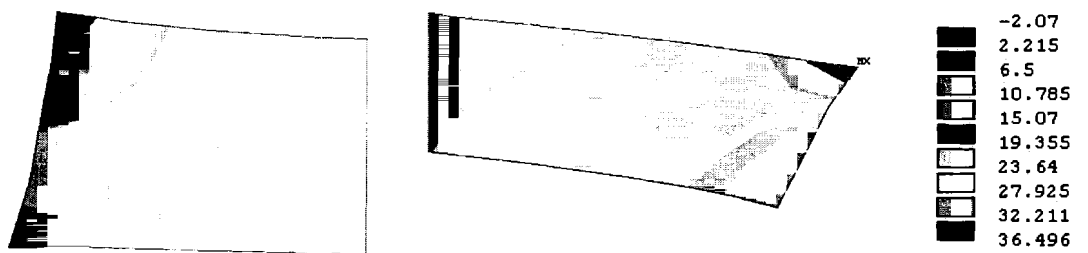


Figure 5.25 Shear Stress Distribution at the Ends of the Adhesive Layer (Mesh 4) for Material System C

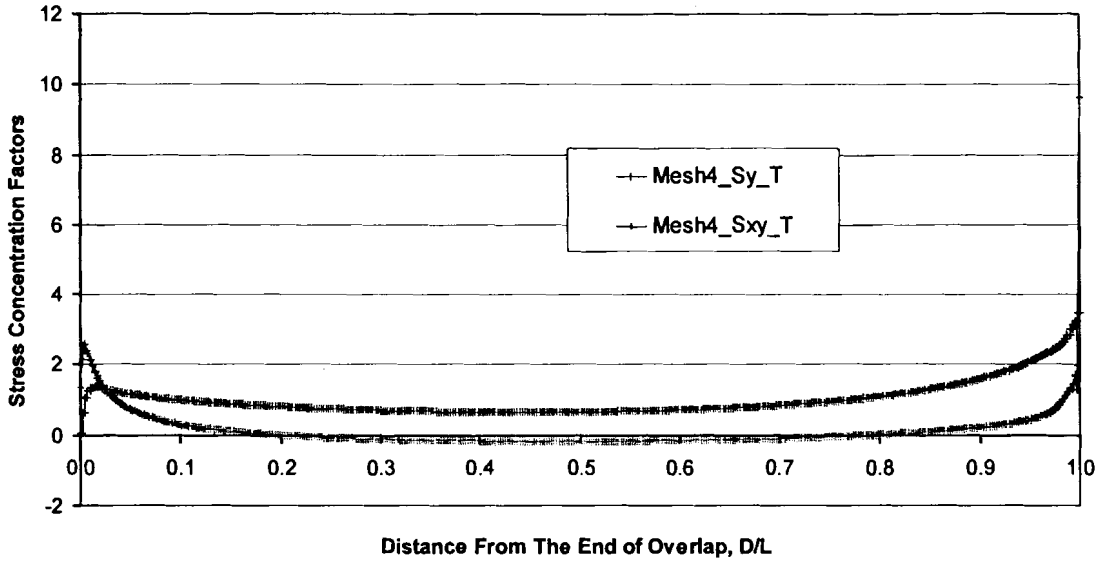


Figure 5.26 Stress Concentration Factors of the Top Surface of the Adhesive Layer (Mesh 4) for Material System B

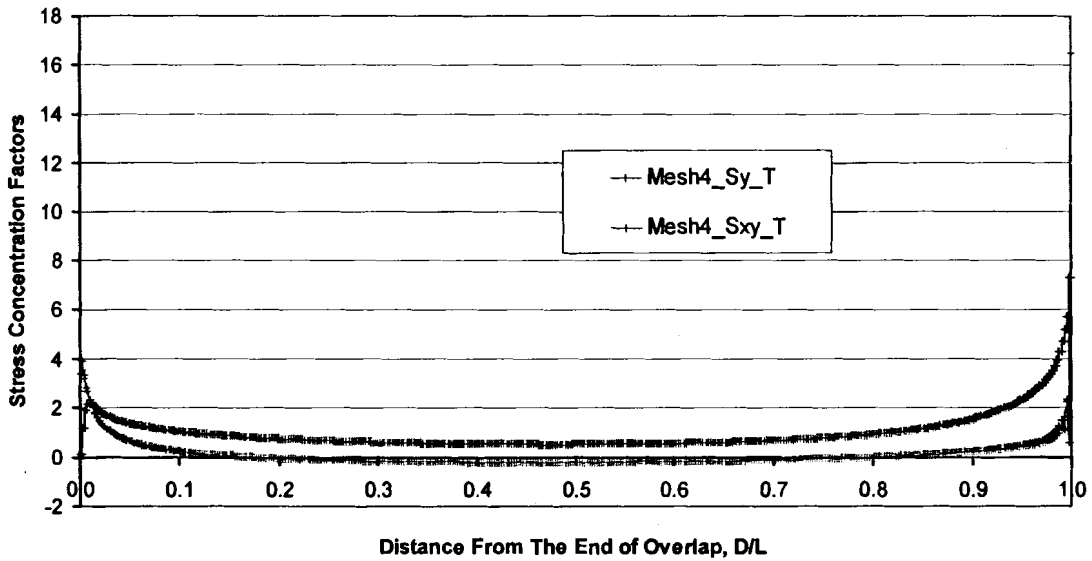


Figure 5.27 Stress Concentration Factors of the Top Surface of the Adhesive Layer (Mesh 4) for Material System C

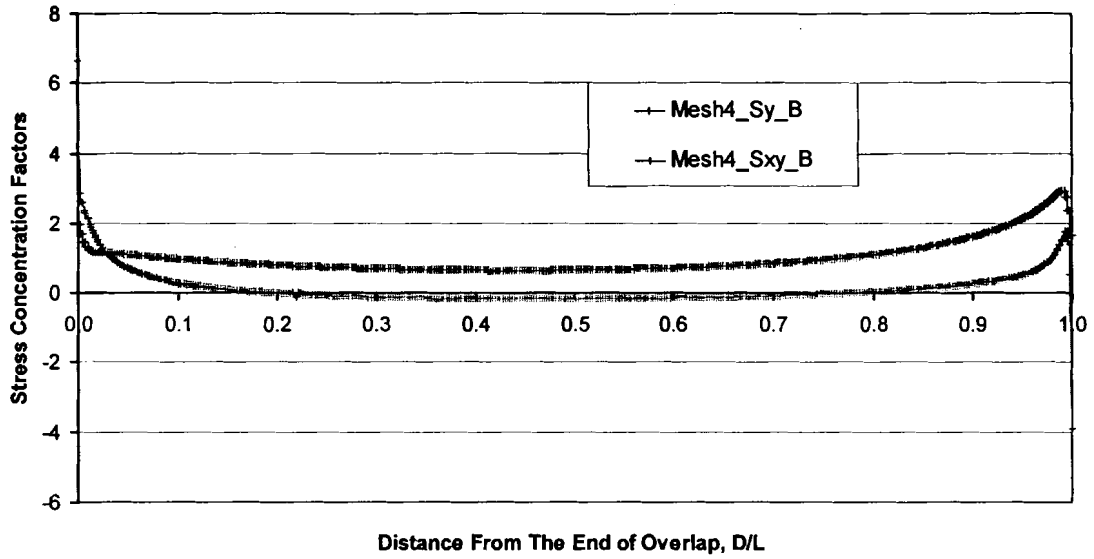


Figure 5.28 Stress Concentration Factors of the Bottom Surface of the Adhesive Layer for Material System B

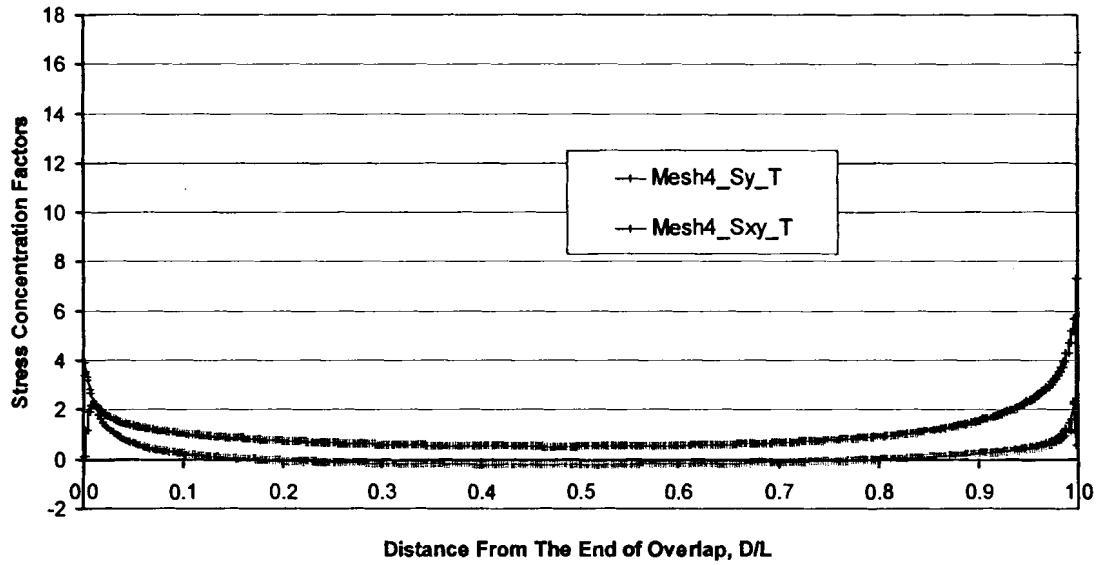


Figure 5.29 Stress Concentration Factors of the Bottom Surface of the Adhesive Layer for Material System C

the adhesive layer starts from the excessive peeling stress at the corner near the notches. Third, the resultants of the peeling stresses and shear stresses of the surfaces of the adhesive layer are constant.

From the comparison, it is shown that material system B has higher stress concentrations than those of material system C, which is mainly due to the significant difference of the elastic modulus between the adhesives. The polyurethane adhesive of material system B is much more ductile than the epoxy adhesive of material system C. It is shown that the adhesive layer is subjected to the combination of peeling stress and shear stress, which may be somehow correlated with the stress condition of beams under flexure loadings. For FRP reinforced glulam beams under flexure loadings, the FRP-wood interface is subjected to the shear stresses as well as peeling stresses. Since the resultants of the peeling stresses and shear stresses of the surfaces of the adhesive layer are constant, the ratio of average peeling stress to average shear stress of the surface of the adhesive layer could be used to characterize this stress condition, as shown in Table 5.7. The maximum number may be used, which is 0.88 for material system B and 0.94 for material system C. The higher ratio indicates more peeling stress exist on the interface, which is undesirable.

5.11 Conclusions and Correlation with Experiments

The FEA shows that the apparent single-lap shear strength of the FRP-wood hybrid specimens was controlled by the tensile (peel) strength of the adhesive/adherend interface in terms of the highest stress concentration factors at the end of the overlap area. The shear and peeling stress distributions are not symmetric. The highest stress

concentration factor occurs at the corner near the FRP notch. Because of mathematical singularities, the peeling stresses are not convergent at that corner.

Table 5.7 Ratios of Average Peeling Stress to Average Shear Stress of the Surface of the Adhesive Layer for Material System B and C

| Mesh | Peeling/Shear Ratio | | | |
|------|---------------------|--------|-------------------|--------|
| | Material System B | | Material System C | |
| | Top | Bottom | Top | Bottom |
| 1 | 0.887 | 0.887 | 0.934 | 0.934 |
| 2 | 0.869 | 0.859 | 0.935 | 0.923 |
| 3 | 0.878 | 0.862 | 0.943 | 0.934 |
| 4 | 0.879 | 0.856 | 0.940 | 0.926 |

The stress condition of the FRP-wood interface may be characterized by the ratio of the average peeling stress to the average shear stress of the adhesive surface. The lower this ratio, the less peeling stresses are developed, and consequently, the more desirable the stress field results. The ratio of material system B, 0.88, is lower than that of material system C, 0.94. Therefore, the stress condition of material system B is more desirable. This ratio can be further used to correlate the results obtained from material level testing and analysis with those from full-scale FRP-glulam girder testing and analysis. It is shown that elastic modulus of adhesives have significant influence on the stress conditions of the single-lap shear configuration.

The failure mode of fatigue tests (shown in Figure 5.30) matched well with the prediction of finite element models, which shows that the cracks always started at a point near the FRP notch. The cracks were usually started at a point near the bondline within the wood layer, and gradually propagated to the wood notch until failure.

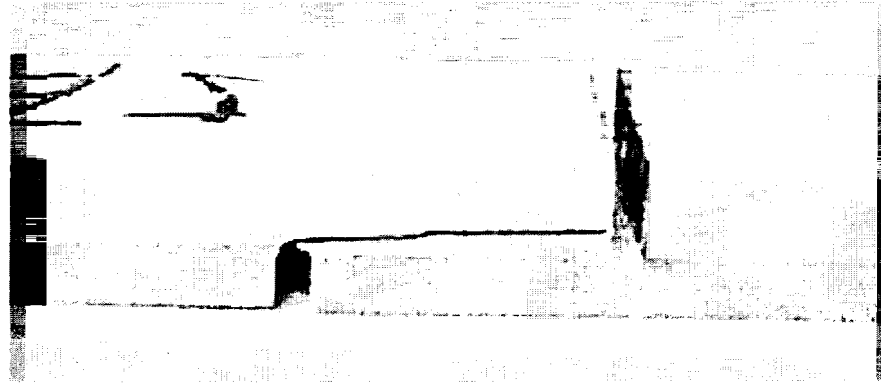


Figure 5.30 Typical Failure Mode of Fatigue Tests

Chapter 6

MODE I FRACTURE TESTING OF FRP-WOOD HYBRID FLAT DCB SPECIMENS

6.1 Summary

The Mode I fracture toughness of FRP composite and wood bonded interfaces was evaluated using flat double-cantilever beam specimens. ASTM standard test procedure D5528 for unidirectional FRP composites was selected and modified to characterize hybrid FRP-wood materials. Modifications to the test protocol were needed to account for specimens made with dissimilar materials (FRP composite and wood). Two material systems that passed the preceding screening tests were investigated: material system B (E-glass/urethane composite with urethane adhesive) and material system C (E-glass/epoxy composite with epoxy adhesive). Crack lengths and crack opening displacements were monitored during the experiments using a CCD digital camera system with digital image correlations. It was found that Mode I fracture toughness of material system B was significantly higher than that of material system C. It was found that this method could be used to quantitatively discriminate and evaluate material systems with different interlaminar toughness.

6.2 Introduction of Fracture Toughness Tests

Adhesive joints are likely to fail by a crack propagating either in the bondline or along the interface between a substrate and the bondline or in a mixture form of both. In a typical fatigue failure, a microscopic crack forms at a point of high stress concentration

and gradually enlarges as the loads are applied repeatedly. When the crack becomes so large that remaining material cannot resist the loads, a sudden fracture of the material occurs (Gere and Timoshenko 1997).

Recently, fracture mechanics has been widely used to correlate crack growth behavior in adhesive joints. In these studies, fracture toughness tests were used to determine the fracture toughness or energy release rates of adhesives sandwiched between substrates. These properties of adhesive bonds are important in terms of characterizing adhesives, predicting adhesive joint strength and service life, and rationally designing adhesive joints (Tong and Steven 1999).

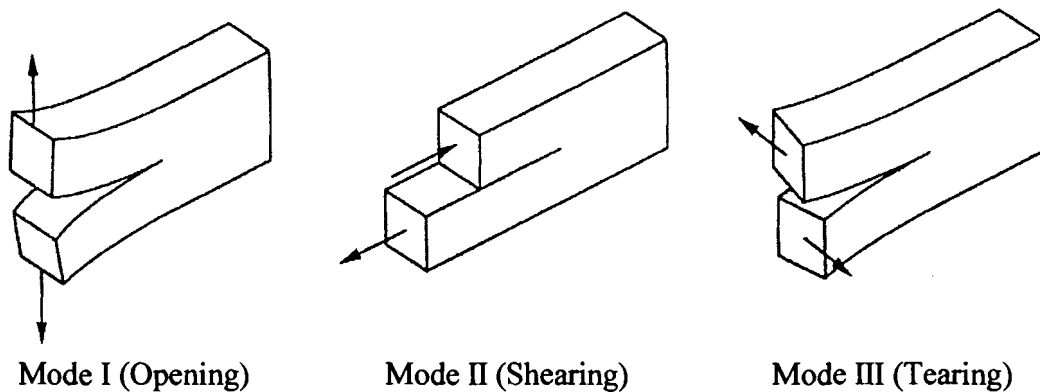


Figure 6.1 Three Crack-propagation Modes

The fracture of a material is described by means of three principal modes. As illustrated in Figure 6.1, the mode of fracture is determined by a combination of the direction of loading and crack propagation. Mode I is designated the opening mode; mode II is termed the shearing mode; mode III is called the tearing mode. Virtually all failure based on fracture of the material can be described in terms of these three modes (Bodig and Jayne 1992).

6.3 Objective and Scope

The general objective of this chapter is to develop a material-level test method to quantitatively discriminate and evaluate interfacial Mode I fracture toughness of FRP-wood bondlines. One ASTM standard test procedure was adapted and modified to account for hybrid FRP-wood materials: the ASTM D5528 Mode I fracture test procedure for FRP-FRP flat double cantilever beam (DCB) adhesive joints. Wood-wood DCB tests were also conducted as controls.

The following steps were conducted to support the chapter objective: a protocol based on the modified ASTM test procedures was developed; the specimen configuration was determined; a standard procedure for specimen fabrications and testing was drafted; acceptance criteria of the experimental results was proposed, and a set of experiments was conducted to validate the test method and acceptance criteria.

6.4 Literature Review of Fracture Test Methods

6.4.1 Adhesive Bonding of FRP-Wood and Wood-Wood

The effects of wood substrate grain angles on the fracture properties and fracture morphology of wood-epoxy adhesive joints were evaluated (Mijovic and Koutsky 1979). The methods of linear elastic fracture mechanics were extended to wood-epoxy joints. Tapered double cantilever beam specimens were used for Mode I fracture testing. The fracture energy for crack initiation was calculated for each sample and plotted as a function of grain angle. Two sets of specimens were used: freshly cut specimens and those previously bonded by a phenolic adhesive with bonding surfaces subsequently

planed down. No significant difference in Mode I fracture energy value was noted between the two types of specimens at grain angles other than 90°.

Because wood contoured double cantilever beam (CDCB) specimens presented experimental difficulties resulting in possible bias and poor reproducibility, a new specimen configuration was developed (River and Okkonen 1993). The specimen was made of oriented strandboard (OSB) and had a concave taper: two contoured OSB beams sandwiched a wood laminate having the test bondline at its center. The compliance and crack-length relationship were experimentally determined. Then, they were used to calculate the strain energy release rate of the adhesive joint. The test results showed that this new specimen could improve both the accuracy and reproducibility.

A new approach was developed to measure adhesive fracture toughness of wood-adhesive joints in Mode I cleavage (Scott *et al.* 1991). It was an extension of the CDCB test and generally followed the procedures outlined in ASTM D3433. Samples were prepared by bonding thin wood laminates to contoured aluminum beams, i.e., used the metal-backed wood beam to measure the toughness of wood-wood bond lines. The results demonstrated that the CDCB test could provide useful information about adhesive fracture properties not obtainable from conventional shear tests.

An experimental characterization of the Mode I fracture toughness of bonded interfaces for hybrid laminates was presented (Davalos *et al.* 1997; Davalos *et al.* 1998; Davalos *et al.* 2000). Bi-layer CDCB specimens for the fracture tests of the wood-wood and FRP-wood bonded interfaces were used. The bi-layer specimen consisted of constant-thickness adherends bonded to straight tapered sections of an easily machinable material. Then, it was contoured to achieve a constant rate of compliance change with

respect to crack length. A numerical method based on the Rayleigh-Ritz solution was developed to design the shape of the test specimens. Based on FEA, the predicted Mode I strain energy release rate by the Jacobian Derivative Method correlated closely with experimental results. The efficient CDCB specimen and experimental/analytical program presented in this research can be used to evaluate the Mode I fracture toughness for hybrid material interface bonds, such as FRP-wood bonds.

Because the use of the CDCB to demonstrate the value of fracture testing for bonded wood was found to be laborious and stringent, a simplified method for Mode I fracture testing of adhesively-bonded wood was developed (Gagliano and Frazier 2001). The flat DCB specimen geometry was applied and a shear corrected compliance method was adapted as the data reduction method, which was derived from beam theory. Digital hardware was used to measure the real-time crack length. It was found that fracture experiments were sensitive to intrinsic adhesive parameters and careful grain angle control may prevent wood failure. It was shown that the flat DCB geometry may greatly simplify sample preparation as well as obtain valuable information.

Experiments were performed under Mode I and Mode III on side grooved Compact-Tension specimens of larch and beech under steady state crack propagation (Tschegg *et al.* 2001). The objective was to study the damage and fracture behaviors and the influence of fiber orientations. It was found that crack initiation energy and specific fracture energy were approximately ten times higher for Mode III loading than for Mode I loading in both wood species.

Finite element models were created to characterize the delaminations found in a bridge using ANSYS (Sanchez 2002). Specifically, the energy release rate, J , was found

for various lengths of delaminations, at various locations throughout the length of the girder. In comprising the results to experimental results obtained by other researchers, it was found that the energy release rates predicted by the model were below the critical energy release rate for an FRP-glulam composite. The delamination growth toward the load was found to be unstable.

6.4.2 Adhesive Bonding of Metal-Metal and FRP-Metal

Mode II type crack propagation had generally been less investigated than that occurring under Mode I (Ede and Verreman 1995). However, in bonded joints, Mode II was shown to be a major contributor to crack propagation. It was suggested that a tapered end-notched flexure (TENF) specimen could be used to solve the deficiencies of regular ENF specimen for the study of fracture and fatigue in Mode II. The proposed contour may prevent the sudden and high acceleration of cracks that hinders usage of the ENF specimen.

A fracture mechanics approach was successfully applied to examine the cyclic fatigue behavior of adhesively bonded joints, which consisted of aluminum-alloy substrates bonded using epoxy structural adhesive (Fernando *et al.* 1996). The fatigue tests were conducted in both dry and wet environments. A TDCB specimen was used to obtain the values of crack growth rate as a function of the maximum strain energy release rate applied in the fatigue cycles. It was found that cyclic fatigue tests conducted in a relatively dry condition led to joint failure at far lower loads and far lower value of the fracture energy than those determined from monotonically loaded fracture tests. On the other hand, the fatigue tests demonstrated that a threshold value of the applied strain-

energy release rate does exist and may be used to rank the fatigue limit behavior of different adhesive systems and their resistance to hostile environments.

Interfacial fracture toughness tests using DCB specimens were performed for studying the role of adhesion between the aluminum and CFRP layer with different aluminum surface treatments (Lawcock *et al.* 1997). One composite layer was sandwiched between two aluminum sheets with the fibers aligned in the aluminum rolling direction. Optical and scanning electron microscopes were used to study the failure behavior and fracture mechanisms. Tensile tests, interlaminar shear strength (ILSS) tests and residual strength tests were also conducted to determine mechanical properties of the joints. No difference was observed in the laminate's in-plane mechanical properties. However, the reduced interfacial bond strength led to decrease in the ILSS of 10%. The results of DCB interlaminar fracture tests indicated an increase in Mode I fracture toughness of up to seven times for the specimens with stronger bonding compared with those with poor bonding.

Epoxy resins are widely employed as the basis for adhesive components because they have many useful engineering properties, such as a relatively high modulus and strength. However, pure epoxy resins are relatively brittle polymers with poor resistance to crack propagation. To improve the crack resistance of epoxy resins, inorganic fillers have been widely used. Crack propagations in epoxy adhesives filled with spherical silica were investigated using epoxy bonded steel DCB specimens (Imanaka *et al.* 2001). The results showed that the fracture toughness increased with particle size and with interfacial strength of silica/matrix.

The wedge-opened DCB method was also used to test the debonding toughness of epoxy-bonded steel plates (Sener *et al.* 2002). In this study, the classical method of crack length measurement by visual observation of the crack tip along the side of the specimen was compared with a method making use of displacement sensors for continuously monitoring the deflection of the plates. The uncertainty arising from the anticlastic effect was enlightened. The experimental reproducibility provided by the different test procedures was also compared.

6.4.3 Adhesive Bonding of FRP-FRP

6.4.3.1 Data Reduction Methods

A modified technique was developed to correct elastic strain energy with crack length of material systems (Berry 1963). It was derived based on the assumption that simple beam theory can be applied to the system, which is not strictly valid. An empirical generalization of this expression was derived from beam theory and verified by experiments. This data reduction method was adopted by ASTM D5528 and named “Compliance Calibration Method” (CC).

Reported values of Mode I fracture energy determined by DCB specimen were noticed to be surprisingly different for supposedly the same fiber-composite material from the literature (Hashemi *et al.* 1989). It was found that the differences might be due to the data reduction methods. A study was conducted to explain the apparently conflicting observations and to rationalize the various analytical approaches by applying an appropriate correction factor. The assumption that the beams act as built-in cantilevers overestimates the fracture energy. To correct this, a method was developed to treat the DCB as if it contained a slightly longer delamination, which may be determined experimentally by generating a least square plot of the cube root of compliance as a

function of delamination length. This data reduction method was adopted by ASTM D5528 and named “Modified Beam Theory Method (MBT)”.

Comprehensive literature review of DCB and ENF test methods and proposed new test procedures were presented (Kageyama and Hojo 1990). For DCB tests, thickness normalized crack length versus cube root of compliance plots were used to determine Mode I fracture toughness. The applicability of this method was confirmed by experiments of four CFRP composite systems. This data reduction method was adopted by ASTM D5528 and named “Modified Compliance Calibration Method (MCC)”.

6.4.3.2 Comprehensive Reviews

A number of approaches to data reduction schemes used in conjunction with the DCB test for determining critical strain energy release rate were discussed, including area method, beam analysis method and empirical method (Whitney *et al.* 1982).

Experimental data on unidirectional tape and bi-directional cloth graphite fiber reinforced polymeric matrix composites was compared to assess the potential of the DCB test as a materials screening tool. The effects of large deflections, shear deformation and viscoelastic behavior were also discussed. It was concluded that the DCB method is an excellent material screening tool for measuring interlaminar Mode I fracture resistance. This method is capable of discriminating between materials of different interlaminar toughness in terms of measurement of the strain energy release rate.

A survey of the current status of test methods for the measurement of delamination resistance of composite materials was presented, with particular emphasis on the work performed in this area by the European Structural Integrity Society (ESIS) (Davies *et al.* 1998). First, the existing Mode I fracture test standards were reviewed.

Then current work of ESIS was presented, both to extend the range of application of these Mode I tests and to standardize Mode II, mixed Mode (I/II) and Mode III tests. Finally, test methods to characterize fatigue crack propagation were also discussed.

Test procedures for Mode I and Mode II critical fracture toughness testing of unidirectional FRP-composites are currently being evaluated for international standardization (Brunner 2000). Recent developments were discussed with emphasis on experimental aspects of fracture toughness testing of FRP-composites in Mode I and Mode II.

6.4.3.3 Studies of Fatigue Behavior

An experimental and analytical investigation was performed based on fracture mechanics methodology to study the fatigue failure of adhesively bonded composite joints (Mall *et al.* 1982). Two configurations of cracked-lap-shear (CLS) specimens were used to simulate real-world conditions of mixed-mode failure (combination of shear and peel stresses). The results showed that the joints were fatigued by cyclic debonding of the adhesive only. The progress of the debonding the interface was tracked by photographing photo-elastic material bonded to the composite. The debonding growth rate was then correlated with different strain-energy-release rates. It correlated very well with total strain-energy-release rate.

In a following study, adhesively bonded composites joints were investigated to characterize both the static and fatigue debonding growth mechanism under Mode I (DCB) and Mixed I and II loadings (cracked-lap-shear) (Mall and Johnson 1986). It was found that total strain-energy release rate (G_T) appeared to be the governing parameter for cohesive debonding growth under static and fatigue loadings. The cyclic debond growth

rate data showed that the debond propagate at G_T values as much as an order of magnitude below the critical static value. Therefore, static data alone is insufficient for safe joint design. Instead, the G_T associated with cyclic debonding at very slow growth rates is more appropriate as a design and as a criterion for adhesive selection. In this case, it would require the characterization of cycle debonding under Mode I loading only, which is simpler and easier to test.

Similar tests with a brittle adhesive were also conducted (Mall and Yun 1987). In all specimens tested, failure occurred in the form of debond growth either in cohesive or adhesive manner. The total strain-energy-release rate was not the criterion for cohesive debond growth under static and fatigue loading in the brittle adhesive as observed in previous studies with the ductile adhesives. Furthermore, the relative fatigue resistance and threshold value of cyclic debond growth in terms of its static fracture strength was higher in the brittle adhesive than those in the ductile adhesive.

In another study, the role of interlaminar fracture toughness on the cyclic delamination growth resistance and interaction of Mode I and Mode II components of cyclic loading were investigated (Mall 1989). Three types of specimens, DCB, CLS and ENF specimens were used to characterize the cyclic delamination (or debonding) growth mechanism under Mode I, Mixed Mode I-II and Mode II conditions, respectively. It was found that the normalized delamination growth resistance for laminated composites under cyclic loading decreased with the increase of static interlaminar fracture toughness. This decrease depended on the loading mode, i.e., maximum for Mode II and minimum for Mode I.

Near-threshold growth of delamination fatigue cracks in unidirectional CFP materials was investigated using DCB specimen (Hojo *et al.* 1989). The crack growth tests were conducted under several stress ratios to find out a fracture mechanics parameter controlling the propagation behavior of fatigue cracks. The tests were conducted both in air and in water. An equivalent stress intensity range was proposed, which was a mixed parameter of the stress intensity range, the maximum stress intensity factor, and an experimental parameter. The crack growth rate under different stress ratios was well correlated the equivalent stress intensity range. This parameter was used to evaluate the environmental effect. Mechanisms of the environmental effect on the delamination fatigue crack growth were discussed based on fractographic observations.

The fracture mechanics data was used to study the fatigue behavior of adhesively bonded composite joints (Kinloch and Osiyemi 1993). First, the strain-energy release-rate in a single-lap joint during cyclic fatigue loading was deduced. Then, DCB specimens were used to get relationship between the rate of crack growth per cycles and the maximum strain-energy release rate by Mode I cyclic fatigue tests. Single-lap fatigue tests by tension loading were also conducted. Finally, the experimental data were modeled and used to predict the fatigue lifetime of bonded single-lap joints. It was found that it is possible to predict the long-term fatigue behavior of common designs of adhesive joints from relatively short-term fracture mechanics tests.

6.4.3.4 Effect of Substrate Material

The effect of the substrate material on the value of adhesive fracture energy was evaluated (Bell and Kinloch 1997). The results were reported for values of the adhesive fracture energies for joints consisting of steel, aluminum alloy or CFRP substrates

bonded using an epoxy adhesive. Two types of specimen were used: DCB and Tapered DCB. Even though the locus of joint failure was observed to be cohesive, the fracture toughness values for the CFRP joints were markedly lower than those for the steel or aluminum alloy joints. It was found that the value of the adhesive fracture energy, G_c , might be dependent upon the type of substrates employed in a TDCB or DCB joint, even when cohesive fracture through the adhesive layer was observed so that the degree of interfacial adhesion did not directly affect the value of G_c . To understand the results, FEA was used to study the form of the stress field ahead of the crack tip in the various types of joint. It was thought that such dependence may arise from the transverse modulus of the substrate influencing the form of the stress-field ahead of the crack in the adhesive layer, which in turn influenced the extent of plastic deformation ahead of the crack tip. However, in the subsequent study, it was found that the value recorded for CFRP was far too low to be explained by this mechanics argument (Blackman *et al.* 2001). Instead, it was assumed that, for the epoxy adhesive, relatively low concentrations of water in the CFRP substrates can lead to a dramatic reduction in the glass transition temperature T_g of cured adhesive, with a corresponding decrease in the value of G_c of the CFRP joint.

6.4.3.5 Effects of Loading Rate

The DCB specimen was utilized to investigate the rate effects on Mode I interlaminar fracture toughness in two composite material systems (Gillespie *et al.* 1987; Smiley and Pipes 1987). Since the adhesive bond was not strong enough to hold the hinge on the specimens at high loading rates, the hinges were mechanically fastened to the composite beams by drilling and tapping holes in the specimen and attaching the hinges with screws. Compliance method and area method were used in the data reduction. The

results indicated that the toughness of both systems was rate sensitive. ASTM D5528 cited this study as a reference of area method.

The rate dependence of Mode I interlaminar fracture behavior in unidirectional CFRP was investigated over a wide range of loading rates using DCB specimens (Kusaka *et al.* 1998; Nojima and Kusaka 1998). The results showed that the fracture toughness decreased stepwise with increasing loading rate showing a distinct rate-sensitive transition region and two rate-insensitive regions above and below. In and below this transition region, the crack grew unstably accompanied by high-speed propagation and arrest; but above the region, the crack grew stably and continuously. A simple model was created to explain this trend incorporating the rate dependence of fracture toughness and the contribution of kinetic energy in the specimen during unstable crack propagation.

6.4.3.6 Effect of Starter Films and Precracking

Results from a series of interlaboratory round robin tests were summarized which were performed to establish a JIS standard for Mode I interlaminar fracture toughness test for CFRP using DCB specimens (Hojo *et al.* 1995). The tests were conducted with two main objectives: first, to examine the influence of starter films and the precracking condition on the initial Mode I fracture toughness values; and second, to establish the definition of initial fracture toughness. It was found that the tests with precracks gave lower values of initial fracture toughness. A 5% offset point was recommended as the initial fracture toughness. The influence of loading apparatus and data reduction methods was also discussed.

6.4.3.7 Effect of Post-cure Conditions

The effect of different post-cure conditions on the Mode I fracture toughness of a vinylester resin and its glass-fibre reinforced composite counterpart was studied (Tucker *et al.* 2001). Following ASTM standards, the single-edge-notch bend (SENB) test and the DCB test were used. It was concluded that the post-cure enhanced the toughness of the glass-fibre/vinylester composite, mainly due to the increase of resin toughness.

6.4.3.8 Effect of Temperature

Mode I constant displacement rate tests on epoxy-bonded CFRP joints were conducted using DCB specimen at -50 , 22 and 90°C (Ashcroft *et al.* 2001). A comparison of experimental compliance and different beam theory approaches indicated that care need to be taken when apply beam theory approaches across a wide temperature range. Temperature was seen to influence the mode of fracture which progressed from stable, brittle fracture at low temperatures to slip-stick fracture at room temperature and finally to stable ductile behavior at elevated temperatures. The critical strain energy release rate was seen to increase with temperature and the failure locus transferred from predominantly in the composite substrate to predominantly in adhesive.

In a subsequent study, the effect of temperature on fatigue crack propagation (FCP) was investigated using the same specimen configuration (Ashcroft and Shaw 2002). Two types of lap joints were manufactured with the same materials and tested in fatigue at the same temperature. The temperature effects on fracture under quasi-static loading were compared with fatigue failure in uncracked lap joints. It was seen that temperature had a significant effect on the locus of failure and FCP. They also evaluated a number of techniques for determining strain energy release rate and crack propagation rate. The applicability of fracture mechanics data to the prediction of fatigue failure in

uncracked lap joints was assessed by attempting to predict fatigue thresholds in different temperatures. Reasonable predictions were made in most cases.

6.4.3.9 Effect of Residual Stresses

The effect of residual stresses on Mode I energy release rate for both adhesive and laminate DCB specimens was evaluated (Nairn 2000). The energy release rate can be partitioned into a mechanical term and a residue-stress term in beam theory. The consequence of ignoring residual stress due to fabrication is that one measures an apparent toughness instead of a true toughness. Such errors can be large for asymmetric laminates and often larger than the correction required for crack-tip rotation effects. Some experimental methods were suggested to correct this effect.

6.4.3.10 Fracture Behavior of Multidirectional Composite Laminates

Fracture toughness of multidirectional CFRP for Mode I and Mode II was investigated using DCB and ENF specimens and Raman Coating Method, which has the advantage of measuring strains of small region (Miyagawa *et al.* 2001). The strain distributions near the crack tip of specimens of 10 different sequences of layers made of CFRP were measured by Raman spectroscopy. Then the results were used to determine the fracture toughness under both Mode I and Mode II. The results were in good agreement with those measured by conventional methods.

6.5 Summary and Discussion of the Literature Review

The approach of using DCB specimen to evaluate wood adhesion is by no means novel. However, it requires visual measurement of the real time crack length, which is laborious, observer dependent and inaccurate using traditional techniques. To overcome

this drawback, significant research efforts have been dedicated to develop contoured DCB (CDCB) specimen to simplify the experimental procedure, such that the compliance varies linearly with crack length. CDCB (or TDCB) specimen configuration has the advantage that the crack length measurements are not required. Furthermore, some techniques were developed to bond flat wood DCB specimens to the contoured metal beams to reduce material variability that is inherent in wood. This geometry is widely accepted by current researchers. However, these methods are suffered from difficult and labor-intensive sample configuration design, calibration and preparation.

On the other hand, the flat DCB geometry greatly eliminates these difficulties. Using digital hardware and state-of-the-art image correlation techniques, real-time crack length measurements required for flat DCB specimens, which is the biggest challenge of the application of this geometry, can be achieved. Therefore, flat DCB geometry was selected to evaluate Mode I fracture toughness of FRP composite and wood bonded interfaces in this study.

One advantage of the DCB specimen is that under displacement control, the strain energy release rate decreases with increasing crack length; thus, a crack may be arrested without complete fracture of the specimen, and therefore, several measurements of fracture toughness are possible from single specimen (Davalos *et al.* 1997).

For plain strain cracks, specimens containing cracks of various sizes appear to fail at the same value of G . This critical value is denoted as G_{Ic} . In the case of plain strain, the crack growth resistance R is equal to G_{Ic} , which is independent of crack size (Anderson 1991). The curve of Mode I energy release rate G_I versus crack length a should be expected to be a straight flat line, i.e., G_I should be a material property of the

system, allowing of course for wood surface variations along the bondline. However, it should be pointed out that this is only true for the onset of crack extension. During crack growth it is not true any more.

6.6 Material Systems

The material systems selected are listed in Table 6.1.

Table 6.1 Material System Selected Based on the Screening Tests

| Material System | FRP composite | FRP fabrication | Wood species | Adhesive | Wood Primer |
|------------------------|------------------------------|--------------------------|----------------------|----------------------------|--------------------|
| B | E-glass/ urethane: w/ CSM | Pultrusion | DF: quarter- sawn | Urethane: ISOGRIP 3030D | HMR |
| C | E-glass/epoxy | Continuous lamination | DF: quarter- sawn | Epoxy: PRO-SET G3 | HMR |

6.7 Modified ASTM D5528: Standard Test Method for Mode I Interlaminar

Fracture Toughness of FRP-Wood Interface

Mode I fracture tests were conducted according to the modified ASTM D5528. A flat DCB configuration was used. The standard was modified to account for the FRP composite substrate. The experiments were used to examine the fracture toughness of two FRP-wood-adhesive material systems in terms of the measurement of strain energy release rate and percentage of wood failure of FRP-wood interfaces. Wood-wood DCB tests were also conducted as control tests

6.7.1 FRP-Wood Specimen Configuration

The DCB configuration of the ASTM D5528 was modified to account for the wood substrate. The wood substrate is used to substitute one FRP substrate. The length of

the specimen was specified as 200 mm based on a previous research (Gagliano and Frazier 2001). For pre-consolidated FRP materials, the thickness of the FRP layer is one consolidated sheet or one fabric layer. For both material system B and C, the FRP materials are pre-consolidated with the thickness of 6.3mm (0.25in).

Since the stiffness of wood and FRP materials are quite different, the configuration is asymmetric. However, it is needed to balance the DCB specimen as much as possible to force the crack to propagate along the FRP-wood interface and prevent premature wood failure, which is the precondition to measure the interfacial fracture toughness. To match the stiffness, tensile tests and 3-point bending tests were conducted for wood and FRP materials to get the approximate stiffness. The thickness of wood was determined based on the test results and preliminary experiments. For DF, the thickness of the wood layer was specified as 8.5 mm and 9.0 mm for material system B and C, respectively.

The load was applied through a pair of hinges bonded to the end of the specimen. Since the available types of commercial hinges restricted the dimensions and strengths of the hinges, the length of the initial crack was increased to assure the hinges were capable of sustaining the applied load without incurring damage. The DCB specimen configuration is shown in Figure 6.2.

6.7.2 FRP-Wood Specimen Fabrication

All of the test specimens were fabricated in the laboratory. Grade structural selected Douglas-fir lumber with a nominal size of 25×150mm (1"×6") was used to fabricate glulam specimens. To get more uniform surface properties for such a small specimen, only Douglas-fir lumbers with a quarter-sawn orientation was used. The

lumber was stored in the conditioning chamber at 24°C and 65% of RH for more than two months. The moisture content was around 12% when fabricating.

From the literature review (Gagliano and Frazier 2001) and preliminary tests, it was learned that careful specimen preparation and grain angle selection might prevent wood failure. This is because wood is weak in shear parallel to grain so that cracks are easier to propagate along the grain direction within wood substrates. For flat sawn lumber, a three-degree grain angle was desired. Although quarter-sawn lumber was used in our case, the grain patterns can still be revealed and selected from the side faces of the wood panels. For FRP-wood specimens, the grain in the wood substrate should orient from the surface toward the bondline along the direction of crack propagation, as shown in Figure 6.2. For wood-wood specimens, two laminates were paired so that the radial grain converged to a “V” shape at the bondline.

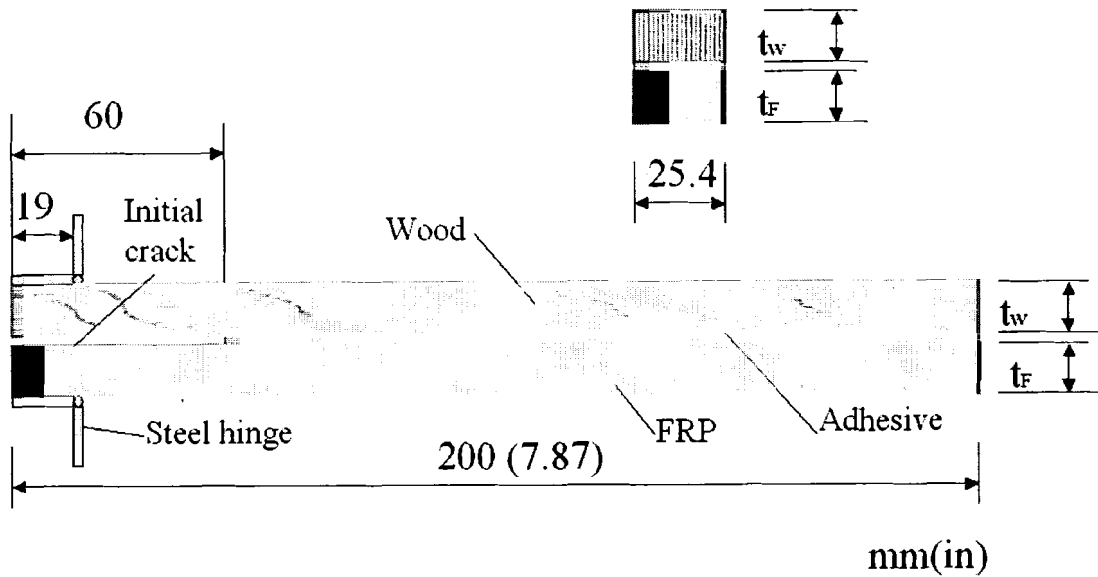


Figure 6.2 Specimen Configuration for Modified ASTM D5528 Mode I Tests

Several nonadhesive materials were screened as insert film to create the initial crack along the interface in the preliminary tests. The PTFE Teflon film (Virgin®) was found to be the best, which was used in the subsequent fabrication.

A pair of moment-free steel hinge tabs was bonded to the end of each specimen to apply the load, as shown in Figure 6.2. The plain steel continuous hinges with 0.06-in thickness, 1.5-in width and 0.5-in knuckle were found to be capable of sustaining the applied load without incurring damage.

The PLIOGRIP structural adhesive from Ashland Chemical was capable of providing adequate bonding strength between steel and FRP. However, the adhesive bond was not strong enough to hold the hinge on the wood surface in the tests. A thin layer of wood fiber under the hinge was always torn off. Therefore, the hinges were mechanically fastened to the wood substrate by drilling and tapping holes in the wood layer and attaching the hinges with wood screws. #6 round head slotted wood screws with 3/8-in length were used.

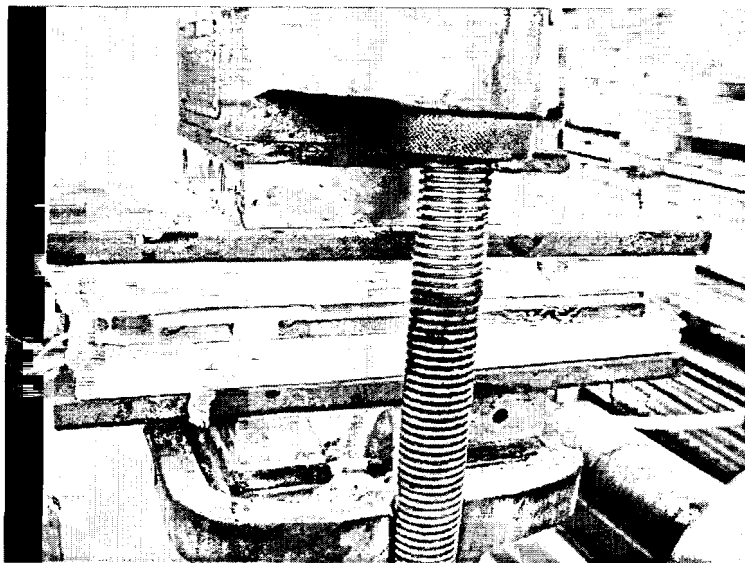


Figure 6.3 Hydraulic Press Used to Fabricate Specimens

The fabrication of FRP-wood laminated specimens was followed by a standard work instruction developed by (AEWC 2002). A standard work instruction for proportioning, mixing, applying and obtaining ingredients for HMR primer for bonding FRP to wood was also applied (AEWC 2001; Lopez-Anido *et al.* 2000).

The test joints were fabricated using a small hydraulic press shown in Figure 6.3, which can automatically be adjusted to apply constant clamping pressure. The assembly time and clamping pressure are listed in Table 6.1.

Table 6.2 Assembly Time and Clamping Pressure of Adhesives

| Adhesive | ISOGRIP Urethane | Epoxy G3 |
|------------------------------------|-----------------------------|---------------------|
| Open/closed Assembly Time (min) | 5/20 | 5/20 |
| Clamping Pressure (psi) | 50 | 20 |



Figure 6.4 Test Panel and DCB Test Sample of Mode I Fracture Tests

For the FRP-wood configuration of each material system, at least 12 specimens were selected and tested, representing at least four different panels. For the wood-wood configuration of each material system, at least 6 specimens were selected and tested, representing at least two different panels. The test panels and test samples are shown in Figure 6.4. The fabrication procedure consists of following steps:

1. Wood and FRP substrates with dimensions of 140 mm (5.5 in) wide and 200 mm (7.87 in) long were prepared. The thickness of wood substrate is 8.5 mm and 9.0 mm for material system B and C, respectively.
2. One surface of the wood lumber was refreshed with a planer. The HMR primer was prepared and applied to that surface 16 hours before the application of the adhesive.
3. A Teflon strip was bonded on the wood surface with spray adhesive. The strip must be parallel the end of the substrate with a distance of 60mm.
4. The bonding surface of FRP substrate was sanded with 80-grit sandpaper and cleaned with Acetone. The surface was wiped with a clean towel before the solvent dried.
5. The adhesive was applied uniformly only to the wood surface in accordance with manufacturer's instructions. Then, the FRP sheet was applied to the wood lumber.
6. The FRP-wood lamination was placed under pressure using the hydraulic press for a period of time and at the glueline temperature specified by the manufacturer of the adhesive.
7. A table saw with the diamond blade was used to trim about a half-inch strip along the longitudinal direction from one side of the test panel and discard the end piece.
8. The lamination was cut to 1-in wide strips along the longitudinal direction as the final samples. It should be able to make 4 test samples out of each test panel.

9. Continuous steel hinges were cut to 1-in wide pieces with the knuckles in the middle. Two holes were drilled on one leaf of the hinge. The surfaces of the hinges were abraded to make flat but rough surfaces.
10. The surfaces of the FRP substrate and the hinge were cleaned with Acetone and wiped with a clean towel before the solvent dried. The wood surface was also wiped with a clean towel.
11. Hinges were bonded to wood and FRP surfaces at the end with initial cracks with PLIOGRIP adhesive and proper clamping pressure. The hinges must be carefully adjusted to make good alignment.
12. Pilot holes were drilled into the wood substrates beneath the holes of the hinges. The pilot holes on the wood must be smaller than the diameter of the wood screws. Wood screws were installed.

The picture of specimen with hinges is shown in Figure 6.5.

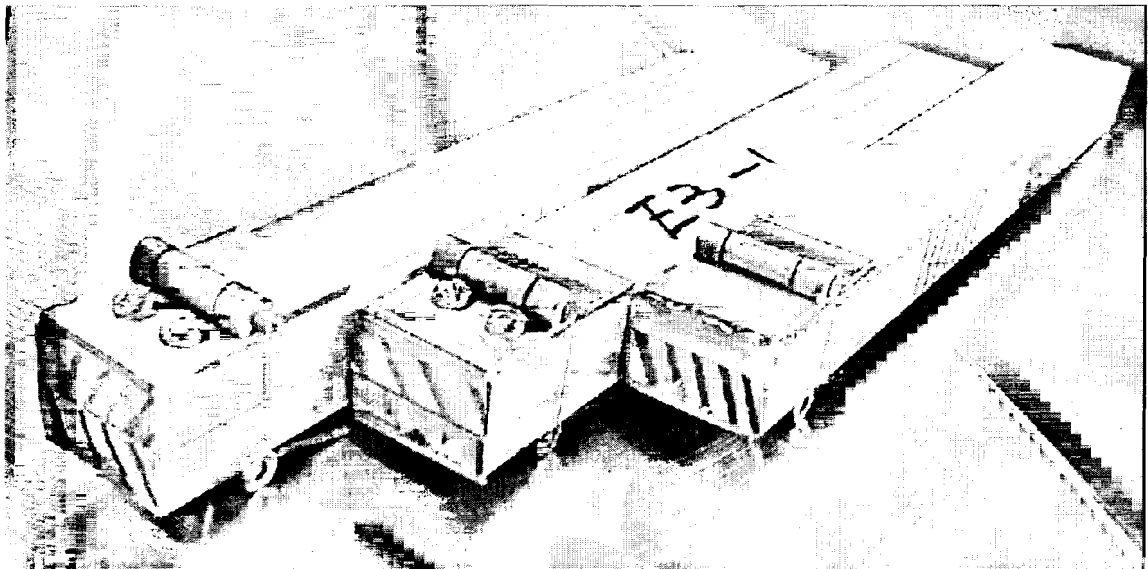


Figure 6.5 DCB Specimen with Hinges

6.7.3 Experimental Procedure

All samples were conditioned in an environmental chamber at 65% RH and 24°C for more than two weeks before testing. An Instron 5500R electro-mechanical testing frame with 2 kN load capacity was used to apply the load. The test setup is shown in Figure 6.6.

The test procedure was adapted from ASTM D5528 (ASTM 2002). Crack opening displacement (COD) and crack length were monitored during testing using a CCD camera with 12X magnification throughout the test. A CCD camera uses a small, rectangular piece of silicon rather than a piece of film to receive incoming light. This is a special piece of silicon called a charge-coupled device (CCD). Pictures were taken at various intervals to save on the computer disk. More pictures were taken during the crack initiation and propagation. The time that picture was taken was also recorded automatically. Data acquisition and system control of the CCD camera were performed with Labview software. The load and displacement of crosshead were recorded as well as time by the data acquisition system of Instron throughout the test.

Both edges of the specimen were coated with a thin layer of water-based typewriter correction fluid, providing a brittle high-contrast coating that simplifies crack visualization. Then, the edges were marked 30 mm with thin vertical lines every 5 mm from the insert. The delamination length is the sum of the distance from the loading line to the end of the insert plus the increment of growth determined from the tick marks. Prior to loading, the free end of the fracture specimen was supported to maintain horizontal placement. The specimen setup is shown in Figure 6.7.

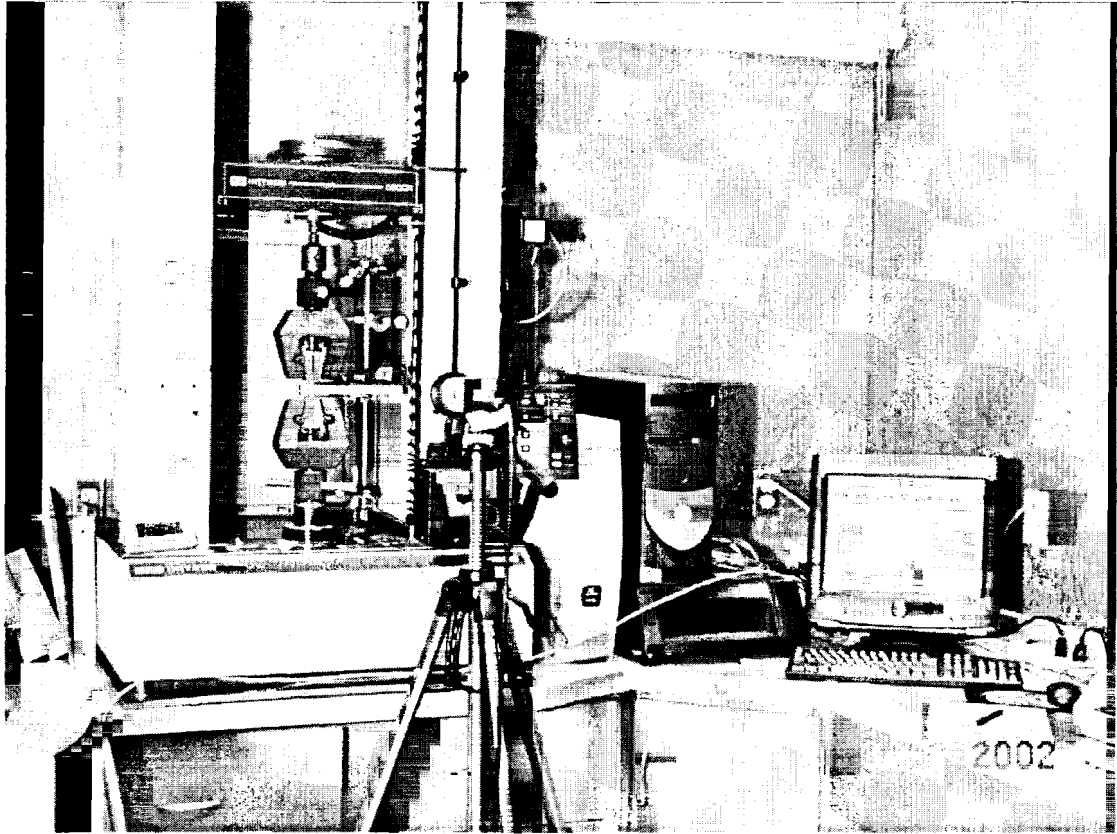


Figure 6.6 Test Setup of the Mode I Fracture Tests

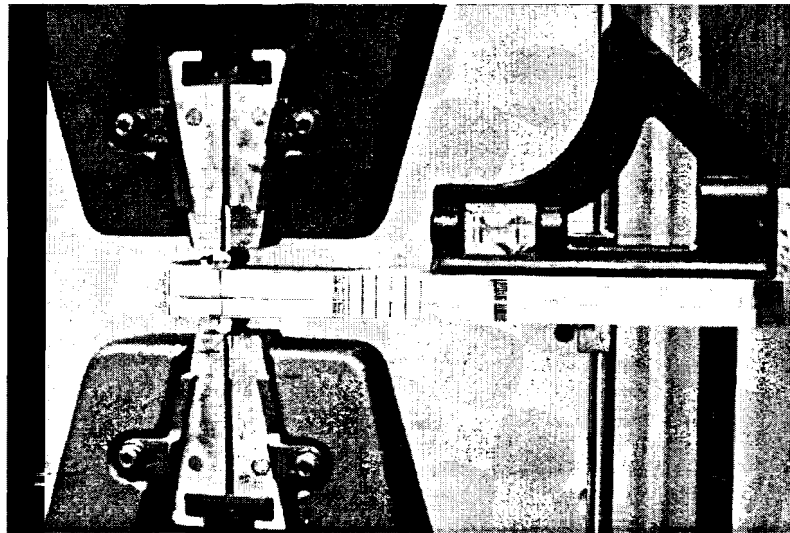


Figure 6.7 The Fracture Specimen Setup

The specimen was loaded continuously in displacement control with a loading rate of 0.5 mm/min, which was also adapted from ASTM D5528. When the delamination extended 30mm, the specimen was unloaded with a constant loading rate of 1 mm/min. Then the test machine was stopped.

6.8 Image Analysis

Sherlock image analysis software was used to measure the COD and crack length from the images with the unit of pixel, as shown in Figure 6.8. Then, they were converted to real unit such as millimeter. The software can be programmed to track the coordinates of COD points automatically for a series of images, as shown in Figure 6.8, which greatly simplifies the data processing. Unfortunately, it couldn't detect the crack tip accurately, which was needed to calculate the crack length. Therefore, the crack lengths were measured manually from the images, which turned out to be laborious and time-consuming. But it may be possible to overcome this drawback by using other softwares.

In ASTM D5528, the displacement of crosshead is used to calculate the fracture toughness, which has to be corrected by a parameter to account for the shortening of the moment arm as well as tilting of the end blocks. By the digital image correlation technique used in this study, it is capable to measure the COD directly, which is easier and more accurate.

Time was used to correlate the load and crosshead displacement recorded by Instron with the COD and crack length measured from the image. To check the accuracy of the time matching, the curves of the crosshead position versus time and the COD versus time were plotted in the same picture. For good time correlation and good

measurements, the two curves should be parallel each other and have the unloading point at the same time, a typical curve is shown in Figure 6.9. By this way, all of the parameters needed to calculate the strain energy release rate for a specific moment can be obtained.

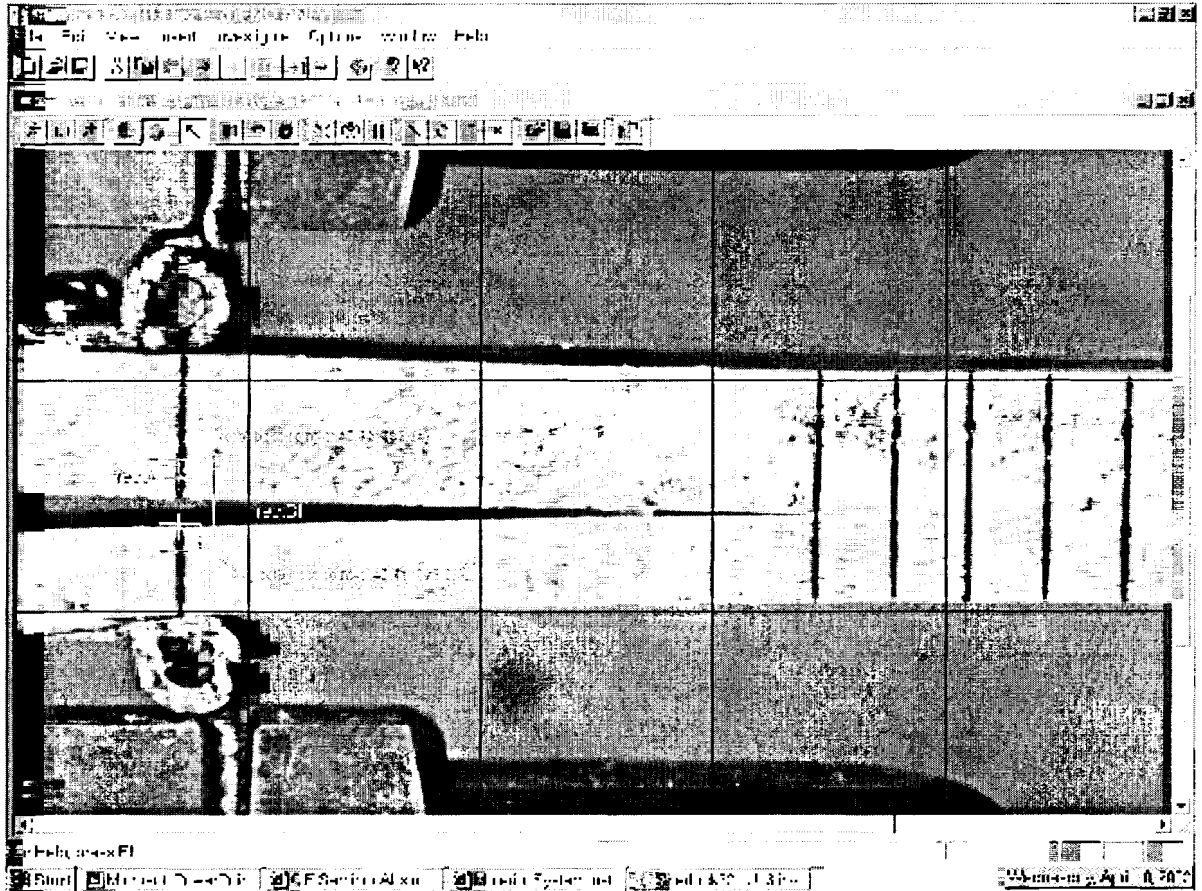


Figure 6.8 Image Analysis Using Sherlock

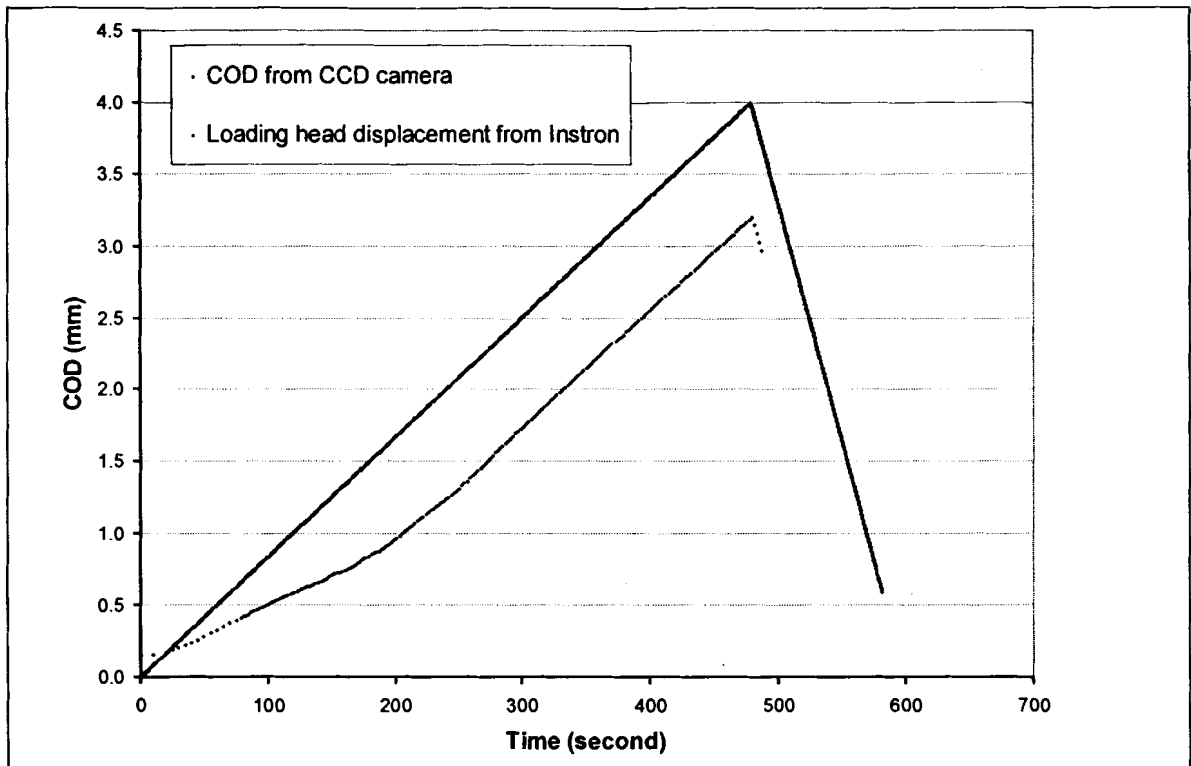


Figure 6.9 Time Correlation of Data from Instron and CCD Camera

6.9 Data Reduction Methods

There are three data reduction methods recommended by the ASTM D5528 for calculating Mode I interlaminar fracture toughness of unidirectional FRP composites in terms of strain energy release G_I . They are Modified Beam Theory (MBT) method, Compliance Calibration (CC) method and Modified Compliance Calibration (MCC) method. The first two methods were adapted by this study for calculating Mode I fracture toughness of FRP-wood interfaces. MCC method requires the thickness of one substrate to calculation the G_I , which is difficult to determine in the configuration of DCB specimen with hybrid substrates with different thickness. Therefore, this method was eliminated from this study.

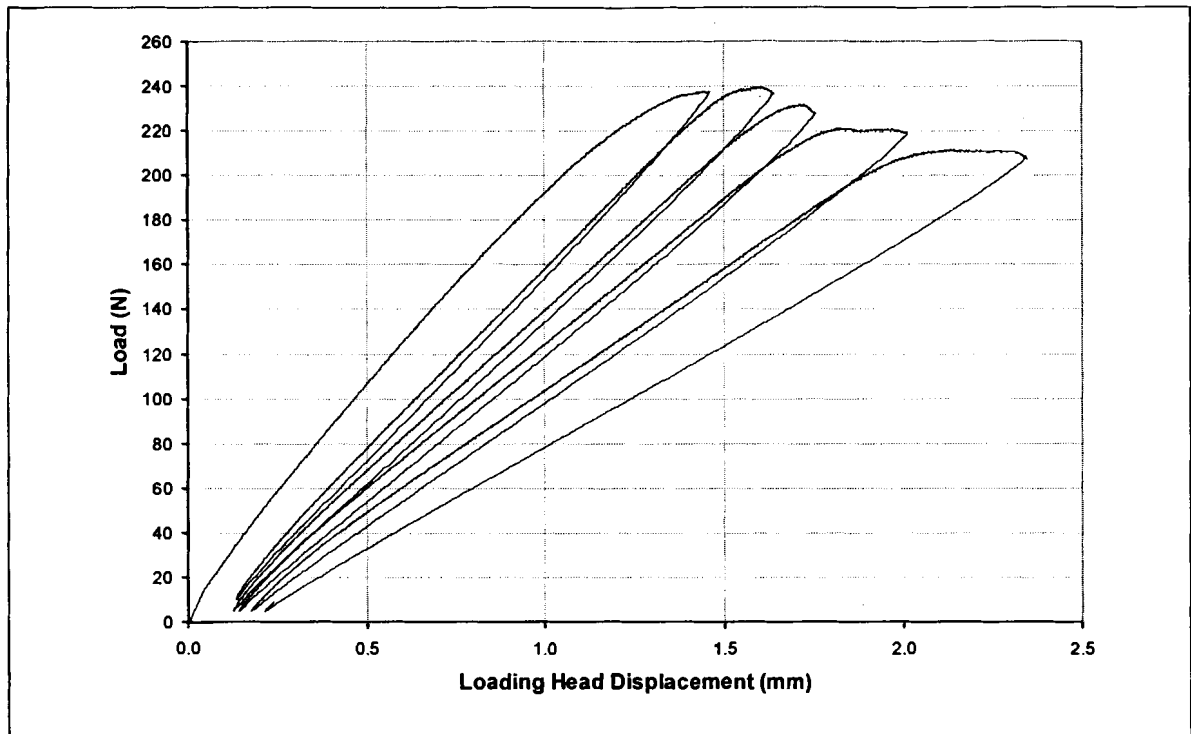


Figure 6.10 Typical Curve of Loading-unloading Cyclic Tests

The area method is another common method, which provides a very direct approach for estimating G_I for materials undergoing elastic response. This method is valid provided that interlaminar crack propagation is the only significant damage induced during the test, which means the unloading curves and subsequent loading curves must be identical. To check the validity of area method, some preliminary tests were conducted consisting of several loading and unloading cycles, based on ASTM D3433 (ASTM 2000a) and previous research (Davalos *et al.* 1997; Gagliano and Frazier 2001). A typical load-displacement curve is shown in Figure 6.10. Obvious hysteresis was observed in the non-coincidence of the loading and unloading curves. Furthermore, a slight displacement offset occurred on each loading cycle. Since these curves were not linear and their end points were significantly different, the area method was proven not to be valid. Therefore, the area method was not considered in this study.

Hashemi et al. developed a modified compliance method to correct for the low shear modulus of FRP composites named Shear Corrected Compliance (SCC) method (Hashemi *et al.* 1990). This method has proven to be very powerful by the research of Gagliano because of its ability to eliminate errors created by modulus variation (Gagliano and Frazier 2001). Such modulus variation greatly confounds traditional shear mode tests. The SCC method assumed perfect linear elasticity of the substrates. However, inelastic behavior may be significant for thinner DCB specimens, for woods of very low specific gravity, or for adhesives with exceptional toughness. Thus, this assumption must be evaluated for each system. This method was also adapted in this study.

Thus, three data reduction methods were adapted in this study: MBT, CC and SCC method. Load, crack length and COD were used for all of the three methods to calculate the strain energy release rate of the FRP-wood hybrid DCB specimens. The equations are listed as following:

6.9.1 Modified Beam Theory (MBT) Method

The Mode I interlaminar fracture toughness should be calculated as follows:

$$G_I = \frac{3P\delta}{2b(a+|\Delta|)} \quad (6.1)$$

where: P is the load, δ is the load point displacement, b is the specimen width and a is the delamination length. The compliance, C , is the ratio of the load point displacement to the applied load, δ/P . These parameters are shown in Figure 6.11. Δ may be determined experimentally by generating a least square plot of the cube root of compliance as a function of delamination length, as shown in Figure 6.12.

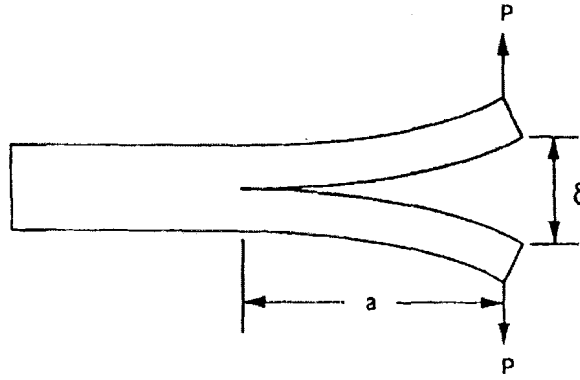


Figure 6.11 DCB for Measurement of Mode I Fracture Toughness (Daniel and Ishai 1994)

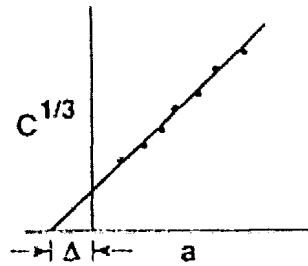


Figure 6.12 Modified Beam Theory (ASTM 2002)

6.9.2 Compliance Calibration (CC) Method

The Mode I interlaminar fracture toughness should be calculated as follows:

$$G_I = \frac{nP\delta}{2ba} \quad (6.2)$$

where the exponent n is determined experimentally from the slope of the least square plot of $\log(C)$ versus $\log(a)$, as shown in Figure 6.13.

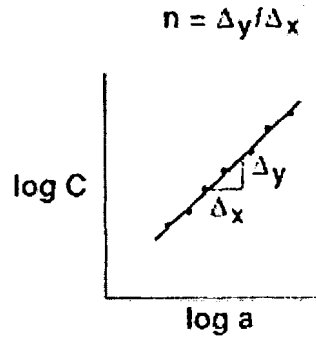


Figure 6.13 Compliance Calibration Method (ASTM 2002)

6.9.3 Shear Corrected Compliance (SCC) Method

The Mode I interlaminar fracture toughness should be calculated as follows:

$$G_I = \frac{P_c^2 (a+x)^2}{b(EI)_{\text{eff}}} \quad (6.3)$$

$$(EI)_{\text{eff}} = \frac{2}{3m^3} \quad (6.4)$$

$$x = \frac{b}{m} \quad (6.5)$$

where m and b are the slope and the y -intercept, respectively, from the linear trendline of the plot of $C^{1/3}$ versus a (Gagliano and Frazier 2001), as shown in Figure 6.14.

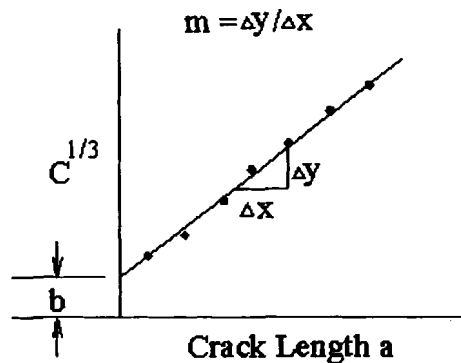


Figure 6.14 Shear Corrected Compliance (SCC) Method (Gagliano and Frazier 2001)

6.10 Experimental Results

A typical load-displacement curve is shown in Figure 6.15. The crack extensions induced changes in compliance, which resulted in losses of strain energy. A typical plot of $\text{Log}(C)$ vs. $\text{Log}(a)$ for the CC method is shown in Figure 6.16. A typical plot of the cube root of compliance versus crack length for MBT and SCC method is shown in Figure 6.17.

Plots of fracture energy versus crack length are shown in Figure 6.19 and Figure 6.20 for FRP-wood specimens of material system B and C, respectively. The comparison of typical plots of G_I versus crack length are shown in Figure 6.18 and Figure 6.21 for wood-wood and FRP-wood specimens of system B and C, respectively.

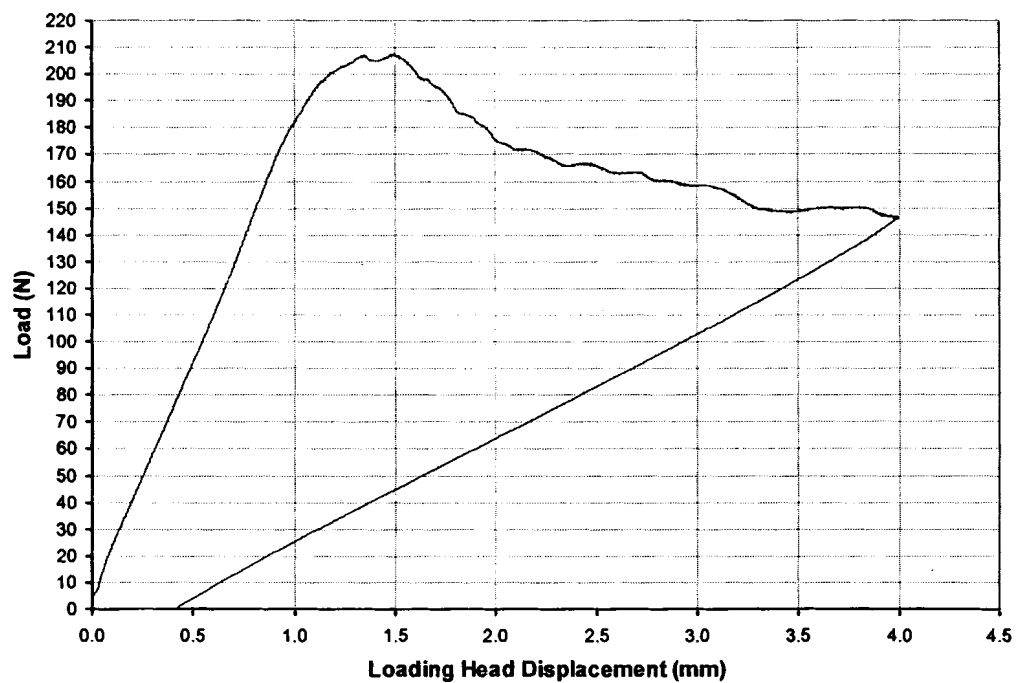


Figure 6.15 Typical Load-displacement Curve for FRP-Wood Specimen of System C

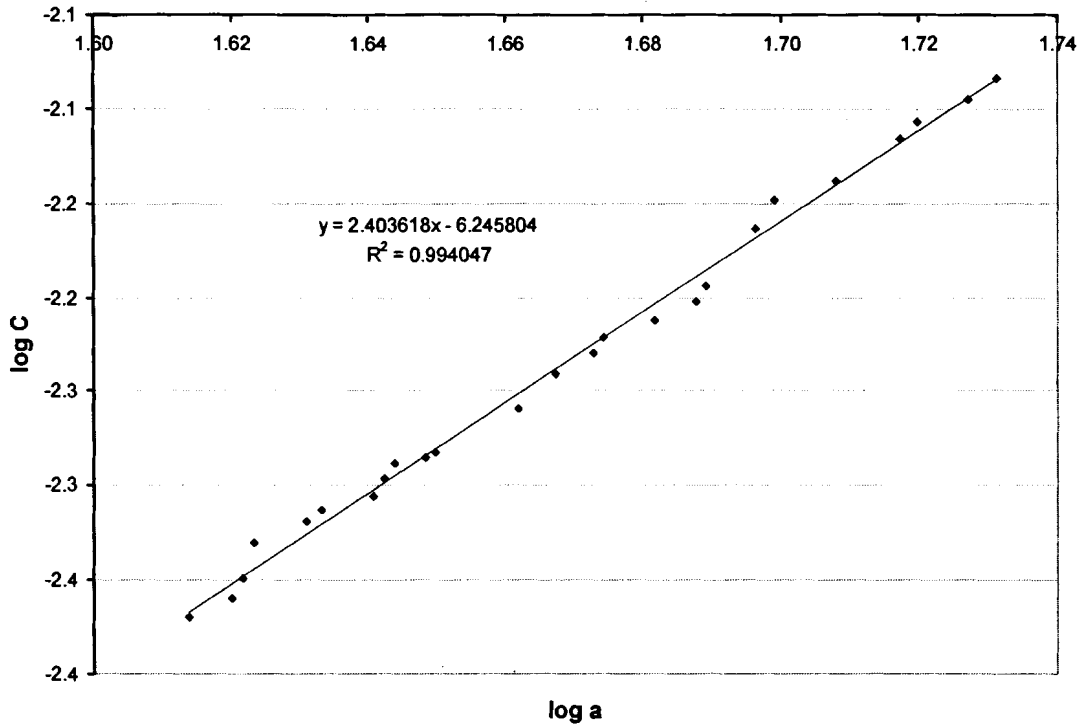


Figure 6.16 Typical Plot of $\log(C)$ versus $\log(a)$ Using the Data from Figure 6.15

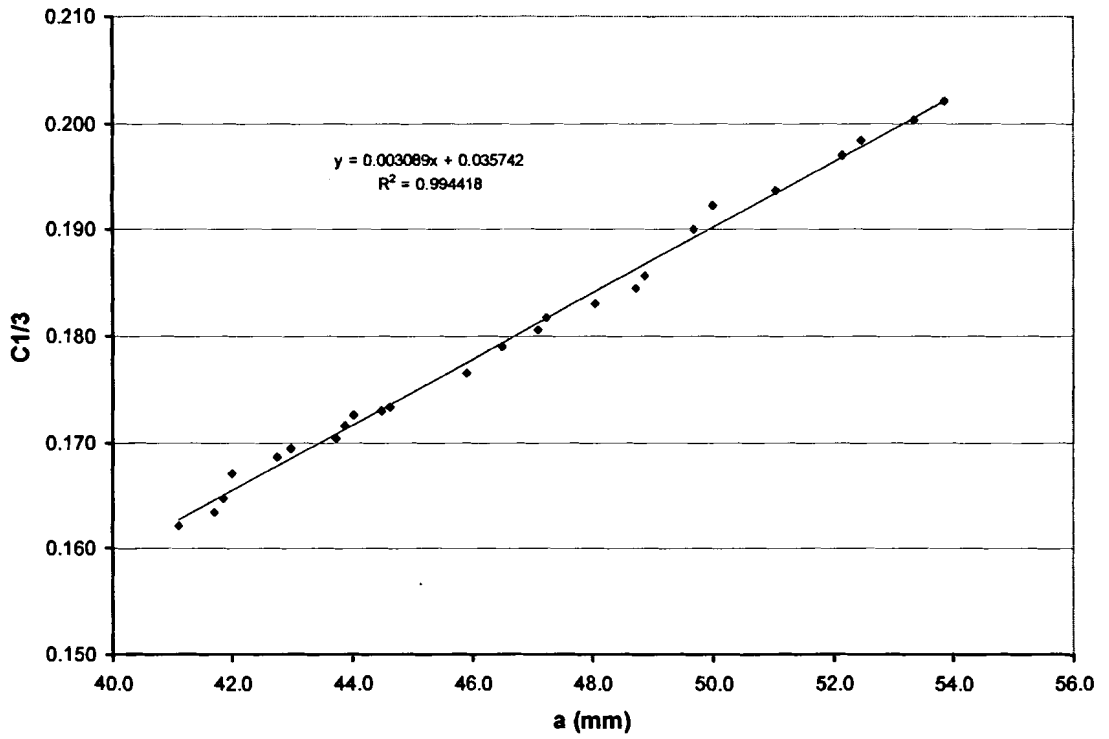


Figure 6.17 Typical Plot of $C1/3$ vs. Crack Length a Using the Data from Figure 6.15

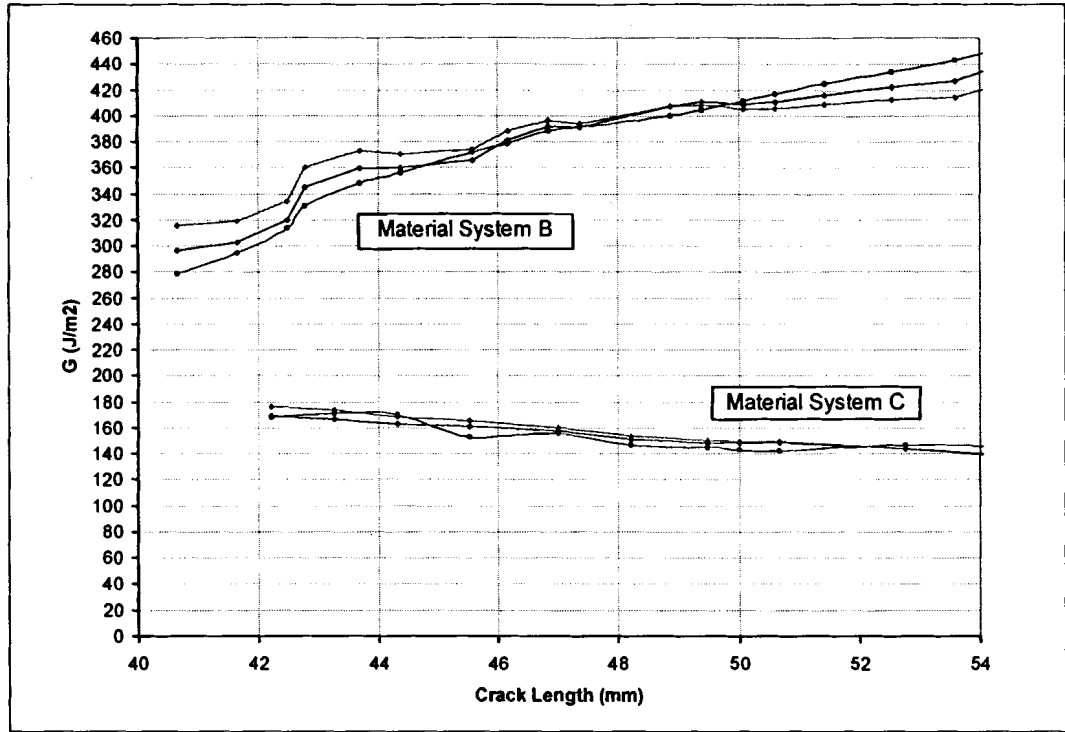


Figure 6.18 Typical G_I vs. Crack Length Plot Comparison for Single Wood-wood Specimen of System B and C

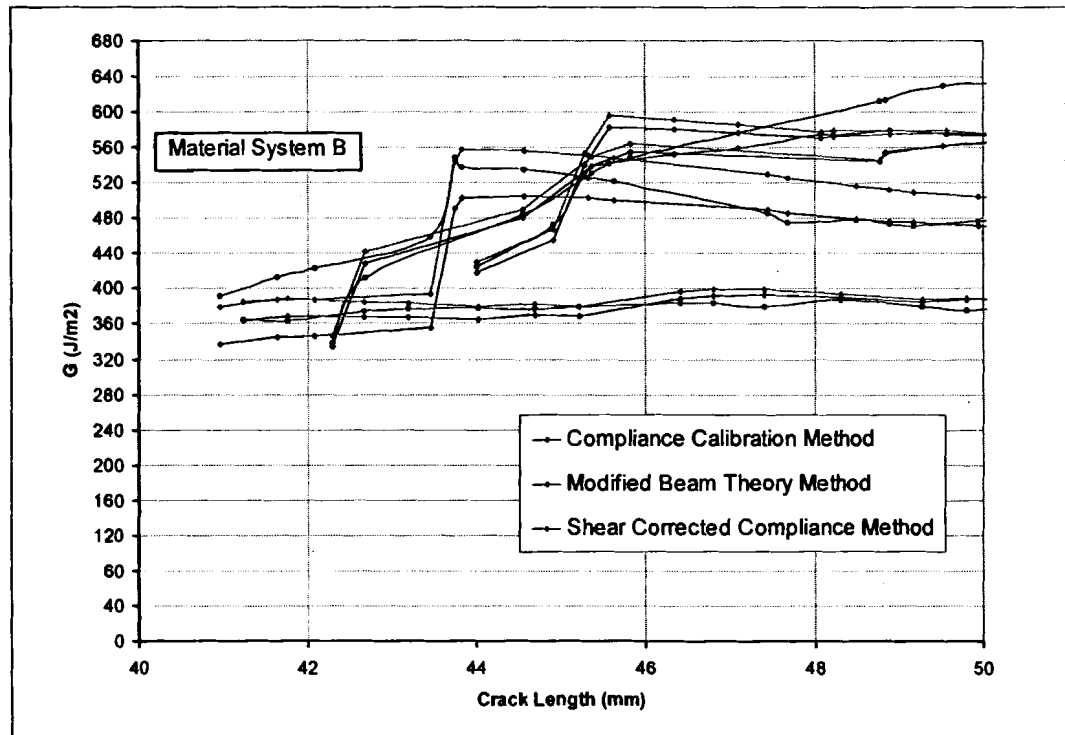


Figure 6.19 G_I vs. Crack Length Plot for four FRP-Wood Specimens of System B

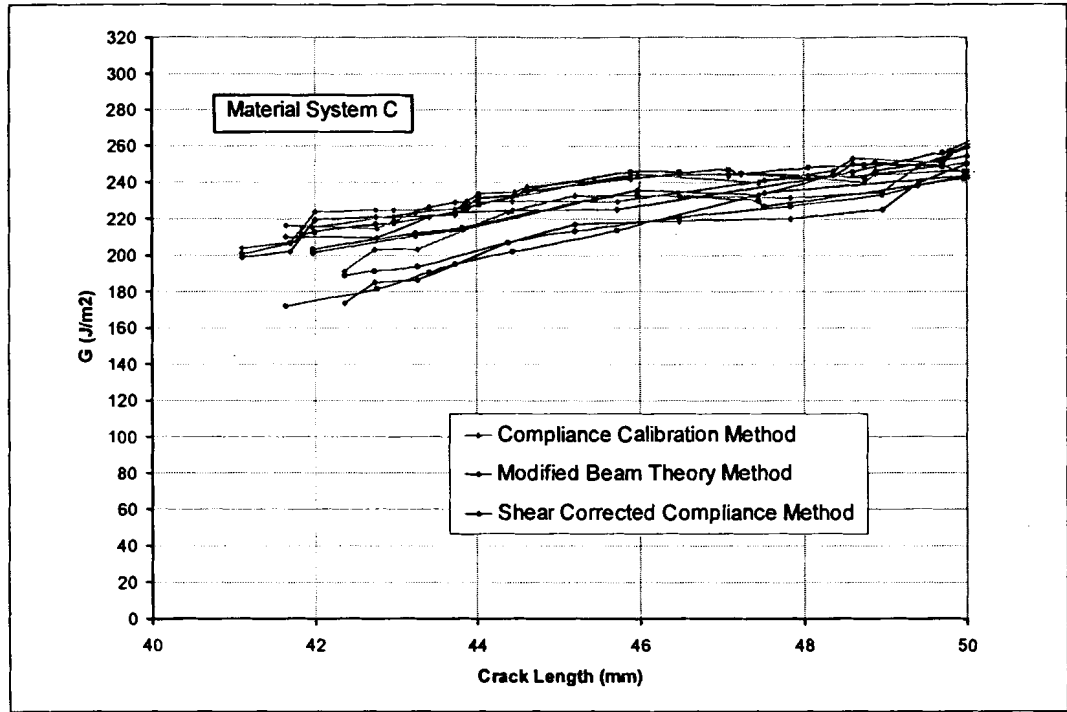


Figure 6.20 G_I vs. Crack Length Plot for four FRP-Wood Specimens of System C

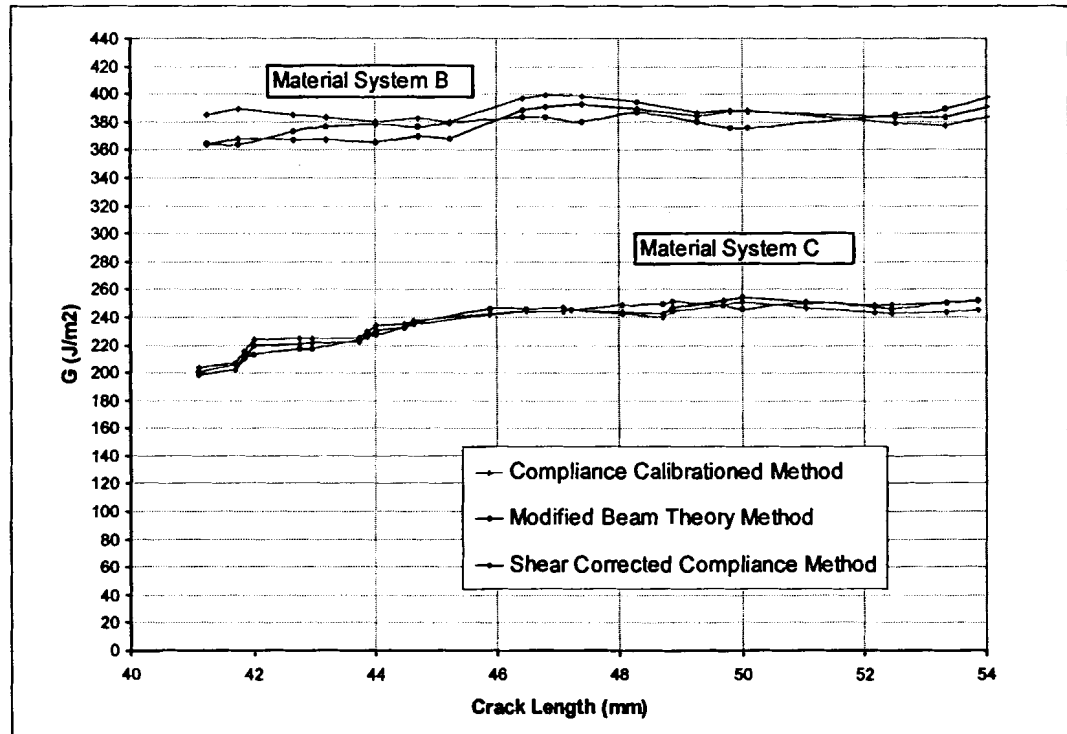


Figure 6.21 Typical G_I vs. Crack Length Plot Comparison for FRP-Wood Fracture Specimens of Material System B and C

6.11 Failure Mode

The photographs of typical failure mode of FRP-wood specimens of material system B and C are shown in Figure 6.22 and Figure 6.23, respectively. The percentage of wood failure of system B was much higher than that of system C. For system B, the cracks usually initiated from the FRP-wood interface and propagated into the wood substrate very soon. The pictures of typical failure mode of wood-wood specimens of material system B and C are shown in Figure 6.24 and Figure 6.25, respectively. For both material systems, the cracks usually propagated along the FRP-wood interface.

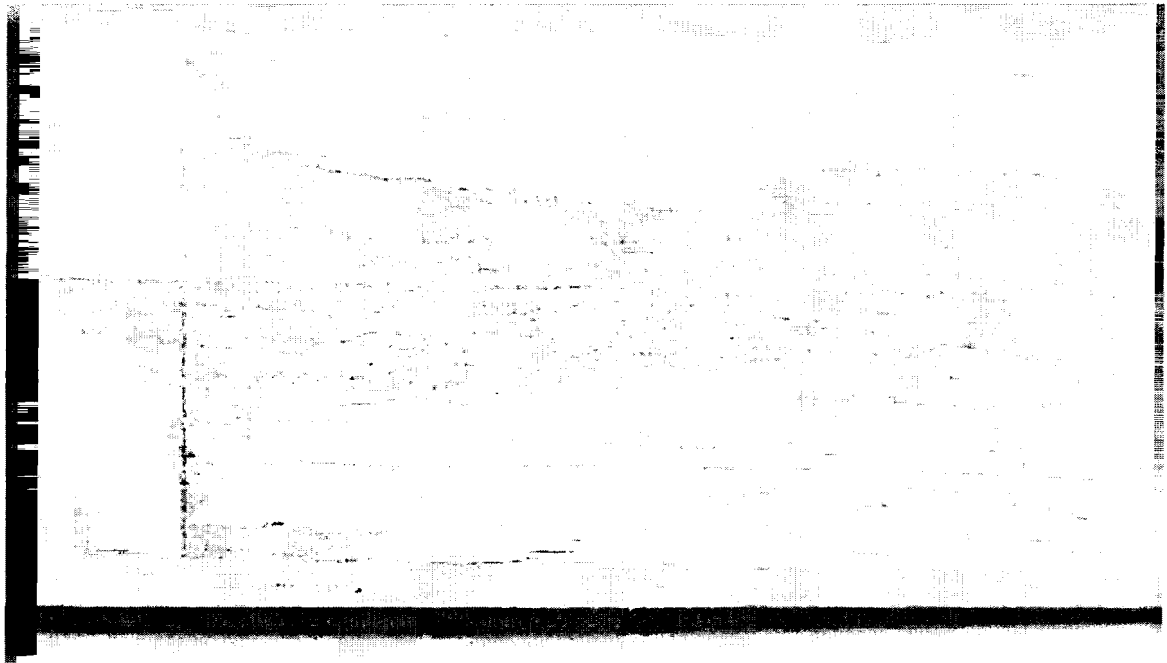


Figure 6.22 Typical Failure Mode of FRP-Wood Specimens of System B

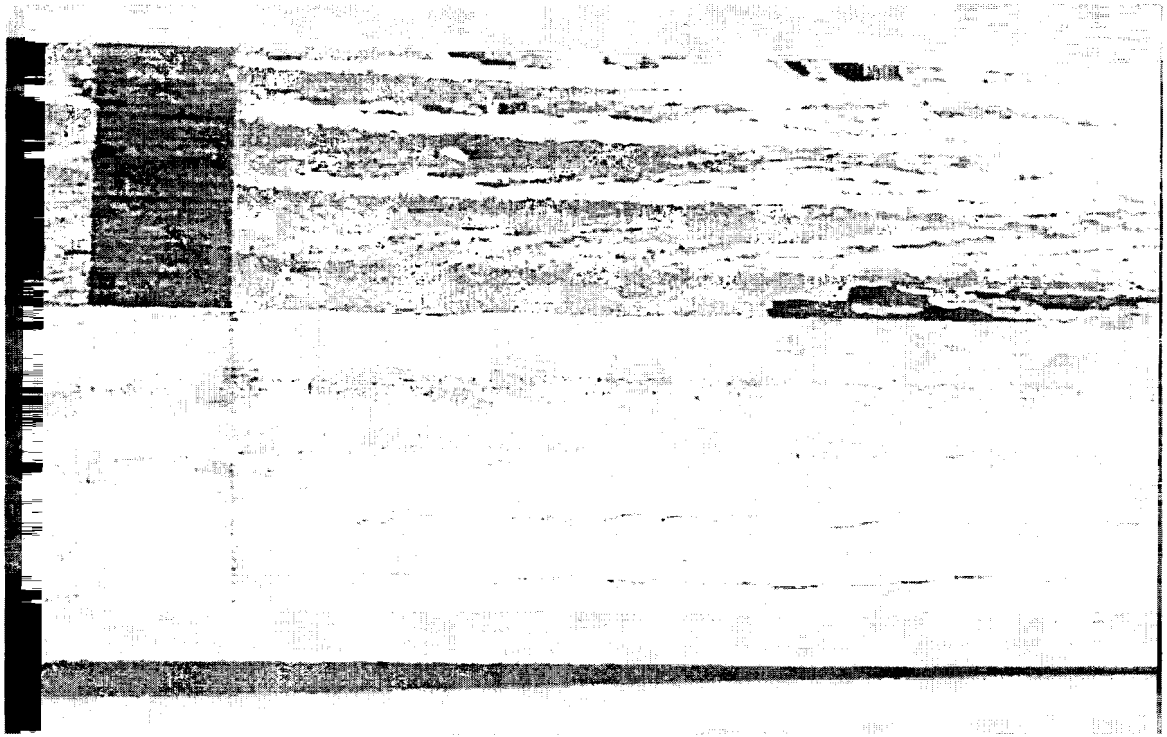


Figure 6.23 Typical Failure Mode of FRP-Wood Specimens of System C

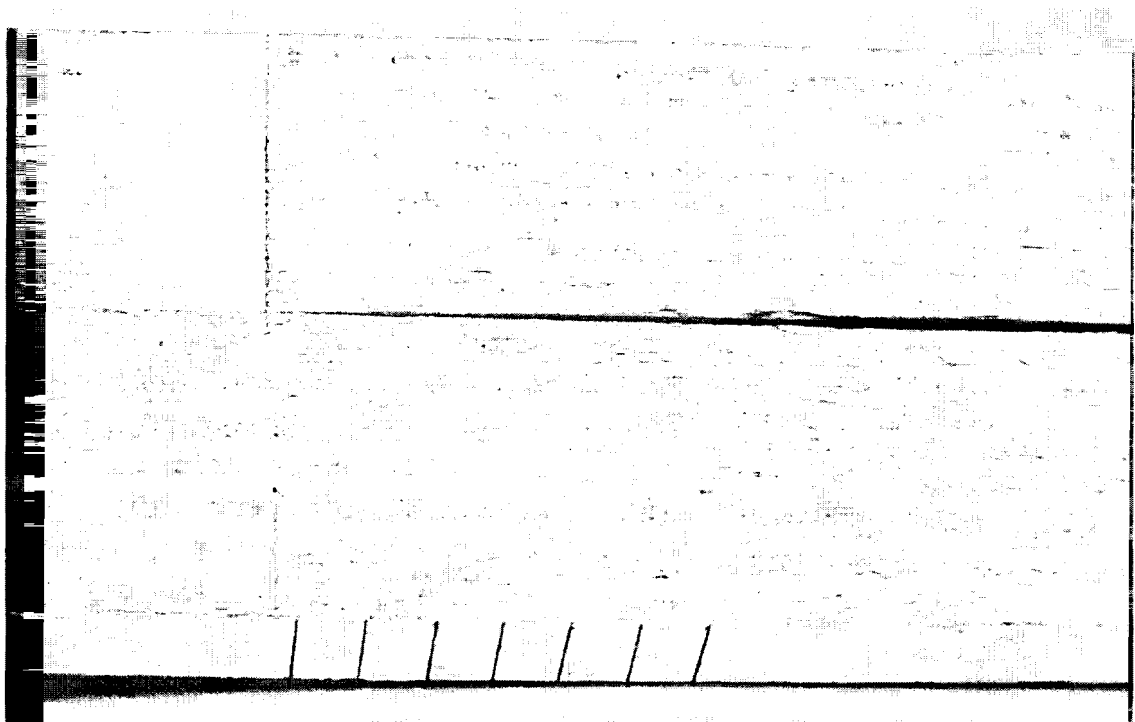


Figure 6.24 Typical Failure Mode of Wood-wood Specimens of System B

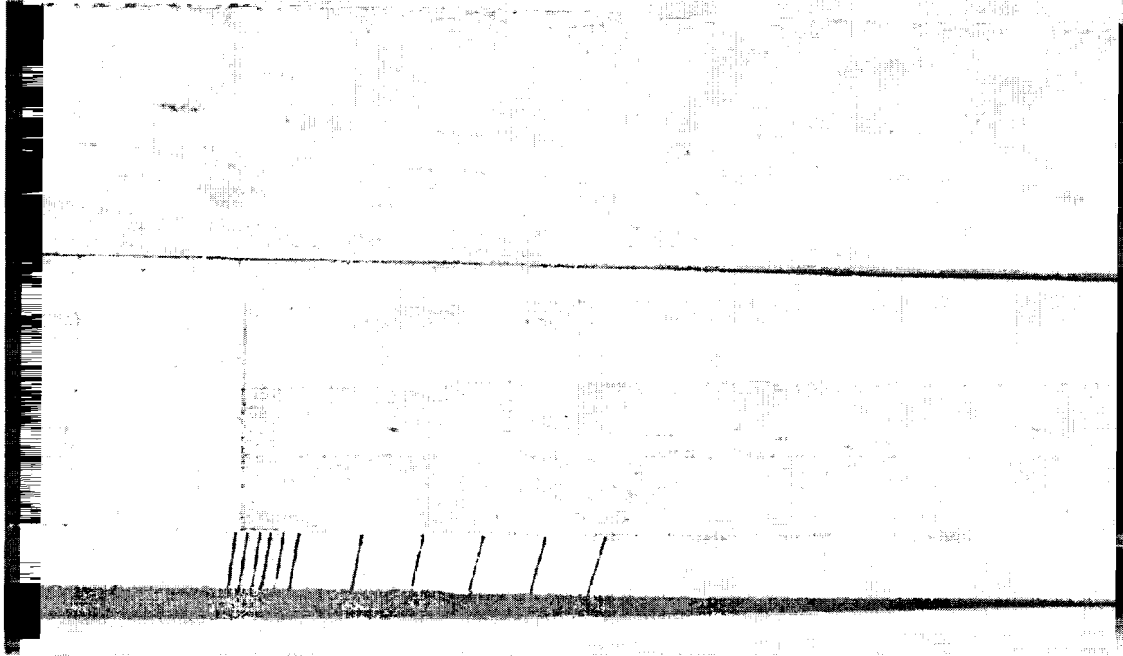


Figure 6.25 Typical Failure Mode of Wood-wood Specimens of System C

6.12 Comparison of Data Reduction Methods

Since quasi-continuous measurements of crack length and COD were achieved by means of the CCD camera, a single fracture specimen can produce up to 15 G_I measurements. Therefore, a coefficient of variation (COV) of G_I could be calculated for each fracture specimen.

The preceding data analyses were conducted with a single data set from a representative fracture specimen of each material system. The result is shown in Figure 6.26. Although COV of CC method was the lowest for specimens from both system B and C, none of the three were clearly superior to the others.

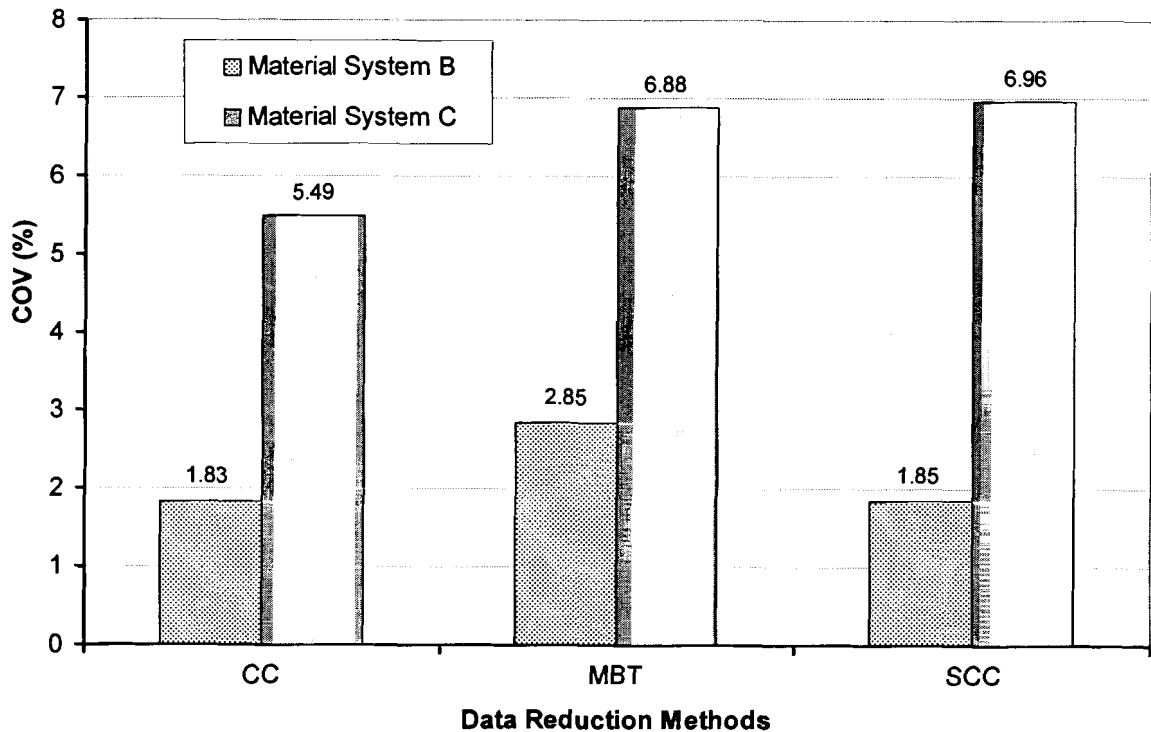


Figure 6.26 COV Comparison of Data Reduction Methods from Data of Single Typical Specimen of System B and C

6.13 Discussion of Experimental Results

A hybrid FRP-wood DCB is asymmetric about the adhesive layer, which often makes the crack path deviate from the FRP-wood interface to the wood substrate. In this study, tensile tests and 3-point bending tests were conducted to estimate the flexural modulus of FRP sheet and wood lumber. Then, these data were used to balance the bending compliance of the wood and FRP substrates by changing the thickness of the wood substrate. However, the results were not quite satisfactory. Only part of the specimens had the ideal interfacial failure, and premature wood failure occurred in most of the specimens.

Previous research showed that careful grain angle selection could prevent premature wood failure. For flat sawn lumbers, a three-degree grain angle was found to

be desired between the radial grain pattern and longitudinal axis of the lumber (Gagliano and Frazier 2001). On the other hand, no significant difference in Mode I fracture toughness values was noted among specimens at different grain angles other than 90° (Mijovic and Koutsky 1979). In this study, only quarter-sawn wood lumber was used to minimize the variation of wood surface properties. In this case, it was very difficult to control the grain angles of the lateral faces. Therefore, for future investigations, flat sawn lumber with similar surface patterns (such as early wood and late wood distribution) and desired grain angles are recommended. Furthermore, since wood density was observed to have a great influence on the surface bonding properties, only wood lumber with similar density should be selected. Techniques may also be improved to get more accurate measurement of the flexural modulus of the substrates.

In the DCB tests of this research, as the delamination grew from the insert, a resistance-type fracture behavior was observed, where the calculated G_I stabilized and increased slightly with the delamination growth. It may be assumed that the principal reason for the observed resistance to delamination was the development of adhesive fiber and wood fiber bridging. Therefore, only initiation values of G_I calculated from the first 15 mm crack length should be counted. Data points above this crack length were questionable.

Since rapid delamination growth may introduce dynamic effects in both the test specimen and in the fracture morphology, the relatively low monotonic loading rate of 0.5 mm/min was used throughout the tests based on the ASTM D5528. The delamination proceeded by a slow stable extension. An unstable jump from the insert was considered

as the indication of defects due to fabrication, e.g., the insert may not completely separate from the substrates.

The test results were very sensitive to the fabrication process and material properties of the substrates. Although only some of the tests were successful, they did give meaningful results and some important information. It was shown that Mode I fracture toughness of material system B was significant higher than that of system C, which proved that pure epoxy resins are relatively brittle polymers with poor resistance to crack propagation (Imanaka *et al.* 2001). The results are in good agreement with the common sense that urethane adhesives usually have higher peel strength than that of epoxy adhesives (Pocius 1997).

Previous researchers showed that the mean values of fracture toughness for the FRP-wood interface bond were slightly less than the corresponding values for the wood-wood interface bond (Davalos *et al.* 1997). It may be assumed that bonding two different adherends with distinct characteristics results in lower bond strength and larger variability. In this study, the fracture toughness values for the FRP-wood interface bond were similar as the corresponding values for the wood-wood interface bond for both material system B and C. This is in reasonable agreement with their results. However, since only a limited numbers of tests gave meaningful results, the statistical response is not fully characterized, which in turn makes it difficult to compare mean values of fracture toughness between FRP-wood interface and wood-wood interface.

In this study, three data reduction methods based on LEFM and empirical generalization of beam theory equations were adapted. Perfect linear elastic behavior was assumed in the calculation of G_I , which is valid when the zone of damage or nonlinear

deformation at the delamination front, or both, is small relative to the smallest specimen dimension, which is the specimen thickness for the DCB test (ASTM 2002).

The beam analysis method is based on the assumption that all of the strain energy in the DCB specimen is stored in the cantilever beams defined by the length of the crack. Since the beams are not rigidly clamped at their ends but supported by an elastic hinge, this assumption is incorrect (Whitney *et al.* 1982). Therefore, all of the three data reduction methods were modified from classic beam theory method to account for this factor. It was shown that all of the three methods were capable of providing useful results. None of them were clearly superior to the others. Although area method is a very direct approach for determining G_I for elastic materials, which assumes all of the energy change goes into interlaminar crack propagation, this method was proven to be not applicable in this study.

6.14 Conclusions and Recommendations

A standard ASTM test method was modified and applied to evaluate Mode I fracture toughness of adhesively bonded FRP-wood flat double cantilever specimens. Based on the research findings presented in this chapter, the following conclusions are drawn:

- 1) A tremendous simplification is realized with the flat FRP-wood DCB geometry. Consequently, crack length measurements are required during testing. However, the application of the state-of-the-art digital hardware and image correlation techniques can greatly reduce the work of real-time crack length measurements as well as improve the accuracy.

- 2) Although this is the first time to apply the flat DCB geometry to evaluate Mode I fracture toughness of FRP-wood hybrid interfaces, this study shows that there is a good potential to develop it to a standard routine test. Since fracture toughness is a material property independent on the size and geometry of the cracked body, this method is capable of discriminating quantitatively between material systems of different interlaminar toughness, making it an excellent material screening tool.
- 3) Three data reduction methods were applied to compute fracture toughness of adhesive-bonded wood joints: modified beam theory method, compliance calibration method and shear corrected compliance method. All of the three methods were shown to be capable to give meaningful results. None of them were clearly superior to the others. The area method was proven to be not applicable in this study.

The following recommendations are suggested:

- 1) The methods of linear elastic fracture mechanics (LEFM) were extended to adhesive-bonded wood joints in this study. Since some deviations from perfect elasticity were observed, an inelastic analysis could be applied. However, the improved accuracy may not outweigh the simplicity and convenience of the linear elastic treatment.
- 2) Only Mode-I fracture toughness of the FRP-wood interface was considered in this study. However, the FRP-wood interface of typical bridge girders are usually subjected to mixed Mode (I/II) delamination loading. Therefore, fracture toughness of Mode II or mixed Mode (I/II) may also need to be evaluated to investigate the overall fracture performance of the FRP-wood interface.

- 3) Another possible improvement may come from the application of precracks. The tests with precracks were found to give lower values of initial fracture toughness (Hojo *et al.* 1995). It may avoid some fabrication defects induced from the insert film, such as the insert is not completely disbanded from the laminates, or the insert is too thick resulting in a large neat resin pocket, or contain a tear or fold (ASTM 2002). These defects may have great influence on the initial value of G_I . To get an initiation value free of fiber bridging, ASTM D5528 doesn't use precracks. However, it may be worth studying the effects of precracking in further investigations.
- 4) In the specimen fabrications of this study, narrow strips of PTFE Teflon film were used to create the initial cracks, as shown in Figure 6.4. For future fabrications, the insert is recommended to cover the whole disbanded area.
- 5) It was shown that fracture mechanics approaches could be applied to examine the cyclic fatigue behavior of adhesively bonded joints. It was found that a threshold value of the applied strain-energy release rate does exist and may be used to rank the fatigue limit behavior of different adhesive systems and their resistance to hostile environments (Fernando *et al.* 1996). Since the objective of this study is to evaluate fatigue performance of the FRP-wood interface, a cyclic fatigue method may be developed to investigate the Mode I fatigue delamination growth onset of the FRP-wood interface based on ASTM D 6115 (ASTM 2000b).

Chapter 7

CONCLUSIONS AND RECOMMENDATIONS

7.1 Development of a Laminating Press

Calibration experiments were conducted to obtain the torque-clamping pressure relationship and the clamping pressure loss-time relationship. The standard operation procedure (work instruction) for the laminating press was developed, and is presented in the Appendix.

Based on the research findings presented in this chapter, the following conclusions are drawn:

- 1) The laminating press is capable of applying reasonably constant and uniform clamping pressure over the time span required to create quality adhesive bonding of the billets for ASTM D2559 and ASTM D905 standard tests. After retightening, the pressure loss over the adhesive curing time (up to 24 hours) was within 19%.
- 2) A phenomenological model and an empirical model were developed to be able to predict the pressure-time behavior of the laminating press system with acceptable accuracy.
- 3) The optimum retightening time and the amount of the initial pressure were determined. For wood billets bonded with this PRF resin, one hour is the proper retightening time, and the initial pressure should be 0.86 MPa (125 psi).

The following recommendations are suggested:

- 1) Lubricant should be applied regularly to reduce the friction between the nuts and the top threads of the guiding posts.

- 2) Since the top plates are relatively heavy (105 kg), two people are needed to operate the press. To operate the system by one person, two jacks may be used to lift up the top plates of the press, one on each side.
- 3) The parameters of the press and the models were calculated specifically for Southern yellow pine and PRF adhesive. If the materials of the lay-ups are changed (wood and/or adhesive), the press has to be recalibrated and the parameters have to be recalculated.

7.2 Material Screening Tests

The following conclusions were drawn based on the experimental findings:

- 1) An effective bonding interface was achieved between E-glass/urethane composite and DF by priming the wood surface with HMR.
- 2) For material system B, both the CSM material sanded by hand and the all roving material sanded by machine passed the delamination tests and shear block tests. Because the extra surface treatment may increase the cost, the all roving material was eliminated from the matrix of the subsequent tests. Only the CSM material was selected for further evaluation.
- 3) An effective bonding interface was achieved between E-glass/epoxy composite and DF by priming the wood surface with HMR.
- 4) It was found that the HMR primer significantly improved the bond strength and durability of the epoxy FRP-wood interface. This experimental findings is in agreement with published results.

5) It was found that the shear block test is not as sensitive as the delamination tests to discriminate adhesive systems. For example, for material system C, all of the three adhesives had good shear strength and wood failure, but only G3 adhesive passed the cycle delamination test. The delamination test of ASTM D2559 was successfully used to discriminate the effect of several bonding parameters and select the best material combinations for further evaluation. These conclusions are in agreement with existing recommendations.

7.3 Single-lap Shear Fatigue Tests

A standard ASTM test method was modified and applied successfully to evaluate fatigue performance of adhesively bonded FRP-wood single-lap shear specimens. The corresponding fatigue performance-based evaluation criteria and associated limits were proposed. Two material systems were evaluated: system B and C. This fatigue test is necessary but not enough to characterize the FRP-wood interface. The advantage of this test is that the interface is subjected to cyclic stress. The disadvantage of this test is the stress concentrations at the notches. Besides, this test does not provide actual material property but an apparent property that depends on a complex stress state including both shear and peeling. However, in actual glulam beam, there is also a complex stress state including both shear and peeling. The main contribution of this study is to establish a protocol to apply single-lap shear under fatigue loading to evaluate FRP-wood interfaces.

Based on the research findings presented in this chapter, the following conclusions are drawn:

- 1) It was shown that material system C presented stronger bonding strength and better fatigue resistance than system B when tested in single-lap shear configuration. Quality bonding was observed for both material systems in terms of high percentage of wood failure.
- 2) Since no statistically significant difference was observed between the control strength and the residual strength for both material systems, it may be assumed that there was no damage accumulation due to fatigue tests.

The following recommendations are suggested:

- 1) Since both material systems B and C passed the delamination tests and shear block tests, ASTM D2559 alone is not sufficient to discriminate the differences between them. Furthermore, performance evaluation tests presented in Chapter 2 are not sufficient to predict whether a bonded interface has good fatigue resistance. Therefore, single-lap shear fatigue tests is considered necessary to evaluate performance requirements of FRP composite reinforcement systems for glulam in highway bridge applications.
- 2) Wood bonding properties (strength and wood failure) are highly dependent on the density of the wood. To evaluate the effects, sample groups with different wood densities should be tested. Within each group, wood lumber should have similar densities and surface pattern to minimize the variation of experimental results.
- 3) The desired SLS strength of an eligible FRP-wood specimen should be controlled by the shear strength of wood parallel to the grain, which is indicated by high wood failure.

- 4) To investigate the effects of possible adhesive strength change due to the post-curing with time, 50% of quasi-static control tests should be conducted after fatigue tests.
- 5) If most of the specimens passed 3 million cycles (e.g., 75%), it may be necessary to increase the stress level to get the information of fatigue failure mode (e.g., the percentage of interface wood failure).
- 6) Since the overlap area is subjected to the shear stresses as well as peel stresses, the fatigue failure process was a process of fracture under the combination of Mode I (Opening Mode) and Mode II (Forward Shear Mode). Therefore, the Mode I fracture toughness may control the overall single-lap shear strength. Thus, the Mode I fracture toughness study presented in Chapter 6 should also be considered as an important indicator of fatigue resistance of FRP-wood bonding.

7.4 Finite Element Analysis of Single-lap Shear Specimen

The FEA shows that the apparent single-lap shear strength of the FRP-wood hybrid specimens was controlled by the tensile (peel) strength of the adhesive/adherend interface in terms of the highest stress concentration factors at the end of the overlap area. The shear and peeling stress distributions are not symmetric. The highest stress concentration factor occurs at the corner near the FRP notch. The peeling stresses are not convergent at that corner.

The stress condition of the FRP-wood interface may be characterized by the ratio of the average peeling stress to the average shear stress of the adhesive surface. The lower this ratio, the less peeling stresses are developed, and consequently, the more desirable the stress field results. The ratio of material system B, 0.88, is lower than that of

material system C, 0.94. Therefore, the stress condition of material system B is more desirable. It is shown that elastic modulus of adhesives have significant influence on the stress conditions of the single-lap shear configuration.

The failure mode of fatigue tests matched well with the prediction of finite element models, which shows that the cracks always started at a point near the FRP notch. The cracks were usually started at a point near the bondline within the wood layer, and gradually propagated to the wood notch until failure.

7.5 Mode I DCB Fracture Tests

A standard ASTM test method was modified and applied to evaluate Mode I fracture toughness of adhesively bonded FRP-wood flat double cantilever specimens. Based on the research findings presented in this chapter, the following conclusions are drawn:

- 1) A tremendous simplification is realized with the flat FRP-wood DCB geometry. Consequently, crack length measurements are required during testing. However, the application of the state-of-the-art digital hardware and image correlation techniques can greatly reduce the work of real-time crack length measurements as well as improve the accuracy.
- 2) Although this is the first time to apply the flat DCB geometry to evaluate Mode I fracture toughness of FRP-wood hybrid interfaces, this study shows that there is a good potential to develop it to a standard routine test. Since fracture toughness is a material property independent on the size and geometry of the cracked body,

this method is capable of discriminating quantitatively between material systems of different interlaminar toughness, making it an excellent material screening tool.

- 3) Three data reduction methods were applied to compute fracture toughness of adhesive-bonded wood joints: modified beam theory method, compliance calibration method and shear corrected compliance method. All of the three methods were shown to be capable to give meaningful results. None of them were clearly superior to the others. The area method was proven to be not applicable in this study.

The following recommendations are suggested:

- 1) The methods of linear elastic fracture mechanics (LEFM) were extended to adhesive-bonded wood joints in this study. Since some deviations from perfect elasticity were observed, an inelastic analysis could be applied. However, the improved accuracy may not outweigh the simplicity and convenience of the linear elastic treatment.
- 2) Another possible improvement may come from the application of precracks. The tests with precracks were found to give lower values of initial fracture toughness. It may avoid some fabrication defects induced from the insert film, such as the insert is not completely disbonded from the laminates, or the insert is too thick resulting in a large neat resin pocket, or contain a tear or fold. These defects may have great influence on the initial value of G_I . To get an initiation value free of fiber bridging, ASTM D5528 doesn't use precracks. However, it may be worth studying the effects of precracking in further investigations.

- 3) In the specimen fabrications of this study, narrow strips of PTFE Teflon film were used to create the initial cracks. For future fabrications, the insert is recommended to cover the whole disbonded area.
- 4) It was shown that fracture mechanics approaches can be applied to examine the cyclic fatigue behavior of adhesively bonded joints. It was found that a threshold value of the applied strain-energy release rate does exist and may be used to rank the fatigue limit behavior of different adhesive systems and their resistance to hostile environments. Since the objective of this study is to evaluate fatigue performance of the FRP-wood interface, a cyclic fatigue method may be developed to investigate the Mode I fatigue delamination growth onset of the FRP-wood interface based on ASTM D 6115.

7.6 Summary

- 1) The HMR primer significantly improved the bond strength and durability of both the urethane and epoxy FRP-wood interface.
- 2) The laminating press is capable of applying reasonably constant and uniform clamping pressure over the time span required for billet fabrications.
- 3) Since the shear block test is easier to conduct than the cycle delamination test, it should be used as the first step of the screening tests. Only those material systems pass the shear block test need to be further investigated.
- 4) The shear block strength is generally higher than the Quasi-static SLS strength for both material systems.

- 5) The single-lap shear fatigue test was proven to be satisfactory to assess FRP-wood bond strength under cyclic loads.
- 6) Apparent SLS strength of the wood-FRP hybrid specimens was controlled by the tensile (peel) strength of the adhesive /adherend interface.
- 7) The stress condition of the FRP-wood interface may be characterized by the ratio of the average peeling stress to the average shear stress of the adhesive surface.
- 8) Mode I DCB fracture test was proven to be satisfactory to assess FRP-wood bond fracture toughness.
- 9) Both single-lap shear tests and Mode I DCB fracture tests are necessary to qualify the FRP-wood bond under quasi-static and cyclic loads.

REFERENCES

- Adams, R. D. (1989). "Strength predictions for lap joints, especially with composite adherends, a review." *Journal of Adhesion*, 30, 219-242.
- AEWC. (2001). "Work Instruction for proportioning, mixing, applying and obtaining ingredients for HMR primer for bonding vinyl ester matrix composites to wood by wet lay-up." Advanced Engineered Wood Composites Center, University of Maine, Orono, ME.
- AEWC. (2002a). "Work Instruction for calibration of cold press screw jacks and calibration of torque wrenches." Advanced Engineered Wood Composites Center, University of Maine, Orono, ME.
- AEWC. (2002b). "Work Instruction for cycle delamination tests based on the modified ASTM D2559." Advanced Engineered Wood Composites Center, University of Maine, Orono, ME.
- AEWC. (2002c). "Work Instruction for Mode I fracture tests based on the modified ASTM D5528." Advanced Engineered Wood Composites Center, University of Maine, Orono, ME.
- AEWC. (2002d). "Work Instruction for shear block tests based on the modified ASTM D905." Advanced Engineered Wood Composites Center, University of Maine, Orono, ME.
- AEWC. (2002e). "Work Instruction for single-lap shear tests based on the modified ASTM D2339." Advanced Engineered Wood Composites Center, University of Maine, Orono, ME.

- Anderson, T. L. (1991). "Fracture mechanics : fundamentals and applications." Boca Raton : CRC Press.
- Andruet, R. H., Dillard, D. A., and Holzer, S. M. (2001). "Two- and three-dimensional geometrical nonlinear finite elements for analysis of adhesive joints." *International Journal of Adhesion and Adhesives*, 21, 17-34.
- ANSYS. (2001). "ANSYS / Multiphysics." ANSYS, Inc, Canonsburg, PA.
- Armstrong, K. B. (1996). "Effect of absorbed water in CFRP composites on adhesive bonding." *International Journal of Adhesion and Adhesives*, 16(3), 21-28.
- Army Research Laboratory. (1999). "The Composite Materials Handbook-MIL-17." Aberdeen Proving Ground, MD.
- Ashcroft, I. A., Hughes, D. J., and Shaw, S. J. (2001). "Mode I fracture of epoxy bonded composite joints: 1. Quasi-static loading." *International Journal of Adhesion and Adhesives*, 21(2), 87-99.
- Ashcroft, I. A., and Shaw, S. J. (2002). "Mode I fracture of epoxy bonded composite joints: 2. Fatigue loading." *International Journal of Adhesion and Adhesives*, 22(2), 151-167.
- ASTM. (2000a). "ASTM D905-98 Standard Test Method for Strength Properties of Adhesive Bonds in Shear by Compression Loading." American Society of Testing and Materials, West Conshohocken, PA.
- ASTM. (2000b). "ASTM D2344-00 Standard Test Method for Apparent Interlaminar Shear Strength of Parallel Fiber Composites by Short-Beam Method." American Society of Testing and Materials, West Conshohocken, PA.

- ASTM. (2000c). "ASTM D2559-00 Standard Specification for Adhesives for Structural Laminated Wood Products for Use Under Exterior (Wet Use) Exposure Conditions." American Society of Testing and Materials, West Conshohocken, PA.
- ASTM. (2000d). "ASTM D2584-00 Standard Test Method for Ignition Loss of Cured Reinforced Resins." American Society of Testing and Materials, West Conshohocken, PA.
- ASTM. (2000e). "ASTM D3039-00 Standard Test Method for Tensile Properties of Polymer Matrix Composite Materials." American Society of Testing and Materials, West Conshohocken, PA.
- ASTM. (2000f). "ASTM D3433-99 Standard Test Method for Fracture Strength in Cleavage of Adhesives in Bonded Metal Joints." American Society of Testing and Materials, West Conshohocken, PA.
- ASTM. (2000g). "ASTM D3535 Standard Test Method for Resistance to Deformation Under Static Loading for Structural Wood Laminating Adhesives Used Under Exterior (Wet Use) Exposure Conditions." American Society of Testing and Materials, West Conshohocken, PA.
- ASTM. (2000h). "ASTM D5379/D5379M-98 Standard Test Method for Shear Properties of Composite Materials by the V-Notched Beam Method." American Society of Testing and Materials, West Conshohocken, PA.
- ASTM. (2000i). "ASTM D6115-97 Standard Test Method for Mode I Fatigue Delamination Growth Onset of Unidirectional Fiber-Reinforced Polymer Matrix

Composites." American Society of Testing and Materials, West Conshohocken, PA.

ASTM. (2002a). "ASTM D4896-01 Standard guide for use of adhesive-bonded single lap-Joint specimen test results." American Society of Testing and Materials, West Conshohocken, PA.

ASTM. (2002b). "ASTM D5528-01 Standard Test Method for Mode I Interlaminar Fracture Toughness of Unidirectional Fiber-Reinforced Polymer Matrix Composites." American Society of Testing and Materials, West Conshohocken, PA.

Barbero, E., Davalos, J., and Munipalle, U. (1994). "Bond strength of FRP-wood interface." *Journal of Reinforced Plastics and Composites*, 13(9), 835-854.

Barger, L. S., Lopez-Anido, R., and GangaRao, H. V. S. (1993). "Experimental Evaluation of Stressed Timber Bridge Systems." *Transportation Research Record*, 1426, 57-61.

Battles, E. P., Dagher, H. J., and Abdel-Magid, B. (2000). "Durability of composite reinforcement for timber bridges." *Transportation Research Record*, 2(1696), 131-135.

Bell, A. J., and Kinloch, A. J. (1997). "The effect of the substrate material on the value of the adhesive fracture energy, G_c ." *Journal of Materials Science Letters*, 16(17), 1450-1453.

Berry, J. P. (1963). "Determination of Fracture Energies by the Cleavage Technique." *Journal of Applied Physics*, 34(1), 62-68.

- Blackman, B. R. K., Kinloch, A. J., and Paraschi, M. (2001). "The effect of the substrate material on the value of the adhesive fracture energy, G_c : Further considerations." *Journal of Materials Science Letters*, 20(3), 265-267.
- Blanchard, C., Chateauminois, A., and Vincent, L. (1996). "New testing methodology for the assessment of fatigue properties of structural adhesives." *International Journal of Adhesion and Adhesives*, 16(4), 289-299.
- Bodig, J., and Jayne, B. A. (1992). "Mechanics of Wood and Wood Composite." Krieger Publishing Company.
- Bond, I. P., and Ansell, M. P. (1998a). "Fatigue properties of jointed wood composites. Part I. Statistical analysis, fatigue master curves and constant life diagrams." *Journal of Materials Science*, 33(11), 2751-2762.
- Bond, I. P., and Ansell, M. P. (1998b). "Fatigue properties of jointed wood composites. Part II. Life prediction analysis for variable amplitude loading." *Journal of Materials Science*, 33(16), 4121-4129.
- Borden. (1993). "Information of Borden Chemical Products."
- Brinson, H. F., and Grant, J. W. (1986). "Mechanical properties for durability predictions of FRP bonded joint." *Composite Structures*, 6(1-3), 107-121.
- Brunner, A. J. (2000). "Experimental aspects of Mode I and Mode II fracture toughness testing of fibre-reinforced polymer-matrix composites." *Computer Methods in Applied Mechanics and Engineering*, 185, 161-172.
- Crews, K. (1998). "International Guidelines for Design of Stress Laminated Timber Bridge Decks." *5th World Conference on Timber Engineering*, Montreux, Switzerland, 24-31.

- Dagher, H. J., Kimball, T., Abdel-Magid, B., and Shaler, S.M. (1996). "Effect of FRP Reinforcement on Low-Grade Eastern Hemlock Glulams." *National Conference on Wood Transportation Structures*, Madison, WI.
- Daniel, I. M., and Ishai, O. (1994). "Engineering Mechanics of Composite Materials." Oxford University Press, Inc.
- Dattaguru, B., Everett, R. A. J., Whitcomb, J. D., and Johnson, W. S. (1984). "Geometrically nonlinear analysis of adhesively bonded joints." *Journal of Engineering Materials and Technology, Transactions of the ASME*, 106(1), 59-65.
- Davalos, J. F., Madabhusi-Ramant, P., and Qiao, P. (1997). "Characterization of Mode-I fracture of hybrid material interface bonds by contoured DCB specimens." *Engineering Fracture Mechanics*, 58(3), 173-192.
- Davalos, J. F., Qiao, P., Madabhusi-Raman, P., and Lang, E. M. (1998). "Mode I fracture toughness of fiber reinforced composite-wood bonded interface." *Journal of Composite Materials*, 32(10), 987-1013.
- Davalos, J. F., Qiao, P. Z., and Trimble, B. S. (2000a). "Fiber-Reinforced Composite and Wood Bonded Interface, Part 1. Durability and Shear Strength." *Journal of Composites Technology and Research*, 22(4), 224-231.
- Davalos, J. F., Qiao, P. Z., and Trimble, B. S. (2000b). "Fiber-Reinforced Composite and Wood Bonded Interface, Part 2. Fracture." *Journal of Composites Technology and Research*, 22(4), 232-240.
- Davids, W. G., Dagher, H. J., and Breton, J. (2000). "Modeling Creep Deformations of FRP-Reinforced Glulam Beams." *Wood and Fiber Science*, 32(4), 426-441.

- Davies, P., Blackman, B. R. K., and Brunner, A. J. (1998). "Standard test methods for delamination resistance of composite materials: current status." *Applied Composite Materials*, 5(6), 345-364.
- Duwadi, S. R., Ritter, M. A., and Cesa, E. (2000). "Wood in transportation program: An overview." *Transportation Research Record*, 1(1696), 310-315.
- Edde, F. C., and Verreman, Y. (1995). "Nominally constant strain energy release rate specimen for the study of mode II fracture and fatigue in adhesively bonded joints." *International Journal of Adhesion and Adhesives*, 15(1), 29-32.
- Fernando, M., Harjopratinno, W. W., and Kinloch, A. J. (1996). "A fracture mechanics study of the influence of moisture on the fatigue behaviour of adhesively bonded aluminum-alloy joints." *International Journal of Adhesion and Adhesives*, 16(2), 113-119.
- FPL. (1999). "Wood Handbook Wood as an Engineering Material." *FPL-GTR-113*, USDA, Forest Products Laboratory, Madison, WI.
- Francis, E. C., and Gutierrez-Lemini, D. (1982). "Effect of scrim cloth on adhesively bonded joints." *The American Chemical Society 184th National Meeting*, Kansas City, MO, 262-266.
- Gagliano, J. M., and Frazier, C. E. (2001). "Improvements in the fracture cleavage testing of adhesively-bonded wood." *Wood and Fiber Science*, 33(3), 377-385.
- Gardner, D., Davalos, J. F., and Munipalle, U. (1994). "Adhesive bonding of pultruded Fiber-Reinforced Plastic (FRP) to Wood." *Forest Products Journal*, 44(5), 62-66.
- Gere, J. M., and Timoshenko, S. P. (1997). "Mechanics of materials." PWS Publishing Company.

- Gillespie, J. W. J., Carlsson, L. A., and Smiley, A. (1987). "Rate-Dependent Mode I Interlaminar Crack Growth Mechanisms in Graphite/Epoxy and Graphite/Peek." *Composites Science and Technology*, 28(1), 1-15.
- Gilmore, R. B., and Shaw, S. J. (1993). "Effect of temperature and humidity on the fatigue behaviour of composite bonded joints." *The symposium on composites bonding*, Airport, TX, 82-95.
- Guess, T. R., Allred, R. E., and Gerstle, J. F. P. (1977). "Comparison of lap shear test specimens." *Journal of Testing and Evaluation*, 5(3), 84-93.
- Harris, J. A., and Fay, P. A. (1991). "Fatigue life evaluation of structural adhesives for automotive applications." *International Journal of Adhesion and Adhesives*, 12(1), 9-18.
- Hashemi, S., Kinloch, A. J., and Williams, J. G. (1989). "Corrections needed in double cantilever beam tests for assessing the interlaminar failure of fiber-composites." *Journal of Materials Science Letters*, 8, 125-129.
- Hashemi, S., Kinloch, A. J., and Williams, J. G. (1990). "The analysis of interlaminar fracture in uniaxial fiber-polymer composites." *Proceedings, Royal Society*, A427, 173-199.
- Hattori, T., and Iwasa, M. (1995). "Fatigue strength of metal/FRP adhesive joints under low temperature." *ASME Design Engineering Technical Conferences*, Boston, MA, USA, 81-86.
- Hojo, M., Kageyama, K., and Tanaka, K. (1995). "Prestandardization study on mode I interlaminar fracture toughness test for CFRP in Japan." *Composite Structures*, 26, 243-255.

- Hojo, M., Tanaka, K., Gustafson, C. G., and Hayashi, R. (1989). "Fracture mechanics for delamination fatigue crack propagation of CFRP in air and in water." *Key Engineering Materials*, 37, 149-160.
- Hu, N., Wang, B., Sekine, H., Yao, Z., and Tan, G. (1998). "Shape-optimum design of a bi-material single-lap joint." *Composite Structures*, 41(3-4), 315-330.
- Imanaka, M., Fukuchi, Y., Kishimoto, W., and Okita, K. (1988). "Fatigue life estimation of adhesively bonded lap joints." *Journal of Engineering Materials and Technology*, 110(4), 350-354.
- Imanaka, M., and Iwata, T. (1996). "Fatigue failure criterion of adhesively-bonded joints under combined stress conditions." *Journal of Adhesion*, 59(1-4), 111-126.
- Imanaka, M., Kishimoto, W., Okita, K., Nakayama, H., and Shirato, M. (1986). "Estimation of fatigue strength of adhesive bonded lap joint." *Journal of the Society of Materials Science*, 35(393), 623-628.
- Imanaka, M., Takeuchi, Y., Nakamura, Y., Nishimura, A., and Iida, T. (2001). "Fracture toughness of spherical silica-filled epoxy adhesives." *International Journal of Adhesion and Adhesives*, 21, 389-396.
- Ishii, K., Imanaka, M., Nakayama, H., and Kodama, H. (1999). "Evaluation of the fatigue strength of adhesively bonded CFRP/metal single and single-step double-lap joints." *Composites Science and Technology*, 59(11), 1675-1683.
- Jain, L. K., Leong, K. H., Mai, Y. W., and Tong, L. (1998). "Effect of through-thickness stitching on the fatigue life of composite single-lap joints." *Applied Composite Materials*, 5(6), 399-409.

- Johnson, W. S., and Mall, S. (1984). "Bonded joint strength: static versus fatigue." *The V International Congress on Experimental Mechanics*, Brookfield Center, CT, 267-271.
- Kageyama, K., and Hojo, M. (1990). "Proposed Methods for Interlaminar Fracture Toughness Tests of Composite Laminates." *Proceedings of the 5th U.S./Japan Conference on Composite Materials*, 227-234.
- Kairouz, K. C., and Matthews, F. L. (1993). "Strength and failure modes of bonded single lap joints between cross-ply adherends." *Composites*, 24(6), 475-484.
- Kayupov, M., and Dzenis, Y. A. (2001). "Stress concentrations caused by bond cracks in single-lap adhesive composite joints." *Composite Structures*, 54(2-3), 215-220.
- Kenig, S., Moshonov, A., Shucrun, A., and Marom, G. (1989). "Environmental effects on shear delamination of fabric-reinforced epoxy composites." *International Journal of Adhesion and Adhesives*, 9(1), 38-45.
- Kinloch, A. J., and Osiyemi, S. O. (1993). "Predicting the fatigue life of adhesively bonded joints." *Journal of Adhesion*, 43, 79-90.
- Kusaka, T., Hojo, M., Mai, Y.-W., Kurokawa, T., Nojima, T., and Ochiai, S. (1998). "Rate dependence of mode I fracture behaviour in carbon-fibre/epoxy composite laminates." *Composites Science and Technology*, 58(3-4), 591-602.
- Lang, T. P., and Mallick, P. K. (1998). "Effect of spew geometry on stresses in single lap adhesive joints." *International Journal of Adhesion and Adhesives*, 18, 167-177.
- Lawcock, G. Y. L., Mai, Y., and Sun, C. (1997). "Effect of adhesive bonding between aluminum and composite prepreg on the mechanical properties of carbon-fiber-reinforced metal laminates." *Composites Science and Technology*, 57(1), 35-45.

- Li, G., and Lee-Sullivan, P. (2001). "Finite element and experimental studies on single-lap balanced joints in tension." *International Journal of Adhesion and Adhesives*, 21(3), 211-220.
- Li, G., Lee-Sullivan, P., and Thring, R. W. (1999). "Nonlinear finite element analysis of stress and strain distributions across the adhesive thickness in composite single-lap joints." *Composite Structures*, 46(4), 395-403.
- Lopez-Anido, R., Gardner, D., Muszynski, L., Goodell, B., Dagher, H., Hong, Y., and Eisenheld, L. (2002). "Performance-based material evaluation of FRP composite reinforcement bonded to glulam members." *Proceedings of the second International Conference (CDCC 02)*, Montreal, Canada, 677-688.
- Lopez-Anido, R., Gardner, D. J., and Hensley, J. L. (2000). "Adhesive Bonding of Eastern Hemlock Glulam Panels with E-Glass/Vinyl Ester Reinforcement." *Forest Products Journal*, 50(11/12), 43-47.
- Lopez-Anido, R., and Karbhari, V. M. (2000). "Chapter 2: Fiber Reinforced Composites in Civil Infrastructure." *Emerging Materials for Civil Engineering Infrastructure - State of the Art*, ASCE Press, Reston, VA, 41-78.
- Lopez-Anido, R., and Xu, H. (2002). "Structural Characterization of Hybrid FRP-Glulam Panels for Bridge Decks." *Journal of Composites for Construction, ASCE*, 6(3), 194-203.
- Mall, S. (1989). "Influence of resin on delamination and debonding mechanisms of composite materials under fatigue loading." *Key Engineering Materials*, 37, 209-224.

- Mall, S., and Johnson, W. S. (1986). "Characterization of mode I and mixed-mode failure of adhesive bonds between composite adherends." *ASTM Special Technical Publication, Composite Materials: Testing and Design (Seventh Conference)*, 322-334.
- Mall, S., Johnson, W. S., and Everett, R. A. J. (1982). "Cyclic debonding of adhesively bonded composites." *The American Chemical Society 184th National Meeting*, Kansas City, MO, 259-261.
- Mall, S., and Yun, K. T. (1987). "Effect of adhesive ductility on cyclic debond mechanism in composite-to composite bonded joints." *Journal of Adhesion*, 23, 215-231.
- Martin, R. H., and Sage, G. N. (1986). "Prediction of the fatigue strength of bonded joints between multi-directional laminates of CFRP." *Composite Structures*, 6(1-3), 141-163.
- Mijovic, J., and Koutsky, J. (1979). "Effect of Wood Grain Angle on Fracture Properties and Fracture Morphology of Wood-Epoxy Joints." *Wood Science*, 11(3), 164-168.
- Miyagawa, H., Sato, C., and Ikegami, K. (2001). "Interlaminar fracture toughness of CFRP in mode I and mode II determined by Raman spectroscopy." *Composites*, 32, 477-486.
- MSC. (1999). "MSC Industrial Supply Co. 1999/2000 big book." 1251.
- Nairn, J. A. (2000). "Energy release rate analysis for adhesive and laminate double cantilever beam specimens emphasizing the effect of residue stresses." *International Journal of Adhesion and Adhesives*, 20, 59-70.

- Nojima, T., and Kusaka, T. (1998). "Fracture behaviours of CFRP laminates in Mode I interlaminar fracture toughness testing." *JSME International Journal*, 41(2), 225-230.
- Ogawa, H. (2000). "Architectural application of carbon fibers development of new carbon fiber reinforced glulam." *Carbon*, 38(2), 211-226.
- Owens, J. F. P., and Lee-Sullivan, P. (2000a). "Stiffness behaviour due to fracture in adhesively bonded composite-to-aluminum joints I. Theoretical model." *International Journal of Adhesion and Adhesives*, 20(1), 39-45.
- Owens, J. F. P., and Lee-Sullivan, P. (2000b). "Stiffness behaviour due to fracture in adhesively bonded composite-to-aluminum joints II. Experimental." *International Journal of Adhesion and Adhesives*, 20(1), 47-58.
- Pandey, P. C., and Narasimhan, S. (2001). "Three-dimensional nonlinear analysis of adhesively bonded lap joints considering viscoplasticity in adhesives." *Computers and Structures*, 79(7), 769-783.
- Pocius, A. V. (1997). "Adhesion and Adhesives Technology." Hanser Publishers.
- River, B. H., and Okkonen, E. A. (1993). "Contoured wood double cantilever beam specimen for adhesive joint fracture tests." *Journal of Testing and Evaluation*, 21(1), 21-28.
- Romanko, J., and Jones, W. B. J. (1980). "Fatigue behavior of adhesively bonded joints." *National SAMPE Symposium and Exhibition 25th*, 154-166.
- Sanchez, O. E. (2002). "Performance study of in-service FRP reinforced glulam bridge girders." University of Maine, Orono.

- Scott, C. T., River, B. H., and Koutsky, J. A. (1991). "Fracture testing wood adhesives with composite cantilever beams." *Journal of Testing and Evaluation*, 20(4), 259-264.
- Segui, W. T. (1998). "LRFD Steel Design." Second, Design and Production Services, Inc.
- Sener, J. Y., Ferracin, T., Caussin, L., and Delannay, F. (2002). "On the precision of the wedge-opened double cantilever beam method for measuring the debonding toughness of adhesively bonded plates." *International Journal of Adhesion and Adhesives*, 22, 129-137.
- Smiley, A. J., and Pipes, R. B. (1987). "Rate effects on mode I interlaminar fracture toughness in composite materials." *Journal of Composite Materials*, 21(7), 670-687.
- Tong, L., and Steven, G. P. (1999). "Analysis and Design of Structural Bonded Joints." Kluwer Academic Publishers, Norwell, MA.
- Tsai, K. T., and Ansell, M. P. (1990). "Fatigue properties of wood in flexure." *Journal of Materials Science*, 25(2A), 865-878.
- Tschegg, E. K., Fruhmann, K., and Stanzl-Tschegg, S. E. (2001). "Damage and fracture mechanisms during mode I and mode III loading of wood." *Holzforschung*, 55(5), 525-533.
- Tucker, R., Compston, P., and Jar, P. (2001). "The effect of post-cure duration on the mode I interlaminar fracture toughness of glass-fiber reinforced vinylester." *Composites*, 32, 129-134.

- Vick, C. B. (1995). "Hydroxymethylated resorcinol coupling agent for enhanced adhesion of epoxy and other thermosetting adhesives to wood." *Wood Adhesives* 1995, 47-55.
- Vick, C. B. (1997). "More durable epoxy bonds to wood with hydroxymethylated resorcinol coupling agent." *Adhesives Age*, 40(8), 24-29.
- Vick, C. B., Christiansen, A. W., and Okkonen, E. A. (1998). "Reactivity of hydroxymethylated resorcinol coupling agent as it affects durability of epoxy bonds to Douglas-fir." *Wood and Fiber Science*, 30(3), 312-322.
- Vick, C. B., and Okkonen, A. E. (1998). "Strength and durability of one-part polyurethane adhesive bonds to wood." *Forest Products Journal*, 48(11-12), 71-76.
- Vick, C. B., and Okkonen, E. A. (2000). "Durability of one-part polyurethane bonds to wood improved by HMR coupling agent." *Forest Products Journal*, 50(10), 69-75.
- Wang, S. S., and Yau, J. F. (1982). "Interface cracks in adhesively bounded lap-shear joints." *International Journal of Fracture*, 19, 295-309.
- Whitney, J. M., Browning, C. E., and Hoogsteden, W. (1982). "Double cantilever beam tests for characterizing mode I delamination of composite materials." *Journal of Reinforced Plastics and Composites*, 1(4), 297-313.
- Williamson, T. G. (1996). "Timber Highway Bridge Construction Practices in the United States." *FPL-GTR-94*, USDA, Forest Service, Forest Products Laboratory and US DOT Federal Highway Administration.

Zalucha, D. J. (1981). "Testing adhesives: philosophy and practice." *Adhesives Age*, 24(4), 17-19.

Zhang, Z. H., Shang, J. K., and Lawrence, F. V. (1995). "A backface strain technique for detecting fatigue crack initiation in adhesive joints." *Journal of Adhesion*, 49, 23-36.

Appendix A Calibration Procedure of the Laminating Press

1) Clamping force versus torque with steel plates

1. Put two thick steel plates on the bottom plate as the spacers;
2. Put the load cell on the top of the steel plates;
3. Put one steel plate on the top of the loading cell;
4. Record the reading of the load cell as the initial load;
5. Use the micro-adjusting torque wrench to tighten the nuts follow the procedures:
 - a. Adjust the torque wrench to a desired torque value;
 - b. Tighten the nuts in a crisscross manner, torque each nut two quarter rounds each time until get the final torque;
 - c. Record the reading of the load cell and loosen the nuts completely. Never torque a nut that is already tightened;
6. Repeat step 5 for following torque levels: 10, 15, 20, 25, 30, 35, 40, 45, 50, and 55 Ft-Lbs;
7. Plot the chart of clamping pressure vs. torque to get the calibration curve;
8. Repeat steps 4 to 7 three times to get more measurements;

2) Clamping force versus torque with wood laminations without adhesive layer

1. Apply hydraulic oil as the lubricant to the top threads of the guiding posts and under the head of the nuts;
2. Put the load cell on the bottom plates;
3. Put a steel plate on the top of the loading cell with an area a little bit bigger than the wood laminations to distribute the clamping pressure;
4. Put four layers of wood between the steel plate and the middle plate. Each of them has a thickness of 0.75-in;
5. Record the reading of the load cell as the initial load;
6. Use the micro-adjusting torque wrench to tighten the nuts follow the procedures:
 - a. Adjust the torque wrench to a desired torque;
 - b. Tighten the nuts in a crisscross manner, torque each nut two quarter rounds each time until get the final torque;
 - c. Record the reading of the load cell and loosen the nuts completely. Never torque a nut that is already tightened;
7. Repeat step 5 for following torque levels: 10, 15, 20, 25, 30, 35, 40, 45, 50, and 55 Ft-Lbs;

8. Plot the chart of clamping pressure vs. torque to get the calibration curve;
9. Repeat steps 4 to 8 three times with new wood billets.

3) Clamping force loss versus time with wood laminations without adhesive layer

1. Apply hydraulic oil as the lubricant to the top threads of the guiding posts and under the head of the nuts;
2. Put the load cell on the bottom plates;
3. Put a steel plate on the top of the loading cell with an area a little bit bigger than the wood laminations to distribute the clamping pressure;
4. Put four layers of wood between the steel plate and the middle plate. Each of them has a thickness of 0.75-in;
5. Record the reading of the load cell as the initial load;
6. Use the micro-adjusting torque wrench to tighten the nuts follow the procedures:
 - a. Adjust the torque wrench to the torque of 55 Ft-Lbs;
 - b. Tighten the nuts in a crisscross manner, torque each nut two quarter rounds each time until get the final torque;
7. Record the reading of the load cell once per minute for the first ten minutes, then once per five minutes for the following 50 minutes;
8. After one hour, loosen the nuts completely and retighten the nuts to the torque of 55 Ft-Lbs;
9. Repeat step 7 for the first hour. Then, record the load once for every one or two hours for the following four hours. At last, record the load at the end of the 24 hours.
10. Plot the chart of clamping pressure vs. time to get the calibration curve;
11. Change wood billets and repeat steps 4 to 10 three times.

4) Clamping force loss versus time with wood laminations and adhesive layers

1. Apply hydraulic oil as the lubricant to the top threads of the guiding posts and under the head of the nuts;
2. Put the load cell on the bottom plates;
3. Put a steel plate on the top of the loading cell with an area a little bit bigger than the wood laminations to distribute the clamping pressure;
4. Put four layers of wood with PRF resin between the steel plate and the middle plate. Each of them has a thickness of 0.75-in;
5. Record the reading of the load cell as the initial load;
6. Use the micro-adjusting torque wrench to tighten the nuts follow the procedures:

- a. Adjust the torque wrench to the torque of 55 Ft-Lbs;
 - b. Tighten the nuts in a crisscross manner, torque each nut two quarter rounds each time until get the final torque;
7. Record the reading of the load cell once per minute for the first ten minutes, then once per five minutes for the following 50 minutes;
 8. After one hour, loosen the nuts completely and retighten the nuts to the torque of 55 Ft-Lbs;
 9. Repeat step 7 for the first hour. Then, record the load once for every one or two hours for the following four hours. At last, record the load at the end of the 24 hours.
 10. Plot the chart of clamping pressure vs. time to get the calibration curve;
 11. Change wood billets and repeat steps 4 to 10 three times.

Appendix B – Standard Operation Procedure of Laminating Press

1. Put two spacers between the middle plate and the bottom plate to keep enough space for the operation;
2. Apply hydraulic oil as the lubricant to the top threads of the guiding posts and under the head of the nuts;
3. Insert three alignment pins on two sides of the clamping area;
4. Always put a piece of plastic between the billets and the press and between different billets as release film;
5. Put billets into the press along the alignment pins;
6. Insert three alignment pins on the other two sides of the clamping area;
7. Take out the spacers and lower the middle plate down to the beams;
8. Use the micro-adjusting torque wrench to tighten the nuts follow the procedures:
 - 1) Adjust the torque wrench to the desired torque; the torque can be calculated according to the calibration curve and the clamping pressure required by the manufacturer of the adhesive;
 - 2) Tighten the nuts in a crisscross manner, torque each nut two quarter rounds each time until get the final torque;
 - 3) Do not over torque the nuts. When the preset torque value has been reached, the wrench indicates by releasing the handle for a few degrees of free travel accompanied by an audible 'click' signal.
9. After one hour, loosen the nuts completely and retighten the nuts to the desired torque;
10. At the end of the clamping time required by the manufacturer of the adhesive, take out the billets and put them into the conditioning chamber.

Appendix C – Work Instruction of Shear by Compression Loading Tests

Objective:

To evaluate the resistance to shear by compression loading of FRP-wood laminations based on modified ASTM D2559-00 and modified ASTM D905-98.

Instruction:

Summary

This work instruction is for the fabrication and testing of FRP-wood shear block samples for the resistance to shear compression loading tests of modified ASTM D 905-98 using the laminating press.

Fabrication Procedure

1. Preparation of wood blocks:
 - 1) Use only flat-sawn lumber;
 - 2) Condition the wood at $23\pm 2^{\circ}\text{C}$ and RH of 50-70% until MC of 9-12% has been attained;
 - 3) Cut each piece of wood to nominal 19-mm (0.75-in) thick, 127 mm (5-in) wide and 602-mm (23.7-in) long (determined by the laminating press);
 - 4) Prepare two pieces of wood of the same species for each laminated wood;
 - 5) Freshly surface each lamination before bonding with the adhesive to tested. Remove at least 0.4 mm from each face within 24 hrs of bonding.
2. Apply HMR Primer (if needed):
 - 1) Prepare HMR Primer according to the corresponding S.O.P.;
 - 2) Apply HMR Primer to the wood surfaces with the spreading rate of 11 g /surface;
 - 3) HMR should be applied 16 hrs before bonding.
3. Preparation of FRP layers:
 - 1) Cut each piece of FRP to 127 mm (5-in) wide and 602-mm (23.7-in) long (determined by the laminating press);
 - 2) Abrade the FRP surfaces with 80-grit sand paper;
 - 3) Wipe the sanded surface with a lint-free, acetone-saturated rag to remove dirt and dust.
 - 4) Wait a minimum of 5 minutes until solvent has evaporated.
4. Fabrication of laminated wood beam:
 - 1) Personal protective equipment- rubber gloves, rubber aprons and protective glasses of goggles-should be worn;
 - 2) Prepare adhesive;
 - 3) Apply the adhesive uniformly to the contacting faces of each lamination in accordance with manufacturer's instructions;

- 4) Place the laminated wood members under proper pressure for a period of time and at the glue line temperature specified by the manufacturer of the adhesive.
5. Prepare test samples
 - 1) Sand the edges of the beams to get smooth side surfaces;
 - 2) Use the table saw for wood to cut through both of the wood layers along the longitudinal direction, make total three cuts and leave 2-in space between them; do not cut FRP layers use this saw which may hurt the blade;
 - 3) Use the tool for shear block fabrication to cut through wood layers along the transverse direction; trim 46-mm (1.8-in) off each end of the beam and discard it;
 - 4) Use the table saw for FRP to cut through FRP layers;
 - 5) Take care in preparing the test specimens to make the loaded surfaces smooth and parallel to each other and perpendicular to the height;
 - 6) Take care also in reducing the lengths of the laminations to 44.3-mm (1.75-in) to ensure that the saw cuts extend to, but not beyond, the glue line.
6. Measure the width and length of the specimen at the glue line to the nearest 0.25-mm (0.01-in) to determine the shear area.
7. Return specimens in the condition chamber until tested.

Conditioning

1. For dry samples: put into the conditioning chamber with 65% RH and 24°C for several days;
2. For wet samples: vacuum-pressure water soak 30 minute vacuum 25 in Hg/30 pressure 75 psi.

Testing and Data Recording

Measure the width and length of the specimen at the glue line to determine the shear area. Place the test specimen in the shearing tool so that the load may be applied as described in Section 5 of ASTM D905. Apply the loading with a continuous motion of the movable head at a rate of 5 mm (0.20 in.)/min to failure. Record the maximum shear force.

Calculations

Calculate the shear stress at failure in pounds-force per square inch based on the glue line area between the two laminations measured to the nearest 0.06 cm² (0.01 in.²), and report for each specimen together with the estimated percentage of wood failure.

Table 1 of ASTM D2559 may be used as a reference of required shear strength for FRP-wood products for different wood species.

Appendix D – Work Instruction of Cycle Delamination Tests

Objective:

To evaluate resistance to delamination during accelerated exposure of FRP-Wood Laminations based on Modified ASTM D2559-00

Summary

This Work Instruction is for the fabrication and testing of FRP reinforced laminated wood beams for the delamination test based on modified ASTM D 2559-00.

Fabrication Procedure

1. Fabricate FRP layers to proper thickness (if needed)
2. Prime the FRP layers if needed
3. Prepare laminated wood test members:
 - 1) Use only flat-sawn lumber;
 - 2) Condition the wood at $23\pm 2^{\circ}\text{C}$ and RH of 50-70% until MC of 9-12% has been attained.
 - 3) Cut each piece of wood to nominal 19-mm (0.75-in) thick, 127 mm (5-in) wide and 602-mm (23.7-in) long (determined by the laminating press). Prepare six pieces of wood of the same species for each laminated wood.
 - 4) Freshly surface each lamination before bonding with the adhesive to tested. Remove at least 0.4 mm from each face within 24 h of bonding.
4. Fabrication of laminated wood beam using PRF adhesive:

The PRF is supplied in two components: 1) LT-5210J Resin; 2) FM-6210 Hardener.

 - 1) Personal protective equipment- rubber gloves, rubber aprons and protective glasses of goggles-should be worn.
 - 2) Apply the adhesive uniformly to the contacting faces of each lamination in accordance with manufacturer's instructions.
 - 3) Place the laminated wood members under pressure of 110 psi for a period of time and at the glueline temperature specified by the manufacturer of the adhesive.
5. Add FRP layers (if not fabricated at the same time)
 - 1) Refresh only one surfaces of wood lamina (if needed). Follow the S. O. P. of the wood planner.
 - 2) Prepare HMR primer according to the corresponding S. O. P.
 - 3) Apply the HMR to the wood surface 16 hours before the application of the adhesive.
 - 4) Clean the FRP surfaces with Acetone. Clean surfaces before sanding to avoid sanding the contaminant into the surface. Sand the surfaces with 80-grit sandpaper. Wipe the surface with clean towels before the solvent dries.

- 5) Apply the adhesive uniformly only to the wood face in accordance with manufacturer's instructions. Apply the FRP layer only to one surface of the laminated wood beam.
 - 6) Place the FRP reinforced laminated wood members under pressure for a period of time and at the glueline temperature specified by the manufacturer of the resin. Follow the S. O. P. of the laminating press to apply the pressure.
6. Prepare test samples
- 1) Trim 46-mm (1.8-in) off each end of the beam and discard it.
 - 2) Cut the remaining trimmed beam into two 254-mm (10-in) sections.
 - 3) Cut each 254-mm (10-in) section into three 76-mm (3-in) specimens with the 76-mm (3-in) dimension parallel to the grain direction in the wood.
7. Conditioning
- Condition the laminated members at $23 \pm 2^\circ\text{C}$ and RH of 50-70% for the minimum time recommended by the manufacture for each curing temperature used during the pressure period, and test immediately.

Testing

First Cycle

1. Weigh and record to the nearest 1 g the weight of each specimen.
2. Place the specimens in the pressure vessel, weigh down and admit water at a temperature of 18 to 27°C (65 to 80°F). Make sure all end grain surfaces freely exposed to the water.
3. Draw a vacuum of at least 25 in-Hg and hold for 5 minutes.
4. Release the vacuum and apply pressure of 75 ± 2 psi for 1 hour.
5. Repeat step 3 and 4, until the weight of specimens reach at least 1.5 times the original weight.
6. Move the test specimens in the oven at $65.5 \pm 2^\circ\text{C}$ ($150 \pm 3.6^\circ\text{F}$) for 21 to 22 hours. Lower their weight to within 15% of the original test specimens' weight. Place the test specimens at least 2 in apart with the end-grain surfaces parallel to the steam of air.

Second Cycle

1. Operate the Steam Generator according to the corresponding S.O.P.
2. Place the specimens to the pressure steam chamber and admit steam at 100°C (212°F) for 1.5 hour, with drain open so the wet condensate is removed as formed.
3. Place the specimens in the pressure vessel, weigh down and admit water at a temperature of 18 to 27°C (65 to 80°F). Make sure all end grain surfaces freely exposed to the water.
4. Apply pressure of 75 ± 2 psi for 40 minutes.
5. Move the test specimens in the oven at $65.5 \pm 2^\circ\text{C}$ ($150 \pm 3.6^\circ\text{F}$) for 21 to 22 hours. Lower their weight to within 15% of the original test specimens' weight.

Place the test specimens at least 2 in apart with the end-grain surfaces parallel to the steam of air.

Third Cycle

Repeat the first cycle, making a total test period of 3 days. Record the data as outlined in 15.4.1 of ASTM D 2559.

Data Recording

At the end of the final drying period, visually examine each specimen. Immediately measure, to the nearest 1.27 mm (0.05 in.), the total length of delamination on each end-grain surface of each specimen and record in Table 2 of ASTM D2559. Record wood-FRP interface delamination and wood-wood interface delamination respectively.

Do not record as delamination any failure in the wood due to checking or small isolated knots. Do not record any delamination that is less than 2.54 mm (0.10 in.) in length and more than 5 mm (0.20 in.) away from any recordable delamination. Record as delamination, any failure that is within the first two layers of wood cells beyond the adhesive layer and in which the fracture path is not influenced by grain angle or growth-ring structure. Do not record as delamination, any failure that is beyond the two layers of wood cells and that is influenced by grain angle and growth-ring structure. Similar rules may be applied to the delamination measurement of wood-FRP bond lines. Measure and record in Table 2 the total length of end grain bond line for each of the specimens.

Calculations

For total delamination length, add together the recorded delamination for all bond lines on the two end-grain surfaces of all the specimens. Report as percent delamination, the total delamination length of all specimens divided by the total length of the bond lines of all specimens multiplied by 100 and record in Table 2.

For wood-wood bond lines, the delamination shall not exceed 5 % for softwoods and 8 % for hardwoods. For FRP-wood bond lines, the delamination limit still need to be determined. But it should not exceed 10%.

Table 2 of ASTM D2559 is provided to record all measurements and calculate percent delamination.

Appendix E – Work Instruction of Single-lap Shear Tests by Tension Loading

Objective:

Use sinusoidal cyclic tension loading to evaluate the single-lap shear fatigue strength of FRP-wood interface based on Modified ASTM D2339-98.

Summary

This Work Instruction is for the fabrication and testing of wood-FRP single-lap shear samples for the fatigue tests in shear by tension loading of modified ASTM D2339-98 and ASTM D3166-99.

Fabrication Procedure

8. Preparation of wood boards:

- 1) Use only vertical-sawn lumber;
- 2) Condition the wood at $23\pm 2^{\circ}\text{C}$ and RH of 50-70% until MC of 9-12% has been attained;
- 3) Cut each piece of wood to nominal 8-mm thick, 127 mm (5-in) wide and 602-mm (23.7-in) long (determined by the laminating press);
- 4) Freshly surface each lamination before bonding with the adhesive to tested. Remove at least 0.4 mm from each face within 24 h of bonding.
- 5) The planer will usually cause snipe at the end of the board. Snipe is when the planer cuts more off of the end than the rest of the board. Run the boards through the planer a few more times and this should reduce or eliminate the snipe.

9. Apply HMR Primer (if needed):

- 1) Prepare HMR Primer according to WI-01-05;
- 2) Apply HMR Primer to the wood surfaces with the spreading rate 0.0945 g / in^2 of $11.2 \text{ g / surface of glue line}$;
- 3) HMR should be applied 16 hrs before bonding.

10. Preparation of FRP layers:

- 1) Cut each piece of FRP to 127 mm (5-in) wide and 602-mm (23.7-in) long (determined by the laminating press);
- 2) Abrade the FRP surfaces with 80-grit sand paper;
- 3) Wipe the sanded surface with a lint-free, acetone-saturated rag to remove dirt and dust.
- 4) Wait a minimum of 5 minutes until solvent has evaporated.

11. Fabrication of FRP-wood laminated boards:

- 1) Personal protective equipment- rubber gloves, rubber aprons and protective glasses of goggles-should be worn;
- 2) Prepare adhesive;

- 3) Apply the adhesive uniformly to the contacting faces of each lamination in accordance with manufacturer's instructions;
- 4) Attach the FRP to the contacting face of each wood lamination. Only the wood is being applied with adhesive.
- 5) Place the laminated wood members under proper pressure for a period of time and at the glue line temperature specified by the manufacturer of the adhesive.

12. Prepare test samples

- 1) Sand the edges of the boards to get smooth lateral surfaces;
- 2) Draw a line at the location of the snipe at each end of the board;
- 3) Use the table saw for FRP with the diamond blade to cut off about quarter-inch strip along the longitudinal direction from one side of the board (get rid of the side piece).
- 4) Cut off about one-inch strip along the transverse direction from one side of the board (get rid of the end piece).
- 5) Cut each board to three 7.25-in long panels along the transverse direction.
- 6) Adjust the height of the blade as the thickness of the FRP layer. Cut a notch on each FRP layer 3-in from the end of the panel parallel to the transverse direction.
- 7) Adjust the height of the blade as the thickness of the wood layer. Cut a notch on each wood layer 3-in from the other end of the panel parallel to the transverse direction. This should leave you one inch between the two notches.
- 8) Cut through the whole panel along the longitudinal direction to make 1-in width coupons. It should be able to get 4 samples out of each panel and 12 samples out of each board.
- 9) Take care to ensure that the saw cuts extend to, but not beyond, the glue line.
- 10) Take care also that the lateral surfaces of the samples should be smooth and perpendicular to the ends of the samples (be square).

13. Measure the width, length and thickness of the specimen at the notches to the nearest 0.25-mm (0.01-in) to determine the shear area.

14. Return specimens in the condition chamber until tested. The configuration of the specimen is shown in Figure C1.

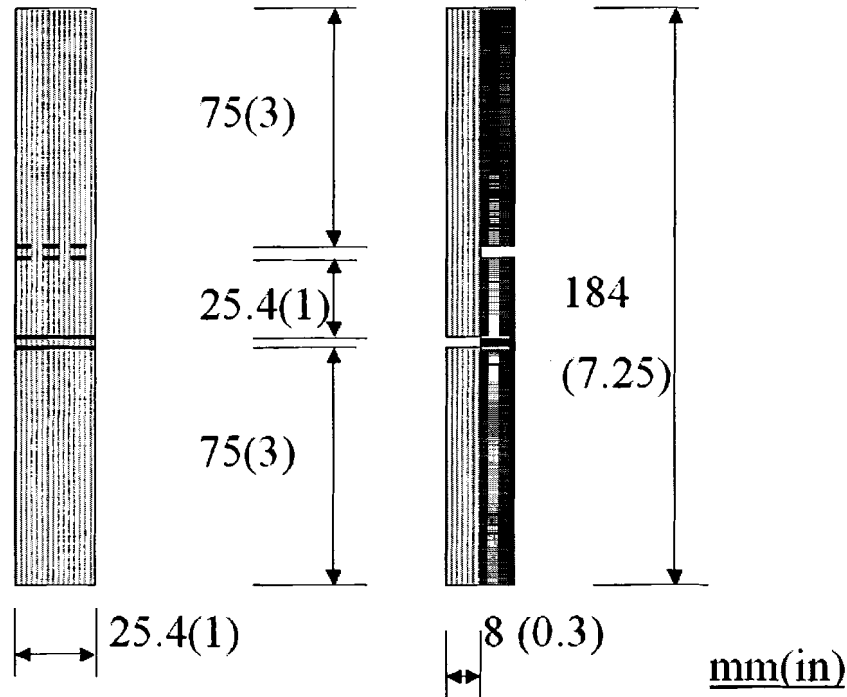


Figure C1 Configuration of the Specimen

Conditioning

Condition the samples at $23 \pm 2^\circ\text{C}$ and RH of 50-70% for at least two weeks before testing.

Testing and Data Recording

1. Three types of experiments were conducted: quasi-static tests, fatigue tests and residue strength tests.
2. Sample size requirement: select and test at least 30 specimens, representing at least four different panels. Use the laminating press to fabricate at least 5 test joints. 12 specimens will be cut from each joint to get total 60 specimens. At least 5 specimens from each panel will be used to do the fatigue tests. At least 5 specimens from each panel will be used to do the quasi-static tests.
3. The test frame is servo hydraulic testing machine (Instron FastTrack 8801 Testing System 22 kip) in the AEW C mechanical testing lab. The crossheads of the testing machine must be carefully aligned manually to prevent premature torsion failure of the specimen. They should be perfectly aligned in such a position that an imaginary vertical line would pass through the center of the bonded area and through the points of suspension. Ensure that the edge of the lap is 25.4 mm (1 in.) from the edge of the grip. The clamping pressure of 40 psi should be used to

prevent crushing failure of the wood layer and slippage in the grip area. The orientation that the wood notch to the upper left should be used to conduct all of the tests.

4. Conduct some quasi-static tests to get the ultimate single-lap shear strength. The loading rate is of 3.5 kN/min.
5. Sinusoidal tension-tension axial load is used to do the fatigue tests. One stress level should be selected, which is determined by 50% of the single-lap shear strength from quasi-static tests. Fatigue tests should be conducted at constant amplitude with a stress ratio of $R = 0.1$ and a frequency of 20 Hz. Specimens should be tested until failure, and the test should be stopped at 3 million cycles if no failure occurred.
6. Residual strength tests should be conducted after fatigue tests if the specimens survive after 3 million cycles. The loading rate should be 3.5 kN/min.
7. In order to minimize possible influence due to post-curing effect of the adhesive, the rest of quasi-static tests should be conducted after the fatigue tests.

Calculations

1. For quasi-static tests and residue strength tests, record the load at failure in kilograms (pounds), and calculate the shear stress at failure as Newtons per square meter (pounds per square inch), based on shear area calculated to the nearest 0.06 mm^2 (0.01 in^2). Estimate the percentage of wood failure to the nearest 5% for each test specimen.
2. For fatigue tests, record the number of cycles to failure. Estimate the percentage of wood failure to the nearest 5% for each test specimen.

Appendix F – Work Instruction of Mode I DCB Fracture Tests

Objective:

Determination of the opening Mode I interlaminar fracture toughness of FRP-wood interface based on Modified ASTM D5528-01.

Summary

This Work Instruction is for the fabrication and testing of FRP-wood flat double cantilever beam samples for the Mode I fracture test of modified ASTM D5528.

Fabrication Procedure

1. Preparation of wood boards:
 - 1) Use only vertical-sawn lumber;
 - 2) Condition the wood at $23\pm 2^{\circ}\text{C}$ and RH of 50-70% until MC of 9-12% has been attained;
 - 3) Cut each piece of wood to nominal 9-mm thick, 140 mm (5.5 in) wide and 200 mm (7.87 in) long (determined by the hydraulic press);
 - 4) Freshly surface each lamination before bonding with the adhesive to tested. Remove at least 0.4 mm from each face within 24 h of bonding.
 - 5) The planner will usually cause snipe at the end of the board. Snipe is when the planer cuts more off of the end than the rest of the board. Run the boards through the planer a few more times and this should reduce or eliminate the snipe.
2. Apply HMR Primer (if needed):
 - 1) Prepare HMR Primer according to WI-01-05;
 - 2) Apply HMR Primer to the wood surfaces with the spreading rate $0.0945 \text{ g} / \text{in}^2$ of $4.1 \text{ g} / \text{surface of glue line}$;
 - 3) HMR should be applied 16 hrs before bonding.
3. Preparation of FRP layers:
 - 1) Cut each piece of FRP to 140 mm (5.5 in) wide and 200 mm (7.87 in) long (determined by the hydraulic press)
 - 2) Abrade the FRP surfaces with 80-grit sand paper;
 - 3) Wipe the sanded surface with a lint-free, acetone-saturated rag to remove dirt and dust.
 - 4) Wait a minimum of 5 minutes until solvent has evaporated.
4. Fabrication of FRP-wood laminated boards:
 - 1) Personal protective equipment- rubber gloves, rubber aprons and protective glasses of goggles-should be worn;

- 2) Bond a Teflon strip on the wood surface with a spray adhesive to create the insert. The strip must be parallel the end of the substrate with a distance of 60mm.
 - 3) Prepare adhesive.
 - 4) Apply the adhesive uniformly to the contacting faces of each lamination in accordance with manufacturer's instructions. Do not apply the adhesive in the insert region.
 - 5) Attach the FRP to the contacting face of each wood lamination. Only the wood is being applied with adhesive.
 - 6) Place the laminated wood members under proper pressure for a period of time and at the glueline temperature specified by the manufacturer of the adhesive.
5. Prepare test samples:
- 1) Sand the edges of the boards to get smooth lateral surfaces;
 - 2) Use the table saw for FRP with the diamond blade to cut off about quarter-inch strip along the longitudinal direction from one side of the board (get rid of the side piece).
 - 3) Cut through the whole panel along the longitudinal direction to make 1-in width coupons. It should be able to get 4 samples out of each panel.
 - 4) Take care that the lateral surfaces of the samples should be smooth and perpendicular to the ends of the samples (be square).
6. Bond steel hinges:
- 1) Cut the continuous steel hinges to 1-in wide pieces with the knuckles in the middle.
 - 2) Drill two holes on one tab of the hinge that will be bonded to the wood substrates.
 - 3) Abrade one tab surface of each hinge that will be bonded to wood and FRP substrates to make flat but rough surfaces.
 - 4) Use the same surface treatment of Step 3 to prepare the contacting face of each hinge.
 - 5) Prepare adhesive. Apply the adhesive uniformly to the contacting face of each hinge in accordance with manufacturer's instructions.
 - 6) Place the bonding area under proper pressure for a period of time and at the glueline temperature specified by the manufacturer of the adhesive.
 - 7) Drill holes into the wood substrates beneath the holes of the hinges. The holes on the wood must be smaller than the diameter of the wood screws. Install the wood screws.
7. Mark specimens:
- 1) Coat both edges of the specimen with a thin layer of water-based typewriter correction fluid, providing a brittle high-contrast coating that simplifies crack visualization.
 - 2) Mark the first 30 mm of the edges with thin vertical lines every 5 mm from the insert.

8. Return specimens in the condition chamber until tested. The configuration of the specimen is shown in Figure D1.

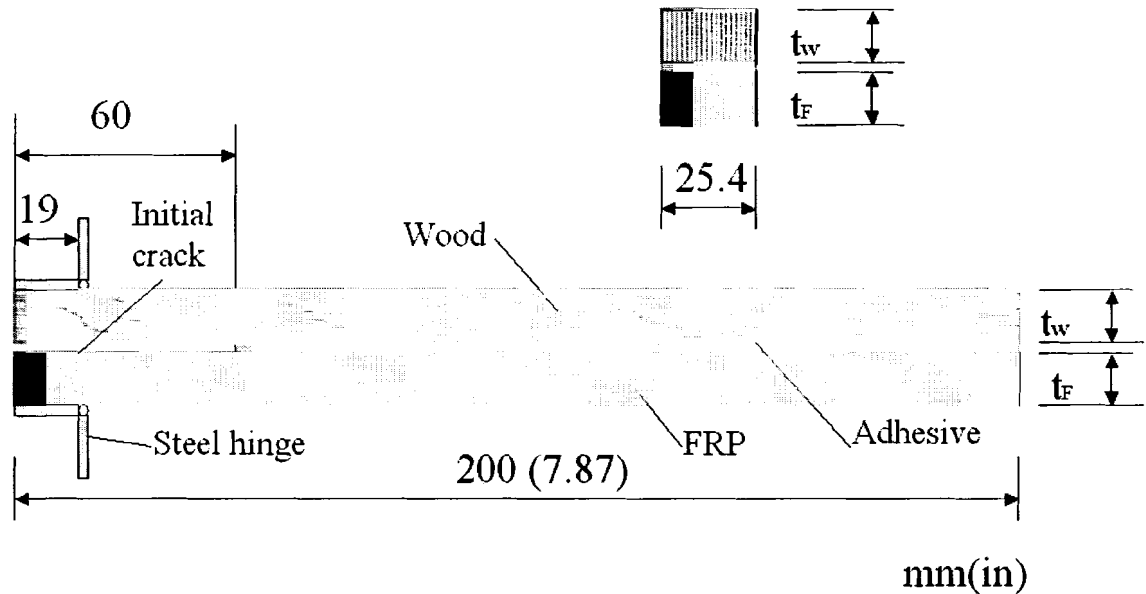


Figure D1 Configuration of the Specimen

Conditioning

Condition the samples at $23 \pm 2^\circ\text{C}$ and RH of 50-70% for at least two weeks before testing.

Testing and Data Recording

1. An Instron 5500R electro-mechanical testing frame with 2 kN load capacity is used to apply the load.
2. Setup the specimen. Prior to loading, the free end of the fracture specimen should be supported to maintain horizontal placement.
3. Setup the CCD camera. Data acquisition and system control of the CCD camera will be performed with Labview software. Crack opening displacement (COD) and crack length will be monitored during testing using the CCD camera throughout the test.
4. Load the specimen continuously in displacement control with a loading rate of 0.5 mm/min. When the delamination has extended 30mm, unload the specimen with a constant loading rate of 1 mm/min. Then stop the test. Load and displacement should be recorded throughout the test, including the unloading cycle.

Image Analysis

Image analysis software Sherlock may be used to measure the COD and crack length from the images with the unit of pixel. Then, they can be converted to real unit such as millimeter. The Sherlock can be programmed to track the coordinates of COD points automatically for a series of images. The crack lengths have to be measured manually from the images.

Calculations

1. Load, crack length and COD are used to calculate the strain energy release rate of the FRP-wood hybrid DCB specimens. Time may be used to correlate the load and crosshead displacement recorded by Instron with the COD and crack length measured from the image.
2. Three data reduction methods may be used to calculate G_I : Modified Beam Theory (MBT) method, Compliance Calibration (CC) method and Shear Corrected Compliance (SCC) method. The equations of the three data reduction method are listed in the Appendix.
3. Plot the curve of the strain energy release rate G_I versus crack length for each specimen.

BIOGRAPHY OF THE AUTHOR

Yong Hong was born in Beijing, P. R. China on July 27, 1970. He graduated from high school in 1989 from Beijing Second High School of Beijing, P. R. China. He attended the Beijing Polytechnic University and graduated in August of 1993 with a Bachelor's degree in Civil Engineering. He worked as a structural design and analysis engineer in China Academy of Building Research (CABR) from 1993 to 1999. He attended the University of Maine since September of 1999. He is a candidate for the Master of Science degree in Civil Engineering from The University of Maine in May, 2003.